

## **General Disclaimer**

### **One or more of the Following Statements may affect this Document**

- This document has been reproduced from the best copy furnished by the organizational source. It is being released in the interest of making available as much information as possible.
- This document may contain data, which exceeds the sheet parameters. It was furnished in this condition by the organizational source and is the best copy available.
- This document may contain tone-on-tone or color graphs, charts and/or pictures, which have been reproduced in black and white.
- This document is paginated as submitted by the original source.
- Portions of this document are not fully legible due to the historical nature of some of the material. However, it is the best reproduction available from the original submission.

5101-228  
Flat-Plate  
Solar Array Project

DOE/JPL-1012-81  
Distribution Category UC-63b

# Proceedings of the Flat-Plate Solar Array Workshop on the Science of Silicon Material Preparation

(August 23, 24, and 25, 1982, The Pointe, Phoenix, Arizona)

(NASA-CR-170318) PROCEEDINGS OF THE  
FLAT-PLATE SOLAR ARRAY WORKSHOP ON THE  
SCIENCE OF SILICON MATERIAL PREPARATION (Jet  
Propulsion Lab.) 316 p HC A14/MF AC1

N83-25034

CSCI 10A G3/44

Unclas  
03535

February 1, 1983

Prepared for  
U.S. Department of Energy  
Through an Agreement with  
National Aeronautics and Space Administration  
by  
Jet Propulsion Laboratory  
California Institute of Technology  
Pasadena, California

JPL PUBLICATION 83-13



5101-228  
Flat-Plate  
Solar Array Project

DOE/JPL-1012-81  
Distribution Category UC-63b

# Proceedings of the Flat-Plate Solar Array Workshop on the Science of Silicon Material Preparation

(August 23, 24, and 25, 1982, The Pointe, Phoenix, Arizona)

February 1, 1983

Prepared for  
**U.S. Department of Energy**  
Through an Agreement with  
**National Aeronautics and Space Administration**  
by

**Jet Propulsion Laboratory**  
California Institute of Technology  
Pasadena, California

JPL PUBLICATION 83-13

**ORIGINAL PAGE IS  
OF POOR QUALITY**

Prepared by the Jet Propulsion Laboratory, California Institute of Technology,  
for the U.S. Department of Energy through an agreement with the National  
Aeronautics and Space Administration.

The JPL Flat-Plate Solar Array Project is sponsored by the U.S. Department of  
Energy and is part of the Photovoltaic Energy Systems Program to initiate a  
major effort toward the development of cost-competitive solar arrays.

This report was prepared as an account of work sponsored by an agency of the  
United States Government. Neither the United States Government nor any  
agency thereof, nor any of their employees, makes any warranty, express or  
implied, or assumes any legal liability or responsibility for the accuracy, com-  
pleteness, or usefulness of any information, apparatus, product, or process  
disclosed, or represents that its use would not infringe privately owned rights.

Reference herein to any specific commercial product, process, or service by trade  
name, trademark, manufacturer, or otherwise, does not necessarily constitute or  
imply its endorsement, recommendation, or favoring by the United States  
Government or any agency thereof. The views and opinions of authors  
expressed herein do not necessarily state or reflect those of the United States  
Government or any agency thereof.

This publication reports on work done under NASA Task RD-152, Amendment  
66, DOE/NASA IAA No. DE-AI01-76ET20356.

ABSTRACT

The Science of Silicon Material Preparation Workshop was held August 23-25, 1982, at The Pointe, Phoenix, Arizona. It was sponsored by the Flat-Plate Solar Array Project (FSA) of the Jet Propulsion Laboratory (JPL). There were six sessions: Silicon Production and Purity; Thermodynamics, Kinetics, and Mechanisms; Particle Formation and Growth; Deposition In Fluidized-Bed Reactors; Chemical Vapor Deposition; and Alternative Polysilicon Processes. Twenty-two invited papers were presented. Discussion periods followed the papers and the sessions. These Proceedings are a record of the papers and the discussions.

Key Words:

Chemical vapor deposition  
Deposition  
Dichlorosilane  
Dichlorosilane process  
Electrochemical deposition  
Fluidized-bed reactor  
Kinetics  
Mechanism  
Particle growth  
Polysilicon  
Process  
Purity  
Silane  
Silane process  
Silicon tetrafluoride  
Solar cell  
Thermodynamics

## FOREWORD

The objectives of this Workshop were: (1) to discuss the chemistry, physical chemistry, and chemical engineering involved in the preparation of semiconductor-grade polysilicon; (2) to review the status of preparation technologies; and (3) to identify critical barriers to improved processes and experimental programs to address the technical problems. Accordingly, the six sessions were for Silicon Production and Purity; Thermodynamics, Kinetics and Mechanisms; Particle Formation and Growth; Deposition In Fluidized Bed Reactors; Chemical Vapor Deposition; and Alternative Polysilicon Processes. A large part of the Workshop dealt with the chemistry and the problems encountered in the use of silane for the deposition of silicon, so that there was some continuity centering on silane through the first five sessions. The papers and the discussions provided a stimulating forum for the exchange information, the pin pointing of problem areas, and the introduction of research ideas.

The Proceedings contain the unedited texts of the papers. These were submitted by the authors before the Workshop. Hence, the actual presentations may have differed somewhat from these papers. The Proceedings also contain the transcribed tapes of the discussions; these were edited, as necessary, to enhance clarity of expression.

The Workshop Committee is grateful to the authors of the papers for making the considerable effort necessary for the preparation of the papers and for their participation in the discussion periods. The audience was very active in raising questions, in presenting additional information, and in discussing areas of uncertainty. The interchanges made the Workshop successful.

PRECEDING PAGE BLANK NOT FILMED

## DEDICATION

The Jet Propulsion Laboratory wishes to dedicate the Proceedings of this Workshop to the memory of the late J. R. (Rannie) Davis. He was a Principal Investigator in the studies performed under JPL Contract 954331 by the Westinghouse Research Center on "Effects of Impurities and Processing on Silicon Solar Cells." The excellence and importance of these investigations of impurity effects have been universally recognized and praised. A large measure of credit is due to his innovative thinking and diligence. His scientific work, his presentations at meetings, and his warm friendship will be missed.

SCIENCE OF SILICON MATERIAL PREPARATION WORKSHOP  
ORGANIZING COMMITTEE:

Anthony Briglio  
George Hsu  
Ralph Lutwack, Chairman  
Andrew Morrison  
Mary Phillips, Conference Coordinator

SCIENCE OF SILICON MATERIAL PREPARATION  
WORKSHOP

AUGUST 23-25, 1982

THE POINTE  
PHOENIX, ARIZONA

PARTICIPANT LIST

ADAMS, Charles C.  
General Atomic Co.  
P. O. Box 81608  
San Diego, CA 92138  
(714) 455-3079

ANDELL, Jonathan  
Solovolt International  
P. O. Box 2931  
Phoenix, AZ 85008  
(602) 244-7324

ATWATER, Harry  
Massachusetts Institute of Technology  
Room 10 - 372 H  
77 Massachusetts Avenue  
Cambridge, MA 02139  
(617) 253-6963

BAILEY, Don  
627 W. Ninth St.  
Traverse City, MI 49684  
(616) 946-2190

BRIGLIO, Anthony  
Jet Propulsion Laboratory  
4800 Oak Grove Dr., M.S. 238-710  
Pasadena, CA 91109  
(213) 354-4883

COLLIER, Jack  
Jet Propulsion Laboratory  
4800 Oak Grove Dr., M.S. 512-103  
Pasadena, CA 91109  
(213) 577-9422

COSTOGUE, E. N.  
Jet Propulsion Laboratory  
4800 Oak Grove Dr., M.S. 507-228  
Pasadena, CA 91109  
(213) 577-9275

DeLUCA, John  
Monsanto  
P. O. Box 8  
St. Peters, MO 63376  
(314) 272-6281

DUDUKOVIC, Milorad (Mike)  
Washington University at St. Louis  
Department of Chemical Eng.  
Campus Box 1198  
St. Louis, MO 63130  
(314) 889-6021

ERK, Henry  
Monsanto  
P. O. Box 8  
St. Peters, MO 63376  
(314) 272-6281, X2628

FELDER, William  
AeroChem Research Laboratories  
P. O. Box 12  
Princeton, NJ 08540  
(609) 921-7070

FITZGERALD, Thomas  
TRW  
One Space Park  
Redondo Beach, CA 90278  
(213) 535-0277

FLAGAN, Richard  
California Institute of Technology  
Eng & Appl Sci, 138-78  
1201 E. California  
Pasadena, CA 91125  
(213) 356-4383

PRECEDING PAGE BLANK NOT FILMED

GAUTREAUX, M. F.  
Ethyl Corporation  
Ethyl Tower - 451 Florida  
Baton Rouge, LA 70801  
(504) 388-7975

GIRAUDI, Ronald V.  
J. C. Schumacher Company  
580 Airport Road  
Oceanside, CA 92054  
(714) 433-1663

GODDARD, William  
California Institute of Technology  
108 Noyes  
Chemistry and Chemical Engineering  
Pasadena, CA 91125  
(213) 356-6544

GOPFFARTH, Gregory  
Texas Instruments  
P. O. Box 84 - M.S. 880  
Sharman, TX 75090  
(214) 892-7158

GRAYSON, Paul  
Eagle Pitcher Industries, Inc.  
P. O. Box 1090  
Miami, OK 74354  
(918) 542-1801

GRIMMETT, Earl. S.  
G & R Technology  
1085 Syringa Drive  
Idaho Falls, Idaho 83401  
(208) 522-5014

HEY, Peter  
University of Arizona  
Optical Sciences Center  
Tucson, AZ 85721  
(602) 626-2864

HOPKINS, Richard  
Westinghouse R&D Center  
1310 Beulah Rd.  
Pittsburgh, PA 15235  
(412) 256-3235

HSU, George  
Jet Propulsion Laboratory  
4800 Oak Grove Dr., M.S. 238-710  
Pasadena, CA 91109  
(213) 354-7428

INGLE, William  
Motorola, Inc.  
5005 E. McDowell Rd.  
Phoenix, AZ 85008  
(602) 244-4415

ISHIGURO, Michi  
OTC America, Inc.  
166 Geary St., Suite 1002  
San Francisco, CA 94108  
(415) 397-7511

IYA, Sridhar  
Union Carbide Corp.  
Electronics Materials Tech. Center  
3333 Index Street  
Washougal, WA 98671  
(206) 835-8720

JACOBSON, Michael R.  
University of Arizona  
Optical Sciences Center  
Tucson, AZ 85721  
(602) 626-2864

JACUBERT, Serge  
Rhone Poulenc Recherches  
12 Rue Des Gardinoux  
Aubervilliers, France 93308  
(1) 834-93-96 (p. 477)

JEWETT, Dave  
Energy Materials Corporation  
P. O. Box 1143 Sterling Rd.  
So. Lancaster, MA 01561  
(617) 365-7383

KAAE, James  
General Atomic Co.  
P. O. Box 81608  
San Diego, CA 92138  
(714) 455-2957



KAYIHAN, Ferhan  
Zeyerhauser Technical Center  
Senior Research Engineer  
WTCLB5  
Tacoma, WA 98477  
(206) 924-6651

KAYSER, R. A.  
Union Carbide Corp  
P. O. Box 180 - State Rte 2  
Sisterville, WVA 26175  
(304) 652-3211 X-1256

KEIL, Dahn  
Solovolt International  
P. O. Box 2934  
Phoenix, AZ 85008  
(602) 244-7324

LEIPOLD, Martin  
Jet Propulsion Laboratory  
4800 Oak Grove Dr., M.S. 238-710  
Pasadena, CA 91109  
(213) 354-3931

LORD, Stephen  
J. C. Schumacher Company  
580 Airport Road  
Oceanside, CA 92054  
(714) 433-1663

LORENZ, James  
Union Carbide Corp.-Elec. Div  
Old Ridgebury Rd. - Sec. F1297  
Danbury, CT 06817  
(203) 794-4612

LUTWACK, Ralph  
Jet Propulsion Laboratory  
4800 Oak Grove Dr., M.S. 238-710  
Pasadena, CA 91109  
(213) 354-7648

MILSTEIN, Joseph  
Solar Energy Research Institute  
1617 Cole Blvd.  
Golden, CO 80401  
(303) 231-7299

MORRISON, Andrew  
Jet Propulsion Laboratory  
4800 Oak Grove Dr., M.S. 238-710  
Pasadena, CA 91109  
(213) 354-7200

MUI, Jeffrey Y. P.  
Solarelectronics Inc.  
P. O. Box 141  
21 Rita Lane  
Bellingham, MA 02019  
(617) 966-1234

McCORMICK, James  
Hemlock Semiconductor Corp.  
12334 Geddes Rd.  
Hemlock, MI 48626  
(517) 642-5203

NODA, Toshio  
Osaka Titanium, Ltd.  
1, Higashihama-Cho  
Amagasaki, Hyogo, Japan 660  
(06) 411-1121

OLSEN, J. M.  
Solar Energy Research Institute  
1617 Cole Blvd.  
Golden, CO 80401  
(303) 231-1801

PELLIN, Remo  
7200 Old Oak Lane  
Charlotte, NC 28212  
(704) 545-9964

PETTIT, Donald  
University of Arizona  
Department of Chemical Engineering  
Tucson, AZ 85721  
(602) 626-1224

PHILLIPS, Mary  
Jet Propulsion Laboratory  
4800 Oak Grove Dr., M.S. 502-422  
Pasadena, CA 91109  
(213) 577-9096

PLAHUTNIK, Frank  
Hemlock Semiconductor Corp.  
12334 Geddes Rd.  
Hemlock, MI 48626  
(517) 642-5203 X-209

PRATURI, Ananda K.  
C. F. Braun  
1000 Fremont  
Alhambra, CA 91802  
(213) 570-2915

REIF, Rafael  
Massachusetts Institute of Tech.  
Dept. of Engr & Computer Sci.  
Dept. of EE-Room 13-3082  
Cambridge, MA 02139  
(617) 253-6879

RING, Morey A.  
San Diego University  
Department of Chemistry  
San Diego, CA 92115  
(714) 265-6271

ROGERS, Leo  
Polycrystalline Silicon Tech. Corp.  
1819 S. Dobson Rd.  
Dobson Ranch  
Mesa, AZ 85202  
(602) 897-2222

ROHATGI, Naresh  
Jet Propulsion Laboratory  
4800 Oak Grove Dr., M.S. 238-710  
Pasadena, CA 91109  
(213) 354-3073

RUZZIER, John  
Continental Industry Inc.  
16441 E. Sullivan  
Fountain Hills, AZ 85268

SANJURJO, Angel  
SRI International  
333 Ravenswood  
Menlo Park, CA 94025  
(415) 859-2455

SARMA, Kalluri R.  
Solovolt International  
P. O. Box 2934  
Phoenix, AZ 85008  
(602) 244-7324

SCHEIDEGGER, Gary  
University of Arizona  
Optical Science Center  
Tucson, AZ 85721  
(602) 626-2864

SCOLARO, M. Anthony  
U.S. Department of Energy  
1000 Independence Ave. 5E066  
Washington, DC 20585  
(202) 252-5548

SCOTT, Bruce  
IBM - Box 218  
Thomas J. Watson Research Center  
Yorktown Heights, NY 10598  
(914) 945-1802

SETTY, H. S. N.  
Motorola, Inc. - Semicond. Grp  
5005 E. McDowell Rd. Mail Drop A128  
Phoenix, AZ 85008  
(602) 244-6154

SHANFIELD, Stan  
Spire Corporation  
Patriots Park  
Bedford, MA 01730  
(617) 275-6000

STEINWANDEL, Jurgen  
Yale University  
Department of Applied Mechanics  
Fluid Dynamics Laboratory  
New Haven, CT 06520  
(203) 436-8675

THORNHILL, Jay  
Jet Propulsion Laboratory  
4800 Oak Grove Dr., M.S. 507-228  
Pasadena, CA 91109  
(213) 577-9040

TUSTIN, David  
Jet Propulsion Laboratory  
4800 Oak Grove Dr., M.S. 502-422  
Pasadena, CA 91109  
(213) 577-9597

## CONTENTS

INTRODUCTION . . . . .	1
SESSION I: Silicon Production and Purity . . . . .	3
The Silicon Challenge: J. H. Lorenz, Union Carbide Corp. . . . .	5
Discussion . . . . .	15
Silicon Purity: Impact on Crystal Growth and Silicon Properties for Photovoltaic Applications: R. H. Hopkins, Westinghouse R&D Center . . . . .	17
Discussion . . . . .	30
SESSION II: Thermodynamics, Kinetics, and Mechanisms . . . . .	31
Chlorosilane Thermodynamic Equilibria Calculations with Applications to High Purity Silicon Preparation: Henry F. Erk, Monsanto Co. . . . .	33
Discussion . . . . .	48
Kinetics and Mechanisms of Chlorosilane Decomposition: Donald F. Bailey, Consultant to Jet Propulsion Laboratory . . . . .	51
Discussion . . . . .	60
Kinetics and Mechanism of the Silane Decomposition: Morey A. Ring, San Diego State University . . . . .	63
Discussion . . . . .	73
Session II General Discussion . . . . .	75
SESSION III: Particle Formation and Growth . . . . .	77
Homogeneous Gas-Phase Condensation of Silicon by Shock Wave Induced Decomposition of $\text{SiH}_4$ : Jurgen Steinwandel, University of Stuttgart . . . . .	79
Discussion . . . . .	88
Kinetics of Particle Growth in Silane Systems: William Felder, AeroChem Research Laboratories, Inc. . . . .	89
Discussion . . . . .	100
Submicron Particle Size Measurement: Don Pettit, University of Arizona . . . . .	101
Discussion . . . . .	105
Factors Governing Particle Size in the Free Space Reactor: Richard Flagan, California Institute of Technology . . . . .	107
Discussion . . . . .	116

Coherent Detection of Scattered Light from Submicron Particles: Donald Pettit, University of Arizona . . . .	121
Discussion . . . . .	123
SESSION IV: Fluidized-Bed Reactor Technology . . . . .	125
The Mechanism of the Chemical Vapor Deposition of Carbon in a Fluidized Bed of Particles:	
James Kaae, General Atomic Company . . . . .	127
Discussion . . . . .	137
A Model for the Growth of Dense Silicon Particles from Silane Pyrolysis in a Fluidized Bed:	
Thomas J. Fitzgerald, TRW Energy Development Group . . . . .	141
Discussion . . . . .	151
Steady-State and Transient Particle Size Distribution Calculations for Fluidized Beds:	
Ferhan Kayihan, Weyerhaeuser Technology Center . . . . .	159
Discussion . . . . .	169
An Update on a Mathematical Model which Predicts the Particle Size Distribution: Earl S. Grinnett, G & R Technology .	171
Discussion . . . . .	190
Session IV General Discussion . . . . .	191
SESSION V: Chemical Vapor Deposition . . . . .	197
Reactor Models for CVD of Silicon: Milorad P. Dudukovic, Washington University at St. Louis . . . . .	199
Discussion . . . . .	227
The Deposition of Low Defect Density Amorphous Semiconductors by Homogeneous Chemical Vapor Deposition:	
Bruce A. Scott, IBM Thomas J. Watson Research Center . . . . .	229
Discussion . . . . .	238
Mechanisms in Plasma Enhanced Deposition of Silicon:	
Kalluri R. Sarma, Solavolt International . . . . .	241
Discussion . . . . .	252
Chemical Vapor Deposition of Epitaxial Silicon:	
Rafael Reif, Massachusetts Institute of Technology . . . . .	253
Discussion . . . . .	263
Chemical Vapor Deposition of Silicon for Optical Uses:	
Michael R. Jacobson, University of Arizona . . . . .	265
Discussion . . . . .	276

SESSION VI: Alternative Polysilicon Processes . . . . .	277
Kinetics of Silicon Electrodeposition: Jerry M. Olson, Solar Energy Research Institute . . . . .	279
Discussion . . . . .	288
The Hemlock Semiconductor Dichlorosilane-Based CVD Process: James McCormick, Hemlock Semiconductor Corp. . . . .	293
Discussion . . . . .	304
Production of Silicon by the Reduction of Silicon Tetrafluoride with Sodium: Angel Sanjurjo, SRI International . .	305
Discussion . . . . .	315
CLOSING COMMENT . . . . .	317

## PROCEEDINGS

### The Science of Silicon Material Preparation Workshop

#### INTRODUCTION

LUTWACK: The workshop will be in six sessions. In the first session, the presentations will deal with aspects of polysilicon preparation encountered in the development of a new low-cost process and with the impact of impurities on the properties of silicon materials and the performance of photovoltaic cells. In the second session, there will be papers on thermodynamic equilibria, kinetics, mechanisms, and models. These will serve as prefaces for the later papers. The third session will deal with particle formation and growth, dealing in particular with systems for silane decomposition. Then, since the development of a fluidized bed reactor is considered to be a primary need in achieving the full effectiveness of the low-cost process using silane and a great deal of attention is being devoted to that development, the next session will deal with the properties, mechanisms, reactions, and modeling of fluidized-bed reactors. The fifth session will deal with the phenomena involved in the chemical-vapor deposition of silicon. In Session 6, the chemistry, kinetics and chemical engineering involved in some alternative processes for producing silicon will be described.

## SESSION I: Silicon Production and Purity

LUTWACK (Chairman): The first session is titled "Silicon Production and Purity." In the first paper Jim Lorenz of Union Carbide will discuss a new low-cost process for polysilicon preparation. In part, the paper will serve as an introduction to the problems of converting silane into semiconductor-grade silicon.

The studies which have been done by the research group at Westinghouse have provided a firm experimental data basis for describing the effects of impurities on the properties of silicon materials and the performance of solar cells. I wish to take this opportunity to pay tribute to the late Rannie Davis, who was one of the principal investigators of this study. The excellence of this work was in large part due to his contributions. Dick Hopkins of Westinghouse, who was the manager and principal investigator of the program, will describe the impact of these investigations on silicon and its uses.

PRECEDING PAGE BLANK NOT FILMED

# THE SILICON CHALLENGE

J. H. LORENZ

UNION CARBIDE CORPORATION

Danbury, Connecticut

**PRECEDING PAGE BLANK NOT FILMED**

## INTRODUCTION

My assignment today is to talk about silicon material preparation. My presentation will include a brief history of the production of pure polysilicon, a status review of the Union Carbide contract programs and current commercial program and the future needs of polysilicon. Dr. Lutwack assures me the solutions to these needs will be given by the experts who follow me today. Thus, I have the easy task of only posing the problems.

Silicon, the second most abundant element on our earth, is found mostly as silica. Thus, with a boundless supply of raw material, our only problem is to get silicon into a usable state required by our technology. If we believe the science fiction writers, then possibly someday we'll find life in outer space is indeed based on silicon rather than carbon, as it is here on the planet earth. However, the quest for pure silicon for terrestrial use is the subject of our concerns here today. This need really began with the invention of the silicon transistor in 1948. It was immediately clear that work was needed on a silicon deposition process. Silicon tetrachloride was the only available silicon compound which could be easily purified, so much of the early work centered on metal reduction reactions. Bell Telephone asked Union Carbide in 1950 to make a pure silicon for the projected semiconductor industry. We were not in a position to respond to this request, but Du Pont did take up the challenge. Just one year later they were producing a form of pure silicon from silicon tetrachloride and zinc. They produced some 100 Kg in 1952 and sold it for \$454/Kg. Many other companies, such as Merck, Grace, Monsanto, Wacker and Texas Instruments, also were looking at ways of producing pure silicon.

Most of the work centered on silicon bromides, fluorides and chlorides, which were reduced on hot wires, with metals or with hydrides. In the 1950's Union Carbide and others were into silicone technology R&D and many different silicon compounds and monomers were being made. Texas Instruments in the late 1950's, requested a sample of the most pure silicon monomer Union Carbide could make. Trichlorosilane was selected - and a five gallon sample proved to be an instant success. Of course, we considered impurities in parts per thousand good in those days. Union Carbide set up to make a million pounds per year - and a business was born. Incidentally, in this same time period we also had made several hundred kilograms of dichlorosilane and monosilane. But we were 30 years too soon! However, progress on using trichlorosilane was rapid. As improved process techniques yielded more pure trichlorosilane, analytical methods had to be developed. We moved from measuring parts per million to parts per billion and onto hundredths of parts per billion. Boron and phosphorous in trichlorosilane were reduced



from 10 parts per million to less than 0.05 parts per billion, over a 12 year period.

This, in 1958, was the beginning of the current trichlorosilane - vapor deposition silicon process. And it has, indeed, served the business very well. There have been substantially no changes in this process to date - except for continuing optimization of yield and costs.

One variation on this process occurred in the late 1960's, when Komatsu Electronic Metals, Inc., a subsidiary of Komatsu, Ltd., began making silicon from monosilane. This was a more costly process, but did make a very pure silicon. Komatsu continues to operate this process today.

#### THE PHOTOVOLTAIC PROGRAM

With the advent of the 1974-75 energy crisis, the Government considered the recommendation of a blue ribbon study group that work be started in many renewable energy areas. The goal was to reduce our dependence on fossil fuels by 1986. Photovoltaics was one suggested area - and Jet Propulsion Labs set up the Low-Cost Solar Array Project (LSA). This was based on the proven performance of silicon solar cells in powering our spacecraft. The major deterrent to their practical use was cost - over \$40 per peak watt. The LSA Project, with a goal of showing industry how to get the cost down to 50¢ a peak watt by 1986, divided the project into 5 tasks. Task I was the development of a lower cost silicon - some 14 companies were funded to develop their favorite polysilicon process. Most of these involved metal reduction of chlorosilanes, fluorides or bromides. Several novel ideas were also funded - like reducing very pure silica and carbon in an electric furnace and the reduction of waste fluorosilicates.

Over the past seven years, the LSA Projects have been screened out and only a few of the most promising survive today. None are currently funded to completion. The new Flat-Plate Solar Array Project (FSA), successor to LSA, has as its primary objective the sponsorship of research and evaluation in technologies for flat-plate photovoltaic arrays. The new Task I, Advanced Materials Research, plans to sponsor research in reactor concepts.

Concurrent with the original JPL/LSA program, the Department of Energy funded additional silicon work, as well as R&D on other materials for solar cells. Among these was the potential use of metallurgical (98%) silicon via purification steps. Industrial firms also pursued this area of multigrained or semicrystalline silicon. Patents have been issued to Wacker, Alcoa, Union Carbide and others on these processes and uses. Most of these processes involve a selective precipitation, directional solidification and casting of shaped blocks, making use of the differing co-efficients of segregation of the contaminants. Several companies are producing solar cells with these materials, but their long-term use remains to be proven.

Other silicon work, in part Government funded, was in the amorphous area. This is promising - but has limited commercial use today, pending further development. It might be interesting to note that the German agencies chose to work only with multigrained silicon, while Japan agencies selected the amorphous area.

9  
Y

The U.S. multifaceted approach to materials has been criticized; however, it appears that our programs will benefit not only the photovoltaic market, but all areas using silicon. Let me now talk about the Union Carbide silicon programs.

#### THE UNION CARBIDE PROGRAM

Union Carbide has been interested in silicon chemistry since the 1930's. Research on silicones was begun then, only to be interrupted by World War II assignments. Work continued sporadically over the next 30 years and included early work on decomposing silane. This was our original work on free space decomposition. Pyrolysis of silicon iodide, carbon reduction of silica and sodium reduction of silicon tetrachloride were investigated. Other units of Union Carbide were doing development work on reducing trichlorosilane inside a quartz tube. On cooling the quartz shattered. We actually had a small pilot plant in operation in 1960. It wasn't a bad technique - if one didn't mind a few quartz chips in the polysilicon. In the 1970's, our silicones unit began producing dichlorosilane, using a UCC patented process. Research on making polysilicon from dichlorosilane in a commercial CVD reactor also resulted in several patents. Another patent of that era was for the preparation of silane from trichlorosilane. These processes were used later in our Government photovoltaic proposals.

In a related activity, Union Carbide also began producing silane commercially in the 1960's using the Ring-Litz Molten salt process.

With the building of the silicones plant in the 1950's, a process was installed for making trichlorosilane with very low levels of Group III and Group V elements - and analytical techniques were developed to analyze fractional parts per billion concentrations of these elements in trichlorosilane. As a feed-stock for the Siemens deposition technique, trichlorosilane was, and still is, used for most of the polysilicon production in the world.

With the energy crisis of 1974-75, and Government's renewable energy programs, Union Carbide joined the Low Cost Solar Array Project, suggesting to Jet Propulsion Labs that less costly silicon might be made from silane.

The Union Carbide process converts powdered, 98% metallurgical grade silicon to trichlorosilane in a fluid bed reactor, fluidized with hot equimolar hydrogen - silicon tetrachloride gas feed (Figure 1). The trichlorosilane is passed through a catalyst in a redistribution reactor to partially convert it to dichlorosilane, which is then passed over a second catalyst bed to form silane. All the chloride materials are repeatedly recycled back to the initial reactors. Silane is distilled for final purification, prior to being decomposed to silicon.

A small silane process development unit was designed, constructed and operated to demonstrate feasibility. This was accomplished.

Concurrent with this process work another Union Carbide group was tackling the problem of how to economically decompose the silane. A small free-

space reactor of 194 mm inside diameter was built. Silane, injected downward as an axial turbulent jet, underwent homogeneous decomposition into a low density sub-micron silicon powder at temperatures between 600-1000°C. Initial results were quite encouraging.

A larger unit, 8 inch diameter by 30 inches long, was designed with induction heating (Figure 2). Several dozen runs were made in Phase III of this program. Operating at about 900°C, 99% of the feed silane was converted to the brown, sub-micron powder at a rate of 2.3/Kg/hr. Sufficient powder was prepared to allow large scale melting and forming tests. This silicon powder did show some metal contamination, probably from the internal stainless steel scraper. However, later melting tests indicated a resistivity of 55 ohm-cm - very adequate for solar cells, but not up to our expectations.

While problems with the free-space reactor were resolved, for the most part, handling the low density (0.2 gr/cm<sup>3</sup>) silicon powder would be a problem. Thus, we looked into various means of consolidating the powder into a more easily handled form.

One possibility was suction casting from a melting pot close-coupled to the reactor. This might have worked - but the cost would be an add-on of \$8-10 per Kg. Compaction, sintering, vacuum casting, and cold mold casting were all tried and rejected as not practical. Even fast pulling of a polycrystalline ingot from a CZ unit would add over \$10 per Kg to the cost.

As part of the free-space reactor program, we issued a subcontract for the design, building and operation of a machine to melt the silicon powder and convert it to shot form. This was done by conveying the powder into an induction heated quartz crucible. The crucible had a 1 mm orifice extending from the bottom, from which molten silicon could free fall some 20 feet in a helium atmosphere. Flow was to be controlled by differential pressure on the top and bottom side of the crucible. The unit did operate to produce silicon shot - but additional developments on crucible design, orifice erosion and powder handling are needed. The silicon shot made from the silicon powder did make good solar cells.

In 1981, further work on the free-space reactor system was suspended in favor of concentrating on the fluidized bed concept of decomposing silane.

Our early work - 1978-80 - in a small fluid bed unit indicated silane could be decomposed at 600 to 900°C to yield a dense silicon plate on seed particles. This work was in a 85 mm reactor, resistance heated and operated in a bubbling mode.

Later, a 6 inch reactor with a static bed height of 3 feet with a unique product collector boot was built (Figure 3). Capacitance heating was tried, to concentrate the heating on the silicon seed particles. Auxiliary based heaters were used to control the wall temperature. This system tended to cause some sintering and was unstable electrically. Even so, some useful data was obtained. A feed of 21% silane, operating at 685°C with a fluidization 4.8 times minimum was 98% deposited on the 90 micron seed particles.

Thus we feel the fluidized bed deposition of silane does show promise but there is much yet to be done. One of the critical parts of a fluid bed system is the gas distribution plate. This must cause even gas distribution, not clog, and allow particle segregation. We believe a conical gas distributor plate with suitable cooling, and a tapered boot section should meet these requirements.

Our fluid bed program was interrupted by a stop work order early 1981. Work has been reinstated for FY '82, with a change back to resistance heating for better control. A limited program will investigate bed temperature, fluid velocity, feed rate relationships.

Concurrent with our program under the FSA project, JPL has been doing related work in their laboratories. Using a 2 inch reactor, and a recently built 6 inch reactor, they are investigating silane feeds up to 50-60% and gas distribution systems. Short duration runs on the 2 inch reactor defined preliminary operating areas which will be used on the 6 inch reactor. They will study the overall mechanism of silicon deposition in a fluidized bed system.

Our program under the DOE/JPL project progressed to the stage that a 25 ton pilot plant design was requested in 1978. In fact, there was such enthusiasm in the DOE that we were called in to argue why we shouldn't immediately build a 1000 ton unit. We compromised on a 100 ton Experimental Process System Design Unit (EPSDU) to be funded to demonstrate technical feasibility of the silane process. Designs were drawn for the silane part of the unit, while the deposition processes were still being researched.

By 1980, construction was well underway at Union Carbide's East Chicago site when the first hints of a change in funding surfaced. In the second quarter of 1981 we were advised that the mechanical contract - this is the connecting up of all the pieces - could not be awarded. Only minimal R&D efforts continued as we - DOE/JPL/UCC - considered how the project might be completed.

With the start of negotiations in August 1981 on how to complete at least the silane portion of this project, Union Carbide provided funds to move the experimental unit from East Chicago to an Electronics Division site at Washougal, Washington. Union Carbide agreed to complete the silane portion of the plant and to continue R&D contract work on fluidized bed deposition.

I'm pleased to confirm that this agreement has been concluded and signed.

In October 1981, the EPSDU unit at East Chicago, Indiana was dismantled and moved to our Washougal, Washington site. This equipment has been re-installed, along with the construction of permanent buildings. The mechanical check out of the silane unit is nearly completed - barely 4 months behind the EPSDU schedule. The start-up phase is now underway.

In the Fall of 1980, Union Carbide Corporation approved the Electronics Division's proposal to produce polycrystalline silicon. The 1000 ton plant is based on converting metallurgical grade silicon, via silane, to pure

semiconductor grade silicon. Technology to decompose silane was purchased from Komatsu Electronic Materials, Ltd., a subsidiary of Komatsu, Ltd., Tokyo. This plant will have sufficient silane capacity, that solar grade silicon can also be made when the market develops.

For the final design of the commercial plant, it would be useful to have the parameters confirmed in a pilot plant. Thus, several decomposers of the Komatsu design will be installed at the Washougal Pilot Plant this Fall. This will allow the operation of the silane unit at full capacity for steady state studies. We will also produce high purity silicon in 1983. Also, this Fall, our fluidized bed equipment will be moved and re-installed at the Washougal Plant, so that FY '83 and later contract work, if funded, can be continued without interruption.

On the Commercial Plant, Union Carbide began engineering studies in 1981. Press releases in May 1981, December 1981 and May 1982 detailed our plans to build this unit at Moses Lake, Washington. Groundbreaking ceremonies were held on July 6, 1982 and civil work will begin in August. The initial silicon production is expected in mid-1984.

Thus - where does all of this leave us? I suggest it leaves us with a definite

#### SILICON CHALLENGE.

There is no question that over the past three decades, the United States developed the semiconductor industry. Over 60% of the world's polysilicon is used here. In the photovoltaic area, the United States has led the world in R&D and in commercialization.

Now - with our recession and the drastic cuts in Government funding - What can we do? John Welty of Motorola states, "we should utilize the best available knowledge in the world to adapt to our plans. We can win because we've done it before". I certainly concur with these thoughts. "If we are concerned about being upstaged in technology, we need not sit idly by and curse the darkness around us - but rather light our candle to see our way out".

What is yet to be done in silicon? Plenty. In the solar area, we need to complete an economical deposition technique. We need to get silicon of adequate purity in an easily handled form - at a reasonable price. Certainly for the immediate future - this decade - flat plate silicon is the material of choice. Silicon will remain the dominant force in the photovoltaic market, with single-crystal cells holding a 40% share as late as 1990 - so states Dr. Paul Maycock, a leading expert. He says any new non-silicon cells would have a tremendous momentum to overcome and a very difficult market entry unless the cost reduction for silicon options was not realized.

In the semiconductor area the needs are for higher purity, including less carbon and for understanding the carbon-oxygen relationship.

The two needs are not necessarily incongruous. Basically, we need to understand the phenomena involved in the conversion of various silicon

9  
Y

compounds to pure silicon. We need this knowledge to design better decomposers and to select optimum operating parameters.

Specifically, a fluidized bed deposition of silane system has a good potential to aid both use areas. We need to define more accurately the deposition rate, the impurity capture rates, the effects of bed diameter and aspect ratios on the fluidization, on particle separation and on the heat transfer. We need to confirm the optimum gas distribution plate, and its operating parameters.

### CONCLUSIONS

In conclusion, I feel we have made significant progress towards our goals. We all hear about the research and development programs to replace silicon - work on selenium, germanium, gallium, arsenic, copper, lead, tellurium, tertiary systems, various liquids and even glass mixtures. Even if one of these turned out to be fantastic, it could not be ready for commercialization within the next ten years. Many of these elements are even in very short supply on earth. Thus, silicon is certainly the material for solar and semiconductor applications for this decade, and perhaps, for all decades.

I'm firmly convinced that silicon has yet to gain its greatest glory. Whether it will be single crystal, up-graded poly, multi-grain, semi-crystalline, purified metallurgical or amorphorous - silicon uses will grow. I also believe researchers like you here today will find new techniques which will accelerate that growth. The ultimate in purity and deposition techniques have not yet been reached. And I believe we have time to do it, as the markets grow.

Government funded research programs have contributed to the advancement of technology for the silicon industry - both the photovoltaic and semiconductor areas. However, one could ask, will there ever be a real photovoltaic market. I believe there will be. The basic question is, when. With little or no Government funding, it may well be into the 1990's or later. The U.S. General Accounting Office, at the request of Representative Dick Ottinger, earlier this year did a study on the possible impact of the federal photovoltaic budget reductions. They concluded and I quote, "The photovoltaic industry is expected to endure even with the reduced fund levels for the photovoltaic program. The current photovoltaic market is expanding and the long-range market has tremendous potential. One well-known research firm estimates that by the year 2000 the photovoltaic market will be \$100 billion annually. Consequently, while a shakeout is expected in the photovoltaic industry, as a result of the budget reduction, the development of photovoltaic technology is expected to continue".

Thus, we hope public funding will continue to help provide the pool of technology for the next generation, while industry provides the means to produce silicon of the purity and in the quantity needed for the next two decades. And indeed that's what these meetings are all about - to develop that pool of technology. And with that, it's time to get on with hearing how we are doing, with your elucidation on our problems.

## UNION CARBIDE

### SILANE - SILICON PROCESS

- METALLURGICAL SILICON IS PURIFIED BY CONVERTING IT TO VOLATILE CHLOROSILANE INTERMEDIATES.
- CATALYTIC REDISTRIBUTION YIELDS SILANE, WHICH IS PYROLYZED TO HIGH PURITY SILICON.
- THE SILICON IS CONVERTED TO CRYSTALLINE FORM, SUITABLE FOR SOLAR CELLS.

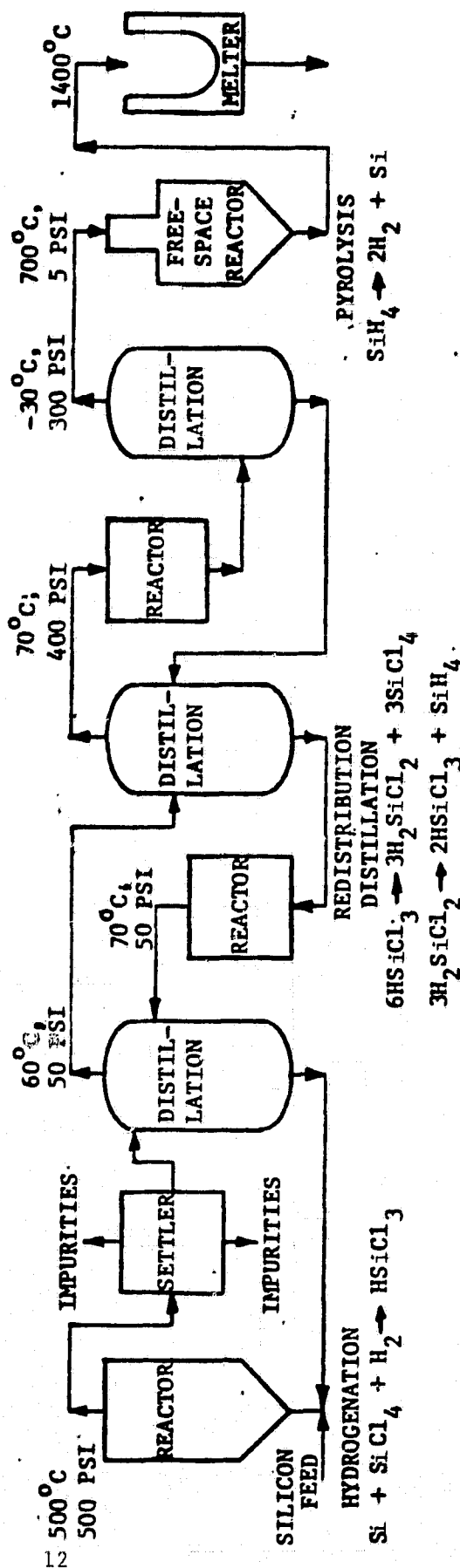
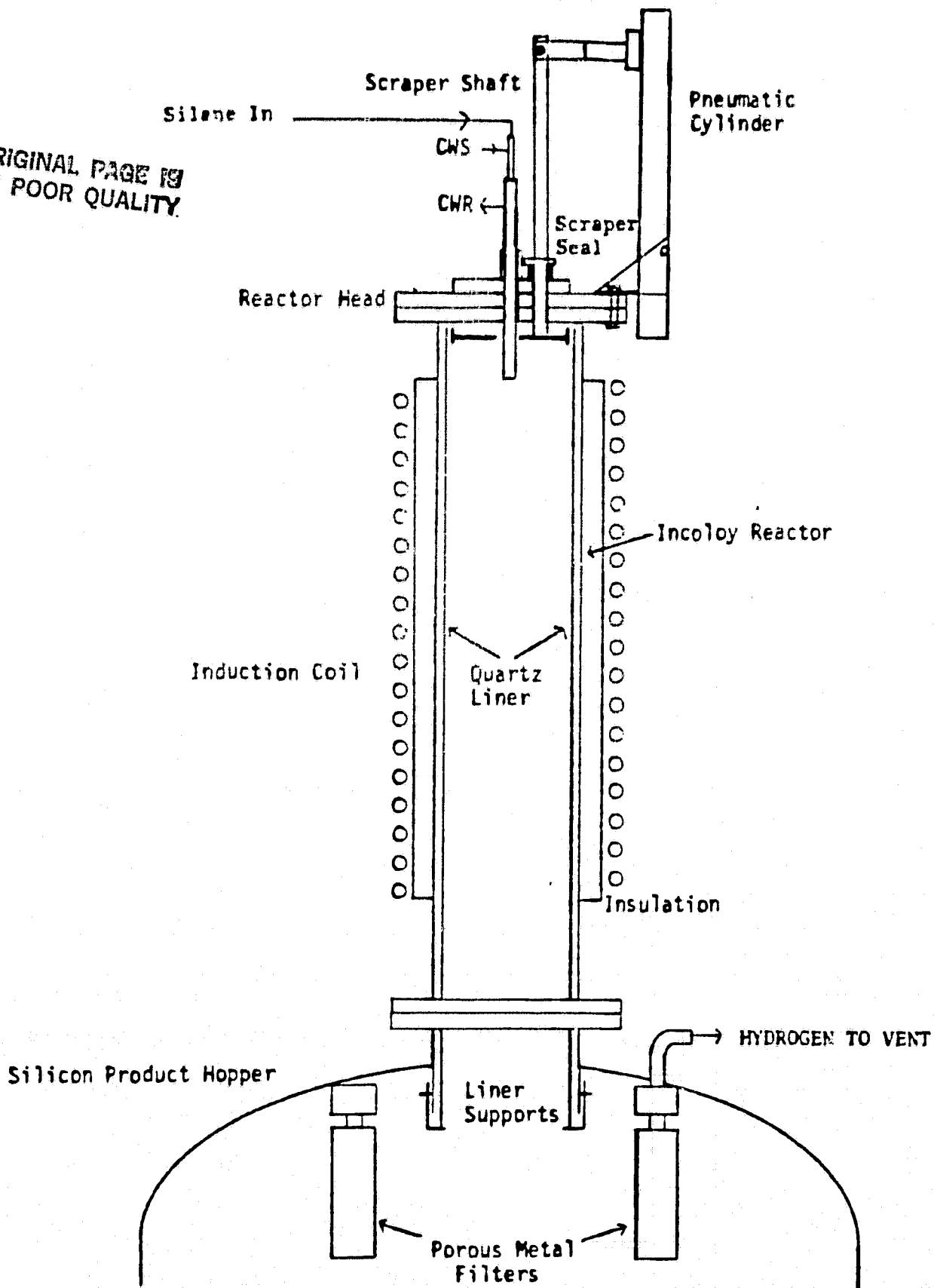


Figure 1

ORIGINAL PAGE 18  
OF POOR QUALITY

### 1.6.1.1 FREE SPACE REACTOR

ORIGINAL PAGE IS  
OF POOR QUALITY



FREE SPACE REACTOR

Figure 2



# FLUID BED REACTOR PDU

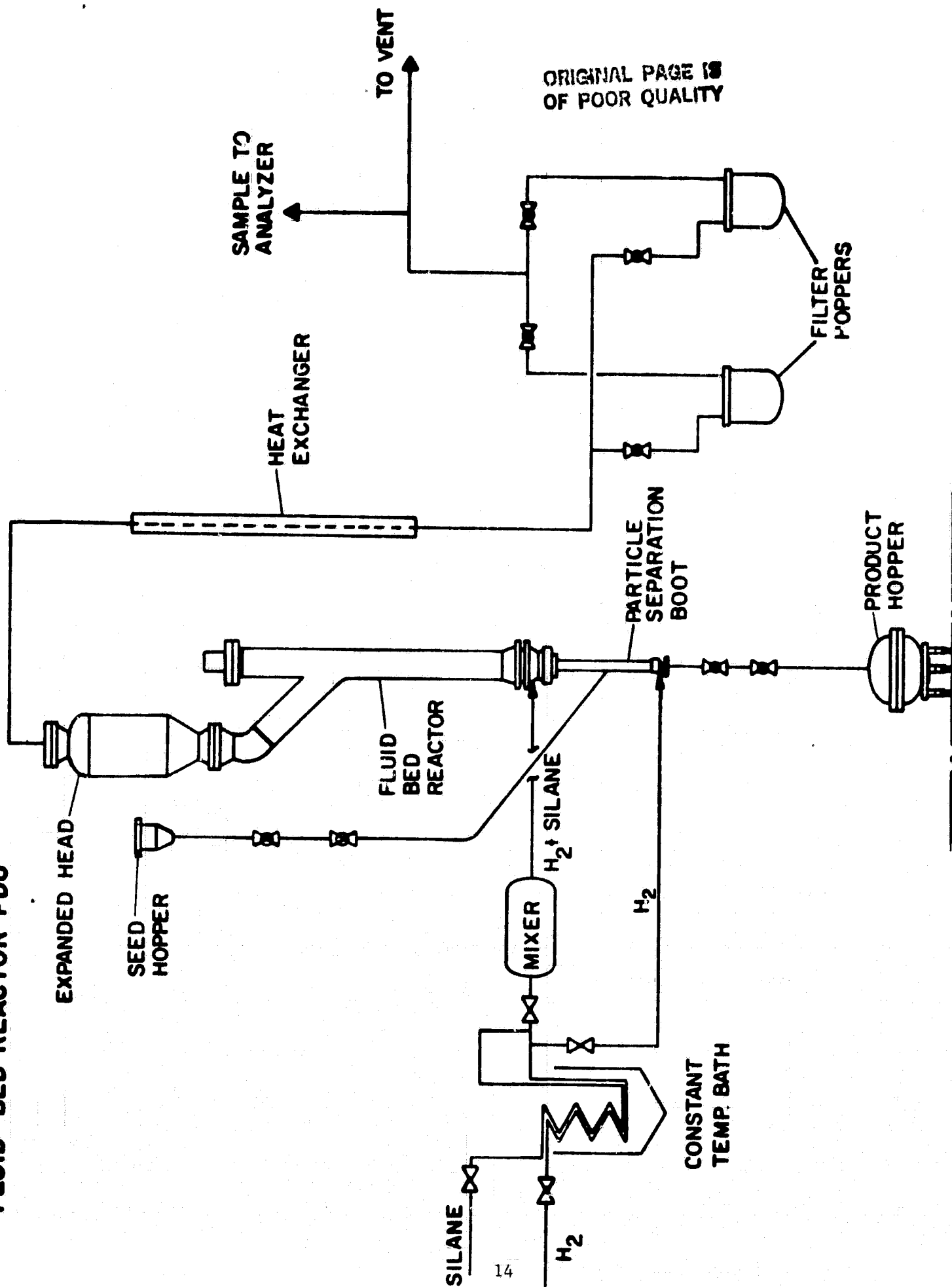


Figure 3

## DISCUSSION

QUESTION: Would you describe the fluidized bed reactor program at Union Carbide?

LORENZ: Dr. Iya, who is in charge of that project, is here, and I'd like to have him comment on the question.

IYA: We have been operating a 6-in. fluidized bed and have a program goal of determining the operating conditions of bed height, temperature, gas velocity, and silane concentration to get the engineering data for design purposes. We have gone up to 20% silane in hydrogen as the feed. The seed particles at the start are typically 90 microns and the product size is of the order of 300 to 320 microns. The longest continuous run has been about 15 hours and a total run time of 40 to 50 hours was accumulated.

LORENZ: We will have quarterly reports available on this program soon.. I'll be glad to talk with you later if you have further specific questions.

# SILICON PURITY: IMPACT ON CRYSTAL GROWTH AND SILICON PROPERTIES FOR PHOTOVOLTAIC APPLICATIONS

R. H. Hopkins, J. R. Davis and A. Rohatgi

Westinghouse R&D Center  
Pittsburgh, PA 15235

## 1. ABSTRACT

Many differing cell designs, fabrication technologies, and crystallization methods are used to produce today's silicon solar cells. Each approach varies in its sensitivity to the purity of the silicon feedstock, making the specification of a universal "solar grade" of silicon elusive. In this article we review how silicon sheet or wafer preparation technology and thermal history influence the relationships between device performance and feedstock purity. We conclude that a range of silicon purity requirements exists for cost-effective manufacturing depending on the overall process sequence employed.

## 2. INTRODUCTION

The impact of impurities on photovoltaic devices has been the subject of intense investigation (e.g. references 1-3) in an attempt to identify a material, "solar grade" silicon, which though lower in cost and less pure than semiconductor silicon is never-the-less suitable for the manufacture of cost-effective terrestrial solar cells. Our studies,<sup>1-4</sup> indicate that cell performance depends on the impurity species and concentrations, method of crystallization, the nature and distribution of defects in the wafer or sheet from which the cell is made, and on the cell design and fabrication process.

In the discussion to follow we fix the cell design and fabrication technique to facilitate a comparison of the impurity behavior as a function of the silicon crystal growth and post growth process history. For our base-line device, a conventional n+p diffused solar cell made on Czochralski (CZ) wafers, a 14% AM1 conversion efficiency is typical in the absence of contaminating impurities.<sup>2</sup> The impact of various metallic impurities and their concentrations in the wafer is illustrated in Figure 1. Minority carrier recombination at deep levels caused by solid solution impurities in the silicon lattice is the dominant performance degradation mechanism.<sup>1</sup>

The concentration, distribution and physical form (solute atom or precipitate) of impurities in a wafer depend on how the silicon ingot was solidified (CZ, casting, ribbon growth, etc.), and on its subsequent thermal history. These two factors strongly impact device performance and are the subject of this paper.

### 3. IMPURITY REDISTRIBUTION DURING SILICON CRYSTALLIZATION

The principal impurity-related phenomena involved during crystal growth are longitudinal segregation along an ingot (macrosegregation) and the formation of second phase particles due to constitutional supercooling (microsegregation).<sup>4-6</sup> The degree of macrosegregation controls the concentration of recombination centers at each location within an ingot, while microsegregation causes the formation of electrically-conductive inclusions which can effectively short circuit the devices.

#### Macrosegregation

A crystal in equilibrium with an impurity-bearing liquid contains an impurity concentration which differs from that liquid by a factor  $k$ , termed the equilibrium segregation coefficient. For most impurities in silicon these factors are much less than unity and may be determined from phase diagram data, if available. In a practical crystal growth situation where liquid mixing occurs, it is more convenient to describe microsegregation in terms of an effective segregation coefficient<sup>5,6</sup>  $k_{\text{(eff)}}$  which is a function of the crystal growth velocity  $R$ , the liquid diffusion coefficient  $D$ , and a diffusion boundary layer  $\delta$  which separates the solid liquid interface from the well-mixed liquid, Figure 2. The relation is

$$k_{\text{(eff)}} = \frac{k}{k + (1-k) \exp\left(-\frac{R\delta}{D}\right)}$$

In the limit as  $R$  or  $\delta$  become zero  $k_{\text{(eff)}}$  approaches  $k$  and segregation along the ingot is maximized as illustrated by the solid curve in Figure 3. Small values of  $\delta$  are expected for stirred CZ growth so that we expect  $k_{\text{(eff)}}$  to approximate  $k$ . Indeed, where comparable equilibrium data exist<sup>7</sup> the values are in good agreement with our  $k_{\text{(eff)}}$  data from CZ crystals, Table 1.<sup>1,2</sup> Clearly, one benefit of CZ growth is that only a minute fraction of the impurities present in the feedstock is incorporated in a crystal. Recombination centers are thus minimized and cell efficiency improves.

In the opposite extreme when  $R$  or  $\delta$  become large,  $k_{\text{(eff)}}$  approaches unity and the concentration of impurities in the solid becomes identical to that in the liquid, as suggested by the dotted curve in Figure 3. This behavior might be expected, for example, with edge-defined ribbon growth (EFG) where fluid flow through the shaping die connecting the melt to the crucible reduces solute redistribution, in effect making  $\delta$  large. This qualitative picture is consistent with available theoretical and experimental results.<sup>8-10</sup> While longitudinal segregation is minimal, considerable lateral segregation from edge-to-edge in EFG ribbons is possible depending on die geometry and growth speed.<sup>10</sup> For unfavorable die designs recombination behavior might vary across the ribbon width. In either case because there is little impurity segregation to the liquid relatively pure silicon feedstock is required to minimize contamination and maximize cell efficiency.

TABLE 1

EFFECTIVE SEGREGATION COEFFICIENTS FOR IMPURITIES IN SILICON

Element	k <sub>(eff)</sub>	Element	k <sub>(eff)</sub>
Ag	1.7x10 <sup>-5</sup>	Mo	4.5x10 <sup>-8</sup>
Al	3x10 <sup>-2</sup>	Nb	<4.4x10 <sup>-7</sup>
Au	2.5x10 <sup>-5</sup>	Ni	1.3x10 <sup>-4</sup>
B	8x10 <sup>-1</sup>	P	3.5x10 <sup>-1</sup>
C	5x10 <sup>-2</sup>	Pd	5x10 <sup>-5</sup>
Co	2x10 <sup>-5</sup>	Sn	3.2x10 <sup>-2</sup>
Cr	1.1x10 <sup>-5</sup>	Ta	2.1x10 <sup>-8</sup>
Cu	8.0x10 <sup>-4</sup>	Ti	2.0x10 <sup>-6</sup>
Fe	6.4x10 <sup>-4</sup>	V	4x10 <sup>-6</sup>
Gd	<4.0x10 <sup>-6</sup>	W	1.7x10 <sup>-8</sup>
Mg	3.2x10 <sup>-6</sup>	Zn	<1.0x10 <sup>-5</sup>
Mn	1.3x10 <sup>-5</sup>	Zr	<1.7x10 <sup>-8</sup>

Between the cases of maximum segregation,  $k_{\text{eff}} = k$ , and no segregation,  $k_{\text{eff}} = 1$ , lies a regime in which some segregation occurs due to partial mixing of the melt, e.g due to thermally driven convective flows. Casting processes used to produce single<sup>11</sup> or polycrystalline<sup>12</sup> ingots may fall in this category. Figure 4, for example, illustrates that the carbon and oxygen concentration both vary systematically along the axis of directionally-frozen SILSO ingots.<sup>12</sup> (Because the segregation coefficient of oxygen is greater than unity in silicon, the oxygen concentration diminishes along the ingot length). Although directional freezing with a heat sink on the ingot bottom as in the Bridgman-Stockbarger or casting methods should minimize convection there is apparently sufficient lateral heat flow to stimulate some mixing.

#### Microsegregation

In addition to the direct effect on the electrical properties of silicon, impurities also limit the conditions under which ingots free of conductive second phase inclusions can be grown. This is because excessive impurity build-up in the solute-rich boundary layer during freezing, Figure 2, causes the breakdown of the planar freezing front to a cellular morphology by process called constitutional supercooling.<sup>4-6</sup> During this transition in silicon portions of the crystal-liquid interface become bounded by {111} facets, Figure 5, whose distribution and geometry vary with the crystal growth direction. The impurity-rich liquid trapped at the cell boundaries later freezes to form inclusions in the crystal.

The onset of cellular breakdown depends on the liquid impurity concentration  $C_L$ , the growth velocity, and the thermal gradients in the solid and liquid.<sup>4,5</sup> For impurities with small values of  $k$  the critical impurity concentration  $C_L^*$  for breakdown during CZ pulling can be found from:<sup>4</sup>

$$C_L^* = -\frac{D}{m} \left( \frac{K_S G_S}{K_L R} - \frac{L}{K_L} \right) \exp \left( -\frac{R\delta}{D} \right)$$

(Here  $m$  is the liquidus slope of the binary phase system,  $K_S$  and  $K_L$  the solid and liquid thermal conductivities,  $L$  the latent heat of fusion per unit volume and  $G_S$  the thermal gradient in the crystal). For commonly used pull rates the model predicts fairly well the concentration at which single crystal growth actually degenerates for a variety of the metal impurities we studied;<sup>1,2</sup> Figure 6. Note that the critical concentration for cellular breakdown is independent of the metallic species and typically is about  $1$  to  $4 \times 10^{20} \text{ cm}^{-3}$  (2000 to 8000 ppm). As the growth rate or crystal diameter increase the value of  $C_L^*$  diminishes.

The microstructure formed under breakdown conditions consists of arrays of metal-rich second phase particles distributed in the silicon crystal matrix, e.g. Figures 7 and 8. Analysis of representative inclusions indicates that they are the most silicon rich phase of the particular binary system involved.<sup>2</sup> The inclusions are electrically very conductive and densely distributed throughout a crystal. As a consequence it is almost impossible to make a non-short-circuited solar cell from such material.

The distribution of inclusions is strongly dependent on crystal orientation as noted above. In Figure 7, a cross section from a  $\langle 110 \rangle$  oriented grain, the second phases align parallel to  $\{111\}$  twin traces as would be expected for impurities trapped at the base of the troughs formed by intersection of  $\{111\}$  facets, Figure 9. Here the impurity content of the cell walls reached the eutectic concentration as indicated by the intimate mixture of Si and Mo silicide. In contrast the microstructure of the  $\langle 111 \rangle$  oriented crystal, Figure 8, is considerably more complicated, comprising tubular Ti silicide particles oriented in a hexagonal array. Similar structures in Ge crystals form when liquid is trapped between macrosteps formed at the intersection of the  $\langle 111 \rangle$  growth plane and the  $\{111\}$  planes at  $70.5^\circ$  and  $109.3^\circ$  to it.<sup>13,14</sup> In each case the inclusions evolve by the solidification of solute-rich liquid trapped at the grooves on the solid-liquid interface formed by intersecting  $\{111\}$  planes.

As illustrated in Figure 7 the liquid trapped at the cell boundaries can be sufficiently enriched in metal to reach the eutectic composition particularly in binary systems where the eutectic temperature and composition lie close to that of pure silicon, Table 2. Clearly system phase relations as well as crystal orientation dictate the morphology of the included second phases.

While most of our data are for CZ crystals we would expect analogous microsegregation patterns in ribbon or cast materials under conditions where high impurity concentrations, low thermal gradients or high crystallization rates prevail. One possible example of this is the "grit" structure formed in cast ingots.<sup>3,12</sup> This fine-grained material encountered at the junction of columnar grains growing in the heat flow direction contains excessive amounts of carbon as well as various transition metals.<sup>12</sup> These impurity-enriched regions may well represent localized areas of cellular breakdown. Their impact on solar cell performance is severe.<sup>12</sup> Devices made on "grit"-containing silicon no longer exhibit diode characteristics and the I-V curve is nearly linear, Figure 10. Clearly, control of the impurity concentration of the silicon feedstock as well as the casting conditions are important in minimizing this structure.

TABLE 2

MICROSEGREGATION IN SILICON-METAL BINARY SYSTEMS  
UNDERGOING CELLULAR CZ GROWTH

Alloying Element	Observed Structure	Eutectic (a/o) Composition	Eutectic Temperature (°C)
V	E	97	1375
W	E	99	1400
Mo	E	98	1410
Cu	P	30	802
Ti	P	85	1330
Zr	P	90	1353
Fe	P	74	1208
Cr	P	85	1320

E - eutectic intergrowth

P - discrete second-phase particles in silicon  
matrix

## 4. IMPURITY REDISTRIBUTION IN THE SOLID STATE

It is important to realize the distribution of impurities formed in a crystal, ribbon or ingot during solidification represents equilibrium with the silicon lattice only at the growth temperature. At ordinary temperatures solubility is much smaller and the impurities can remain in the lattice only in a quenched metastable state or be precipitated as a second phase. Thus the concentration of electrically-active impurities—those which form deep levels and degrade carrier lifetime—is a function of post growth thermal history including the cell fabrication process itself.

For example, Figure 11 illustrates that only a fraction of the Cr, V, and Ti incorporated in a CZ silicon crystal during freezing remains electrically active at room temperature.<sup>1,2</sup> Note in particular that species like Cr which diffuse rapidly in silicon, viz. Table 3, thus facilitating precipitation, show relatively small electrically-active fractions.

In our experiments a thermal gradient of  $\sim 100^\circ\text{C}/\text{cm}$  combined with the 7cm/hr growth rate produces a nominal  $700^\circ\text{C}/\text{hr}$  crystal cooling rate. Under these conditions the data of Figure 11 suggest that about 77% of the Cr, 72% of the V and 60% of the Ti originally incorporated in a crystal remains electrically active, the rest having precipitated as a second phase. Mo which diffuses very slowly in silicon, Table 3, remains completely active. X-ray topographs of Cu-doped crystals taken subsequent to growth vividly illustrate the precipitation behavior, Figure 12. Cu is among the most rapidly diffusing species in silicon, Table 3, and no electrically-active deep levels are found in our crystals.

Since each crystal growth process involves a different time-temperature history we expect the concentration of electrically active impurities to vary with the process. For example castings produced over many hours of cooling as by the heat exchanger method<sup>11</sup> might show very low concentrations

of electrically-active impurities while rapidly frozen ribbons<sup>8</sup> might exhibit higher concentrations of deep levels if the same feedstock material were employed.

TABLE 3  
DIFFUSION CONSTANTS OF SOME IMPURITIES IN SILICON  
AT 900°C<sup>2,15,16</sup>

Impurity	Diffusion Constant (cm <sup>2</sup> /sec)
Copper	10 <sup>-6</sup>
Iron	6x10 <sup>-6</sup>
Chromium	10 <sup>-7</sup>
Vanadium	8x10 <sup>-10</sup>
Titanium	2x10 <sup>-10</sup>
Molybdenum	< 10 <sup>-14</sup>
Tungsten	< 10 <sup>-14</sup>

Besides the growth process, the thermal history of silicon can be altered by processes such as annealing, gettering, or junction diffusion employed in device fabrication. For example, the electrically-active Cr concentration in a Czochralski wafer monotonically decreases as the annealing temperature is raised until at 500°C no active Cr can be detected by deep level spectroscopy,<sup>2</sup> Figure 13. Clearly processes which may be used to activate desirable dopants can also affect the state of harmful impurities as well.

Figure 14 illustrates a third interaction between impurities and thermal processing, the diffusion of an impurity to a wafer surface in the presence of a chemically-active species  $\text{POCl}_3$ .<sup>2,16</sup> The concentration profiles measured by deep level spectroscopy (DLTS) were fit to a diffusion model<sup>17</sup> to derive the indicated diffusion constants. An Arrhenius plot of D versus 1/T yields an activation energy for Ti diffusion of 1.66eV in good agreement with the literature.<sup>18</sup> Data for V and Cr follow a similar pattern while little or no Mo diffusion could be detected consistent with the values of D in Table 3. Apparently the surface of the wafer acts as a sink for impurities at which they are electrically-deactivated by complexing with phosphorous or by precipitation.<sup>19</sup>

Finally because impurities can be redistributed in the solid state we expect the underlying silicon microstructure to strongly influence the final impurity concentration and distribution. This is indeed the case. We found that the electrically-active impurity concentration in polycrystalline silicon ingots varies both with the wafer defect structure and with the impurity species.

Deep level spectroscopy was used to measure the impurity concentration in the vicinity of grain boundaries, twins and defect-free regions in ingots bearing Mo, Ti and Cr, respectively. We found the Mo concentration essentially invariant within a wafer. In striking contrast the Cr concentration of grain boundary-free regions was often an order of magnitude larger than the Cr content the vicinity of a grain boundary, Figure 15. No



**ORIGINAL PAGE IS  
OF POOR QUALITY**

depression in electrical activity was noted at twin boundaries. For the Ti-doped ingots the electrical activity near the grain boundaries was about half that of defect free regions in keeping with the lower diffusion coefficient of Ti as compared to Cr.

We conclude that on cooling from the solidification temperature impurities precipitate preferentially at grain boundaries and become electrically inactive. The process is most noticeable for rapidly diffusing species like Cr, and relatively ineffective for slowly diffusing species like Mo.

It is clear that the choice of post growth process sequence to optimize solar cell efficiency depends on the impurity concentration and microstructure of the silicon wafer. While precipitation can be used to enhance device performance, the approach is only viable if the conductive particles are excluded from the junction region of the devices where they induce junction recombination, shunting or even shorting of the cell, Figure 10. Moreover, while grain boundaries are impurity sinks, they also can degrade device performance by acting as recombination sites.

## 5. CONCLUSIONS

The acceptable impurity concentration in the silicon feedstock depends on the crystal growth process and post growth thermal history thus no generally acceptable specification of "solar grade" silicon is possible. Impurities produce two dominant device-related effects: (1) carrier-lifetime reduction by recombination and yield reduction caused by conductive inclusions or precipitates in the silicon base material.

The implication of these effects on "solar grade" silicon requirements depends on the manufacturing strategy chosen. If the approach involves producing high efficiency single-crystal or very large grain polycrystal devices then a high purity feedstock is required for lifetime reasons and the precipitate effect vanishes. If production is aimed at efficiencies of 10% to 12% using smaller grain material then the cell performance will be limited by grain boundary recombination. In this case higher concentrations of recombinations centers can be present without added performance loss. However, precipitates decorating grain boundaries which penetrate the junction are especially prone to produce shorting and must be avoided.

The data<sup>1-4</sup> now available will aid a silicon refiner or cell manufacturer to estimate the cell performance from the impurity content of the silicon feedstock within the context of a particular fabrication technology. This permits assigning a value to further purification of the silicon or other performance improving processes, thus optimizing the material cost/device performance tradeoffs.

## ACKNOWLEDGEMENT

In Memoriam: J. R. "Ranny" Davis died May 23, 1982. Ranny provided both spirit and intellectual spark for this effort. We dedicate this

paper to him.

We gratefully acknowledge support for portions of this study by the JPL Flat Plate Solar Array Project.

#### REFERENCES

1. J. R. Davis, et al, IEEE Transactions of Electron Devices, ED-27, 677 (1980).
2. R. H. Hopkins, et al., Final Report "Effect of Impurities and Processing on Silicon Solar Cells", DOE/JPL-954331-81/14, February (1982).
3. J. Dietl, et al "Solar Silicon" in Crystals, Growth, Properties and Applications 5, 43 (1981).
4. R. H. Hopkins, et al. J. Crystal Growth, 42, 493 (1977).
5. B. Chalmers, Principles of Solidification, John Wiley, NY (1964).
6. M. C. Flemings, Solidification Processing, McGraw-Hill, NY (1974).
7. F. A. Trumbore, Bell System Technical Journal 39, 205 (1960).
8. J. C. Swartz, et al., J. Electr. Materials 4, 255 (1975).
9. S. Matsuma and T. Fukudor, J. Crystal Growth 34, 350 (1976).
10. J. P. Kalejs, J. Crystal Growth 44, 329 (1978).
11. F. Schmid, Proceedings of 12th IEEE Photovoltaic Specialists Conf. IEEE, NY 146 (1976).
12. K. Roy et al., Proceedings of 14th IEEE Photovoltaic Specialists Conf. IEEE, NY, 897 (1980).
13. W. Bardsley et al. J. Crystal Growth 49, 612 (1980).
14. W. Bardsley, et al. Solid State Electronics 5, 395 (1962).
15. H. F. Wolf, Silicon Semiconductor Data, Pergamon Press (1969).
16. A. Rohatgi, unpublished results, Westinghouse R&D Center, (1982).
17. J. Crank, Mathematics of Diffusion, Oxford University Press, London, 45 (1964).
18. V. Boldgrev, et al. Sov. Phys. Semicond. 11, 709 (1977).
19. D. Lecrosnier, et al. ECS Extended Abstracts, Boston #160, 426 (1979).

ORIGINAL PAGE IS  
OF POOR QUALITY

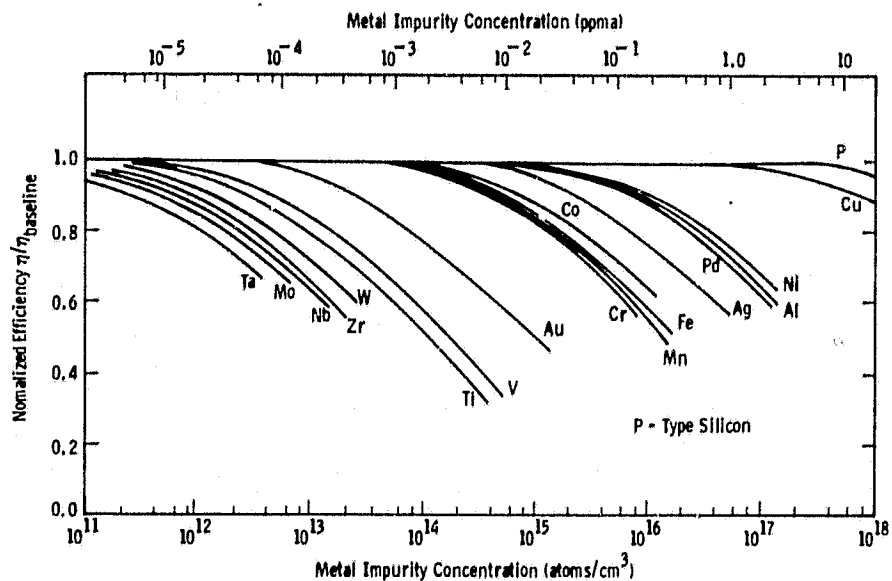


Figure 1. Impurity-Performance Curves for CZ Solar Cells

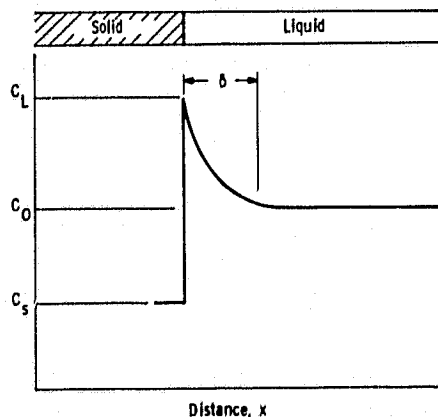


Figure 2. Impurity Redistribution During Solidification from a Stirred Liquid

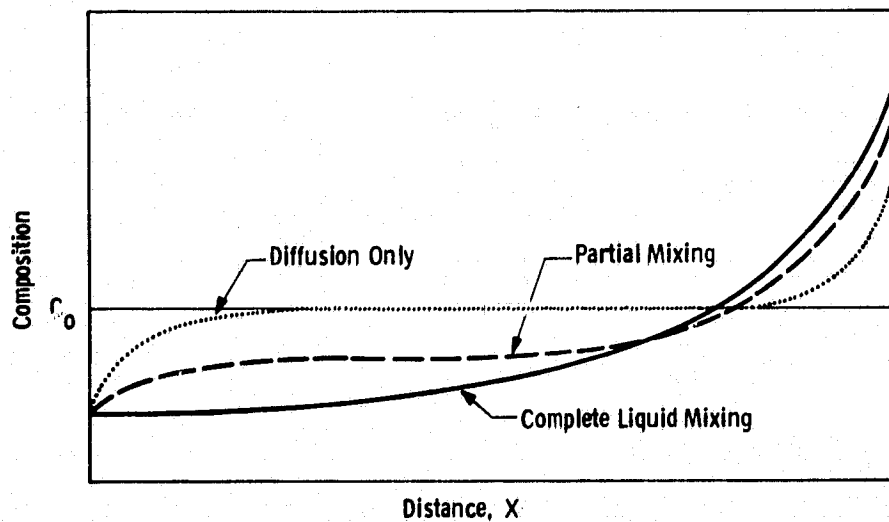


Figure 3. Crystal Impurity Profiles for Different Liquid Mixing Conditions

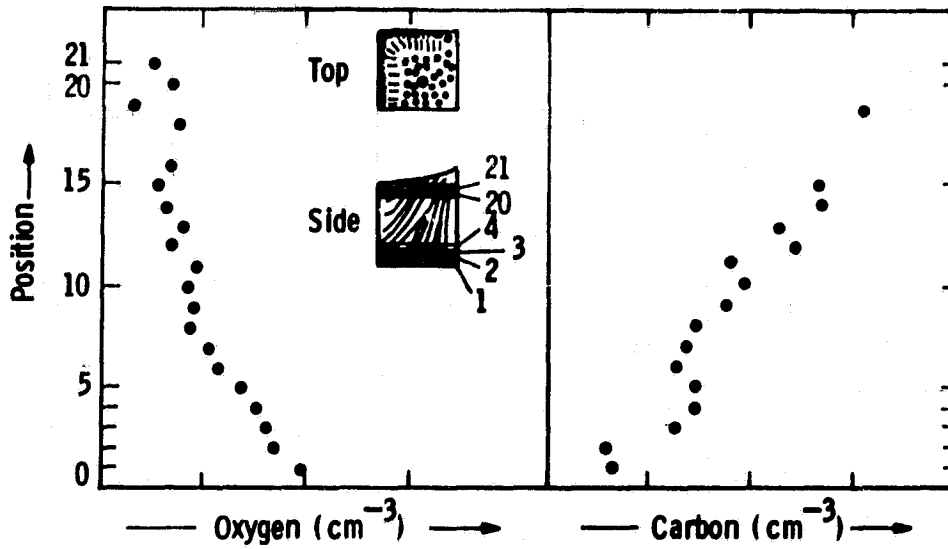


Figure 4. Carbon and Oxygen Profiles in SILSO Ingots (After Roy, et al.)

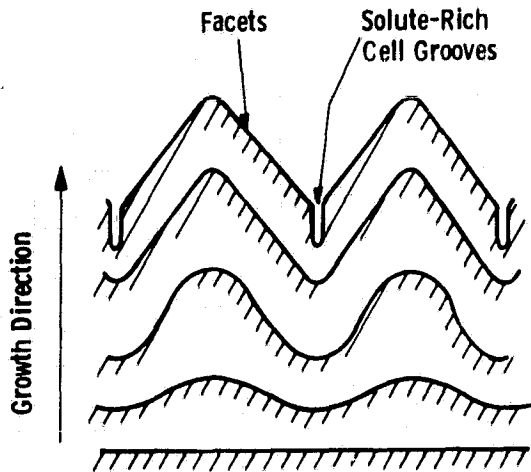


Figure 5. Breakdown of Planar Freezing Front to Faceted Cells

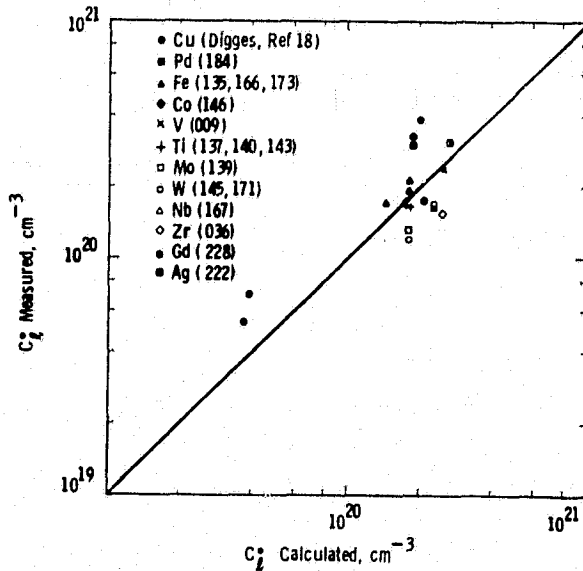


Figure 6. Critical Impurity Concentrations for Breakdown of CZ Growth

ORIGINAL PAGE IS  
OF POOR QUALITY

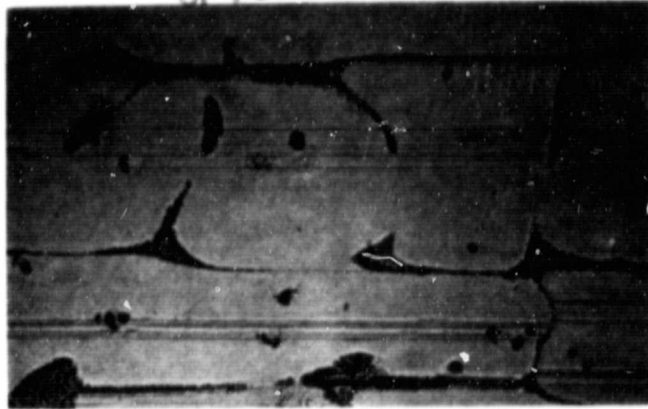


Figure 7. Mo Silicide-Silicon Eutectic in a  $\langle 110 \rangle$  Oriented Silicon Crystal (100X)

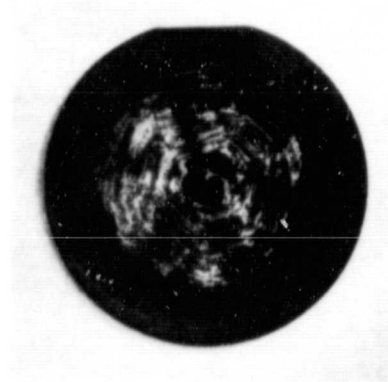


Figure 8. Hexagonal Array of Ti Silicide Inclusions in a  $\langle 111 \rangle$  Silicon Wafer (Wafer Diameter 3 cm)

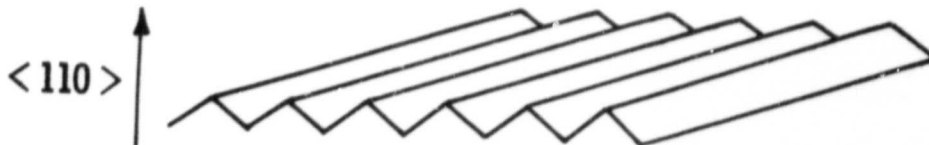


Figure 9. Illustration of Facetted Cell Morphology at Solid-Liquid Interface of a  $\langle 110 \rangle$  Silicon Crystal

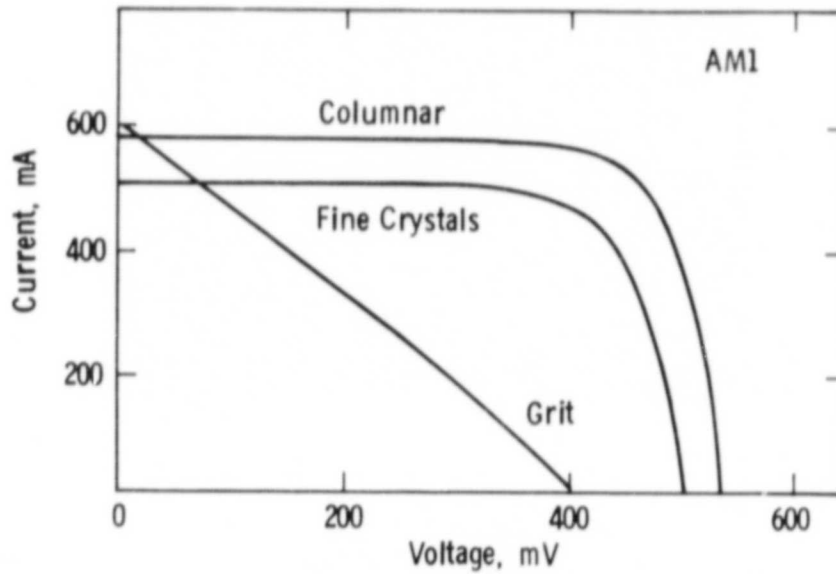


Figure 10. Solar Cell I-V Curves for SILSO Material (After Roy, et al.)

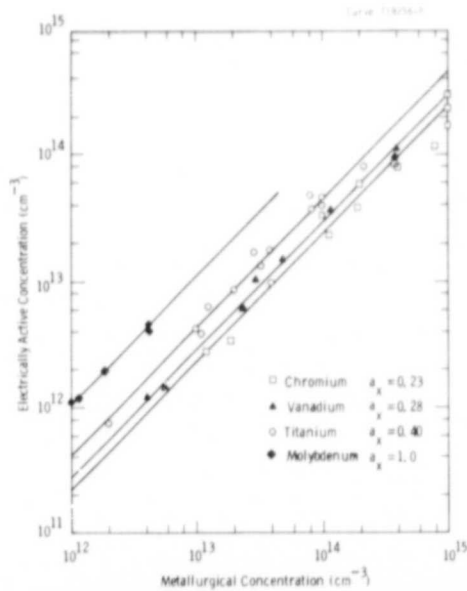


Figure 11. Electrically-active Impurity Fraction (by DLTS) in CZ Wafers

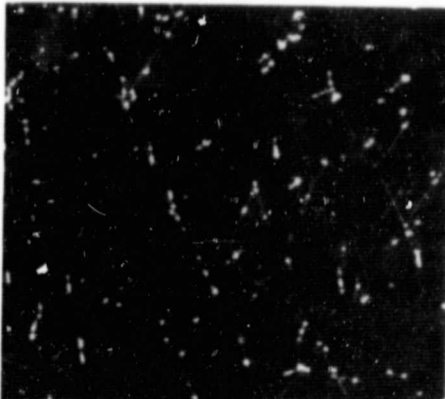


Figure 12. Cu Silicide Precipitates in CZ Silicon. (220) X-ray Topography; 20X.

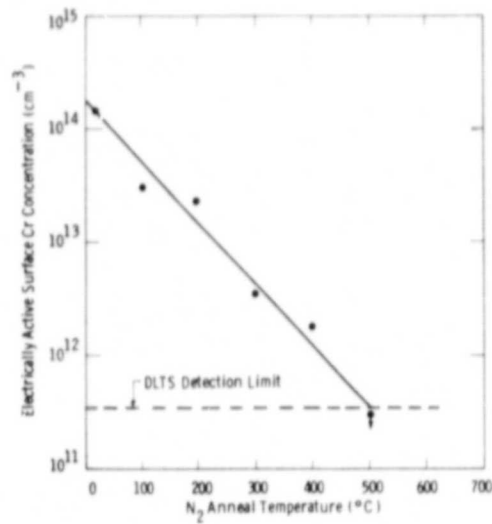


Figure 13. Electrically-active Cr Concentration (by DLTS) After Heat Treatment

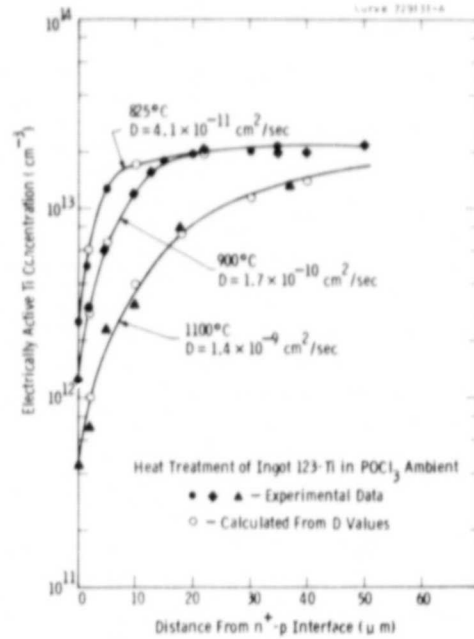


Figure 14. Profiles of Electrically-active Ti Following 50 min  $POCl_3$  Gettering

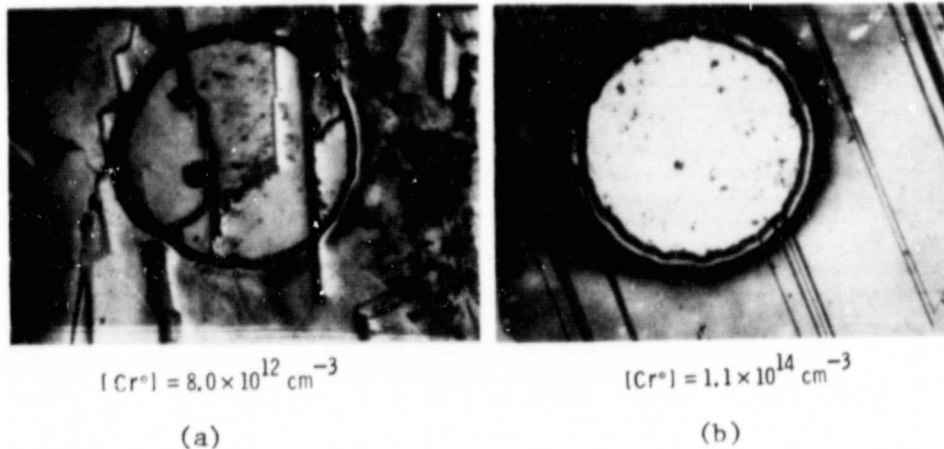


Figure 15. Electrically-active Cr At Grain Boundary (a) and (b) Twinned Area

## DISCUSSION

MILSTEIN: Have you, by any chance, done any EBIC work on those materials?

HOPKINS: We've not done the EBIC work. We have done some laser-induced recombination studies but not in great detail. This was a segment of the work which came very near the end of the program, which we finished early in February. I'll have to admit there are a lot of things we would really like to do if we had the opportunity to do them.

MILSTEIN: OK, one comment if I might; I think you've got something there that's extremely interesting in the sense that in the past people have observed enhancement as well as reduction in current and grain boundaries. It appears that you have the answer.

REIF: How much of a problem is oxygen for solar cell performance?

HOPKINS: Well, that's not an easy question to answer, but let me try to answer it in the following way. Most of the work we did was with conventional Cz material, into which we purposely infused one or another of the transition metal impurities. All of those ingots contained the 10 to 40 ppm of oxygen typically present in a Cz crystal. Hence, we really can't distinguish what the effect of oxygen would be. We did a little bit of work using a few float zone ingots, and there seemed to be an indication of interactions of some of these impurities, for example aluminum and titanium, with the oxygen. This was deduced by comparing the cells made from the float zone materials with the solar cells made by the same process using Cz, but the data were so limited that we've really been very hesitant to draw any kind of conclusions from them. I think it would be something very interesting to look at, particularly in the context of high efficiency devices. We've been doing some work using passivation techniques for the surfaces of silicon solar cells; and we're making some devices in the 16% to 17% range. I think that a very interesting research project would be to study the effects of impurities, especially of carbon and oxygen, on really high efficiency solar cells, since the extra efficiency can really buy something by getting lower cost devices. That's something I think that would be very very nice to do.

JEWETT: In the EFG material program work was done using crucibles and dies made entirely from carbon. There appeared to be a substantial problem, I believe, when carbon crucibles were used. The use of quartz in the crucible was a source of oxygen. So materials of construction can be related in some way to impurities in silicon.

HOPKINS: I agree.



## SESSION II: Thermodynamics, Kinetics, and Mechanisms

BAILEY (Chairman): This area of thermodynamics, kinetics, and mechanisms is very controversial. Many of the ideas that are presented will be useful to you. Please feel free to ask questions and even raise controversial points.

# CHLOROSILANE THERMODYNAMIC EQUILIBRIA CALCULATIONS WITH APPLICATIONS TO HIGH PURITY SILICON PREPARATION

by  
Henry F. Erk  
Research Engineer  
Monsanto Co.

P. O. Box 8, St. Peters, MO 63376

## Introduction

Many industrial processes for the production of high purity silicon are based upon chlorosilane chemistry; e.g., the formation of trichlorosilane in a fluid bed, the subsequent pyrolysis of the trichlorosilane in a Siemens decomposer, and the pyrolysis of silicon tetrachloride in an epitaxial reactor. Other processes proposed for the manufacture of low-cost, pure silicon are also based upon chlorosilane chemistry; e.g., fluid bed pyrolysis of trichlorosilane and production of silane by chlorosilane disproportionation. An excellent benchmark for evaluating the performance of these processes and others is the approach of the reaction system to thermodynamic equilibrium. In several cases, particularly in trichlorosilane reduction to silicon, thermodynamic equilibrium is the point of optimal operation. The ability to calculate equilibrium compositions in the silicon-chlorine-hydrogen system is therefore useful to the high-purity silicon industry.

Many workers have performed Si-Cl-H thermodynamic equilibria calculations. One of the earliest efforts was made by Lever (1) who solved the ideal gas equilibrium equations for a ten component system. About the same time Niederkorn and Wohl (2) and Harper and Lewis (3) also performed detailed equilibrium calculations. Then Hunt and Sirtl, (4) and (5), used minimization of free energies and developed a thermodynamic data base which has been widely used throughout the years. They illustrated the importance of accurate thermodynamic data. More recently Kokovin, Kuznetsov, et al., (6) and (7), presented calculations based upon the equation solving approach. Langlais, Hottier and Cadoret (8) presented calculations using an updated version of Hunt and Sirtl's data and the concept of homogenous/heterogenous equilibrium.

The present work deals with the development of user-friendly computer programs which rapidly perform equilibria calculations for the Si-Cl-H system. The programs are used with a variety of thermodynamic data to calculate equilibrium composition, silicon to chlorine ratios (Si/Cl), equilibrium yields ( $\eta$ ), at different temperatures, pressures and chlorine to hydrogen ratios (Cl/H). One objective of this work is to illustrate the importance of and the need for accurate thermodynamic data for the chlorosilanes, particularly  $\text{SiCl}_4$ ,  $\text{SiHCl}_3$ ,  $\text{SiCl}_2$ , and  $\text{SiH}_2\text{Cl}_2$ . By introducing small errors in the standard heat of formation of trichlorosilane [similar to the treatment performed by Hunt and Sirtl (5)], large errors appear in the molar ratio of  $\text{SiHCl}_3$  to  $\text{SiCl}_4$ , as well as significant errors in Si/Cl (or yield), and molar ratio of  $\text{SiCl}_2$  to  $\text{SiCl}_4$ .

A second objective is to apply these calculations to three important processes: the production of trichlorosilane in a fluidized bed of silicon,

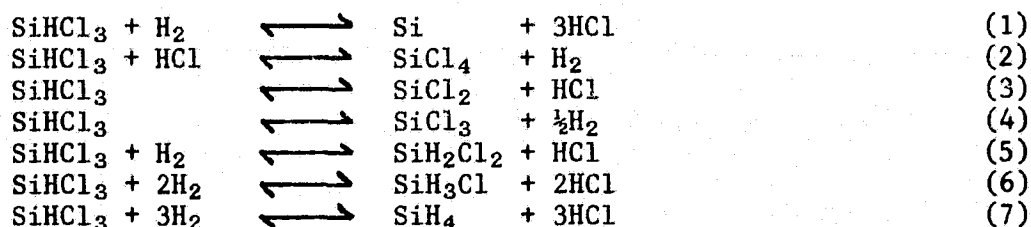
the production of polysilicon from trichlorosilane in a high pressure Siemens decomposer, and the production of silicon from trichlorosilane in a fluidized bed reactor. Comparisons of equilibrium calculations with patent literature data for each of these processes provides insight into the closeness of the individual process to chemical equilibrium. In the fluidized bed production of trichlorosilane, for example, the hydrogenation of silicon tetrachloride does not approach equilibrium for small bed residence and low temperatures (9); however, at high temperatures and longer residence times equilibrium is attained. The second process studied, the production of polysilicon in Siemens decomposers, never completely approaches equilibrium since the bulk gas temperature of the reactants is lower than the temperature of the polysilicon surface; although for temperatures above approximately 1000°C local chemical equilibrium on the hot silicon surface can be assumed (10). In contrast to the Siemens decomposer, the production of polysilicon in a fluidized bed of silicon could be limited by chemical equilibrium since the reactant gas is at the same high temperature as the silicon.

#### Thermodynamic Model and Its Solution

In the Si-Cl-H system the major chemical species (neglecting polymers of Si-Cl-H are:  $H_2$ ,  $HCl$ ,  $SiCl_4$ ,  $SiCl_2$ ,  $SiHCl_3$ ,  $SiH_2Cl_2$ , and  $Si$ , (5) and (11). For the sake of completeness silane is included. Although  $SiH_4$  is not a major specie at equilibrium, it is sometimes used as a feedstock, particularly for epitaxial growth of silicon. Several proposed low-cost routes to high purity silicon center around silane decomposition and its production by disproportionation of chlorosilanes. Three additional species -  $SiHCl_3$ ,  $SiCl_3$ , and inert gas - are also included in the model.

With the chemical species defined one has two approaches to performing equilibrium calculations: minimization of free energies and equation solving of a system of chemical equilibria expressions combined with mass balance constraints. Both approaches are reliable. The equation solving approach was selected in this work.

A set of seven independent chemical equations interrelating the ten active species can be formulated:



The stoichiometric-coefficient matrix rank is 7 indicating three degrees of freedom. Equations (1) through (7) describe a pathway, albeit not necessarily the actual chemical pathway, the system takes to equilibrate; since thermodynamics is path independent, any pathway can be used.

Ideal gas behavior is assumed; this assumption is valid at the high temperatures and moderate pressures where chlorosilane chemical equilibrium

exists. The ideal gas equilibrium expressions for the seven chemical reactions are illustrated in Table 1, equations (8a) to (8g), where P is the total system pressure;  $\theta$  is the total number of moles in the gas phase;  $K_i$  for  $i=1, 2, \dots, 7$ , is the equilibrium constant for the  $i$ th reaction; and  $n_{HCl}$ ,  $n_{H_2}$ ,  $n_{SiHCl_3}$ , etc., are the number of moles of HCl,  $H_2$ ,  $SiHCl_3$ , etc. These equilibrium expressions are coupled with the mass balance constraints, equations (9a) to (9k), shown in Table 1, where  $n_0^0$  is the moles of inert gas;  $n_{SiHCl_3}^0$ ,  $n_{H_2}^0$ ,  $n_{HCl}^0$ , etc., are the initial number of moles of  $SiHCl_3$ ,  $H_2$ , HCl, etc., fed the system; and  $\xi_i$  for  $i=1, 2, 3, \dots, 7$ , is the number of moles of  $SiHCl_3$  which is consumed in the  $i$ th reaction. The solution of equations (8a) through (9k), the general case equations, represents the chemical equilibrium in the Si-Cl-H system.

In the conventional Siemens decomposition process only  $SiHCl_3$  and  $H_2$  are fed to the reactor, consequently it is of interest to simplify the model equations based upon a feed of only these two species. Assume a basis of one mole of  $SiHCl_3$  fed, and define  $x_j$ , for  $j=1, 2, \dots, 7$ , to be the fractional number of moles of  $SiHCl_3$  consumed in each reaction. Define A as the number of moles of  $H_2$  fed to the system, then the equilibrium and mass balance equations become equations (10a) to (11d) shown in Table 1, where I is the total moles of inert gas fed to the system;  $x_0$  is the equilibrium number of moles of  $SiHCl_3$ ;  $x_{H_2}$  is the equilibrium number of moles of  $H_2$ ; and  $x_{HCl}$  is the equilibrium number of moles of HCl. These equations represent the simplified case equations for the Si-Cl-H system.

As a consequence of the Gibbs phase rule, the Si-Cl-H system has three degrees of freedom. If the three degrees: temperature (T), pressure (P), and molar ratio of chlorine of hydrogen (Cl/H) are fixed, the equilibrium mole fraction of each gas phase specie is completely determined. It is possible to define many hypothetical mixtures of chlorosilanes,  $H_2$ , and HCl which all have the same Cl/H. Consequently a transformation exists for converting any Si-Cl-H feed to a hypothetical mixture of 1 mole of  $SiHCl_3$ , A moles of  $H_2$ , I moles of inerts, and EXCESS moles of elemental silicon. The transformation is accomplished as follows:

1. Compute Cl/H of the feed, the total number of moles of chlorine (CLMOLE), inert gas (IMOLE), and silicon (SIMOLE).
2. Let
 

$A = (3 - Cl/H)/(2 Cl/H)$  (12a)  
 $SCALER = CLMOLE/3$  (12b)  
 $I = IMOLE/SCALER$  (12c)  
 $EXCESS = (SIMOLE/SCALER) - 1.$  (12d)

And the transformation from an equilibrated simplified case system to the actual system is accomplished by the inverse transformation:

$n_{SiHCl_3}$	$= (x_0)$	SCALER	(13a)
$n_{H_2}$	$= (x_{H_2})$	SCALER	(13b)
$n_{HCl}$	$= (x_{HCl})$	SCALER	(13c)
$n_{SiCl_4}$	$= (x_2)$	SCALER	(13d)
$n_{SiCl_2}$	$= (x_3)$	SCALER	(13e)
$n_{SiCl_3}$	$= (x_4)$	SCALER	(13f)
$n_{SiH_2Cl_2}$	$= (x_5)$	SCALER	(13g)
$n_{SiH_3Cl}$	$= (x_6)$	SCALER	(13h)
$n_{SiH_4}$	$= (x_7)$	SCALER	(13i)
$n_{Si}$	$= (x_1 + EXCESS)$	SCALER	(13j)

This transformation is useful in converting from the general case equations [(8a) through (9k)] to the simplified case equations [(10a) through (11d)].

Two different solution algorithms have been developed. One algorithm solves the general case, while the other solves the simplified case. Because there are three mathematical degrees of freedom (10 specie and 7 reactions) one can reduce the system of equations in either case to a system of three nonlinear equations in three unknowns. For the general case solution the three unknowns were chosen to be  $n\text{SiHCl}_3$ ,  $n\text{H}_2$ , and  $\theta$ . A set of properly scaled equations to be solved is shown in Table 1 [equations (14a)-(14c)], where substitution for  $\xi_1$  through  $\xi_7$ ; and  $n\text{HCl}$ ,  $n\text{SiCl}_4$ , etc., can all be made in terms of  $n\text{SiHCl}_3$ ,  $n\text{H}_2$ , and  $\theta$  alone. The solution algorithm is:

1. Guess a starting value for  $n\text{SiHCl}_3$ ,  $n\text{H}_2$ , and  $\theta$ .
2. Calculate  $n\text{HCl}$ ,  $n\text{SiCl}_4$ ,  $n\text{SiCl}_2$ ,  $n\text{SiCl}_3$ ,  $n\text{SiH}_2\text{Cl}_2$ ,  $n\text{SiH}_3\text{Cl}$ ,  $n\text{SiH}_4$  from equations (8a), (9f) through (9k).
3. Evaluate right hand side (RHS) of equations (14a) to (14c) and calculate the errors (1-RHS) for each equation.
4. Use a nonlinear equation solving routine; e.g., BSOLVE Algorithm, see (12), to correct estimates  $n\text{SiHCl}_3$ ,  $n\text{H}_2$  and  $\theta$  based upon the errors.
5. If the errors in equations (14a) to (14c) are sufficiently small ( $< 10^{-4}$ ) stop, otherwise go to step 2 for another iteration.

For the simplified case solution a Gauss-Sidel successive substitution scheme has been developed by Dr. Warren Groves at Monsanto (13). As in the general case, three nonlinear equations must be solved. The basis variables are chosen to be  $x_2$ ,  $x\text{H}_2$  and  $\theta$ . The solution algorithm is:

1. Initialize
 
$$\begin{aligned} x_7 &= 0 \\ x_2 &= 0.75 \\ x_{\text{H}_2} &= A + 0.5 \\ \theta &= 1.25 + A + I \end{aligned}$$
2. Calculate
 
$$x_0 = [(x_2/K_1)^3 x_{\text{H}_2}^2 P/K_2\theta]^{1/4} \quad (15a)$$

$$\text{Calculate: } x_{\text{HCl}} = x_2 x_{\text{H}_2} / K_2 x_0 \quad (15b)$$

$$\text{Calculate: } x_3 = K_3 x_0^2 \theta / P x_{\text{HCl}} \quad (15c)$$

$$\text{Calculate: } x_4 = K_4 x_0 (\theta / P x_{\text{HCl}})^{1/2} \quad (15d)$$

$$\text{Calculate: } x_5 = K_5 x_0 x_{\text{H}_2} / K_5 x_{\text{HCl}}^2 \quad (15e)$$

$$\text{Calculate: } x_6 = x_5 K_6 x_{\text{H}_2}^2 / x_{\text{HCl}} \quad (15b)$$

$$\text{Calculate: } x_7 = x_6 K_7 x_{\text{H}_2}^2 / K_6 x_{\text{HCl}} \quad (15c)$$
3. Calculate the ratio of  $x_7^1/x_7^2$  where  $x_7^1$  is the previous value of  $x_7$ . If  $\log(x_7^1/x_7) < 10^{-5}$ , Stop - otherwise continue. If  $[x_7^1/x_7] > 1$ , set INDEX = 0.
4. Calculate  $x_1 = (1 - x_0 - 2x_3 - x_4 - 2x_5 - 3x_6 - 4x_7 + x_{\text{HCl}})/4$  [a combination of equations (33) and (34)] (15d)
5. Correct the basis variables  $x_2$ ,  $x_{\text{H}_2}$ ,  $\theta$  by:
 
$$\text{INDEX} = \text{INDEX} + .3 \quad (15e)$$

$$\text{SUMMA} = \sum_{j=0}^7 x_j \text{ INDEX} \quad (15f)$$

$$x_2 = x_2^1 / \text{SUMMA} \quad (x_2^1 \text{ previous value of } x_2) \quad (15g)$$

$$x_{\text{H}_2} = (A + x_1 - x_2/4 + x_5 + 2x_6 + 3x_7) / \text{SUMMA} \quad (15h)$$

$$\theta = (1 + A + I + x_1 + x_3 + x_4/2) / \text{SUMMA} \quad (15i)$$

Branch to step 2.

9  
Y

Groves' algorithm is efficient and simple to implement, and has been programmed on a TI-59 hand-held calculator as well as on the computer.

Using the two solution algorithms, a set of user-friendly, Fortran IV computer programs have been written for Monsanto's Interactive Computer Facility (ICF). Average computation time ranges from .05 to .2 CPU seconds. A full screen input version of the program is used to perform calculations interactively on IBM 3270 terminals using the programs. Figure 1 is an example of a typical graph which can be generated, the Si-Cl-H triangular diagram. Thermodynamic data (for the constants  $K_1$  through  $K_7$ ) from the JANAF thermochemical tables (14) was used to produce this figure; however, a variety of other thermodynamic data from other sources can be used in the programs.

### Thermodynamic Property Bases

Very accurate thermodynamic property data is required in equilibrium calculations. Hunt and Sirtl (5) illustrated this by observing the effect of small errors in the standard enthalpy of formation of  $\text{SiHCl}_3$  upon the molar ratio of  $\text{SiCl}_4$  to  $\text{SiHCl}_3$ . Table 2 shows the results of some equilibrium calculations using the Hunt and Sirtl thermodynamic data and introducing small errors in the enthalpy of formation for  $\text{SiHCl}_3$ , in intervals of 2.5% around Hunt and Sirtl's value of 116.9 kcal/mole. The 5% error limit is larger than the reported accuracy of  $\Delta H_f^\circ \text{SiHCl}_3$  (14); however, errors in the data for other species such as  $\text{SiCl}_4$  and  $\text{SiCl}_2$  have been neglected. Also, for the sake of simplicity, errors in the entropy and heat capacity data have been neglected, although they too effect calculation accuracy.

The effect of errors in thermodynamic properties varies with conditions. Table 2 shows that calculated values, especially for molar ratio of  $\text{SiHCl}_3$  to  $\text{SiCl}_4$ , are extremely sensitive to  $\Delta H_f^\circ \text{SiHCl}_3$ , at low temperatures and low Cl/H, where the  $\text{SiHCl}_3$ - $\text{SiCl}_4$  equilibrium is dominant. At high temperatures and high Cl/H,  $\text{SiCl}_2$ - $\text{SiCl}_4$  equilibrium dominates, and so calculations are less sensitive to  $\Delta H_f^\circ \text{SiHCl}_3$ .

Errors in  $\text{SiHCl}_3$  properties propagate to effect other species composition as shown in the molar ratios of  $\text{SiCl}_2$  to  $\text{SiCl}_4$  in Table 2. Errors in Si/Cl are also evident. The errors may appear to be small, but they are magnified in the equilibrium yield  $\eta$ :

$$\eta = [(\text{Si/Cl}) \text{ feed} - (\text{Si/Cl}) \text{ equilibrium}] / (\text{Si/Cl}) \text{ feed}, \quad (16)$$

especially when  $\text{SiHCl}_3$  (Si/Cl = .333...) is used as a feed.

Besides the Hunt and Sirtl data, another set of thermodynamic properties is found in the JANAF thermochemical tables. The properties listed in JANAF tables are obtained from a compilation of various sources, including Hunt/Sirtl's data and much more recent works. Figures 2 and 3 are plots of equilibrium Si/Cl versus Cl/H for the Hunt and Sirtl, and JANAF data bases respectively. Both data bases predict similar overall trends, but for a given Cl/H, the JANAF data consistently predicts higher Si/Cl (and thus lower yields) than the Hunt and Sirtl data.

Table 3 shows a comparison of calculated Si/Cl for both data bases with experimental data obtained by Kokovin, et al., (15). At high temper-

atures the experimental Si/Cl is bracketed by JANAF-data calculations on the high side and Hunt/Sirtl-data calculations on the low side. At low temperatures (700°C) the experimentally obtained Si/Cl is above calculated values, and closest to the Si/Cl calculated with JANAF data. As the temperature increases the error between calculated Si/Cl and experimental Si/Cl decreases for both JANAF and Hunt/Sirtl data bases.

Another source of experimental data for comparison to equilibrium calculations is the mass spectrometric work of Ban, (16) and (17). Table 4 shows a comparison of Ban's data with equilibrium calculations. Using JANAF data, calculated concentrations of HCl and SiCl<sub>4</sub> are slightly lower than those calculated using Hunt/Sirtl data. Concentrations of SiHCl<sub>3</sub> using JANAF data are slightly higher than those using Hunt/Sirtl data. Because of the scatter in the experimental results, it is difficult to access which of the two data bases is more accurate. Within experimental error both adequately predict the concentrations of key components at temperatures above 700°C.

In light of the analysis of Tables 2, 3, 4 and Figures 2 and 3 one concludes that at temperatures above 700°C both JANAF and Hunt/Sirtl thermodynamic properties can adequately be used in equilibrium calculations. At lower temperatures accuracy of calculations are very dependent on the accuracy of the properties. Since low temperature data (200°C-400°C) is not accessible, it is difficult to determine whether JANAF or Hunt/Sirtl are viable data bases.

### Applications to Industrial Process

*Manufacture of Trichlorosilane.* Table 5 lists fractions of SiHCl<sub>3</sub> and SiCl<sub>4</sub> from various patents describing processes for manufacturing SiHCl<sub>3</sub> and compares the values with equilibrium calculations using both JANAF and Hunt/Sirtl properties. The patents describe many processes for hydrogenating SiCl<sub>4</sub> and etching silicon with HCl in fixed or fluidized beds of low-grade silicon. Also presented in Table 5 are maximum and minimum fractions of SiHCl<sub>3</sub> assuming all other silicon containing species (SiCl<sub>2</sub>, SiCl<sub>3</sub>, SiH<sub>2</sub>Cl<sub>2</sub>, SiHCl<sub>3</sub> and SiH<sub>4</sub>) are converted to SiHCl<sub>3</sub> and SiCl<sub>4</sub> respectively; some conversion of the less stable silicon species to SiHCl<sub>3</sub> or SiCl<sub>4</sub> does occur when the product gases are cooled and analyzed.

In Table 5 neither the JANAF nor the Hunt/Sirtl calculations compare closely with all literature values. At high temperatures and long residence time the measured fraction of SiHCl<sub>3</sub> is generally lower than the calculated fraction. At low temperatures the measured fraction of SiHCl<sub>3</sub> is generally much higher than the calculated fractions. An inaccuracy of less than 1% in the thermodynamic data can cause the fraction of SiHCl<sub>3</sub> to vary by more than the difference between the calculated and experimentally determined values of Table 5; inaccurate thermodynamic properties is the most plausible explanation for the discrepancies.

Some of the experimental values of Table 5 are below the equilibrium calculated value. As temperature and residence time increases, however, the experimental values approaches the calculated value. This indicates that for low temperature and short residence times the manufacture of SiHCl<sub>3</sub> is

governed by kinetics. Various catalysts such as copper (18) and (19) or iron (21), (22) and (23) are used to enhance the kinetics of  $\text{SiHCl}_3$  production.

*Decomposition of Trichlorosilane in High Pressure Siemens Decomposer.* The atmospheric-pressure Siemens decomposer has always dominated the production of high purity silicon. One drawback to this decomposer is the fact that thermodynamic equilibrium is not attained. Silicon yields in the Siemens decomposer can be as low as 30% of the equilibrium yield based upon polysilicon rod temperature.

U.S. Patent 4,173,944 describes a high pressure (5 atmospheres) Siemens decomposer. High pressures reduce the thermodynamic equilibrium yield as illustrated in Figure 4, which is a plot of yield versus pressure at a temperature of  $1050^\circ\text{C}$  for various feed conditions. The effect of pressure is less dramatic when the molar ratio of  $\text{H}_2$  to  $\text{SiHCl}_3$  in the feed is small (less than 5 to 1). The patent describes a process, operating at  $1050^\circ\text{C}$  and 4.93 atmospheres, where the feed is one mole of  $\text{H}_2$  to one mole of  $\text{SiHCl}_3$ . With this feed the yield obtained in the decomposer was 0.12 moles of silicon per mole of  $\text{SiHCl}_3$  fed. The thermodynamic equilibrium calculation using JANAF properties give an equilibrium yield of 0.18 moles of Si per mole of  $\text{SiHCl}_3$ , while the calculation using Hunt/Sirtl properties gives a yield of 0.21. Thus the high pressure decomposer operates at approximately 60% of equilibrium based upon silicon deposition. Without any data at lower pressure it is difficult to say whether increased pressure enhances or retards the performance of the decomposer.

*Closed-Loop Manufacture of Silicon.* The closed-loop silicon-to-silicon process (25) has been proposed as a route to low-cost silicon. In one version of the concept (26) chlorosilanes are manufactured in a fluidized bed of metallurgical-grade silicon, then the chlorosilanes are purified and separated. The purified chlorosilanes are pyrolyzed in a fluidized bed decomposer. Table 6 compares equilibria calculations for the chlorosilane generator and decomposer with mass balance qualities listed in (26). For the decomposer, it is difficult to compare one-for-one compositions with calculations, since the compositions of chlorosilane mixtures are measured at a lower temperature than the decomposer's operating temperature. The decomposer exhaust composition presented in (26) might represent a chlorosilane mixture which has reequilibrated as it is cooled, prior to being analyzed. For simplicity it was assumed that species such as  $\text{SiCl}_2$  or  $\text{SiCl}_3$ , which are unstable at temperatures below  $1000^\circ\text{C}$ , decompose to form  $\text{SiHCl}_3$  and  $\text{SiCl}_4$  respectively.

Table 6 reveals that both equilibrium calculation compositions compare poorly with the offgas composition for the chlorosilane generator. One can only conclude that both thermodynamic property bases have small errors in the properties for  $\text{SiHCl}_3$  and/or  $\text{SiCl}_4$ . The fluidized bed decomposer offgas composition, however, is very close to the equilibrium calculations based upon JANAF properties. Hunt/Sirtl property based calculations are not as close, but also indicate the fluidized bed decomposer is operating close to equilibrium. One might expect a fluidized bed decomposer could be operated close to the equilibrium state because of the type of contacting of silicon particles with reacting  $\text{SiHCl}_3$ .



## Conclusions

A set of user-friendly interactive computer programs developed at Monsanto are extremely useful in analyzing the thermodynamics of the Si-Cl-H system. The mathematical model for the system of 11 chemical species is easily solvable by the two solution algorithms presented. Sensitivity analysis indicates, however, that the accuracy of equilibrium calculated quantities (particularly the ratio of  $\text{SiHCl}_3$  to  $\text{SiCl}_4$ ) are extremely dependent upon the accuracy of the thermodynamic-property data base, especially at low temperature.

Two thermodynamic property bases have been considered: the Hunt/Sirtl data and the JANAF data. For high temperatures used in chlorosilane decomposers both bases are fairly reliable, although the Hunt/Sirtl base predicts higher yields of silicon than the JANAF base. At lower temperatures (used in the chlorosilane generators) comparison of calculated  $\text{SiHCl}_3$  to  $\text{SiCl}_4$  ratios with values presented in the patent literature indicate noticeable discrepancies which can only be explained by inaccuracies in the thermodynamic properties or in the literature values.

Despite the discrepancies between calculations and patent literature values, one can see that the production of  $\text{SiHCl}_3$  from  $\text{SiCl}_4$ ,  $\text{H}_2$ ,  $\text{HCl}$  and  $\text{Si}$  is kinetically controlled for small reactor residence times. In the high pressure Siemens decomposer, the silicon yield is only 60% of the equilibrium yield, which can be expected from this type of decomposer. In the fluidized bed production of silicon, however, one might expect equilibrium operation and calculations indicate this is the case.

## References

1. R. F. Lever, IBM J. Res. Develop. 8, 460 (1964).
2. I. Niederkorn and A. Wohl, Rev. Roumaine Chem., 11, 85 (1966).
3. M. J. Harper and T. J. Lewis, U. K. Ministry of Aviation Report ERDE (1966), CFSTI AD 641310.
4. L. P. Hunt and E. Sirtl in "Chemical Vapor Deposition; Second International Conferences", J. M. Blocher, Jr., and J. C. Withers, Editors; The Electrochemical Society, Symposium Series, New York (1970).
5. L. P. Hunt and E. Sirtl; J. Electrochem. Soc., 119, 1741 (1972).
6. G. A. Kokovin, T. A. Fedorova, T. V. Kuznetsov, Report "Comparison of the Results of Thermodynamic Analysis with Experimental Data from Silicon Growth by the Chloride Method", Inst. Neorg. Khim, Novosibirsk, USSR, Viniti 2332-74 (1974).
7. F. A. Kuznetsov, G. A. Kokovin, Ya. M. Buzhdan, Izvestiya Sibirskogo Otdeliniya Akademii Nauk SSSR Serya Khimicheskikh Nauk, 1, 5 (1975).
8. F. Langlais, F. Hottier and R. Cadoret, J. Cryst. Growth, 56, 659 (1982).
9. Union Carbide Final Report, "Feasibility of the Silane Process for Producing Semiconductor-Grade Silicon", work performed under JPL Contract 954334, Chapter 4.
10. J. Bloem, W.A.P. Claasen, and W.G.J.N. Valkenburg, J. Cryst. Growth, 57, 177 (1982).
11. V. S. Ban, J. Japan Assoc. Crystal Growth, 5, 119 (1978).

12. Kuester and Mize, "Optimization Techniques with FORTRAN", McGraw Hill, New York (1968).
13. W. O. Groves, Personal Communications, January-March 1981.
14. Joint Army, Navy, Air Force Thermochemical Tables; D. R. Stull and H. Prophet, Editors, NSRDS-NBS37 (1971) (1974) (1975) (1978).
15. S. V. Sysoev, A. N. Golubenko and G. A. Kokovin, Izvestiya Sibirskogo Otdeliniya Akademi Nauk SSSR Serya Khimichiskikh Nauk, 2, 98 (1977).
16. V. S. Ban and S. L. Gilbert, J. Electrochem. Soc., 122, 1382 (1975).
17. V. S. Ban, J. Electrochem. Soc., 122, 1389 (1975).
18. USSR. Patent No. 833,494, Russian Cl. 661.68 (088.8), June (1981).
19. Japanese Kokai Patent No. Sho 56[1981]-73617, June (1981).
20. Japanese Kokai Patent No. Sho 56[1981]-169119, December (1981).
21. U.S. Patent No. 4,044,109, August (1977).
22. U.S. Patent No. 3,681,036, August (1972).
23. FRG Patent No. DE 3,024,319 A1 Offenlegungsschrift, January (1982).
24. U.S. Patent No. 4,173,944, November (1979).
25. R. A. Roques, G. F. Wakefield, J. M. Blocher, Jr., M. F. Browning and W. Wilson; LSA Silicon Material Task Closed-Cycle Process Development; Texas Instrument Interim Summary Report No. 03-79-17, March (1979).
26. U.S. Patent No. 4,092,446; May (1978).

TABLE 1  
MAJOR EQUATIONS FOR THE  
GENERAL CASE AND  
SIMPLIFIED CASE EQUILIBRIA  
CALCULATION

GENERAL CASE EQUATIONS		SIMPLIFIED CASE EQUATIONS	
$K_1 = P \frac{n_{HCl}^3}{\theta} \frac{n_{SiHCl_3}}{n_{H_2}}$	(8a)	$K_1 = \frac{1}{\theta} \frac{P}{x_1} \frac{x_{HCl}^3}{x_{H_2}}$	(10a)
$K_2 = \frac{n_{SiCl_4}}{n_{H_2}} \frac{n_{H_2}}{n_{SiHCl_3}} \frac{n_{HCl}}{n_{H_2}}$	(8b)	$K_2 = \frac{x_{H_2}}{x_0} \frac{x_{HCl}}{x_{H_2}}$	(10b)
$K_3 = P \frac{n_{HCl}}{n_{H_2}} \frac{n_{SiHCl_3}}{n_{SiHCl_3}} \frac{n_{SiHCl_3}}{n_{H_2}}$	(8c)	$K_3 = \frac{P}{\theta} \frac{x_{HCl}}{x_0}$	(10c)
$K_4 = P \frac{n_{H_2}}{n_{H_2}} \frac{n_{SiHCl_3}}{n_{SiHCl_3}} \frac{n_{SiHCl_3}}{n_{H_2}}$	(8d)	$K_4 = \left(\frac{P}{\theta}\right) \frac{x_{H_2}^2 x_{HCl}}{x_0}$	(10d)
$K_5 = \frac{n_{HCl}}{n_{H_2}} \frac{n_{SiHCl_3}}{n_{SiHCl_3}} \frac{n_{SiHCl_3}}{n_{H_2}}$	(8e)	$K_5 = \frac{x_{HCl}}{x_0} \frac{x_{HCl}}{x_{H_2}}$	(10e)
$K_6 = \frac{n_{HCl}}{n_{H_2}} \frac{n_{SiHCl_3}}{n_{SiHCl_3}} \frac{n_{SiHCl_3}}{n_{H_2}}$	(8f)	$K_6 = \frac{x_{HCl}}{x_0} \frac{x_{HCl}}{x_{H_2}}$	(10f)
$K_7 = \frac{n_{HCl}}{n_{H_2}} \frac{n_{SiHCl_3}}{n_{SiHCl_3}} \frac{n_{SiHCl_3}}{n_{H_2}}$	(8g)	$K_7 = \frac{x_{HCl}}{x_0} \frac{x_{HCl}}{x_{H_2}}$	(10g)
$\theta = n_0^0 + n_{SiHCl_3} + n_{H_2} + n_{HCl} + n_{SiCl_4} + n_{SiCl_2} + n_{SiCl_3} + n_{SiH_2Cl_2} + n_{SiH_3Cl} + n_{SiH_4}$	(9a)		
$n_{SiHCl_3} = n_0^0 - \xi_1 - \xi_2 - \xi_3 - \xi_4 - \xi_5 - \xi_6 - \xi_7$	(9b)		
$n_{H_2} = n_0^0 - \xi_1 + \xi_2 + \frac{1}{2}\xi_4 - \xi_5 - 2\xi_6 - 3\xi_7$	(9c)		
$n_{HCl} = n_0^0 + 3\xi_1 - \xi_2 + \xi_3 + \xi_5 + 2\xi_6 + 3\xi_7$	(9d)		
$n_{Si} = n_0^0 + (n_{SiHCl_3}^0 - n_{SiHCl_3}) + (n_{SiCl_4}^0 - n_{SiCl_4}) + (n_{SiCl_2}^0 - n_{SiCl_2}) + (n_{SiCl_3}^0 - n_{SiCl_3}) + (n_{SiH_2Cl_2}^0 - n_{SiH_2Cl_2}) + (n_{SiH_3Cl}^0 - n_{SiH_3Cl}) + (n_{SiH_4}^0 - n_{SiH_4})$	(9e)		
$n_{SiCl_4} = n_0^0 - n_{SiCl_4} + \xi_2$	(9f)		
$n_{SiCl_2} = n_0^0 - n_{SiCl_2} + \xi_3$	(9g)		
$n_{SiCl_3} = n_0^0 - n_{SiCl_3} + \xi_4$	(9h)		
$n_{SiH_2Cl_2} = n_0^0 - n_{SiH_2Cl_2} + \xi_5$	(9i)		
$n_{SiH_3Cl} = n_0^0 - n_{SiH_3Cl} + \xi_6$	(9j)		
$n_{SiH_4} = n_0^0 - n_{SiH_4} + \xi_7$	(9k)		
MASS BALANCE: $SiHCl_3 - 1 = x_0 = \sum_{j=1}^7 x_j$		MASS BALANCE: $SiHCl_3 - 1 = x_0 = \sum_{j=1}^7 x_j$	
MASS BALANCE: $H_2 - x_{H_2} = A - x_1 + x_2 + \frac{1}{2}x_4 - x_5 - 2x_6 - 3x_7$		MASS BALANCE: $H_2 - x_{H_2} = A - x_1 + x_2 + \frac{1}{2}x_4 - x_5 - 2x_6 - 3x_7$	
MASS BALANCE: all species - $\theta = 1 + x_0 + (x_2^2 x_3) + x_3 + x_4 + x_5 + x_6 + x_7 + x_{HCl} + x_{H_2}$		MASS BALANCE: all species - $\theta = 1 + x_0 + (x_2^2 x_3) + x_3 + x_4 + x_5 + x_6 + x_7 + x_{HCl} + x_{H_2}$	
$1 = (n_{SiHCl_3}^0 + \sum_{i=1}^7 n_{SiHCl_3}^i) / (n_{SiHCl_3}^0 + 10^{-10})$		$1 = (n_{SiHCl_3}^0 + \sum_{i=1}^7 n_{SiHCl_3}^i) / (n_{SiHCl_3}^0 + 10^{-10})$	
$1 = (n_{H_2}^0 + \xi_1 - \xi_2 - \frac{1}{2}\xi_4 + \xi_5 + 2\xi_6 + 3\xi_7) / (n_{H_2}^0 + 10^{-10})$		$1 = (n_{H_2}^0 + \xi_1 - \xi_2 - \frac{1}{2}\xi_4 + \xi_5 + 2\xi_6 + 3\xi_7) / (n_{H_2}^0 + 10^{-10})$	
$1 = (\theta - n_{SiHCl_3} - n_{H_2} - n_{HCl} - n_{SiCl_4} - n_{SiCl_2} - n_{SiCl_3} - n_{SiH_2Cl_2} - n_{SiH_3Cl} - n_{SiH_4}) / (n_0^0 + 10^{-10})$		$1 = (\theta - n_{SiHCl_3} - n_{H_2} - n_{HCl} - n_{SiCl_4} - n_{SiCl_2} - n_{SiCl_3} - n_{SiH_2Cl_2} - n_{SiH_3Cl} - n_{SiH_4}) / (n_0^0 + 10^{-10})$	

TABLE 2

Temp. °C	Pressure atm.	Cl/H	SiHCl <sub>3</sub> /SiCl <sub>4</sub>					SiCl <sub>2</sub> /SiCl <sub>4</sub>					Si/Cl				
			-5	-2.5	0	2.5	5	-5	-2.5	0	2.5	5	-5	-2.5	0	2.5	5
400	-1	67.4	4.02	.340	3.65x10 <sup>-2</sup>	4.08x10 <sup>-3</sup>	3.22x10 <sup>-6</sup>	9.00x10 <sup>-7</sup>	5.06x10 <sup>-7</sup>	4.59x10 <sup>-7</sup>	4.53x10 <sup>-7</sup>	5	.331	.312	.267	.253	.251
400	1.0	165.0	8.25	.630	1.065	7.25x10 <sup>-3</sup>	1.48x10 <sup>-6</sup>	3.81x10 <sup>-7</sup>	1.74x10 <sup>-7</sup>	1.47x10 <sup>-7</sup>	1.46x10 <sup>-7</sup>	7	.332	.322	.279	.256	.253
400	10.0	-1	311.0	17.3	1.118	1.30x10 <sup>-2</sup>	6.86x10 <sup>-7</sup>	2.68x10 <sup>-7</sup>	6.28x10 <sup>-8</sup>	4.79x10 <sup>-8</sup>	4.62x10 <sup>-8</sup>	8	.333	.329	.295	.266	.260
400	-1	1.0	23.0	1.65	1.86x10 <sup>-2</sup>	2.10x10 <sup>-2</sup>	6.49x10 <sup>-7</sup>	1.80x10 <sup>-7</sup>	1.19x10 <sup>-7</sup>	1.72x10 <sup>-7</sup>	1.71x10 <sup>-7</sup>	7	.329	.296	.259	.251	.250
400	1.0	1.0	48.7	3.17	.302	.373x10 <sup>-2</sup>	3.12x10 <sup>-7</sup>	9.53x10 <sup>-8</sup>	5.92x10 <sup>-8</sup>	5.46x10 <sup>-8</sup>	5.41x10 <sup>-8</sup>	8	.331	.319	.266	.256	.251
400	1.0	104.0	6.27	.546	5.91x10 <sup>-2</sup>	6.62x10 <sup>-2</sup>	1.43x10 <sup>-7</sup>	3.89x10 <sup>-8</sup>	2.00x10 <sup>-8</sup>	1.76x10 <sup>-8</sup>	1.72x10 <sup>-8</sup>	7	.332	.319	.276	.256	.253
400	-1	10.0	.569	.349	6.16x10 <sup>-2</sup>	7.35x10 <sup>-2</sup>	1.23x10 <sup>-4</sup>	1.18x10 <sup>-7</sup>	1.10x10 <sup>-7</sup>	1.08x10 <sup>-7</sup>	1.08x10 <sup>-7</sup>	7	.250	.250	.254	.267	.275
400	1.0	10.0	.569	.451	.104	.013	3.90x10 <sup>-3</sup>	3.81x10 <sup>-8</sup>	3.51x10 <sup>-8</sup>	3.42x10 <sup>-8</sup>	3.42x10 <sup>-8</sup>	7	.275	.271	.256	.251	.250
400	10.0	10.0	.570	.520	.170	2.27x10 <sup>-2</sup>	1.23x10 <sup>-8</sup>	1.22x10 <sup>-8</sup>	1.13x10 <sup>-8</sup>	1.09x10 <sup>-8</sup>	1.08x10 <sup>-8</sup>	8	.275	.273	.260	.252	.250
1200	-1	5.62	1.31	.690	.252	9.26x10 <sup>-2</sup>	21.7	19.9	19.2	18.9	18.8	7	.176	.171	.169	.168	.168
1200	1.0	7.70	2.46	.837	.298	1.08x10 <sup>-2</sup>	42.6	3.22	2.77	2.59	2.52	5	.252	.192	.181	.175	.173
1200	10.0	-1	14.0	4.10	1.31	.447	1.36	.876	.657	.576	.532	7	.260	.239	.219	.206	.199
1200	-1	1.37	.480	.173	6.33x10 <sup>-2</sup>	2.32x10 <sup>-2</sup>	2.79	2.51	2.39	2.36	2.34	7	.307	.304	.302	.302	.302
1200	1.0	2.40	.804	.284	.103	3.77x10 <sup>-2</sup>	.765	.612	.551	.528	.519	8	.293	.277	.267	.262	.260
1200	10.0	1.0	4.63	1.47	.508	.182	.274	.195	.162	.150	.145	7	.305	.285	.267	.256	.251
1200	-1	.269	.115	4.50x10 <sup>-2</sup>	1.68x10 <sup>-2</sup>	6.30x10 <sup>-3</sup>	1.25	1.23	1.22	1.21	1.21	5	.332	.329	.327	.327	.327
1200	1.0	.381	.196	8.30x10 <sup>-2</sup>	3.20x10 <sup>-2</sup>	1.22x10 <sup>-2</sup>	.316	.306	.300	.297	.296	7	.288	.282	.277	.274	.273
1200	10.0	10.0	.478	.304	1.46	5.99x10 <sup>-2</sup>	9.39x10 <sup>-2</sup>	9.09x10 <sup>-2</sup>	8.80x10 <sup>-2</sup>	8.63x10 <sup>-2</sup>	8.56x10 <sup>-2</sup>	7	.277	.271	.263	.259	.257

TABLE 3

Temp. °C	Pressure atm.	Cl/H	JANAF Based Si/Cl	Hunt/Sirtl Based Si/Cl	Experimental Si/Cl
950	1	1.00	.265	.256	.260
950	1	0.30	.260	.248	.254
950	1	0.20	.256	.241	.248
950	1	0.10	.242	.223	.235
950	1	0.07	.230	.209	.225
800	1	1.00	.266	.261	.262
800	1	0.20	.268	.260	.260
800	1	0.15	.267	.258	.262
800	1	0.10	.265	.255	.254
800	1	0.07	.261	.250	.252
750	1	1.00	.267	.263	.270
750	1	0.10	.271	.262	.265
700	1	1.00	.268	.264	.261
700	1	0.64	.270	.265	.289
700	1	0.50	.270	.266	.287
700	1	0.20	.274	.268	.286
700	1	0.10	.276	.268	.287

ORIGINAL PAGE IS  
OF POOR QUALITY

TABLE 4  
COMPARISON OF CALCULATED  
EQUILIBRIUM COMPOSITIONS  
WITH EXPERIMENTALLY DETERMINED COMPOSITIONS\*

Temp. °C	Species	Pp** (SiCl <sub>2</sub> H <sub>2</sub> )	Pp*** (SiCl <sub>3</sub> H)	Pp**** (SiCl <sub>4</sub> )	Pp (Hunt/Sirtl)	Pp (JANAF)
726.85	HCl	1.7x10 <sup>-2</sup>	1.4x10 <sup>-2</sup>	1.9x10 <sup>-3</sup>	1.1x10 <sup>-2</sup>	8.5x10 <sup>-3</sup>
	SiCl <sub>2</sub>	5.2x10 <sup>-3</sup>	4.0x10 <sup>-3</sup>	< 10 <sup>-5</sup>	6.6x10 <sup>-2</sup>	1.3x10 <sup>-4</sup>
	SiH <sub>2</sub> Cl <sub>2</sub>	5.2x10 <sup>-3</sup>	3.6x10 <sup>-4</sup>	< 10 <sup>-5</sup>	1.3x10 <sup>-3</sup>	1.8x10 <sup>-4</sup>
	SiHCl <sub>3</sub>	3.6x10 <sup>-2</sup>	1.6x10 <sup>-2</sup>	1.2x10 <sup>-2</sup>	1.9x10 <sup>-2</sup>	2.2x10 <sup>-2</sup>
	SiCl <sub>4</sub>	9.8x10 <sup>-3</sup>	1.2x10 <sup>-2</sup>	3.8x10 <sup>-2</sup>	3.0x10 <sup>-2</sup>	2.1x10 <sup>-2</sup>
	H <sub>2</sub>	0.9268	0.954	0.9478	0.939	0.939
926.85	HCl	6.5x10 <sup>-2</sup>	4.2x10 <sup>-2</sup>	2.8x10 <sup>-2</sup>	4.0x10 <sup>-2</sup>	3.2x10 <sup>-2</sup>
	SiCl <sub>2</sub>	8.5x10 <sup>-3</sup>	1.1x10 <sup>-2</sup>	2.8x10 <sup>-3</sup>	1.5x10 <sup>-3</sup>	2.7x10 <sup>-3</sup>
	SiH <sub>2</sub> Cl <sub>2</sub>	1.4x10 <sup>-3</sup>	1.1x10 <sup>-3</sup>	< 10 <sup>-5</sup>	1.4x10 <sup>-3</sup>	1.7x10 <sup>-3</sup>
	SiHCl <sub>3</sub>	1.3x10 <sup>-2</sup>	1.0x10 <sup>-2</sup>	1.8x10 <sup>-2</sup>	1.5x10 <sup>-2</sup>	1.7x10 <sup>-3</sup>
	SiCl <sub>4</sub>	1.4x10 <sup>-2</sup>	2.2x10 <sup>-2</sup>	2.5x10 <sup>-2</sup>	2.4x10 <sup>-2</sup>	2.2x10 <sup>-2</sup>
	H <sub>2</sub>	0.900	0.914	0.9256	0.918	0.921
1026.85	HCl	1.1x10 <sup>-1</sup>	8.4x10 <sup>-2</sup>	6.4x10 <sup>-2</sup>	6.4x10 <sup>-2</sup>	5.1x10 <sup>-2</sup>
	SiCl <sub>2</sub>	1.4x10 <sup>-2</sup>	1.8x10 <sup>-2</sup>	1.7x10 <sup>-2</sup>	5.0x10 <sup>-3</sup>	7.7x10 <sup>-3</sup>
	SiH <sub>2</sub> Cl <sub>2</sub>	6.6x10 <sup>-3</sup>	5.3x10 <sup>-3</sup>	5.3x10 <sup>-3</sup>	1.3x10 <sup>-3</sup>	1.5x10 <sup>-3</sup>
	SiHCl <sub>3</sub>	4.0x10 <sup>-3</sup>	5.7x10 <sup>-3</sup>	3.9x10 <sup>-3</sup>	1.2x10 <sup>-2</sup>	1.3x10 <sup>-2</sup>
	SiCl <sub>4</sub>	6.5x10 <sup>-3</sup>	1.1x10 <sup>-2</sup>	1.7x10 <sup>-2</sup>	2.0x10 <sup>-3</sup>	1.6x10 <sup>-2</sup>
	H <sub>2</sub>	0.859	0.876	0.872	0.898	0.906

\* At 1 atm. system pressure and Cl/H = 1

\*\* Composition obtained by starting with SiCl<sub>2</sub>H<sub>2</sub> and H<sub>2</sub>

\*\*\* Composition obtained by starting with SiCl<sub>3</sub>H and H<sub>2</sub>

\*\*\*\* Composition obtained by starting with SiCl<sub>4</sub> and H<sub>2</sub>

ORIGINAL PAGE 17  
OF POOR QUALITY

TABLE 5  
COMPARISON OF EQUILIBRIUM CALCULATIONS  
WITH LITERATURE DATA FOR MANUFACTURE  $\text{SiHCl}_3$

Reference	Cl/H	Temp. C°	Pressure atm.	Estimated Residence Time, Sec.	Experimental $\text{SiHCl}_3/\text{SiCl}_4$	JANAF Calculated $\text{SiHCl}_3/\text{SiCl}_4$	JANAF Limits High	JANAF Limits Low	Hunt/Sirtl Calculated TCS/TEI	Hunt/Sirtl Limits High	Hunt/Sirtl Limits Low
18	1	700	1	N.A.	.715/.285	.268/.713	.279/.721	.264/.736	.229/.771	.236/.764	.226/.774
19	1	350	1	~ 1*	.803/.197	.300/.700	.305/.695	.298/.701	.230/.770	.234/.766	.230/.700
	1	600	1	~ 1*	.369/.631	.275/.725	.287/.717	.273/.721	.230/.770	.245/.755	.225/.775
	2	350	1	~ 4*	.059/.941	.243/.757	.242/.758	.232/.768	.186/.814	.188/.812	.185/.815
	2	600	1	~ 3*	.318/.782	.222/.778	.228/.772	.221/.779	.185/.815	.188/.811	.184/.816
20	.054	750	1	10	.210/.790	.484/.515	.517/.483	.453/.546	.431/.569	.396/.604	.413/.587
	.117	800	1	50	.250/.750	.422/.577	.457/.542	.397/.603	.374/.626	.396/.604	.361/.639
	.470	1000	1	100	.340/.660	.313/.687	.431/.569	.258/.742	.273/.725	.327/.673	.255/.745
21	1	478	1	12	.140/.860	.287/.713	.243/.707	.285/.715	.232/.768	.236/.764	.231/.769
	1	426	1	11	.260/.740	.293/.707	.298/.702	.291/.709	.232/.768	.236/.764	.231/.769
	1	331	1	9	.800/.200	.304/.696	.308/.692	.302/.698	.231/.769	.234/.766	.230/.770
22	9.9x10 <sup>-3</sup>	400	1	190	.709/.290	.295/.705	.301/.698	.294/.706	.232/.768	.235/.765	.231/.769
	1	800	1	4	.970/.030	.640/.360	.664/.336	.638/.362	.550/.450	.571/.429	.524/.478
	9.9x10 <sup>-3</sup>	800	1	118	.172/.827	.621/.379	.283/.717	.255/.745	.226/.774	.235/.765	.215/.485
	1	1000	1	2	.742/.257	.631/.369	.690/.310	.530/.469	.586/.413	.636/.364	.651/.349
	9.9x10 <sup>-3</sup>	1000	1	99	.140/.860	.254/.746	.364/.636	.217/.783	.222/.718	.264/.736	.210/.790
23	1.333	320	1.3	2	.602/.398	.720/.280	.828/.172	.696/.307	.700/.300	.851/.149	.651/.349
	3	320	4	3	.388/.612	.295/.705	.299/.701	.293/.707	.223/.771	.225/.775	.222/.778
	.222	320	4	40	.279/.719	.275/.725	.280/.720	.272/.728	.210/.790	.212/.780	.209/.791
					.635/.365	.519/.481	.532/.468	.505/.495	.417/.583	.427/.573	.410/.590

\*Estimated assuming a 1 m tall 10 cm  $\phi$  fluid bed.

TABLE 6  
COMPARISON OF EQUILIBRIUM CALCULATIONS  
WITH CLOSED-LOOP MANUFACTURING OF SILICON

Chlorosilane Generator Offgas Composition, lb-moles/hr	JANAF Calculations Chlorosilane Generator	Hunt/Sirtl Calculations Chlorosilane Generator	Fluidized Bed Decomposer Offgas Composition lb-moles/hr.	JANAF * Calculated Composition	Hunt/Sirtl* Calculated Composition
H <sub>2</sub>	4.79	4.88	142.2	141.5	139.8
HCl	0.0331	0.0420	7.78	7.70	11.6
SiH <sub>2</sub> Cl <sub>2</sub>	0.0265	0.326	0.326	0.314	0.422
SiHCl <sub>3</sub>	0.938	0.782	5.915	6.76	6.00
SiCl <sub>4</sub>	2.32	2.44	7.171	6.56	6.09
Si			2.48	2.25	3.35
Temperature °C	625	625	1100	1100	1100
Pressure, atm	1.61	1.61	2.0	2.0	2.0

\* Assuming the reactions  $\text{SiCl}_2 + \text{HCl} \rightarrow \text{SiHCl}_3$   
 $\text{SiCl}_3 + \text{HCl} \rightarrow \text{SiCl}_4 + \frac{1}{2} \text{H}_2$

ORIGINAL PAGE IS  
OF POOR QUALITY

FIGURE 1

# The Si - Cl - H Triangular Diagram

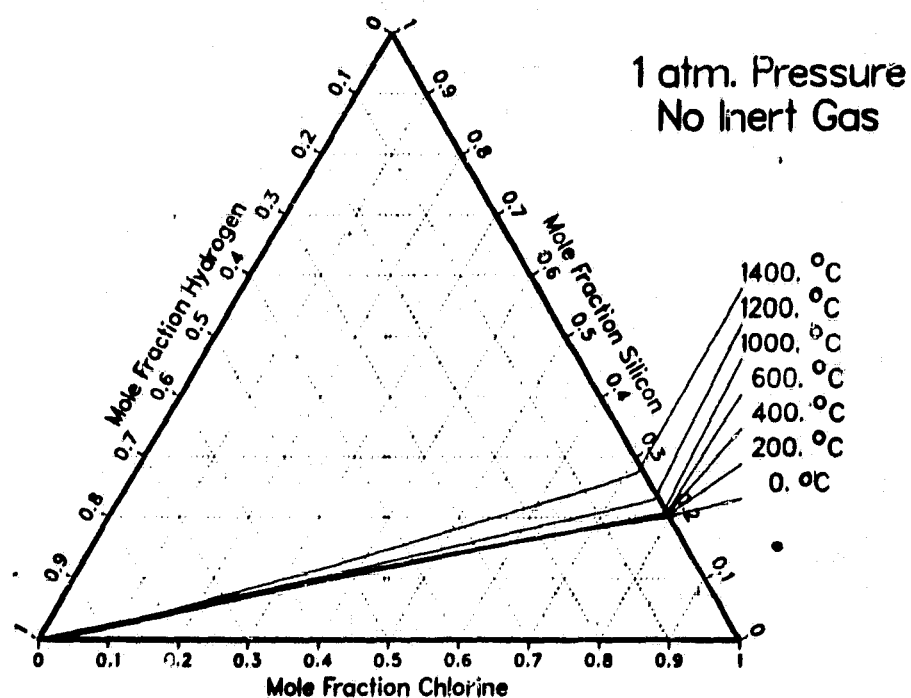


FIGURE 4

# Equilibrium Yield: Effect Of Pressure

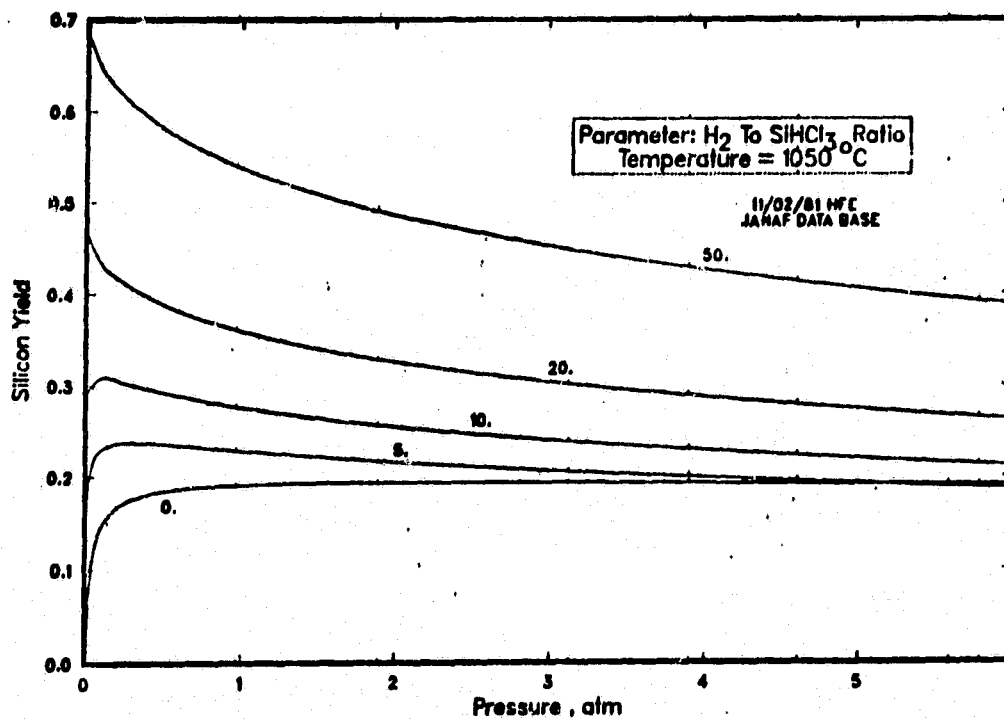


FIGURE 2  
Thermodynamics Of The  
Silicon, Chlorine,  
Hydrogen System

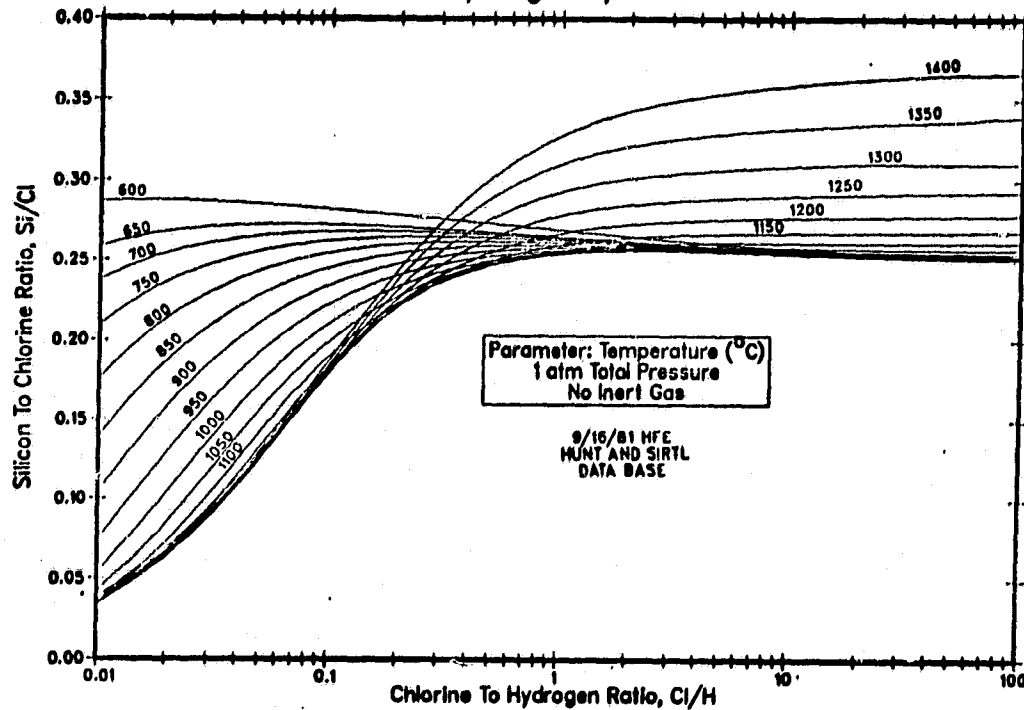
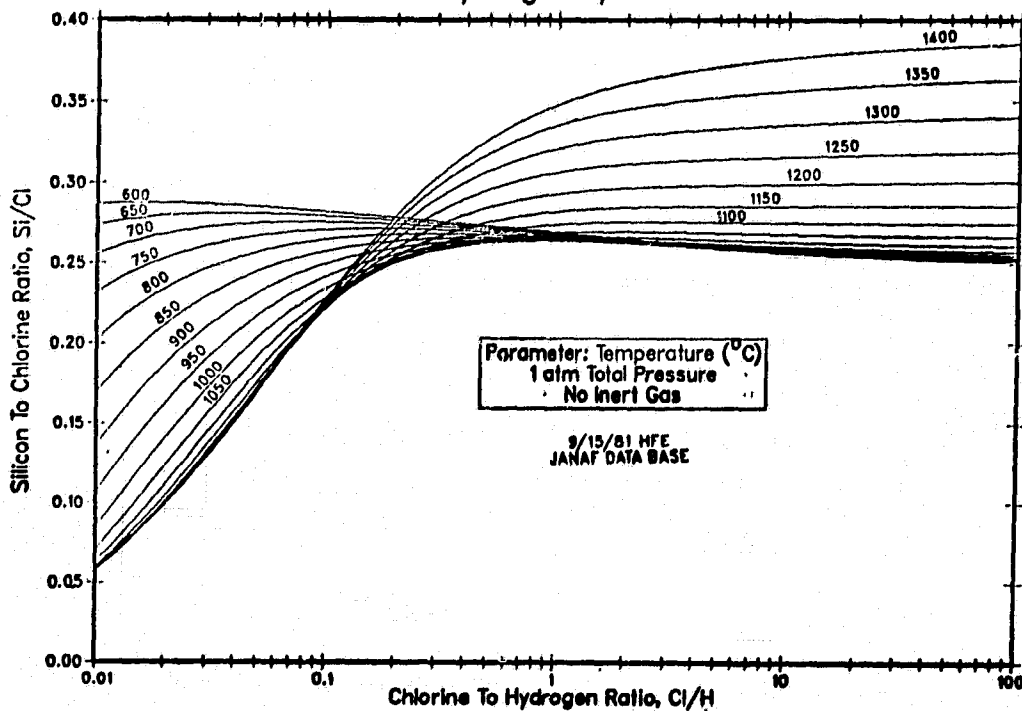


FIGURE 3  
Thermodynamics Of The  
Silicon, Chlorine,  
Hydrogen System





DISCUSSION

PRATURI: You mentioned that the Siemens decomposer operates at 60% equilibrium. Does that mean it's not constrained by equilibrium but that there is a kinetic constraint? Or, did it not reach equilibrium?

ERK: It did not reach equilibrium. It's constrained by a combination of the kinetics and the mass transfer of the system.

PRATURI: Can you say a few words about the heterogeneous and homogeneous equilibria concept?

ERK: Well, basically the concept permits the calculation of the partial pressure of silicon in a system in which homogeneous and heterogeneous reactions occur and there is an equilibrium. Beyond a silicon pressure limit of the super-saturation pressure of silicon, so-called homogeneous nucleation of silicon occurs. The concept of supersaturation leads to the addition of an extra equilibrium between the supersaturated silicon and the solid silicon.

REIF: I just want to make sure that I understood something. Does the condition of high temperatures and long residence time imply that the trichlorosilane process is dominated by equilibrium, that is, by thermodynamics?

ERK: Apparently, yes.

REIF: Now, is it correct that at high temperatures and a short residence time the process is dominated by kinetics or some sort of a mass transfer limitation?

ERK: Could be.

REIF: Now, are your computations compatible with the conditions of high temperature and a short residence time?

ERK: They're close, but not exact. Much smaller fractions of trichlorosilane are described in the patents than the calculations predict. In other words, processes apparently produce less than predicted by thermodynamic equilibrium calculations.

LEIPOLD: Could you comment on how easily your technique could be extended to systems in which there is no chlorine, silicon, or hydrogen?

ERK: Essentially what would have to be done is to eliminate all the mass balance equations that have any kind of silicon containing species. The approach is basically the same and the equations are written slightly differently. The Russian Kokovin has a paper which describes in great detail the procedure for a general system. It gets extremely simple when there is only silicon and hydrogen; in fact, it could almost be done without a computer.

MILSTEIN: You made a comment very early in the paper, and I think it was touched upon later, that thermodynamically you look at circumstances which are independent of pathway. I think I would agree with that for making calculations, whereas when you talk about the actual circumstance, the kinetic aspects are very important. With regards to an earlier question about the residence time, one might imagine a reaction where there is a forward reaction and a back reaction. Until the forward reaction has built some reactant up to a sufficient concentration, the back reaction has no way of proceeding. From that point of view, if one is a rapid reaction and the other one is slow, the residence time is going to become a very critical issue; thermodynamically you are not going to see that, though.

ERK: This is a question of thermodynamics versus kinetics. Thermodynamics assumes that there is an infinite amount of time to let the system equilibrate. The mechanism that I propose is a purely computational mechanism. In no way whatsoever is it intended to model reality in terms of kinetics.

BAILEY: I have a question concerning the very unusual chemical behavior at lower temperatures. If you'll notice from those curves, at lower temperatures the higher the chlorine-to-hydrogen ratio, the higher the yield of silicon at low temperatures, and that's a very unusual circumstance. Do you have any explanation? I'm looking at some of the data you showed from the Hunt/Sirtl paper.

ERK: Yes, it does go slightly down, but under those conditions the reactions are constrained by other limitations in the reactor, i.e., the kinetics of the system. The reaction rates decrease with decreasing temperature. Also, at the lower temperatures, although there is a higher yield of silicon, more unwanted by-products (such as silicon tetrachloride, for example) are produced.

BAILEY: My second question has to do with the fact that in thermodynamics you make use of the initial and final states, but in the calculations, I see very little evidence of any consideration of what I call the "silicon-silicon" compounds that are formed in the silicon-hydrogen-chlorine system. I have some information that leads me to believe that these compounds are extremely stable at low temperatures.

ERK: The so-called silicon polymers.

BAILEY: Right.

ERK: Yes, that's probably one point that really needs to be addressed. These other compounds need to be included in the calculations and the failure to account for these species, which are in the system, probably causes a large error in the calculations at the lower temperatures.

9  
Y

INGLE: Earlier somebody said that some of the differences result from the way equilibrium is reached. Using one reaction path, polymer materials result; using a different path, polymers may not be formed. So, it's a lot more complex than just simply looking at one system. A number of different reaction approaches need to be examined to see whether different numbers for theoretical equilibria are obtained. The real world is not the theoretical world. In certain approaches, polymers will be formed and a system containing polymers will be a different equilibrium system.

ERK: We need more data on the polymers.

DUDUKOVIC: I strongly disagree with the last comment. I think the real world is a theoretical world if you do the calculations correctly. I think these calculations at high temperatures show that you do it right, because at high temperature you don't have those problems. If  $\Delta G$  and  $\Delta H$  values are made available for low temperatures, the physicist, or the chemist, will do the calculations. They will derive information concerning the amounts of polymers, and it will be totally independent of the path. The system at the lower temperatures could then be described. This cannot be done now; the data are not available.

MILSTEIN: You're right in the sense that you ought to be able to calculate everything, but I think the other point that has to be remembered is that if some reaction proceeds at an extremely low rate due to kinetics, while the calculated equilibrium value may be a larger value, realistically very little or no reaction will be observed.

DUDUKOVIC: I agree with that. At least the calculations will reveal the equilibrium concentrations of those compounds at lower temperatures. Without such calculations there is no information on the maximum concentrations. I'm not saying that equilibrium will be reached and that equilibrium concentrations will be measured. I am very well aware of the difference between kinetics and thermodynamics, but the thermodynamic calculations should be made to determine the possible concentrations.

# KINETICS AND MECHANISMS OF CHLOROSILANE DECOMPOSITION

Donald L. Bailey

Consultant to Jet Propulsion Laboratory

Traverse City, Michigan

Chlorosilanes containing the elements silicon, hydrogen and chlorine are important intermediates in the manufacture of silicone products and in the production of high purity polycrystalline silicon for the electronics industry. A wealth of information exists for chemical processes which either are used to prepare chlorosilanes or to convert them into silicon chemicals containing carbon-silicon bonds. These include the reaction of hydrogen chloride with silicon to give trichlorosilane and the addition of trichlorosilane (or dichlorosilane) to olefinic compounds to produce organic substituted chlorosilanes. In the temperature range that such reactions occur (300-700°K) thermal decompositions of chlorosilanes are relatively slow. The kinetics and mechanisms for such decompositions have been investigated only qualitatively. High temperature decompositions of chlorosilanes where silicon is a major product take place rapidly with the result that conclusions drawn have been based on thermodynamics and physical considerations such as surface area and diffusion rather than on the chemical steps involved. While this treatment has been quite helpful in defining the silicon-hydrogen-chlorine system it seemed desirable to review both high and low temperature chlorosilane decompositions including those where catalysts are employed. This presentation will provide an overview of chlorosilane reactions with the objective of pointing out their implications in the production of polycrystalline silicon metal.

## I. Hydrogen Chloride-Silicon Reaction

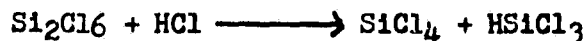
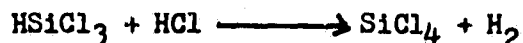
The direct synthesis of trichlorosilane from hydrogen chloride and metallurgical grade silicon metal is a widely used commercial process.



By-products in the above reaction include  $\text{SiCl}_4$ ,  $\text{H}_2\text{SiCl}_2$ ,  $\text{HSi}_2\text{Cl}_5$ ,  $\text{Si}_2\text{Cl}_6$  and  $\text{Si}_3\text{Cl}_8$ . Copper is sometimes used as a catalyst but is unnecessary for trichlorosilane production. Up to 30 percent dichlorosilane can be obtained by use of special Cu-Si masses and short contact times. Dichlorosilane is unstable under the reaction conditions and rapidly dissociates into other products. This infers that the reaction involves dichlorosilane as an intermediate. Equilibrium conditions are not attained. By way of contrast pure semiconductor grade silicon does not react well with hydrogen chloride under comparable conditions.

ORIGINAL PAGE IS  
OF POOR QUALITY.

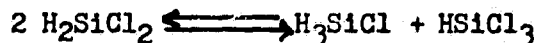
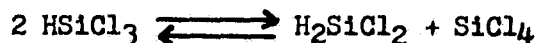
Hydrogen chloride can also react with chlorosilanes containing hydrogen or with disilanes and polysilanes.



Below 500°C the above reactions require a catalyst such as copper. Above this temperature they occur thermally. Dichlorosilane and monochlorosilane can be expected to be more reactive with hydrogen chloride than trichlorosilane and hexachlorodisilane. The  $\text{HCl-HSiCl}_3$  reaction is reversible but the equilibrium lies far to the right (ca. 99 percent  $\text{SiCl}_4$ ).

## II. Disproportionation and Redistribution of Chlorosilanes

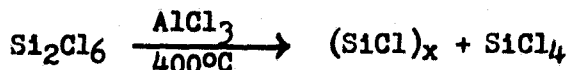
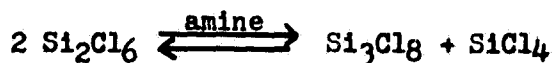
The redistribution of Si-H and Si-Cl bonds in trichlorosilane to give dichlorosilane and silicon tetrachloride takes place with a tertiary amine catalyst (such as dry A-21 Amberlyst Resin) at room temperature. Subsequent redistributions with dichlorosilane yield monochlorosilane and finally silane.



At 60-80° equilibrium (10-11 percent dichlorosilane) is achieved with trichlorosilane over A-21 catalyst in less than one minute. No significant by-products are formed. The above reactions involve mutual equilibria and can be treated as a single system defined by the Si/Cl ratio (or by the Cl/H ratio since no hydrogen is formed). Amine catalyzed redistributions of chlorosilanes are part of the Union Carbide and Hemlock Semiconductor processes for producing pure silicon currently under development.

Aluminum chloride is also a catalyst for the disproportionation of trichlorosilane at 375°C. In this case small amounts (2-5 percent) of hexachlorodisilane are found in the product. Thermal disproportionation takes place at 700°C (973°K). It is noteworthy that this temperature is lower than that at which silicon deposition from trichlorosilane becomes kinetically significant (1000°K). The first step in the silicon deposition mechanism may involve dichlorosilane as an intermediate.

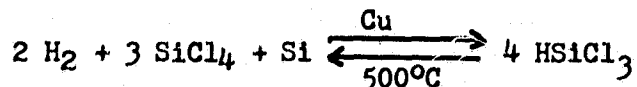
In addition to the above, the Si-Si and Si-Cl bonds in disilanes can undergo redistribution to form polysilanes.



With aluminum chloride catalyst at  $400^\circ\text{C}$  the polymeric  $(\text{SiCl})_x$  obtained was a brittle, deep orange solid which formed as a continuous block on the walls of the reactor. After 16 hours reaction was substantially complete and irreversible. Chemical analysis gave a Si/Cl ratio of one. A similar polymer obtained by pyrolysis of  $\text{SiCl}_4$  has been reported as an amorphous yellow powder stable to  $400^\circ\text{C}$  (1). It is doubtful that polymeric silicon chlorides of this type can be considered as chemical intermediates in silicon decomposition processes at high temperatures. The silicon-silicon bond is relatively unstable. However they may be significant in low temperature thermal decompositions below  $1000^\circ\text{F}$ . Polysilanes disproportionate thermally to higher polysilanes and silicon tetrachloride at about  $600^\circ\text{C}$ .

### III. Hydrogenation of Silicon Tetrachloride

In 1947 E.O. Brimm (2) established that an equilibrium amount of trichlorosilane could be obtained by passing silicon tetrachloride and hydrogen over silicon metal at  $500^\circ\text{C}$  using copper as the catalyst.



More recently this reaction, which is a step in Union Carbide's semiconductor silicon process, has been studied in considerable detail by J.Y.P. Mui (3). Equilibrium (20-35 percent  $\text{HSiCl}_3$ ) is reached at contact times of 30-60 seconds. Higher pressures give higher conversions but slower rates. The reaction rate appears to be independent of silicon surface area in the range studied. This suggests that the reaction mechanism involves a slow reaction of hydrogen with silicon tetrachloride followed by a fast reaction of hydrogen chloride with silicon metal.

It is noteworthy that hydrogenation of silicon tetrachloride over silicon is the reverse reaction to silicon deposition. Some interesting studies could be made at  $500-700^\circ\text{C}$  which would give considerable insight as to the role of redistribution, polysilane formation and other variables in a temperature range where chemical kinetics are measurable. However, these studies would have limited interest when applied to the high temperature processes generally employed for producing polycrystalline silicon. Above  $1200^\circ\text{K}$  the chemical reactions take place so rapidly

that factors such as diffusion and mass transfer become rate-controlling.

#### IV. Thermal Decompositions

Some qualitative data exists (4) for the thermal decomposition of chlorosilane-hydrogen mixtures in a quartz tube. The incipient decomposition temperature was measured. This is the temperature at which a significant silicon deposit can be observed. Results are tabulated below.

<u>Chlorosilane</u>	<u>Percent Molar Conc. in Hydrogen</u>	<u>Incipient Decomposition Temp. °K</u>
$\text{SiCl}_4$	10	1150
$\text{HSiCl}_3$	10	1000
$\text{H}_2\text{SiCl}_2$	10	850
$\text{H}_3\text{SiCl}$	--	700 (estimated)

As expected from bond energy data chlorosilanes containing a greater number of hydrogen substituents were found to be thermally less stable. Homogeneous decomposition of dichlorosilane to silicon was observed in the gas phase in addition to deposits along the tube. (This did not occur with trichlorosilane). The silicon deposits were amorphous, non-crystalline, and may have contained high molecular weight chlorine-substituted polysilanes. Analyses of the exit gases gave little evidence for monochlorosilane indicating that silicon deposition can proceed faster than dichlorosilane redistribution. At 1000°C (1273°K) the deposition of silicon metal from trichlorosilane was observed to approach equilibrium in about 0.1 seconds.

#### V. Thermodynamic Equilibria

A number of papers (5, 6, 7) have appeared which present a thermodynamic analysis of the silicon-hydrogen-chlorine system. R.F. Lever showed that, at equilibrium with silicon metal, chlorosilane systems can be defined in the gas phase as a function of temperature, pressure and the Cl/H ratio. From enthalpies of formation and entropy data equilibria for various species in the Si-H-Cl system have been calculated. While as many as fourteen gaseous species can be considered to be in equilibrium with silicon the principal ones are hydrogen, hydrogen chloride,  $\text{SiCl}_4$ ,  $\text{HSiCl}_3$ ,  $\text{SiCl}_2$ ,  $\text{H}_2\text{SiCl}_2$  and  $\text{H}_3\text{SiCl}$ . Traces of  $\text{SiH}_4$ ,  $\text{SiCl}$  and  $\text{SiCl}_3$  appear in the calculations but rarely exceed partial pressures of  $1 \times 10^{-4}$  atm. at one atmosphere. By way of example, values calculated by V. Ban and S. Gilbert (7) are presented.

EQUILIBRIUM PARTIAL PRESSURES OF  
VAPOR SPECIES IN THE SILICON-HYDROGEN-CHLORINE  
SYSTEM Cl/H RATIO = 0.1  
(CALCULATED IN ATMOSPHERES)

<u>T, °K</u>	<u>1000</u>	<u>1200</u>	<u>1400</u>
H <sub>2</sub>	.939	0.918	0.881
HCl	0.011	0.04	0.086
SiCl <sub>4</sub>	0.030	0.024	0.012
HSiCl <sub>3</sub>	0.019	0.015	0.009
H <sub>2</sub> SiCl <sub>2</sub>	0.001	0.001	0.001
SiCl <sub>2</sub>	0.00007	0.002	0.011

In addition to calculated values Ban and Gilbert also carried out experimental measurements with dichlorosilane using a tubular quartz reactor closely connected to a mass spectrometer through a small heated quartz capillary tube. The results showed certain deviations from thermochemical equilibrium calculations but were of the same order of magnitude. They attributed the deviations to retarded HCl adsorption on silicon and to incomplete dichlorosilane decomposition.

Since reaction kinetics are extremely fast above 1200°K equilibrium calculations can be valuable in predicting the extent of silicon deposition from various chlorosilane-hydrogen mixtures. The deposition of silicon takes place when the Si/Cl ratio in the starting mixture exceeds that of gaseous products at equilibrium. Otherwise, etching of the silicon substrate occurs as in hydrogenation of SiCl<sub>4</sub>. The theoretical yield of silicon deposited from various chlorosilanes is profoundly affected by both the Cl/H and the Si/Cl concentration in the feed as illustrated in the following table.

CALCULATED DEPOSITION OF SILICON  
FROM ONE KILOGRAM OF VARIOUS CHLOROSILANES AT  
1400°K (5 MOLE PERCENT IN HYDROGEN)

<u>Chlorosilane</u>	<u>Cl/H Ratio</u>	<u>Si/Cl Ratio (Feed)</u>	<u>Silicon Yield (Grams)</u>
SiCl <sub>4</sub>	.105	.25	39.5
HSiCl <sub>3</sub>	.077	.33	97
H <sub>2</sub> SiCl <sub>2</sub>	.050	.50	199
H <sub>3</sub> SiCl	.024	1.00	385



Neglecting practical considerations such as cost and availability it is evident that monochlorosilane would be the chlorosilane of choice for obtaining high yields of silicon.

In the trichlorosilane-hydrogen system it has been shown that conversion to silicon is markedly affected by hydrogen concentration (Cl/H ratio). Data obtained in a quartz tube at 1450-1550°K by H.W. Pattin (8) demonstrated that a plot of log mole percent trichlorosilane in hydrogen versus percent silicon deposited gave a straight line relationship. The yields ranged from 52.3 percent silicon at 1.43 mole percent trichlorosilane to 18.8 percent silicon at 10.3 mole percent. These values are significantly lower than those reported from thermodynamic calculations. In the experiments carried out the silicon deposition took place in the first part of the heated quartz tube; the remaining section of the tube was clean and free of silicon except at the exit end where the temperature dropped. It was concluded that the system was substantially at equilibrium when silicon no longer deposited along the tube. Other researchers have reported different results (9).

## VI. Kinetic Considerations

The kinetics of silicon deposition from a mixture of trichlorosilane and hydrogen were studied in some detail by D. Laskafeld and T. Roznov (10). They established that in the range of 1350-1500°K the controlling factor of the reaction is diffusion of gaseous compounds of silicon to the surface of the rods used for the deposition. Silicon deposition rate was found to be proportional to the square root of flow rate and trichlorosilane concentration in the feed. The experimental reactor used was similar in design to Siemens-type reactors for commercial production of polycrystalline silicon.

The above findings were confirmed by M. Bawa, R. Goodman and J. Truitt (11) in the temperature range of 1300-1500°K. They described the kinetics of silicon deposition by the equation:

$$R = 1.425 L D^{0.56} V^{0.56} \exp(-7000/T) P (1-2.2 Cl/H)$$

R = silicon deposition rate, grams/minute

L = length of rod, cm.

D = rod diameter, cm.

V = flow rate, liters/minute

P = partial pressure of chlorosilanes, atm.

Temperature increases deposition rate up to the melting point of silicon. This represents the change-over point from diffusional control to control of the deposition by chemical kinetics. Above 1700°K the deposition rate is linear with surface area, flow rate and partial pressure of the chlorosilane.

$$R = 1.85 \times 10^{-7} A P V \exp(13,500/T)$$

A = surface area (cm<sup>2</sup>)

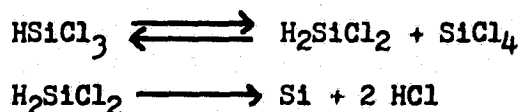
Below 1200°F chemical kinetics play an important role in silicon deposition. Sirtl, Hunt and Sawyer (9) have presented general outlines as to the extent that surface-controlled or diffusion-controlled reactions play the dominant role irrespective of different types of equipment or experimental conditions. The variables of low flow rate, low mole fraction chlorosilane, high substrate temperature, low temperature gradient, high surface site density and high silicon surface to reactor volume all favor a diffusion-controlled reaction; the reverse situation favors a surface-controlled reaction. Siemens type polycrystalline silicon reactors probably operate under conditions where the kinetics are surface-controlled when the rods are small and the temperature gradient between the feed gases and the silicon surface is high. In experimental work by N.R. Berlat (12) using a CVD reactor of the Siemens type with an 18 inch quartz bell jar it was observed that a linear relationship existed between average growth rate in grams per hour of silicon and pounds per hour of trichlorosilane fed to the reactor regardless of trichlorosilane concentration or flow rate. This data was collected during six hours at 1150°C. It would appear that deposition rate was surface-controlled rather than diffusion-controlled. At a later stage in the deposition when the silicon rods are large diffusion would be expected to be rate-controlling.

## VII. Mechanisms

Deposition of silicon on a heated substrate is considered to be a heterogeneous reaction with the bulk of chemical processes taking place on the solid surface. In the temperature range of 1300-1500°K (conditions generally used in polycrystalline silicon manufacture) reactions take place at the surface more rapidly than the rate of diffusion of chlorosilanes. As a result the kinetics are controlled by the diffusion rate. Since equilibria of the various chemical species are established in a short time thermodynamics calculations are useful in predicting the results and, for practical purposes, chemical pathways are unimportant.

It is well recognized that a boundary layer (with a thermal gradient) exists between the hot silicon substrate and the chlorosilane-hydrogen gas mixture used as feed. Chemical processes also occur in this boundary layer since chlorosilanes must diffuse through before they react with the silicon surface and gaseous species formed must diffuse out before leaving the reactor. It would be most surprising if a highly unstable specie such as  $\text{SiCl}_2$  did not undergo further reactions with chlorosilanes in the boundary layer.

The thermal disproportionation of trichlorosilane may be an intermediate step in silicon deposition.



9  
Y

In decomposition studies disproportionation was favored over silicon deposition. Since dichlorosilane undergoes decomposition to silicon at lower temperatures than trichlorosilane it would be an expected intermediate in silicon deposition. Decomposition of dichlorosilane may involve an  $\text{SiHCl}$  intermediate. This chemical specie would be too unstable to be identified in the gas composition. Formation of  $\text{SiCl}_2$  from dichlorosilane seems less likely, particularly for silicon formation in the vapor phase.

At high temperatures polysilanes probably do not enter into the chemical process steps due to the inherent instability of the Si-Si bond. They may be significant in low temperature decompositions below  $1000^\circ\text{F}$ .

### VIII. Dichlorosilane

Deposition of silicon using dichlorosilane as a feedstock in Siemens-type reactors is under investigation by Hemlock Semiconductor Corporation. The advantage of using dichlorosilane over trichlorosilane or silicon tetrachloride can be predicted from thermodynamic data. In addition, experiments carried out in an 18 inch reactor (12) have shown that addition of small amounts (10-15 weight percent) dichlorosilane to trichlorosilane can increase the deposition rate of silicon by as much as 30-40 percent. The advantages and disadvantages are outlined below:

#### I. Advantages over Trichlorosilane

1. Higher deposition rates
2. Lower temperature of decomposition. (Translates to lower power consumption).
3. Can be used at higher mole-percent concentrations in hydrogen.
4. Higher conversions to silicon.

#### II. Disadvantages Compared to Trichlorosilane

1. Homogeneous decomposition at high temperatures. More likely to deposit silicon on the quartz bell jar.
2. Higher cost due to an additional processing step (disproportionation).
3. Safety. Greater flammability. Lower autoignition temperature. Gas at room temperature.

Recent progress in the development of economical processes for dichlorosilane coupled with further resolution of difficulties inherent in its use for silicon deposition should make this chlorosilane a preferred starting material over trichlorosilane for high purity silicon.

### Bibliography

1. R. Schwarz and Ch. Danders; Chem. Ber., 80, 444 (1947)
2. E.O. Brimm, Unpublished Work (1947)
3. J.Y.P. Mui and D. Seyferth, "Investigation of the Hydrogenation of  $\text{SiCl}_4$ " Final Report. DOE/JPL-955382-79/8
4. J.D. Reedy, Unpublished Work (1972)
5. R.F. Lever, IBM J.Res. Develop., 8, 460 (1964)
6. L.P. Hunt and E. Sirtl, J. Electrochem. Soc., 119, 1741 (1972)
7. V.S. Ban and S.L. Gilbert, J. Electrochem. Soc., 122, 1382 (1975)
8. H.W. Patten, Unpublished Data (ca. 1960)
9. E. Sirtl, L.P. Hunt and D.H. Sawyer, J. Electrochem. Soc., 121, 919 (1974)
10. D. Laskafeld and T. Roznov, Int. Chem. Eng., 9, 440 (1969)
11. M. Bawa, R. Goodman and J. Truitt, SC Eng. J., 42 (1980)
12. N.R. Berlat, Unpublished Work (1972)

## DISCUSSION

5  
Y

DUDUKOVIC: Mass transfer is known to depend a lot on the reactor type used and on the gas injection geometry. If the conditions of the decomposer and the temperatures at which it operates are considered, the growth rates can be determined. Then, the rate of reaction per unit surface can be calculated and one can find out that the rate of reaction is very small. If a mass transfer coefficient is calculated from it, the coefficient would be very small. So for those gases at those temperatures and at a constant pressure it is expected to be higher. So it is possible that those reactions are still controlled by kinetics.

BAILEY: I'd like to comment as follows. Sirtl, Hunt and Sawyer have covered the conditions in their paper. I believe that one can characterize the reaction above 1200°C as being diffusion-controlled and below 1200°C as not diffusion-controlled. The basis for this statement is some Union Carbide data and the fact that there are different conditions used in the Siemens-type reactor. So that when there is a small boundary layer, when there is a very large differential between the temperature of the gas and the hot rod, when there is a large volume-per-surface ratio, when a high flow rate is used, and when there is a low trichlorosilane concentration, there will be a greater tendency for a surface-controlled reaction; and the reverse is true for the opposite conditions. I think that below 1200°C, just to pick a point, the reaction is more likely to be surface-controlled than controlled by chemical kinetics. For a reaction run above that temperature, the type of control will depend on the conditions. I would say though that if you were running a fluidized-bed reaction above 1200°C, you will have a reaction, for all intents and purposes, if you can measure it, which is under diffusion control but the diffusion is so simple that I doubt if the chemical kinetics are important even there.

DUDUKOVIC: Well, I tend to disagree a little. I think that there is so much surface in a fluid-bed reactor that for the first time there is a chance of running the reaction at equilibrium. Because the mass transfer coefficients are so much higher than in a CVD decomposer and especially so much higher than in an epitaxial reactor, there are probably no mass-transfer limitations. My understanding is that this myth of mass-transfer control above 1200°C started because people studied the decomposition very extensively in epitaxial reactors in which there are Reynolds numbers which range from 50 to 100, at the most. Therefore, the deposition is taking place at rates that are much lower than in a decomposer. In those reactors probably there are mass-transfer limitations. However, this does not mean that there are mass transfer limitations in a decomposer, especially not in a fluid bed. The reaction rate is about  $10^{-7}$  moles/cm<sup>2</sup> sec and if you calculate the mass transfer coefficient, assuming mass-transfer control, the coefficient would be very small.

BAILEY: Let me make one statement that may clarify this question. The chemistry has been reported. I have already said that I think that this boundary layer has a lot to do with the kind of chemical processing which will occur. The assumption has been made that the reaction takes place on the surface. When the kinetics are fast enough so that chemical reaction at the surface is faster than diffusion to the surface, there will be a diffusion-controlled mechanism. The conditions for this mechanism, however, remain to be established.

## Kinetics and Mechanism of the Silane Decomposition

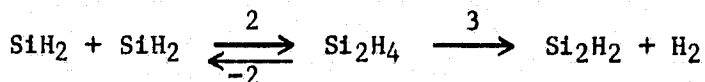
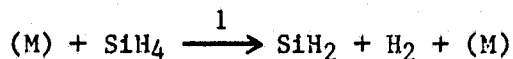
Morey A. Ring and H. Edward O'Neal  
San Diego State University  
San Diego, California 92182

The thermal decomposition of silane in static and flow systems ( $T = 400-600^\circ\text{C}$ ) progresses through several stages of changing rates, changing reaction orders, and varying products. In the initial stages (0-3%) the reaction follows  $3/2$  order kinetics and the principal products are  $\text{H}_2$  and  $\text{Si}_2\text{H}_6$ , trisilane is also formed at rates roughly an order of magnitude lower than those for disilane.<sup>1</sup> In later stages (5% and up), reaction rates become faster by factors of 3-5,<sup>1</sup> the products produced are mainly  $\text{H}_2$  and solid polymer, and reaction orders have been reported as 1.0 ( $400^\circ\text{C}$ , static system),<sup>1</sup> 1.5 ( $485^\circ\text{C}$ - $530^\circ\text{C}$ , flow)<sup>2</sup> and 0.75 ( $530$ - $589^\circ\text{C}$ , flow). Clearly the reaction is very complex and we are far from understanding it in any kind of detail. However, correlation of data from prior studies<sup>1,2</sup> with data of several recent studies in our laboratories (single pulse shock tube pyrolysis,<sup>3,4</sup> and our static system pyrolyses in the presence and absence of additives),<sup>5</sup> has, we feel aided in the identification of the reactions and intermediates involved in the two reaction stages. The purpose of this paper is to present our current thoughts on the silane pyrolysis system in both reaction stages.

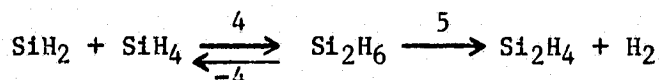
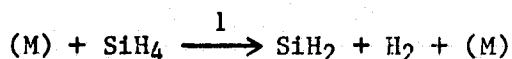
We can now say that, with regard to the initial reaction stage (0-3%), most aspects of the mechanism are reasonably well understood. The reaction is 'mainly' gas phase homogeneous and initiation is via a 3-center molecular hydrogen elimination reaction of silane in its pressure dependent regime. Silylene and hydrogen are the primary products, and the subsequent reactions are dominated by silylene reactions. This stage of the pyrolysis can be described by the following reactions.

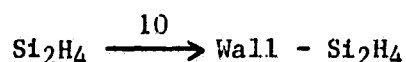
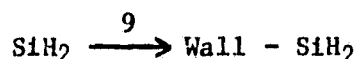
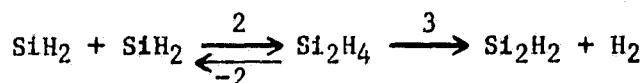
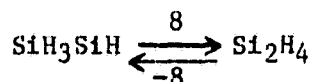
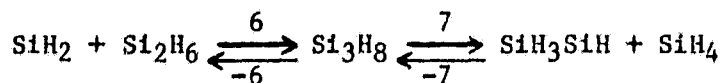
### Initial States of Reaction (0-3%)

#### shock tube (1100-1300 K)



#### static system (650-725 K)





The Arrhenius parameters of these reactions are given in Table 1. The Arrhenius parameters for the 1,2-H shift reactions for trisilane (rxn 6, rxn 7) and for disilane (rxn-4) are well established and require no additional discussion. The very important (to the silane decomposition mechanism) primary dissociation processes (rxn 1, and 3), do however, merit more attention. This is because rxn 1 is the dominant initiation reaction, and because rxn 3 provides both an important sink for  $\text{SiH}_2$  (when  $\text{Si}_2\text{H}_4$  is removed at the walls) and an additional source of  $\text{H}_2$  production.

We have demonstrated that rxn 1 is the initiation reaction of the decomposition.<sup>3</sup> Thus in the shock tube pyrolysis, in which only homogeneous unimolecular initiation reactions can occur, the decomposition kinetics gave at  $P = 4900$  torr,  $T = 1035\text{--}1184$  K,  $\log k_{\text{exp}} \text{SiH}_4 = 13.3\text{--}52.7/2.3\text{RT}$ . Such a low activation energy excludes single bond rupture ( $\text{SiH}_4 \rightarrow \text{SiH}_3 + \text{H}$ ) as the initiation reaction and demands a concerted process like rxn 1. Further, by performing RRKM fall-off calculations based on our SPST rate constant using different transition state models for rxn 1 it was found that with a high pressure limiting A-factor model of  $A_1(\infty) = 10^{15.5} \text{ sec}^{-1}$ , the RRKM predictions of the reaction rates for the

Purnell and Walsh conditions were in good agreement with their reported values. Also the RRKM calculated unimolecular rate constants showed a pressure fall-off in the P & W pressure and temperature range which matched very nicely their experimental 3/2 order reaction behavior. That this 3/2 order dependence is only apparent and also completely fortuitous was then demonstrated by studying the reaction under static conditions at constant total pressure but varying silane pressure. Under these conditions the reaction was found to be first order in silane, thus demonstrating conclusively that rxn 1 is a unimolecular process in its pressure dependent regime.<sup>3</sup>

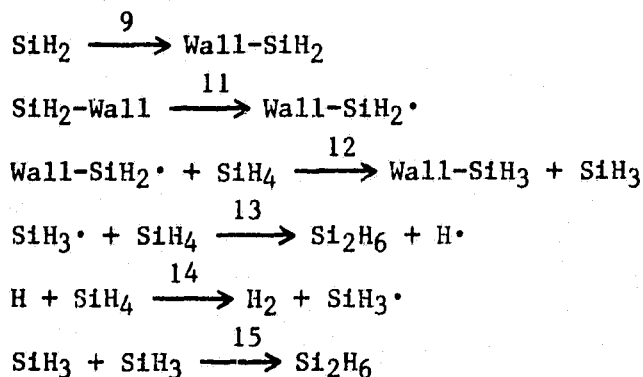
The shock tube pyrolysis of an equimolar  $\text{SiH}_4/\text{SiD}_4$  mixture gave statistical yields of  $\text{HD}/\text{D}_2/\text{H}_2$ , with an overall hydrogen yield of  $1.85 \pm 0.15$  and disilane was not a reaction product. This prompted us to propose that the silylene sink under shock tube conditions is the rxn (2,-2,3)<sup>3</sup> sequence. Confirmation of this sequence comes from a shock tube study of the disilane decomposition<sup>4</sup> ( $P \sim 2500$  torr,  $850\text{--}1030$  K). Here the constant yields of  $\text{SiH}_4$  (80%) and  $\text{H}_2$  (20%) over decomposition from 10-65% showed that two primary



ORIGINAL PAGE IS  
OF POOR QUALITY

dissociation reactions occur for disilane, rxns -4 and 5. But more important, at temperatures above about 970 K, hydrogen yields in the SPST disilane pyrolysis increased with increasing temperature; this is clearly due to the turning on of rxn 3. A computer modeling of the rxn system (rxns 4, -4, 5, 6, -6, 7, 8, -8 and 1) gave a good fit to the data for  $k_3 = 10^{14.5} \times e^{-53,000/RT} \text{ sec}^{-1}$ .

Statistical yields of  $\text{H}_2/\text{HD}/\text{D}_2$  have also been observed in the static system pyrolysis of equimolar mixtures of  $\text{SiH}_4/\text{SiD}_4$ .<sup>9</sup> This was originally attributed to the involvement of H atoms<sup>9</sup>, but after the SPST silanes study we suggested that as in the shock tube reaction, the statistical  $\text{H}_2/\text{HD}/\text{D}_2$  yields were probably due to the same silylene dimer formation-decomposition sequence (rxns 2, -2, 3)<sup>3</sup>. It is now clear that the revised hypothesis cannot be valid. Reaction 3 is too slow under static system conditions to be a significant source for  $\text{H}_2$  production. Thus the single most important question about the silane static system pyrolysis remains unanswered, i.e., what reaction is the silylene sink? Our recent static system studies strongly indicate that first order wall removal (rxn 9) is the static system pyrolysis silylene sink.<sup>5</sup> In addition, we also will provide data which suggests that silylene on the walls initiates silyl radical production, which in turn propagates a free radical chain reaction. The onset of this silyl radical chain is, we feel, the beginning of the second (or latter) reaction stage and is the cause of the higher reaction rates. Thus we feel the latter reaction stage of the static system silane pyrolysis can be represented by the following additional reactions:



Reactions 13-15, proposed originally by P & W,<sup>1</sup> are obviously consistent with the large HD yields. The data supporting wall removal of silylene (rxn 9) as the silylene sink rxn are shown in Table 2. The term of importance is the ratio,  $R = (\text{Si}_2\text{H}_6/\text{SiH}_4)$ , which we followed in time for reaction mixtures of varying total pressure at three different temperatures. We found the R increased in time to a maximum (at about 10% reaction) and then slowly decreased in value. The higher the reaction pressure, the higher the value of R at maximum\* (i.e.,  $R_{\text{max}}$ ). Also, as the data show,  $R_{\text{max}}$  increased about a factor of  $2.7 \pm .1$  over the  $64^\circ\text{C}$  temperature range of study. This rather minimal temperature dependence (corresponding to an activation energy of only about + 13 kcal) proves that reaction 9 is the silylene sink. The argument is as follows. When  $(\text{Si}_2\text{H}_6/\text{SiH}_4)$  reaches its maximum value, reactions 4, -4, 5 and

\*The  $R_{\text{max}}$  plateau regime also lasted for a longer time at high silane pressures

ORIGINAL PAGE 13  
OF POOR QUALITY

and 6,-6,7,-7 are clearly in steady state (and probably close to their equilibrium conditions). At this point the rate of production of silylene must equal its rate of removal by the sink reaction. In general terms then,

$$\text{Rate SiH}_2 \text{ formation} \approx k_1(\text{SiH}_4)^x = \text{Rate}(\text{SiH}_2) \text{ removal} \approx k_{\text{sink}} (\text{SiH}_2)^y (\text{SiH}_4)^z$$

Since reaction 4,-4 close to equilibrium, to a good approximation  $[\text{SiH}_2]_{\text{max}}$  is directly proportioned to  $R_{\text{max}}$ .

$$[\text{SiH}_2]_{\text{max}} \approx \left[ \frac{\text{Si}_2\text{H}_6}{\text{SiH}_4} \right]_{\text{max}} \times \frac{1}{K_{4,-4}} \approx R_{\text{Max}} \frac{1}{K_{4,-4}}$$

Substituting into the above equation and rearranging to solve for  $R_{\text{Max}}$  gives,

$$R_{\text{Max}} = \left[ \frac{k_1 [\text{SiH}_4]^{x-z}}{k_{\text{sink}}} \right]^{1/y} \times K_{4,-4}$$

Hence the temperature dependence of  $R_{\text{Max}}$  (at constant silane concentration) is given by,

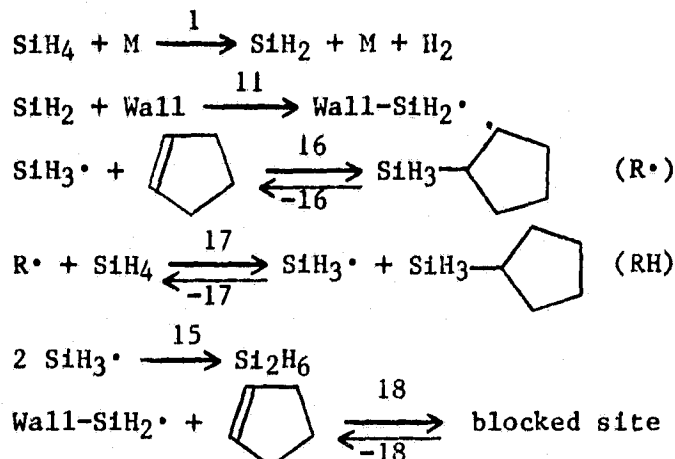
$$E_{\text{max}} = \frac{E_1 - E_{\text{sink}}}{y} + \Delta H^\circ_{4,-4}$$

Since silylene is formed only by reaction 1 and  $E_{\text{sink}}$  should be close to zero, and  $\Delta H^\circ_{4,-4} \approx -47$  kcal

$$E_{\text{Max}} = \frac{56-0}{y} - 47; E_{\text{Max}}(\text{exp}) \approx 13 \text{ kcal}$$

Hence the only reasonable value for the silylene reaction order (y) is y = 1, and the only reasonable first order silylene sink reaction is rxn 9. There are other interesting features to these data, but because of time and space limitations, these cannot be made here, rather we move on to the final important point which is the mechanism of the latter stages of the silane pyrolysis and the involvement of the silyl radical chain sequence (rxns 13-15). We are in the process of studying the static system silane pyrolysis in the presence of cyclopentenes. Preliminary data from this study are shown in Table 3. The main products are the usual ones (disilane, trisilane,  $\text{H}_2$ ), but silylcyclopentane (RH) is also formed. As in the neat system, disilane and trisilane rise to their maximum yield values (0-8% reaction), at which time the rate of silylcyclopentane formation accelerates. This product also eventually reaches a maximum (steady state) value (~ 20% reaction) and then slowly decreases. Of particular interest is

the correlation in silane disappearance rates with the onset of RH formation and its attainment of steady state. In the 3-30% reaction period the silane disappearance rates are 3-4 times faster than the silane initiation reaction. Beyond 40% reaction, the silane disappearance rates drop back to values very close to those calculated for rxn 1 alone.<sup>1</sup> Our current explanation of these observations is given by the following reactions.



RH is formed by the silyl radical chain 16,17, which is reversible. Hence RH formation ceases when the equilibrium condition is achieved. The silane decomposition falls back to the rate of rxn 1 when RH reaches maximum because the rate of silyl radical generation at the walls (rxn 12) is much reduced in the presence of cyclopentene (i.e., cyclopentene blocks the wall sites leading to silyl radical production (rxn 18,-18).

The data are consistent with this explanation. Thus experimentally, the rate of silane loss is about three times as fast as the initiation reaction 1. Therefore,

$$\frac{\text{Rate silane loss (by silyl chain)}}{\text{Rate silane loss (rxn 1)}} \approx \frac{2}{1} \approx \frac{k_{16}(\text{SiH}_3) \left( \text{Cyclopentene} \right)}{k_1(\text{SiH}_4)^{3/2}}$$

From this we calculate (using  $k_{16} \approx 10^{9.0} \times e^{-8,500/RT} \text{ M}^{-1} \text{ sec}^{-1}$ )  $(\text{SiH}_3)_{\text{ss}} \approx 1.1 \times 10^{-10} \text{ M}$  at  $673^\circ\text{K}$ . At steady state, Rate ( $\text{SiH}_3$  production by rxn 12) = Rate termination (rxn 15), and we can estimate the rate of rxn 12 to be about Rate 12  $\approx 1.3 \times 10^{-10} \text{ M sec}^{-1}$ . Since Rate 1 =  $k_1(\text{SiH}_4)^{3/2} \approx 8.1 \times 10^{-7}$ , it is clear that only about  $1.3 \times 10^{-10}/8.1 \times 10^{-7} = 1.6$  wall-SiH<sub>2</sub>·sites in  $10^4$  leads to silyl radical production.

It is very interesting to note that the rate acceleration in the silane disappearance for neat silane is very similar to that observed for the silane-cyclopentene reaction mixtures. This is an accidental result which occurs because of balancing factors. Thus while silyl production at the walls is much more efficient in neat silane (i.e., the active silylene absorption sites on the walls are not blocked by cyclopentene),

$$\text{*Rate (12)} = k_{15}(\text{SiH}_3)^2 \approx 1 \times 10^{10} (1.1 \times 10^{-10})^2$$

ORIGINAL PAGE IS  
OF POOR QUALITY

the silyl chain propagation is much slower in neat silane. Thus we estimated\*\* the propagation reaction in the silane-cyclopentene system to have a rate constant about  $k_{16} \approx 10^{9.0} \times e^{-8500/RT} \text{ M}^{-1} \text{ sec}^{-1}$ , and we estimate the rate constant for the propagation reaction in the neat silane system to be about  $k_{13} \approx 10^{10} \times e^{-18,000/RT} \text{ M}^{-1} \text{ sec}^{-1}$ \*\*\*.

It is also interesting to note that our suggested mechanism is in quantitative agreement with the latter stage rate observations. Thus using the P & W rate constants for silane disappearance via rxn 1, and using our estimated rate constant for the silyl chain propagation, and further assuming that every silylene produced by rxn 1 and removed at the walls generates a silyl radical by rxn 12, we calculate the reaction rates of silane disappearance shown in Table 4. The total rates at 653 and 703 K predict an activation energy of 50.2 kcal and an A-factor of  $8.5 \times 10^{12} \text{ sec}^{-1}$ . The observed values (by P & W) are  $A = 10^{13.2} \text{ sec}^{-1}$ ,  $E = 51.2 \text{ kcal}$ . We do not claim to have proven the mechanism of the static system pyrolysis of silane at this time. However, we do feel that the present mechanism is quite consistent with the experimental facts, and that it is a promising premise which is worth further experimental study.

REFERENCES

1. J. H. Purnell and R. Walsh, Proc. Roy. Soc., A, 293, 543 (1966).
2. G. Cochet, H. Mellottee and R. Delbourgo, J. de Chim. Phys. 71, 1363 (1974).
3. C. G. Newman, H. E. O'Neal, M. A. Ring, F. Leska and N. Shipley, Int. J. Chem. Kinetics, 11, 1167 (1979).
4. J. Dzarnoski, S. F. Rickborn, H. E. O'Neal and M. A. Ring, Organometallics (September 1982).
5. R. L. Espino-Rios, R. White, M. A. Ring, H. E. O'Neal, to be published.
6. I. M. T. Davidson, F. T. Lawrence and N. A. Ostah, J. Chem. Soc., Chem. Comm., 859 (1980).
7. M. Bowery and J. H. Purnell, Proc. Roy. Soc., A, 321, 341 (1971).
8. A. J. Vanderwielen, M. A. Ring and H. E. O'Neal, J. Am. Chem. Soc., 97, 993 (1975). 9. M. A. Ring, M. J. Puentes and H. E. O'Neal, J. Am. Chem. Soc., 92, 4845 (1970).
10. P. S. Neudorfl and O. P. Strausz, J. Phys. Chem., 82, 241 (1978).

\*\*By analogy with methyl radical addition to  $\pi$  bonds. This is not too unreasonable a model since the exothermicities of the methyl and silyl radical addition reactions should be similar.

\*\*\*This assumes  $A_{13} \approx 10^{11} \text{ M}^{-1} \text{ sec}^{-1}$  (very reasonable for an H-atm reaction which have steric factors near unity), and  $E_{13} \approx 2.0 \text{ kcal}$  (a guess).

TABLE 1

ORIGINAL PAGE IS  
OF POOR QUALITY

## Arrhenius Parameters for Silane Decomposition Reactions

Rx	log A	E <sub>act</sub>	Ref.
1	15.5 ± .4	59.6 ± 1.5	3 <sup>a</sup>
3	14.5 ± .6	53.0 ± 2.2	4
4	10.3	1.0	6 <sup>b</sup>
-4	14.4 ± .2	48.8 ± .3	7,4 <sup>c</sup>
5	15.3 ± .6	55.0 ± .2.2	4 <sup>d</sup>
-6	15.7 ± .3	53.0 ± .6	8
7	14.7 ± .3	49.2 ± .6	8

- a) The parameters listed are for the high pressure values ( $k_{\infty}$ ). Calculated<sup>3</sup> RRKM ratios for  $\text{SiH}_4$  are:  $k_1/k_{\infty} = 0.15$  and  $0.12$  at 80 torr ( $T = 650$  and  $710$  K, respectively);  $k_1/k_{\infty} = 0.36$  and  $0.30$  at 400 torr ( $T = 650$  and  $710$  K, respectively).
- b) The A factor is that calculated from the experimental value of  $A_{-4}$  and a calculated (but very reasonable) value for  $\Delta S_{4,-4}$ . The insertion of  $\text{Me}_2\text{Si}$  into the Si-H bond in  $\text{Me}_3\text{SiH}$  was examined in competition with surface polymerization between 410 and 510 K. No change in relative rates were observed.<sup>6</sup> Thus it appears that  $\text{Me}_2\text{Si}$  insertion into the Si-H bond has a near zero activation energy and  $\text{SiH}_2$  and  $\text{Me}_2\text{Si}$  seem to have very similar reactivities.
- c) These parameters are from an Arrhenius plot (550-1005 K) of static<sup>7</sup> and SPST<sup>4</sup> decompositions of disilane.
- d) These Arrhenius parameters were obtained from the experimental rate constant of the SPST decomposition of  $\text{Si}_2\text{D}_6$  along with an assumed A-factor based on the A-factor from the methylsilane decomposition.<sup>10</sup> The activation energy is in good agreement with one obtained from the SPST and static disilane data for the  $k_4/k_5$  ratio as a function of temperature.

TABLE 2

---

Values of  $R = \left( \frac{\text{Si}_2\text{H}_6}{\text{SiH}_4} \right)$  at Their Maxima<sup>a</sup> in the Pyrolyses of Silane<sup>b</sup>



---

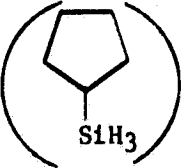
<u>Temperature</u>	<u>P(Total = 106 torr)</u>	<u>P(Total = 150 torr)</u>
367°C:	$R_{\text{Max}} = 6.6 \times 10^{-3}$	$R_{\text{Max}} = 9.0 \times 10^{-3}$
400°C:	$R_{\text{Max}} = 8.5 \times 10^{-3}$	$R_{\text{Max}} = 17 \times 10^{-3}$
430°C:	$R_{\text{Max}} = 17 \times 10^{-3}$	$R_{\text{Max}} = 26 \times 10^{-3}$
$\frac{R_{\text{Max}} (430^\circ\text{C})}{R_{\text{Max}} (367^\circ\text{C})}$ :	2.58	2.88

---

- a) The maxima were reached between 3-10% reaction. The lower the pressure, the earlier  $R_{\text{Max}}$  was established.
- b) Reactant mixtures were  $[\text{SiH}_4/\text{nBu}] = 10/1$ . The n-Butane was present as GLC internal analytical standard.

TABLE 3

SiH<sub>4</sub> Decomposition (SiH<sub>4</sub>/  /  = 52/40/8) Total Pressure = 342 torr,  
T = 400°C

Rx. Time min.	$\left( \frac{\text{Si}_2\text{H}_6}{\text{SiH}_4} \right)$	$\left( \frac{\text{Si}_3\text{H}_8}{\text{Si}_2\text{H}_6} \right)$		(% SiH <sub>4</sub> loss)
6	.013	.091	0.62	10.6
11	.023	.11	3.68	19.4
14	.026	.11	5.16	25.0
21	0.26	.10	6.96	34.0
30	.022	b	5.13	44.4
50	.021	b	6.31	49.5

a) Relative GC peak areas (uncorrected for sensitivity) with cyclohexane as the internal standard.

b) Peak observed but not integrated correctly.

TABLE 4

---

Results of Rate Constant Estimates for Latter Stages of the Silane Pyrolysis (Static System)

---

Silane Reaction Rate Components

<u>T(K):</u>	<u>Initiation</u> ( $M_{\text{sec}}^{-1}$ ) <sup>a,c</sup>	<u>Chain</u> ( $M_{\text{sec}}^{-1}$ ) <sup>b,c</sup>	<u>Total</u> ( $M_{\text{sec}}^{-1}$ )
653:	$5.6 \times 10^{-5}$	$7.2 \times 10^{-5}$	$1.28 \times 10^{-4}$
703:	$1.2 \times 10^{-3}$	$8.5 \times 10^{-4}$	$2.05 \times 10^{-3}$

---

- a) Rate constants (pseudo first order) for silane loss via the initiation reaction (rxn 1) for silane pressures of 335 torr.

$$k_{\text{initiation}}(\text{sec}^{-1}) = 2 k_1 (\text{SiH}_4)^{1/2}$$

- b) Rate constants (pseudo first order) for silane loss via the silyl radical chain sequence (rxns 13,14) for silane pressures of 335 torr.

$$k_{\text{chain}}(\text{sec}^{-1}) = 2 k_{13} (\text{SiH}_3) = 2 k_{13} \left[ \frac{k_1 (\text{SiH}_4)^{3/2}}{k_{15}} \right]^{1/2}$$

c)  $k_1 = 10^{15.2} \times e^{-55,900/RT} M^{-1/2} \text{ sec}^{-1}$

$$k_{13} = 10^{9.9} \times e^{-18,000/RT} M^{-1} \text{ sec}^{-1}$$

$$k_{15} = 10^{10.0} M^{-1} \text{ sec}^{-1}$$



## DISCUSSION

FLAGAN: I'd just like to mention a point that I raised after the meeting. You discussed at length the possible role of surface reactions, labeling them as wall reactions. However, since the time-scales for the formation of particles in the reacting system could be extremely short, the surface reactions might indeed be taking place on aerosol particles rather than on walls of the reactor.

RING: I thought about that point after you mentioned it. There is a high concentration of silane in the lower-temperature, static system. I wonder if silylene isn't trapped readily, so that the silylene concentration would be fairly small. At 400 to 500°C the dimerization reaction might be very slow and at the temperatures of about 450°C there may be essentially no dimerization taking place. The times are short in the shock tube. Here we think that the silylene dimerized to give  $\text{Si}_2\text{H}_4$ . So under static conditions at these lower temperatures in the shock tube I don't believe that we could get solid particles. If particles do form, the reactions could take place on their surfaces. I would like to make another comment. I mentioned some static disilane and trisilane kinetics measurements; the values given were always for the initial rates. Starting with disilane or trisilane for the kinetic studies, the rates were determined for about the first few percent of the reaction.

LUTWACK: Is there a way of shielding the wall so that you must use the particles in the gas phase and therefore can distinguish between the two mechanisms?

RING: That would be interesting.

FLAGAN: Instead of shielding the wall, one could simply introduce sufficient particles into the system to guarantee that the surface area of those particles would dominate. I could give you a reference where a study was conducted for a carbon system.

MILSTEIN: The other way to do it is to make the system very large so that the relative wall area is small compared to the volume.

BAILEY: Are you planning to do any other shock-tube work with some chlorosilanes?

RING: At the moment we are working with alkylsilanes, because they're easier to work with. We did start with chlorosilanes once and the trouble with the shock-tube work is that we have to open it up after every shock. As you all know, siloxanes form at low concentrations of chlorosilanes and we ended with siloxane and not chlorosilane. Now we are studying alkylsilane decompositions. It would be interesting to go to the halosilanes, but I think we would have a hydrolysis problem. We would have to either modify our shock tube or pump on it for a very long time in between shocks. So, I guess the answer is, right now, no.

BAILEY: What kind of a mechanism is involved in a thermal reaction between an olefin such as cyclopentene and trichlorosilane as compared with silane and cyclopentene? The purported mechanism is the homolytic cleavage of trichlorosilane into trichlorosilyl radical and the hydrogen radical and subsequent addition to the olefin. Hydrogen is presumably not a product of this cleavage in the presence of the olefin. These reactions can take place thermally in the range of 300 to 400°C. If a decomposition of trichlorosilane take place in the absence of the olefin, nothing is seen. So the purely thermal disassociation is very different than the reaction in the presence of an olefin.

RING: The SiH bond energy in trichlorosilane is about 91 or 92. You could not get silicon-hydrogen rupture at 400 or 500°C and certainly not at 300°C. So if trichlorosilane reacts with an olefin in the 300 to 400°C range it would almost look like it might well be bimolecular. We thought this might occur with silane in acetylene, and we've looked at the decomposition of vinyl silane and thought silane may add to the acetylene, but it doesn't. So at least for silane and acetylene at 400°C the radical reaction is faster than the bimolecular addition reaction.

## SESSION II GENERAL DISCUSSION

INGLE: I have a question for the group. When dichlorosilane is used for the preparation of a-Si, what is the H:Cl ratio in the product?

SCOTT: I don't have the answer; however, in the case of  $\text{SiH}_4$ , the question is how much H is in the a-Si product. It turns out that it is very temperature-dependent. So if one could deposit under conditions in which the Cl could be retained, for example at low substrate temperatures (plasma decomposition of a chlorosilane at a low substrate temperature), a fair amount of Cl would probably remain in the product, perhaps 1:1. But with higher temperature depositions, the Cl content would decrease if the Cl system behaves similarly to the  $\text{SiH}_4$  system.

INGLE: What about the Cl:H ratio?

SCOTT: I would guess that more Cl than H would be incorporated and that would be temperature-dependent, also.

BAILEY: There are a number of publications on the decomposition of certain halosilanes, such as bromosilanes and even iodosilanes. It is quite surprising that the polymeric substances obtained from the bromosilane reactants do not contain the bromine moiety but rather the hydrogen moiety. Using these precursors, then, the polymers which were prepared were comprised of hydrogen and silicon but no bromine. The reference is a monograph on the silicon to silicon; it deals mainly with organo-silicon chemistry.

### SESSION III: Particle Formation and Growth

FLAGAN (Chairman): This is the session on Particle Formation and Growth. We will have five papers. The work of the first paper was done at the Department of Physical Chemistry of the University of Stuttgart by Steinwandel, Dietz, and Hoeschele. The paper is entitled "Homogeneous Gas Phase Condensation of Silicon by Shock Wave Induced Decomposition of Silane" and will be presented by Jurgen Steinwandel. In the second paper, Bill Felder of AeroChem Research Laboratories will describe the Kinetics and Particle Growth in Silane Systems. Then, in the third paper, Don Pettit, who is a graduate student of chemical engineering at the University of Arizona, will present a paper co-authored with Tom Peterson. The title is "Submicron Particle Sizes." I will present the fourth paper; it is based on the thesis research of M. K. Alam, who is a graduate student working with me at Caltech. Don Pettit will give the final paper of this session. He will describe a new method for making optical particle measurements.

PRECEDING PAGE BLANK NOT FILMED

HOMOGENEOUS GAS-PHASE CONDENSATION OF SILICON  
BY SHOCK WAVE INDUCED DECOMPOSITION OF  $\text{SiH}_4$ .

by

J. Steinwandel\*, Th. Dietz, J. Hoeschele and M. Hauser

Department of Physical Chemistry  
University of Stuttgart, West Germany

Abstract

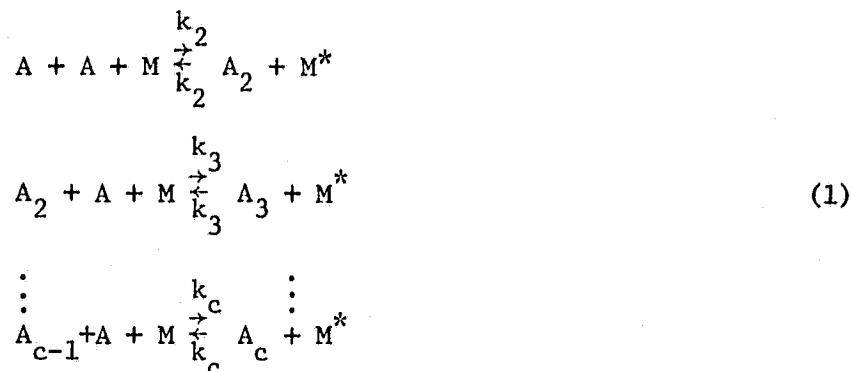
The gas phase condensation of silicon was studied using a membrane shock tube. Supersaturated silicon vapors were generated by thermal decomposition of  $\text{SiH}_4$  in strong shock waves. The initial compound concentration in the shock wave carrier gas argon ( $n_{\text{SiH}_4} < 5 \cdot 10^{15} \text{ cm}^{-3}$ ) was sufficiently low for the ideal shock tube operation equations to hold and isothermal reaction conditions to prevail during the phase transition. In varying shock wave temperatures and initial compound concentration in the carrier gas, various supersaturated states of atomic silicon vapor were produced in the region between incident and reflected shock waves. The vapor condensed to form small silicon clusters with a maximum size of about 50 Å during the undisturbed observation time of 2 msec. The rate of formation of the clusters was detected using atomic ( $\text{SiI}$ ) and molecular ( $\text{Si}_2$ ) spectroscopy and dynamical extinction measurements ( $\text{Si}$ -clusters) respectively. Our experimental data cannot be described by the classical theory of homogeneous nucleation; we have instead used a simple kinetic model based on classical collision theory assuming a constant number of growing particles. Due to the spectroscopic identification of the  $\text{Si}_2$ -molecule, we assume this number to be the equilibrium concentration of the molecule.

Introduction

The formation of a new phase appearing in a homogeneous medium is important in various fields. Phase transitions must be considered in meteorology, where the condensation of water dominates in the physical-chemical processes of the lower atmosphere. Gas phase reactions related to the condensation in metal vapors are important in metallurgy. An understanding of small clusters of metals and metal compounds produced by the physical-chemical processes of the vapor-liquid/solid phase transition is also important for a complete understanding of the interstellar chemistry. Condensation reactions from the gas-phase are further important in thin film technology; in particular, silicon condensation processes are of increasing practical importance in the context of the production of  $\alpha$ -silicon for solar energy conversion. Phase transitions are usually classified as first, second or higher order depending on whether the first, second or a higher derivative of the free energy functions describing the phase equilibria possesses a discontinuity. A first-order transition is therefore characterized by a discontinuity in entropy and volume according to  $(\partial G / \partial T)_p = -S$  and  $(\partial G / \partial p)_T = V$  at the transition point. All gas-phase condensation processes therefore are first-order phase transitions and the entropy discontinuity is related to the latent heat of the transition.

\* Applied Mechanics, Yale University, New Haven, CT 06520.

According to the classical theory of homogeneous nucleation (Volmer, 1939, Becker and Doering, 1935), a supersaturated homogeneous vapor can condense only if, in equilibrium prevailing prior to condensation, small particles of the new phase are formed by statistical fluctuations, resulting in a local decrease of entropy. The nucleation process must be assumed as follows:



the subscript c denotes the so-called critical cluster assumed to be in metastable equilibrium with the supersaturated vapor, and its rate of dissociation is equal to its rate of growth. The classical nucleation theory (capillary approximation) relates the formation of a critical cluster to the mechanical work necessary for the formation of a liquid surface:

$$\Delta W = \frac{1}{3} \sigma \Omega \quad (2)$$

where  $\sigma$  is the surface tension and  $\Omega = 4\pi r_c^2$  is the critical cluster surface area.

The radius  $r_c$  of the critical cluster as a function of  $\sigma$  and the degree of supersaturation  $n/n_\infty(T)$ , where  $n_\infty(T)$  is the flat surface equilibrium density of the vapor, is assumed to be given by the Gibbs-Thomson equation:

$$r_c = \frac{2m\sigma}{k_B T \rho} (\ln n/n_\infty(T))^{-1} \quad (3)$$

where  $m$  is the monomeric mass and  $\rho$  the bulk material density. The kinetic treatment finally leads to the expression of the rate of formation  $J$  in  $\text{cm}^{-3} \text{sec}^{-1}$ :

$$J = Z \exp \left\{ - \frac{16 \pi}{3 \ln(n/n_\infty)^2} \frac{m^2 \sigma^3}{\rho^2 (k_B \cdot T)^3} \right\} \quad (4)$$

where  $Z$  is the collision frequency of the dimension of  $J$ . It can be seen, that  $J$  depends strongly on the quantities  $n/n_\infty(T)$  and  $\sigma$ . Especially in the case of metal clusters, the latter is poorly known and the classical theory is therefore subject to fundamental errors if applied to metal condensation, even ignoring the fundamental doubts in the validity to small clusters of the thermodynamic and kinetic concepts of the theory.

#### Experimental procedure

In order to generate supersaturated silicon vapors, we decomposed the volatile compound  $\text{SiH}_4$  using strong shock waves. The shock waves were generated in a membrane shock tube (diameter 12.7 cm) having 3.6 m length of the driver section and 5.4 m in length of the driven section (shock wave side). A view of the mechanical setup and gas handling instrumentation is shown in

Fig. 1. Driver gas was 99.999% helium, shock wave carrier gas was 99.999% argon. Variable amounts of  $\text{SiH}_4$  could be added to the carrier gas as shown in Fig. 1. Concentration of  $\text{SiH}_4$  in the carrier gas did not exceed 0.5%  $n_{\text{Ar}}$  and we therefore can assume ideal shock tube operation and isothermal reaction conditions. The shock

wave is produced by rupturing the diaphragm which originally separates the two shock tube parts having different pressures. ( $p_{\text{He}} \leq 10$  at,  $p_{\text{Ar}} \leq 20$  torr) The shock wave is an entropy discontinuity travelling with supersonic speed into the test gas  $\text{Ar}/\text{SiH}_4$ . The discontinuity results in an increase in temperature and pressure of the gas through the shock front to constant variables behind it. The shock wave Mach number  $M = u_s/a_s$ , where  $u_s$  is the shock speed and  $a_s$  the sound speed of the gas in front of the shock wave, was measured using platinum resistance elements connected to differential amplifiers giving impulses due to the shock wave arrival at the elements. Shock wave damping could also be measured and only experiments with less than 1% damping were used for analysis, so that the ideal gasdynamic equations (Oertel 1966) could be applied. Constant temperature  $T_2$  is maintained for an undisturbed observation time of about 2 msec. Particle formation was detected by optical spectroscopy as shown schematically in Fig. 2. For absorption and extinction measurements (Si, Si-clusters), a Xenon-plasma lamp (450 watt) was used. Emission spectra were recorded without the lamp. Time-dependent measurements were detected by the two simultaneously operated monochromators and photomultipliers recorded by a two-channel transient recorder. A separate marker channel of the recorder detects the impulses of the platinum resistance elements for shock speed determination (see rectangular marks at the bottom of Fig. 6).

The detection of silicon atoms

Silicon atoms were detected using the technique of integral resonance absorption spectroscopy as reported by Naumann and Michel (1972) and Steinwandel et al. (1981). We used the Si-atomic (SiI) resonance transition  $3P_1 \rightarrow 3P_0$  at 251.621 nm. In the following, we outline the manner in which measurements on the integral absorption of isolated spectral lines were used for

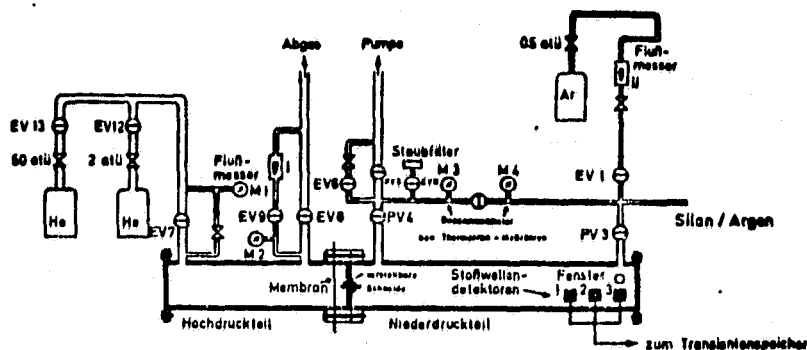


Fig. 1 Schematic of shock tube arrangement

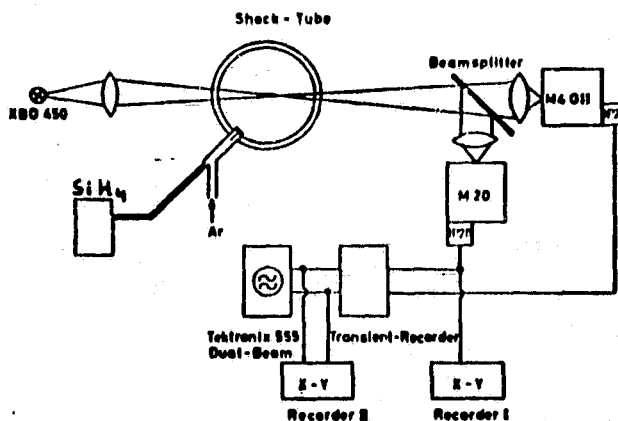


Fig. 2 Schematics of optical detection instrumentation

determining the combination of the two quantities:

- a) The population density  $n_i$  of the lower state of the observed optical transition at wavelength  $\lambda_i$
  - b) the line-broadening cross section  $\sigma_L$  which represents the efficiency of silicon-argon collisions in broadening the spectral line.
- Assuming uniform density of absorbing species over the shock tube diameter  $\ell$ , the spectral absorption behind a gas layer of thickness  $\ell$  at a distance  $\Delta \lambda$  from the line center is given by:

$$I(\Delta \lambda)/I_0 = e^{-k(\Delta \lambda) \cdot \ell} \quad (5)$$

where  $k(\Delta \lambda)$  is the absorption coefficient and  $I_0$  the primary intensity of the light. The integral absorption measured at the slit of the detecting monochromator is then governed by  $k(\Delta \lambda)$  and, in addition, the slit function  $g(\Delta \lambda)$ . One obtains for the integral absorption in percent:

$$A = 100 \cdot \left[ 1 - \frac{\int_{-\infty}^{\infty} g(\Delta \lambda) \exp[-\ell \cdot k(\Delta \lambda)] d(\Delta \lambda)}{\int_{-\infty}^{\infty} g(\Delta \lambda) d(\Delta \lambda)} \right] \quad (6)$$

if the transmission maximum is at the wavelength center. Under the present experimental conditions,  $A$  is exclusively governed by regions in the line profile, which are dominated by collision broadening due to Ar-Si-interactions. Then,  $k(\Delta \lambda)$  is given by:

$$k(\Delta \lambda) = r_0 \frac{\bar{v}}{2\pi c} \lambda_i^4 f_i \sigma_L n_{Ar} n_{Si} (\Delta \lambda)^{-2} \quad (7)$$

where  $r_0$  is the classical electron radius,  $\bar{v}$  the mean relative collision velocity,  $c$  is the speed of light,  $n_{Ar}$  and  $n_{Si}$  are the corresponding number densities;  $f_i$  is the oscillator strength of the electronic transition. For the analysis, all quantities in Eq. (7) except  $n_{Si}$  are known and with the measured integral absorption, we found the ground-state population density  $n_{Si}$  to be  $10^{14} \text{ cm}^{-3} \leq n_{Si} \leq 10^{15} \text{ cm}^{-3}$  behind the shock waves. In the analysis, we have neglected contributions of natural dumping and Si-Si resonance broadening. The latter can be assumed if the density ratio Si/Ar does not exceed about  $5 \cdot 10^{-3}$ , which is the case for the present experiments.

#### The detection of silicon dimers

Spectra of diatomic molecules are much more complex than the atomic spectra. This is due to the additional degrees of freedom of vibration and rotation resulting in a high variety of the electronic transition possible.

An electronic transition in a diatomic molecule is related to a change in the vibration and rotation quantum numbers. For the term energies, one writes:

$$T = (T'_e - T''_e) + (G'_v - G''_v) + F'_j - F''_j \quad (8)$$

where  $T'_e$ ,  $G'_v$  and  $F'_j$  are the electronic, vibronic and rotational levels of the higher energy terms and  $T''_e$ ,  $G''_v$  and  $F''_j$  those of the lower energy terms. The factors  $G_v$  and  $F_j$  are given by the following series:

$$G_v = \omega_e \left( v + \frac{1}{2} \right) - \omega_e x_e \left( v + \frac{1}{2} \right)^2 + \dots \quad (9)$$



$$F_j = B_j(j+1) - D_j^2(j+1)^2 + \dots \quad (10)$$

where  $\nu$  is the vibrational and  $j$  the rotational quantum number.  $\omega$  is the ground state vibration wave number.  $x_e$  is the first evaluation coefficient for the anharmonic oscillator.  $B$  is the rotational constant,  $D$  the first evaluation coefficient for the non-rigid rotor both given in wave number units. The difference in the electronic terms ( $T'_e - T''_e$ ) is a constant and given by the difference in the zero-energy levels of the two potential curves under consideration ( $\nu' = \nu'' = 0$ ).

We used the X-H band of the silicon dimer molecule for identification (Huber-Herzberg, (1979), Suchard (1976)). We have calculated the potential energy curves of the state  $^3\Sigma_u^-$  (excited state) and  $^3\Sigma_g^-$  (ground state) by the method of Rydberg, Klein and Rees. The result is shown in Fig. 3. The

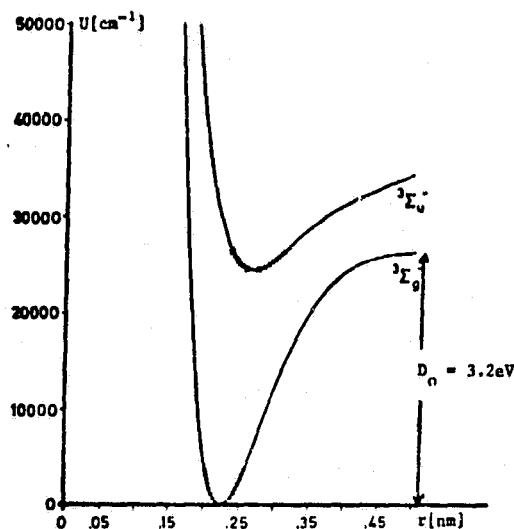


Fig. 3 Potential energy curves for the  $\text{Si}_2$  X-H transitions calculated by the RKR-method

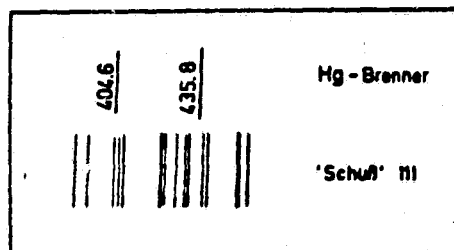


Fig. 4 Experimental  $\text{Si}_2$  X-H spectrum with Hg-calibration lines

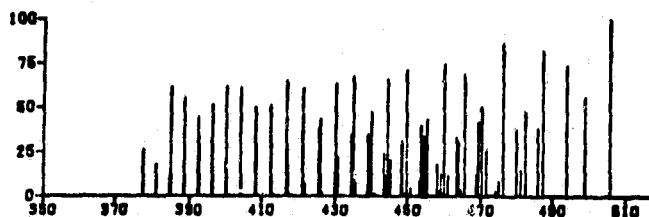


Fig. 5 Calculated X-H spectrum and relative intensities of electronic transitions

potential energy curves are of interest not only in calculating the term energies, but also for a calculation of the intensity distribution of the spectral lines. For a reliable identification of the  $\text{Si}_2$ -molecule, the intensity distribution is also required and we have therefore calculated the Franck-Condon factors for the X-H transitions by quantum-mechanical methods. Calculated optical transitions and corresponding Franck-Condon factors are shown in Fig. 5. An integral photographic spectrum of the X-H-band with mercury calibration lines is shown in Fig. 4. The line emission intensities cannot be explained by simple thermal activation of the molecule at temperatures below 3500 K and we therefore have to assume a chemiluminescence process due to the reaction  $\text{Si} + \text{Si} \rightarrow \text{Si}_2 + h\nu$ , where the release in reaction enthalpy results in the emission of a photon. It can be seen from Fig. 3, that highly vibronic excited states of the ground-state  $^3\Sigma_g^-$  can have a resonance coupling with low vibronic energy levels of the electronic excited state  $^3\Sigma_u^-$  which is a required condition for a chemiluminescence process. Time-

dependent measurements of the  $\text{Si}_2$ -emission show that the molecule is present immediately behind the shock wave within the principal gasdynamic time resolution of 1  $\mu\text{sec}$ . We suggest that the reaction equilibrium  $\text{Si} + \text{Si}_2^{\text{KP}} \rightleftharpoons \text{Si}_2$  is reached within this time.

#### The detection of silicon clusters

It is not possible yet to detect the smaller silicon molecules like  $\text{Si}_3$ ,  $\text{Si}_4$  ... because the electronic spectra of this species are not known. It is instead possible to detect clusters once they have grown up to sufficiently high population numbers allowing the optical behavior to be described by the optical properties of the liquid or solid material. The optical behavior of small particles in scattering and absorbing electromagnetic radiation can be expressed in terms of the complex refractive index of the particles using the general Mie theory (1908), which can be applied for particles of any size assuming spherical shape. The radius and the complex refractive index  $m = n - ix$  of the particle dominates the amount of electromagnetic radiation which is scattered and absorbed from an incident light beam. The complex refractive index  $m$  with its real part  $n$  and its imaginary part  $ix$  is for all substances a function of the wavelength and therefore  $m(\lambda) = n(\lambda) - ix(\lambda)$ . For metal-like particles,  $m(\lambda)$  is characterized by a considerable contribution of the imaginary part  $ix(\lambda)$  and this is due to the excitation of the plasma electrons of the metal. The combined process of scattering and absorption, where in the case of small metal particles the absorption dominates substantially, is called the extinction. In Fig. 6, we have shown such an extinction measurement of growing silicon clusters, simultaneously recording the growth process at two different wavelengths ( $\lambda_1 = 254 \text{ nm}$ ,  $\lambda_2 = 365 \text{ nm}$ ). The increasing signals in Fig. 6 mean increasing optical extinction by the absorption of the clusters. The time dependent extinction intensity can be correlated to the radius development of the clusters which will be outlined in the following; the extinction is defined by:

$$\begin{aligned} - \ln I/I_0(\lambda, r) &= E(\lambda, r) \\ &= \sigma_{\text{ext}}(\lambda, r) \cdot n \cdot \ell \quad (11) \\ &= \pi r^2 Q_{\text{ext}}(\lambda, r) \cdot n \cdot \ell \end{aligned}$$

where  $I$  is the incident light intensity of wavelength  $\lambda$ ,  $r$  is the radius of the droplets (assuming a delta distribution) present in the concentration  $n$ ,  $\sigma_{\text{ext}}$  is the photon extinction cross section and  $Q_{\text{ext}}$  the extinction efficiency factor;  $\ell$  is the optical path. Mass conservation during the condensation process leads to clusters, assumed to be of spherical shape.

$$(n_0 - n)m_{\text{at}} = \frac{4}{3} r^3 n \cdot \rho \quad (12)$$

where  $n_0$  is the initial monomeric density and  $n$  the monomeric density at the

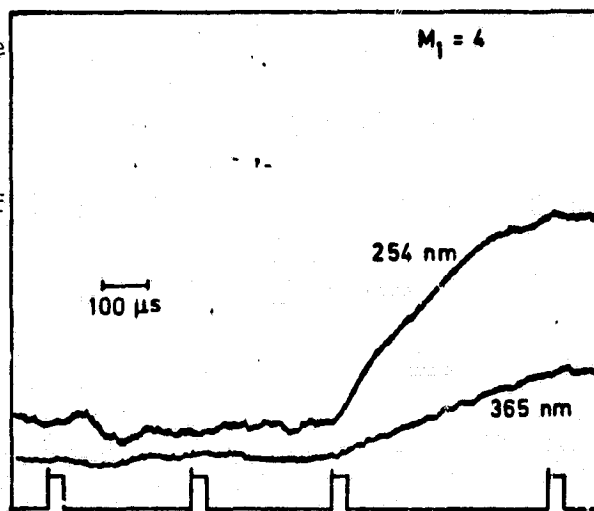


Fig. 6 Growth of silicon clusters by dual trace optical extinction measurement

ORIGINAL PAGE IS  
OF POOR QUALITY

time of observation.  $\rho$  is the density of the bulk material.  $m_{at}$  is the monomeric mass. A combination of Eq.(11) and (12) leads to:

$$r = \frac{3}{4} \frac{m_{at}(n_o - n) \cdot \ell}{\rho} \cdot \frac{Q_{ext}}{E} \quad (13)$$

the simultaneous measurement at two different wavelengths leads to:

$$\begin{aligned} r &= \frac{3}{4} \frac{m_{at}(n_o - n) \cdot \ell}{\rho} \cdot \frac{Q_{ext}(\lambda_1)}{E_1} \\ r &= \frac{3}{4} \frac{m_{at}(n_o - n) \cdot \ell}{\rho} \cdot \frac{Q_{ext}(\lambda_2)}{E_2} \end{aligned} \quad (14)$$

the efficiency factors  $Q_{ext}(\lambda_1)$  and  $Q_{ext}(\lambda_2)$  as a function of the wavelength and the radius were calculated from general Mie-theory using the complex refractive index at the particular wavelength. Because the radius at a given observation time is equal for both observation wavelength, (14) reduces to a simple expression:

$$\frac{Q_{ext}(\lambda_1)}{E_1} = \frac{Q_{ext}(\lambda_2)}{E_2} \quad (15)$$

where  $E_{1,2}$  are known from the experiment. From the known radius-dependence of  $Q_{ext}$ , the final radius of the particles at a given time can be found, fulfilling Eq.(15). This method can only be applied in the region in which Mie-oscillations in  $Q_{ext}$  do not occur. This is the case for the present experiments and with this method we found radii up to 50 Å at the end of the observation time of about 2 msec.

The measured radius development is consistent with the kinetic description of the growth process which assumes constant total mass of the condensing system, constant concentration of growing particles where this concentration is produced instantaneously and given by the dimer equilibrium concentration, and further that the particles have spherical shape. The monomeric flux to a cluster of radius  $\hat{r}$  present at a number density  $\hat{n}$  is given by:

$$i_1 = (n_o - \hat{n}) \hat{r}^3 \frac{4\pi}{3 v_1} \bar{v} \pi \hat{r}^2 \quad (16)$$

where  $n_o$  is the initial monomeric density, and  $v_1$  the cluster volume. The change in time in the actual monomeric density is given by:

$$d n_1 / dt = - \hat{n} i_1 \quad (17)$$

where  $n_1$  is given by the bracket expression in Eq. (16). The increase in volume of condensed matter is now given by:

$$d\bar{v}/dt = v_1 n_1 \bar{v} \pi \hat{r}^2 \quad (18)$$

and the corresponding change in radius:

$$d\hat{r}/dt = 0.25 \bar{v} v_1 n_o - \hat{n} \left( \frac{\hat{r}}{r_1} \right)^3$$

$$= \frac{1}{3} \pi \hat{n} \bar{v} (a^3 - \hat{r}^3) \quad (19)$$

where  $a^3 = r_1^3 n_0 / \hat{n}$ . The differential Eq.(19) can be solved analytically giving the functional dependence of  $t$ , and momentum radius  $R$  to be:

$$t = \frac{1}{a^2 \hat{n} \pi \bar{v}} \left[ \ln \frac{(R-a)(a^2 + ar + r^2)}{(r-a)(a^2 + aR + R^2)} + \frac{1}{\sqrt{3}} \left( \operatorname{atn} \frac{2r+a}{a\sqrt{3}} - \operatorname{atn} \frac{2R+a}{a\sqrt{3}} \right) \right] \quad (20)$$

The implicit function  $R(t)$  is shown in Fig. 7 calculated for an initial silicon monomeric density of  $10^{14} \text{ cm}^{-3}$ . The corresponding  $\text{Si}_2$ -density at temperature  $T = 2500 \text{ K}$  of about  $10^{12} \text{ cm}^{-3}$  was calculated from the tabulated values of the dimerisation equilibrium  $\text{Si} + \text{Si} \xrightleftharpoons{K_p} \text{Si}_2$  (JANAF, 1971). The time constant of the growth process as given by Eq.(20) in the kinetic description of the condensation is mainly governed by the initial monomeric concentration  $n_0$  and the effective concentration  $\hat{n}$  of particles assumed to grow further. As the initial monomeric density is known in the experiments, only the assumption of dimers present in their equilibrium concentration defined by  $K_p$  appears to be capable of correlating the theoretical and experimental time constants.

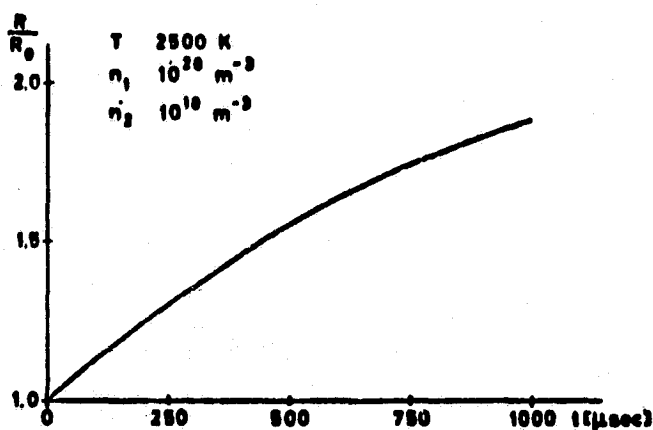


Fig. 7 Calculated particle growth process

The temperature influence in  $\bar{v}$  is given by

$$\bar{v} = \left[ \frac{8 k_B \cdot T}{\pi} \left( \frac{1}{m_{\text{Si}}} + \frac{1}{m_{\text{Si}_n}} \right) \right]^{\frac{1}{2}} \quad (21)$$

In the temperature range of interest ( $1500 \text{ K} \leq T \leq 3000 \text{ K}$ ), Eq.(21) shows that the influence on  $\bar{v}$  is minimal.

### Conclusion

The classical theory of homogeneous nucleation does not contribute to the fact that dimer molecules can be present in a considerable amount compared to the monomeric concentration of a condensing vapor. We have identified the  $\text{Si}_2$  molecule in the condensation processes and shown that the experimental time constants of the reaction can be explained by a kinetic model based on classical collision theory introducing the equilibrium concentration of silicon dimers at given temperature and initial monomeric pressure in Eq. (20). The resulting dimer concentrations can reach up to 1% compared to the monomers and this number must be considered as too high for the thermodynamic and kinetic treatment of the classical theory to hold. In addition, as there

is no physical-chemical relevance in describing the formation of a dimer molecule by any extrapolation of macroscopic surface tension values, we assume the classical theory to be inapplicable to the present experiments. It should further be noted that, according to the basic thermodynamic and kinetic concepts of this theory, critical nuclei should be formed by statistical fluctuations, where the rate of these fluctuations is given by Eq.(4). As the term  $\ln(n/n_\infty)$  in Eq.(4) decreases, finally approaching zero, so does the nucleation rate. This should result in highly increased induction periods for condensation to be detected, after the shock wave has passed the observation station and silicon atoms are produced by the decomposition of  $\text{SiH}_4$ . There is no experimental evidence for this fact. In all experiments where we could detect a gas phase condensation, this process starts immediately behind the shock wave. This seems to us to be supportive of the assumption that silicon dimers affect the condensation in a manner quite different from that usually assumed in thermodynamic and kinetic treatments of nucleation theories.

#### Acknowledgement

This work was supported by the "Fonds der Chemischen Industrie" and by a Feodor-Lynen Fellowship of the Alexander-von-Humboldt Foundation for J. St, which made this work possible.

#### References

- R. Becker and W. Doering, Ann. Phys. 24, 719 (1935).
- K.P. Huber and G. Herzberg, IV Constants of Diatomic Molecules, van Nostrand N.Y. (1979).
- JANAF, NSRDS-NBS 37, Washington 1971.
  - 1974 Supplement: J. Phys. Chem. Ref. Data 3, 311.
  - 1975 Supplement: J. Phys. Chem. Ref. Data 4, 1.
  - 1978 Supplement: J. Phys. Chem. Ref. Data 7, 793.
- G. Mie, Ann. Phys. 25, 377 (1908).
- F. Naumann and K.W. Michel, Z. Phys. 255, 348 (1972).
- H. Oertel, "Stossrohre", Springer, Wien, N.Y. (1966).
- J. Steinwandel, Th. Dietz, V. Joos and M. Hauser, Ber. Bunsenges, 8, 85 (1981).
- S.N. Suchard, "Spectroscopic constants for selected homonuclear diatomic molecules", SAMEO-TR-76-31, Los Angeles (1976).
- M. Volmer, "Kinetik der Phasenbildung", Steinkopff, Dresden (1939).

## DISCUSSION

LUTWACK: Could the light emitted due to thermal excitation of the silicon atoms at high temperatures hide the other phenomenon that you are trying to see because you are getting an increase in light?

STEINWANDEL: No.

GODDARD: I would have guessed that rather than having a gas-phase reaction for the formation of silicon particles by decomposing the silane all the way down to silicon atoms and recombining them to make  $\text{Si}_2$ , etc., that the process would involve, for example, the formation of silylene which then attacks silane to make an  $\text{Si}_2$  species. When the pressure is not too high,  $\text{H}_2$  can be eliminated to make a silylene and to yield silicon species that have hydrogen. By gradually losing hydrogen, larger and larger species form. These eventually form a silicon cluster from which a moderate amount of hydrogen can be lost by dehydrogenation processes. The dominant pathway would not be to make silicon atoms and then  $\text{Si}_2$ , etc. This reaction path would be more analogous to what has been observed in other systems.

STEINWANDEL: I see the point, but I would say at temperatures of about 3000 or 3500°K, these polysilicon species should exist; but yours is a possible explanation.

RING: Just a comment on your mechanism versus ours. Even at only 1800°C, which is before your reflection wave, the SiH bond rupture would be  $10^6$  to  $10^7$  times faster at 1800°K than compared to, say, 1200°C. So, I think it's not surprising that your mechanism and ours are different. I think this relates to his other point. At these temperatures, these single unimolecular reactions are awfully fast.

PETTIT: Why do you use Mie theory, a more complicated theory, for these 50 Å particles which could be handled with a Rayleigh-scattering regime?

STEINWANDEL: Well, that's very easy to answer, because we have a Mie program, and therefore we use this. It saves us a Rayleigh calculation; that's the only thing. One could, of course, use the Rayleigh approximation. We didn't know, a priori, which kind of particles we had to expect, and therefore to be safe, we used the Mie calculations.

PETTIT: Well, a lot of these Mie programs become unstable when you get to real small particle sizes. I was wondering whether you noticed that when you were using it for particles in the range of 50Å?

STEINWANDEL: Yes, we checked our particular Mie program, and it is stable at the Rayleigh approximation.

# KINETICS OF PARTICLE GROWTH IN SILANE SYSTEMS

by

C.R. Dickson\* and W. Felder  
AeroChem Research Laboratories, Inc.  
Princeton, N.J.

## INTRODUCTION

The objective of this exploratory work was to provide kinetic and mechanistic information on the formation and growth of silicon particles arising from the pyrolysis of silane ( $\text{SiH}_4$ ) gas. Experiments were carried out in heated, dilute, flowing mixtures of  $\text{SiH}_4$  in Ar to determine the sizes and rates of growth of silicon particles, the rates of growth of silicon seed particles, the amount of  $\text{SiH}_4$  decomposed, and the number of particles formed. Thus, the studies encompassed the homogeneous decomposition of  $\text{SiH}_4$ , gas-surface interactions, and particle growth phenomena. Detailed investigations of these processes were not intended; rather, an overview of the mechanisms and the time and temperature dependences were sought. The work reported here also was aimed at demonstrating the utility of the flow tube method for providing kinetic information on gas particle systems.

The experiments were carried out in the AeroChem High-Temperature Fast-Flow Reactor [1]. The HTFFR is a heated flow tube device designed for rate coefficient measurements on gas and gas particle systems over wide temperature ranges (300-2000 K). It permits independent control of reactant concentrations, total pressure, temperature, and residence time. In this work, particle sizes were determined as functions of these experimental parameters using in situ laser light absorption and scattering. Silane decomposition was measured by comparing inlet and outlet  $\text{SiH}_4$  concentrations. In some experiments, particle samples were withdrawn to compare the sizes measured by the optical diagnostics with those measured by electron microscopy.

Two results of this work appear applicable to technologies for the production of silicon from the pyrolysis of  $\text{SiH}_4$ :

1. Particle growth rates increase with increasing temperature. Thus, higher process temperatures will probably favor the growth of larger particles.

2. Particle growth rate appears to be independent of silane concentration. Thus, at a given temperature, addition of silane to a process will result in formation of additional particles rather than in the growth of larger particles.

---

\* Present address: RCA Sarnoff Laboratories, Princeton, N.J.

Although the results demonstrate that useful kinetic information can be obtained using the flow tube technique for studying gas particle systems, several questions remain unanswered. More detailed experimental measurements are needed to verify the basic conclusions stated above and to compare these measurements with the work of others on silane decomposition and silicon particle growth. In particular, a quantitative particle sampling system is needed to determine particle concentrations more accurately than the semi-quantitative methods we used. This sampling system should be combined with more detailed absorption or forward scattering measurements than were made in this work to provide real-time, calibrated, in situ particle concentration values.

## EXPERIMENTAL

The AeroChem HTFFR used has been described in detail elsewhere [1]. Briefly, the apparatus, shown schematically in Fig. 1, consists of a resistance-heated tube through which gas flows. The gas is preheated by contact with the hot walls in the upstream portion of the 2.5 cm i.d. high purity alumina reaction tube and achieves a uniform, selectable temperature in the downstream sections. Additional heat may be applied to these sections to maintain a uniform axial temperature profile. Typically, temperature uniformity is better than  $\pm 3\%$  in the 1000-1800 K range. The uniform temperature region includes the optical ports and extends ca. 12 cm downstream of these ports. Temperatures are measured [1,2] using a movable Pt vs. Pt/10% Rh thermocouple.

Reagents are introduced to the heated gas flow through a movable, water-cooled inlet. The time base for the measurements is established by the position of the reagent inlet and the (known) constant velocity gas flowing in the heated tube. The inlet could be positioned anywhere up to 30 cm upstream of the observation ports. Room temperature  $\text{SiH}_4$  could be delivered into the heated Ar flow at any point in this region.

Optical observations were made through coplanar, mutually perpendicular (1 cm diam) ports. Figure 2 shows the observation plane layout schematically. A 1 mW He-Ne or a 0.1 W argon ion laser beam was chopped at 1 kHz and used for scattering or absorption measurements. Graphite disc light baffles with 0.6 cm diam holes spaced 1.0 cm apart defined the optical paths and eliminated scattered light. The laser beam exited through a Brewster angle window mounted on a light trap to prevent back reflections. The scattered light detector was a trialkali photomultiplier tube mounted on the port perpendicular to the laser beam. A limited number of attenuation measurements was made by using a silicon photodiode to determine the intensities of the incident ( $I_0$ ) and transmitted ( $I$ ) laser beams.

The amount of silane decomposed on passing through the heated tube was determined from the difference between the measured input flow of  $\text{SiH}_4$  and its concentration at the outlet of the flow tube. A long-path (97 cm) absorption cell connected to the exhaust line of the HTFFR was used to determine the  $\text{SiH}_4$  concentration. The absorption optical system consisted of a resistively heated SiC (Globar) light source, a pinhole collimator, two planoconvex  $\text{CaF}_2$  lenses to form a parallel beam through the absorption cell, a 4.2 to 4.8  $\mu\text{m}$  bandpass filter and a PbSe detector. Figure 3 shows the ir absorption system schematically and Fig. 4 depicts the response characteristics of the detector



and bandpass filter in the relevant region of the  $\text{SiH}_4$  absorption spectrum. Figure 5 shows the calibration curve for pure  $\text{SiH}_4$  and for mixtures of  $\text{SiH}_4$  in Ar at total pressures of 100 and 500 Torr. The presence of Ar did not noticeably affect the absorption calibration.

In some experiments, silicon particles were seeded into the gas flow using the fluidized bed feed system shown in Fig. 1. A portion of the Ar main gas flow was diverted through the bed to fluidize it before it entered the HTFFR. Some Si particles were suspended above the bed and entrained in this flow for transport to the HTFFR. A calibrated optical extinction monitor at the exit of the bed was used to measure the relative concentration of particles in the flow. This value was found, by collection measurements, to be directly proportional to the particle concentration in the HTFFR. Si particles as large as 150  $\mu\text{m}$  diam were fluidized and transported into the HTFFR in this manner. For the measurements reported here, seed particles of 0.15 and 5.0  $\mu\text{m}$  were used.

The basic measurement made in this work was of the scattered laser intensity at  $90^\circ$  from the incident beam. From such measurements and a knowledge of the refractive index of the silicon particles, the diameters of the (assumed to be spherical) particles can be computed using the Mie theory. Mie theory is fully described in standard references [3,4] on light scattering. The theory yields cross sections for the extinction and scattering of radiation of wavelength  $\lambda$  by particles of radius  $r$ . The solutions for the cross section are expressed as series of complex spherical Bessel functions and their derivatives. The coefficients are functions of the complex index of refraction and the size parameter,  $x = 2\pi\lambda/r$ .

For convenience, the cross sections,  $C_{\text{ext}}$  and  $C_{\text{scat}}$  are often expressed as extinction (absorption) and scattering efficiencies,  $Q$ . These are defined as the ratio of the Mie cross section to the geometrical cross section:

$$Q_{\text{ext}} = C_{\text{ext}}/\pi r^2$$

and

$$Q_{\text{scat}} = C_{\text{scat}}/\pi r^2.$$

When these efficiencies are plotted as a function of the size parameter, they often exhibit oscillatory behavior which converges to a value of 2. The convergence is due to removing light by both particle geometry (a shadow) and interference or diffraction effects. The oscillations are also distinct functions of the particle size and they thus form one basis for determining that size experimentally. For example, Vietti and Schuster [5] showed that the oscillations in scattered light intensity that they observed in a cloud chamber where water droplets were condensing could be correlated with the growth of the droplets in time.

In this work, distinct oscillations in the scattering and absorption data were also observed. Unlike the cloud chamber measurements [5], the flow tube method used here independently establishes a time base due to the flow time-distance proportionality. Thus it was possible to trace out an efficiency vs. residence time curve by moving the cooled  $\text{SiH}_4$  inlet relative to the observation plane. Curves showing distinct oscillations such as Fig. 6 for scattering at  $90^\circ$  resulted. To relate these oscillations to silicon particle sizes,

a computer calculation was used to generate an ideal scattering or extinction (absorption) efficiency curve. For such a calculation, input data required are the complex refractive index, the wavelength, and a nominal particle concentration. The computer program yields the relative intensity of scattered (or transmitted) light for any input particle radius. Figure 7 shows a curve generated by the program for the He-Ne laser scattering. The individual peaks are numbered and those numbers correspond to the labels in Fig. 6. Thus, simply by "counting peaks" the size of the silicon particles formed from decomposing silane can be determined at any time in the process history.

The value of the complex refractive index used here was computed from data obtained by Dash and Newman [6]. From their observed absorption coefficient,  $\alpha$ , we compute the extinction index,  $k$ , through

$$k = \lambda\alpha/4\pi$$

where  $\lambda$  is the wavelength of light. The refractive index,  $m$ , is given by

$$m = m_0(1 - ik)$$

Figure 8 shows the calculated variation in  $k$  for the laser wavelengths available in this work.

## RESULTS AND DISCUSSION

### Light Scattering and Extinction

The finding in the initial phases of this work that distinct Mie oscillations occur in the scattering and extinction data and that those oscillations correlate with residence time in the heated reactor means that particle growth is proceeding proportional to that time. Furthermore, the sharpness of the observed oscillations is taken to indicate that at any time in their growth history, the particles have a relatively narrow size distribution. This latter conclusion is generally assumed to be valid when sharp oscillations in the Mie scattering are observed. Vietti and Schuster [5] showed that the width of such peaks is directly related to the standard deviation of the normal distribution of sizes which they assumed in their work. When the standard deviation of the size parameter grew to a value of 2, the Mie oscillations disappeared. Direct measurements of particle size in the present work were also made by withdrawing samples from the flow at the observation port and obtaining scanning electron microscope photographs. The measured particle sizes were found to agree within 5% with the values calculated from "counting peaks" in all cases. In addition, insofar as it was possible to determine from the photographs, spherical particles with a "narrow" range of sizes were found.

### Particle Growth Rates

Particle formation and growth were examined at three temperatures (873, 1173, and 1473 K) and at three total pressures (120, 200, and 350 Torr) at each temperature. Light scattering at 90° was observed using either the 514.5 nm Ar or the 632.8 nm He-Ne laser lines. Better data were produced from the more distinct oscillations observed in the Ar<sup>+</sup> laser scattering.

These data are shown in Figs. 9-11. One general feature is apparent: the particle radius growth rate decreases with increasing time while its volume rate of growth increases. Taking the initial radius growth rates ( $dr/dt$ ) gives the results shown in Table I:

Table I  
SILICON PARTICLE GROWTH RATES FROM SCATTERING AT 514.5 AND 632.8 nm

Pressure (Torr)	dr/dt ( $\mu\text{m/ms}$ ) at T (K)		
	873	1173	1473
120	0.055	0.084	0.225
200	0.069	0.124	0.16
350	0.078	0.176	0.12 <sup>a</sup>

<sup>a</sup> Only 632.8 light scattering used.

Several trends in the particle growth rates can be seen. At 120 and 200 Torr, particle growth rate increased with increasing temperature. At 350 Torr, particle growth rate apparently decreased at the highest temperature. More striking is the apparent reversal in pressure dependence of the growth rate at 1473 K. At the lower temperatures, growth rate increased with increasing total pressure, while at 1473 K it apparently decreased. A plot of  $\ln(dr/dt)$  against  $1/T$  (Arrhenius type plot) is non-linear for these data, showing an upward curvature for the low pressure results and a downward curvature for the high pressure data. It is tempting to speculate that more than one mechanism is operational, but more data are required before doing so. Specifically, constant total density (rather than total pressure) measurements are needed as a function of temperature.

Some additional measurements were made at 1173 K and 200 Torr in which the initial silane concentration was varied (in the data above, the initial  $\text{SiH}_4$  concentration was  $0.9 \times 10^{16} \text{ cm}^{-3}$ ). The relative intensity of scattered light for a particular particle size was measured as a function of the silane concentration. The scattered intensity is directly proportional to the number density of particles of the given size being measured. The results for particles of 0.4, 0.6, and 1.0  $\mu\text{m}$  radii are shown in Figs. 12 and 13. For the smallest particle, no change in the number density was seen; however, for the larger particles, increasing numbers are observed. For the 1.0  $\mu\text{m}$  radius particle, there appears to be a limit to the number density of particles which may be present. It may be that the unchanging number density of the 0.4  $\mu\text{m}$  radius particles indicates that the limiting number density for that size has already been achieved. In addition, the positions of the specific Mie oscillations did not change (within experimental uncertainty) as the initial silane concentration was varied. This means that over the range of silane concentrations tested here, the rate of growth to that particle size was independent of silane concentration. Thus, these results suggest that there is a limit both to the rate of growth and to the number density of any particular size of particle, but they do not suggest a limit to the maximum size of the particle which may be grown. It appears that other factors such as growth time available and the local temperature and silane concentration in the gas surrounding each particle are more important in determining the ultimate particle size than the rate coefficients of the gas-surface interactions of importance in the present results.

## Silane Decomposition

The fraction of silane decomposed as a function of residence time was measured at 873, 1173, and 1473 K and for the pressures of 120, 200, and 350 Torr. Again, the initial silane concentration was kept at a constant  $0.96 \times 10^{16}$  for these measurements. Since a portion of the HTFFR is heated downstream of the optical observation plane where the particle growth rates are measured, the silane decomposition results must be offset by at least the time required for the gas flow to traverse that region (assuming that once the gas exits the heated region decomposition ceases instantly). Thus, correlating the observed decomposition fractions with the particle growth rates is difficult. In addition, to obtain early time decomposition data, the flow speed had to be increased. Using a flow speed of 1.0 m/s (compared to 0.5 m/s used in the particle growth rate measurements) and moving the cooled inlet slightly above the observation plane, data were obtained at a minimum residence time of 9.5 ms. At 1473 K under all flow conditions, decomposition was essentially complete at the earliest times that could be measured. The results for 873 and 1173 K are displayed in Figs. 14 and 15. All of the data indicate an initial rapid increase in the rate of silane decomposition followed by a leveling off. The exact nature of the initial rise could not be determined. It seems reasonable that all of the decomposition curves will eventually reach 100%. The apparent inverse pressure dependence of the decomposition is unexplained. It is consistent with a diffusion-limited gas particle interaction rate. If this is indeed the case, then the missing early time data should provide information on the homogeneous gas phase silane decomposition. Again, as in the case of the particle growth rate measurements, use of the flow tube technique has apparently separated the two decomposition mechanisms. Obviously more data are needed to verify these conclusions. Straightforward apparatus modifications would allow the optical observation plane and the sampling port for silane decomposition measurements to be coincident. Somewhat more difficult would be a means to cool the sampled gas instantaneously to retard further silane decomposition; a supersonic nozzle for sampling would appear useful.

## Additional Observations from Particle Collection

The most interesting observation other than the narrow size distribution and spherical nature of the collected particles is that the samples appear to consist of smaller particles having radii of ca. 0.05  $\mu\text{m}$ . This "microsphere" size lies just below the calculated lower limit for detection by Mie scattering shown in Fig. 7. The time for particles to grow to this small size is shown by the present work to be less than 1-2 ms. It is tempting to speculate that the observed particle growth rates reflect, at least in part, agglomeration of these small particles. Unfortunately, when seed particles are introduced into a flow containing decomposing silane, the resulting collected samples do not show clear evidence for the presence of microspheres. In fact, some of the collected particles appear glassy, suggesting direct growth from the vapor phase.

## CONCLUSIONS

The present study should be considered exploratory in nature. It has shown the utility of applying the flow tube technique for addressing basic kinetic and mechanistic questions in two phase reacting flows. Detailed, quantitative measurements on decomposing silane and seeded flows are needed to verify the preliminary conclusions presented here. Accurate measurements of particle concentration are a definite requirement. Recent work in soot formation has shown the utility of multiple wavelength absorption methods [7, 8] for determining particle concentrations when the size distribution is known (as it is in the present work). Knowledge of the particle concentration and size distribution would allow an accurate mass balance to be made for the HTFFR studies. Detailed kinetic information would then be available from such work.

## ACKNOWLEDGMENTS

This work was sponsored by the Department of Energy through the Jet Propulsion Laboratory under Contract No. 955491, subcontract under NAS7-100.

## REFERENCES

1. FONTIJN, A. and FELDER, W., in Reactive Intermediates in the Gas Phase, D.W. Setser, Ed. (Academic Press, New York, 1979) Chap. 2.
2. FONTIJN, A. and FELDER, W., J. Phys. Chem. 83, 24 (1979).
3. KERKER, M., The Scattering of Light and Other Electromagnetic Radiation (Academic Press, New York, 1969).
4. VAN DE HULST, H.C., Light Scattering by Small Particles (Wiley, New York, 1969).
5. VIETTI, M.A. and SCHUSTER, B.G., J. Chem. Phys. 58, 434 (1973).
6. DASH, W.C. and NEWMAN, R., Phys. Rev. 99, 1151 (1955).
7. BARD, S. and PAGNI, P.J., ASME J. Heat Transfer 103, 357 (1981).
8. OLSON, D.B., "Soot Formation in Synfuels," Fourth Quarterly Report, AeroChem TN-223, DOE PC 30304-4, December 1981.

## FIGURE CAPTIONS

- FIG. 1 HTFFR FOR MEASUREMENTS OF Si PARTICLE FORMATION AND GROWTH KINETICS
- FIG. 2 OPTICAL OBSERVATION PLANE OF HTFFR
- FIG. 3 IR ABSORPTION SYSTEM FOR SILANE CONCENTRATION MEASUREMENTS
- FIG. 4 DETECTION SYSTEM CHARACTERISTICS COMPARED TO SILANE ABSORPTION SPECTRUM
- FIG. 5 CALIBRATION CURVE FOR SILANE INFRARED ABSORPTION SYSTEM  
(○) pure silane; (△) 100 Torr Ar added, (□) 500 Torr Ar added.
- FIG. 6 EXPERIMENTAL SCATTERED LIGHT INTENSITY AT 90°
- FIG. 7 CALCULATED SCATTERED LIGHT INTENSITY AT 90°
- FIG. 8 CALCULATED VARIATION OF EXTINCTION INDEX OF Si PARTICLES WITH WAVELENGTH
- FIG. 9 SILICON PARTICLE GROWTH RATES AT 873 K
- FIG. 10 SILICON PARTICLE GROWTH RATES AT 1173 K
- FIG. 11 SILICON PARTICLE GROWTH RATES AT 1473 K
- FIG. 12 SCATTERING INTENSITY AT 90° FOR 0.4 AND 0.6  $\mu\text{m}$  PARTICLES AS A FUNCTION OF SILANE CONCENTRATION
- FIG. 13 SCATTERING INTENSITY AT 90° AS A FUNCTION OF SILANE CONCENTRATION FOR 1.0  $\mu\text{m}$  PARTICLES
- FIG. 14 SILANE DECOMPOSITION AS A FUNCTION OF RESIDENCE TIME AT 873 K FOR ARGON PRESSURES SHOWN
- FIG. 15 SILANE DECOMPOSITION AS A FUNCTION OF RESIDENCE TIME AT 1173 K FOR ARGON PRESSURES SHOWN

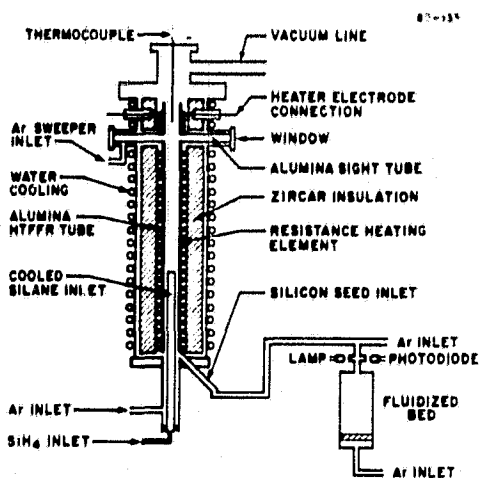


FIG. 1

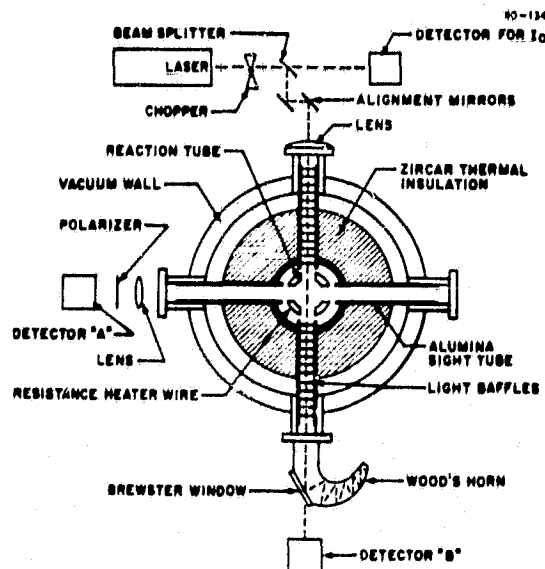


FIG. 2

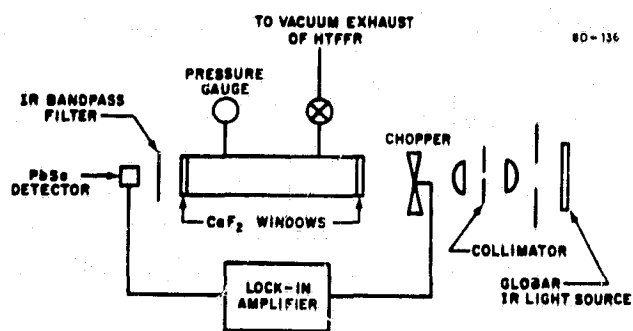


FIG. 3

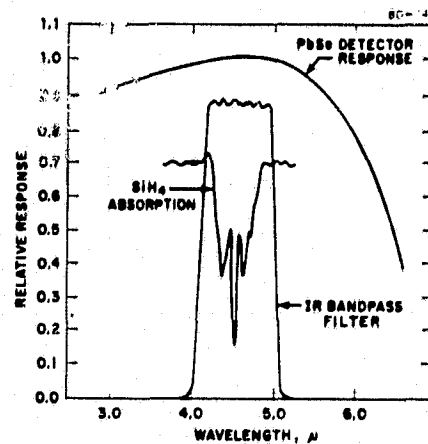


FIG. 4

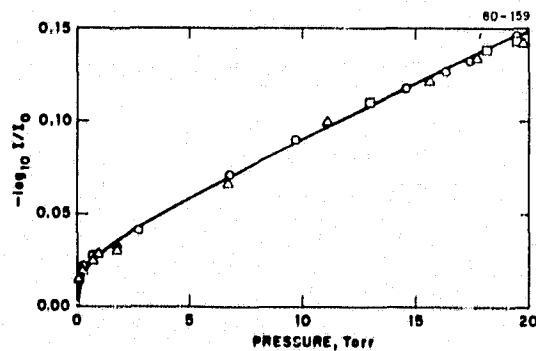


FIG. 5

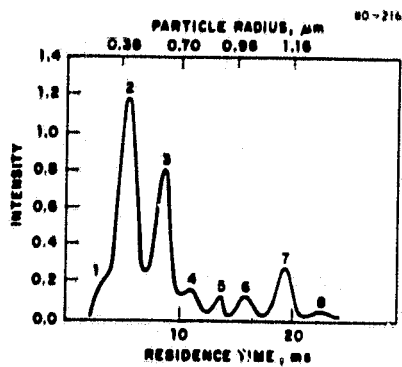


FIG. 6

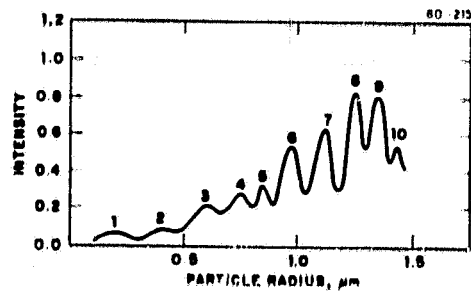


FIG. 7

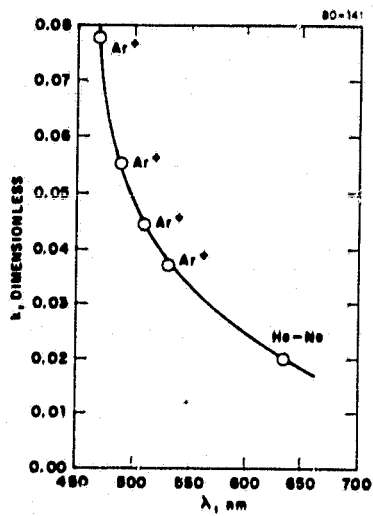


FIG. 8

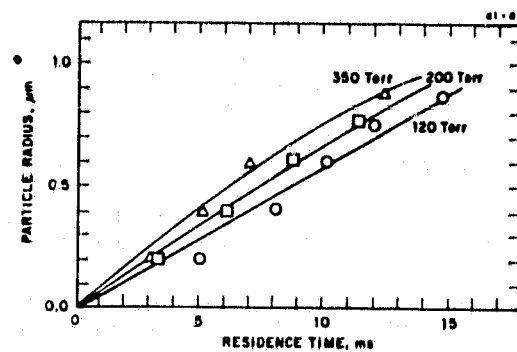


FIG. 9

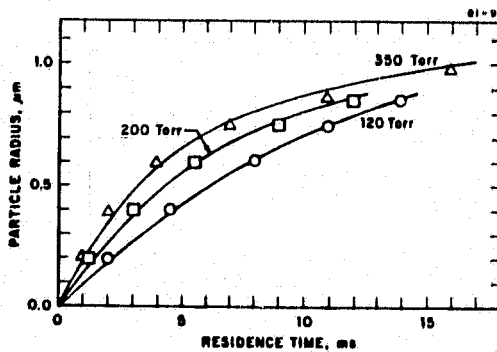


FIG. 10



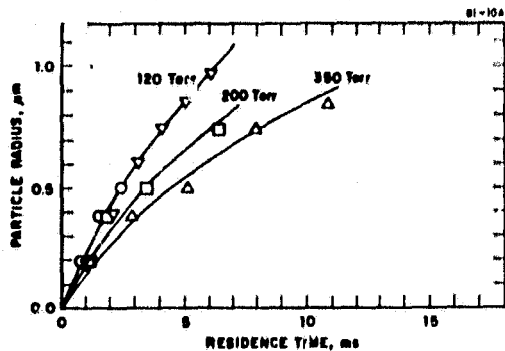


FIG. 11

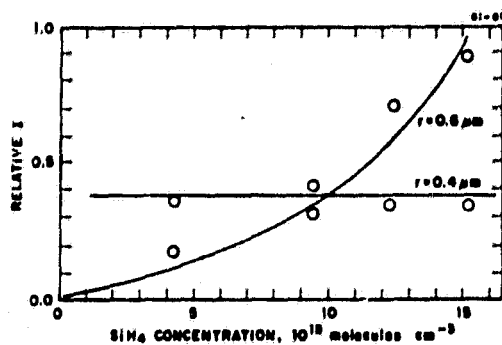


FIG. 12

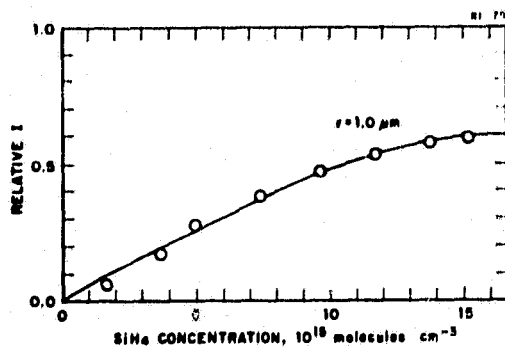


FIG. 13

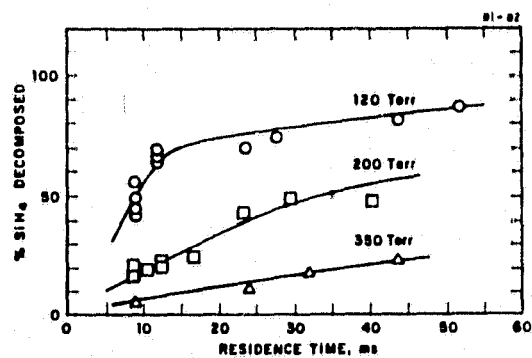


FIG. 14

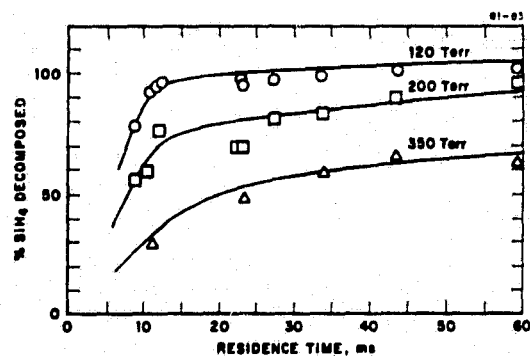


FIG. 15

## DISCUSSION

DUDUKOVIC: I have a couple of questions. Are those runs (for growth rates) that you presented done with small seeds of .15 micron particles?

FELDER: No.

DUDUKOVIC: There were no particles introduced?

FELDER: No particles were introduced in any of those.

DUDUKOVIC: I see. When you change the pressure in the system, what was the dependence of the linear velocity in the system? Did you keep the total molar feed rate constant or did you adjust that to keep the velocity constant?

FELDER: The velocity was kept constant at  $1/2 \text{ m sec}^{-1}$ .

PRATURI: I would like to know whether the diameter of the microspheres that consist of the big particles is constant?

FELDER: From all we can tell from the few collections we made, yes. At about .05 microns radius.

PRATURI: Do you think that that fact would suggest a severe change in the mechanism for increasing the size of the particles? For example, could the mechanism be that they grow up to that diameter and then there is a coagulation type mechanism after that?

FELDER: No.

BAILEY: In your abstract, you pointed out that the concentration seemed to be independent of particle size and you mention the fact that there were a greater number of particles in the concentration. I understand that to mean that the weight of the silicon decomposed is greater with greater concentration. In other words, particle size is one measurement but what about the total weight of the silicon produced?

FELDER: Well, there appears to be an increase in the number of particles at a given size as a function of the silicon introduced. That's a factor of at least five. Does that answer your question?

BAILEY: You found that as the concentration was increased there was particle growth which was independent of the concentration. If the number of particles increased, does that mean that the overall weight under a given circumstance goes up with the concentration increase?

FELDER: Do you mean do the particle densities go up? That's possible.

BAILEY: A point of clarification. If particle growth is independent of concentration, you can conclude that the weight of silicon produced is also independent of silicon concentration. That's not true, is it?

FELDER: No.

## SUBMICRON PARTICLE SIZE MEASUREMENT

Don Pettit and Thomas Peterson

University of Arizona

Fine particles can be a product of a process or they can be a problem. In dealing with collections of small particles, the concern is not with how many arms and legs each particle is going to have but rather with some characteristic dimension that represents the size of that particle. Particles of interest are typically .001 microns in diameter (these are just above molecular cluster dimensions) and range upwards to 10 microns. Particles in the size range from .01 microns to 1 microns are the most interesting because mechanisms such as coagulation, light scattering, and health effects dominate. Typical concentrations for room air are about 100 particles  $\text{cm}^{-3}$  (this is cumulatively summed up over the particle size ranges of interest). In a combustion environment, like flue gas, there will be  $10^7$  or  $10^8$  particles  $\text{cm}^{-3}$  and in smoke there will be as many as  $10^{10}$  particles  $\text{cm}^{-3}$ . Aerosol systems on the industrial level typically fall in the higher concentrations. In ambient studies or in a clean room environment, the particles are less than 100  $\text{cm}^{-3}$ .

The characterization of these aerosol systems requires an instrument capable of measuring the particle number and size so that a size distribution can be determined. This instrument should be capable of an in situ analysis, eliminating the need for sample probes that disrupt stream lines and cause sampling errors. This instrument should be capable of providing information on a real time basis so that on-line analysis can be used for process control. In the present particle counting technology there are two basic techniques being used. For small particle sizes of .01 to 1 microns the instruments use electric mobility methods which take aerosol particles, charge them and then measure the rates of migration as these particles go in between capacitor plates. Electrical mobility techniques will handle concentrations up to  $10^6$  particles  $\text{cm}^{-3}$ . A sample probe must be used because the aerosol must be removed from the system and transferred into the electrical aerosol analyzer. There are optical techniques which are used for particles sized from .1 to 10 microns. It is difficult to go below the .1 micron limit, the typical being .3 microns. Optical techniques can handle concentrations up to  $10^3$ , with some as high as  $10^6$ , particles  $\text{cm}^{-3}$ . Optical systems are of considerable advantage in view of the in situ possibilities. Among the optical techniques are those based on ensemble measurements. Collections of many particles scattering light are observed as extinction-type measurements and these give statistical information about the aerosol system where the moments of a distribution are determined.

There are single particle count techniques in which particles can be counted one at a time as they go through some inspection region. The single particle counting techniques basically work by focusing a beam of light down to a small beam waist and use an off-axis detector to gather the light from a small inspection region. The measurement is of the intensity of light scattered out of the inspection region when single particles pass through. If

there is more than one particle, there will be a sampling error known as coincidence. The probability of a coincidence error occurring can be calculated as a function of the size of the inspection region and the total aerosol concentration. If the measured aerosol concentration is  $N_i$  and the actual aerosol concentration  $N_t$ , the coincidence error is equal to  $N_i/N_t = 1 - N_t V$  where  $V$  is the volume of the inspection region. The typical procedure is to set  $N_i/N_t$  equal to 0.95 so that 5% of the time more than one particle will be in the inspection region. The volume of the inspection region is set by the parameters used in building the instrument. A calculation can be made of the total maximum aerosol concentration which can be counted and still be assured that 95% of the time only one particle is in the inspection region. To give you an idea of the typical calculation, I have done a few sample calculations for the condition of a 5% coincidence error. For an inspection region of 1000 microns in diameter and 700 microns long, which would be a typical inspection region for a commercial optical particle counter like the Climat 208, 80 particles  $\text{cm}^{-3}$  is the maximum concentration which can be counted. On some custom built research particle counters, an inspection region as small as 25 microns in diameter and 100 microns long can be obtained and up to about  $10^6$  particles  $\text{cm}^{-3}$  can be measured.

The signal from such an instrument will give a series of pulses in the time domain so that the width will be the time of flight of the particle through the inspection region and the height will be the scattered intensity. The height can be related to particle diameter through scattering mechanisms. What is needed at this point is an electronic box that sorts out the pulses according to height and stores them so the particle size distribution can be recorded.

Scattering theory can be used to relate the pulse height to particle diameter for the physical geometry of the instrument used. Usually a plot is made of log scattered intensity vs log particle diameter. One problem with these intensity measurements is that two orders of magnitude of particle diameter typically span eight orders of magnitude in signal intensity. It is difficult to design an electrical device that will handle this range of signal; available instruments will typically handle only one decade of particle size.

An important question is what determines the detection limit in these optical devices. Why does .1 micron seem to be the lower limit? The detection limit is reached when the background scattering in the inspection region equals the scattering of a single particle contained within this region. The smaller the inspection region, the lower the detection limit. The present practical limits on the size of the inspection region lead to the lower limit of .1 micron with intensity based instruments. Two kinds of light sources can be used in these optical particle counters: white light and laser light. With white light, a spectrum of wavelengths strikes the particle. This tends to smear out the calibration curve, removing the Mie wiggles and giving a monotonic response. A disadvantage with white light is the limitation to intensities less than 40 watts  $\text{cm}^{-2}$  (based on a large quartz halogen high pressure type lamp). White light provides a uniform intensity

9  
Y

profile throughout the inspection region. This is important in order to avoid the circumstance in which the incident intensity on the particles varies with trajectory through the inspection region. Laser light produces discrete wavelengths causing Mie wiggles in the scattering calibration curves. This non-monotonic response is troublesome. Laser systems with intensities as high as  $4000 \text{ watts cm}^{-2}$  are obtained in intercavity scattering experiments in which the particles are passed through the interior of the laser. Lasers are notorious for producing Gaussian intensity profiles. The Gaussian profile will be superimposed on top of the inspection region, and particles going near the edge will have a lower incident intensity than those going through the middle. There will be a path dependent function for the incident intensity. The problem of non-monotonic response can be minimized by angle averaging in which a range of angles is viewed with a detector.

There are compromises with each system. In general, the extent of the inspection region will affect several parameters, like the minimum and maximum detectible particle sizes. For a small inspection region there will be a small amount of background scattering and an associated minimum range of detectible particle sizes. The maximum particle size is also dictated by the size of the inspection region, because as the size of the particles approaches that of the inspection region near miss and partial eclipse problems will occur. Hence, the largest particle should be much smaller than the size of the inspection region to minimize these kinds of problems.

The inspection region will affect the aerosol flow rate. As the pulses become extremely narrow, the band width of the amplifiers in the electronics which process these pulses will have to be increased, probably causing the signal to noise ratio in the electronics to be the limiting factor. The minimum and maximum aerosol concentrations which can be counted are also dictated by this inspection region. The maximum aerosol concentration is based on the time required for counting a distribution. Since individual particles are counted, the counting should be done at a reasonable rate so that a statistically significant number of particles can be counted in a reasonable period of time. The acceptable values for a minimum count rate and the maximum aerosol flow rate will dictate the minimum acceptable aerosol concentration needed to give an adequate count rate.

As an example, for an inspection region that is 25 microns in diameter and 100 microns long, the minimum particle size is of the order of .1 micron in diameter based on the background scattering measurement. The maximum particle size will be about 5 microns due to partial eclipses. The maximum aerosol flow rate through this inspection region will be around  $.7 \text{ cm}^3 \text{ min}^{-1}$  based on 5 microsecond wide pulses. The maximum aerosol concentration based on the coincidence equation is  $10^6 \text{ particles cm}^{-3}$  and the minimum aerosol concentration is  $5 \times 10^4 \text{ particles cm}^{-3}$  for a 500 Hertz count rate. If a machine with this kind of inspection region was used to count room air there would be a signal once every two seconds, and it would take a week of counting to obtain a significant distribution. Hence, to obtain an adequate system for counting, the specifications of the viewing zone of the instrument should be made precisely and correctly.

The calibration for an instrument will be a function of the particle characteristics. For ambient-type aerosols the real part of the refractive index will vary from 1.3 to 1.5 and for combustion generated aerosols from 1.5 to 1.7. The calibration system should mimic the actual system to be counted in order to minimize counting error. If the characteristic dimension is of interest, the instrument can be designed to look at near forward scattered light, and the particle shape factors are not as critical.

In conclusion, it is important in the measurement of aerosol systems that the proper configuration of particle instrumentation be used to ensure reliable results.

## DISCUSSION

LUTWACK: Could you say a bit more about the shape factor in your calibration?

PETTIT: If you're interested in knowing what the shape of the particle is, you typically look at back scattered light which has more fingerprint regions for the Mie calculations. If you're only interested in the characteristic dimension of a particle and not so much in what its actual shape is, near forward scattered light is the best way to go.

# FACTORS GOVERNING PARTICLE SIZE IN THE FREE SPACE REACTOR

R. C. Flagan and M. K. Alam  
California Institute of Technology  
Pasadena, California 91125

## 1.0 INTRODUCTION

A number of approaches are being considered in the attempt to reduce the cost and improve the purity of silicon manufactured for photovoltaic and other semiconductor applications. A common feature of many of the methods is the conversion of metallurgical grade silicon to volatile compounds such as silicon tetrachloride, di- or tri-chlorosilane, other halo-silanes, or silane. Distillation methods are then used to remove impurities from these materials. Once the volatile species has been purified, the precursor compounds are reacted to produce solid silicon. The conventional Siemens process for producing silicon involves direct chemical vapor deposition on a heated substrate. The vapor deposition is slow due to mass transfer limitations. The slow deposition and large heat losses make the silicon produced by this method quite expensive. Nevertheless, Siemens-type reactors currently account for the vast majority of the silicon produced for semiconductor applications.

Entrained bed or "free-space" reactors have been considered as an alternate method for silicon production. Both JPL and Union Carbide have experimented with free-space reactors designed to generate a silicon powder by the thermally induced decomposition of silane gas (Levin, 1980; Lay and Iya, 1981). The pyrolytic decomposition of silane is sufficiently rapid at high temperatures that efficient conversion of silane to condensed phase products (silicon and silicon hydrides) can be achieved in residence times less than a few seconds. The silicon powder generated by the JPL and Union Carbide bench scale reactors consisted of particles in the 0.1 to 0.9 micron size range, as estimated by electron microscopy and surface area measurements. Such small particles are most readily separated from the carrier gas by filtration since their terminal settling velocities are below 1 mm/sec and their aerodynamic relaxation times are well below 1 msec.

If larger particles could be generated directly from gaseous precursors in a free space reactor, the problems associated with particle collection, transport, melting, and contamination could be greatly reduced. The present theoretical study of silicon aerosol formation in entrained flow reactors has been undertaken in order to elucidate those factors which limit particle growth in such systems, and to identify alternate approaches which are capable of generating larger particles by pyrolysis of silane gas.

PRECEDING PAGE BLANK NOT FILMED



## 2.0 THEORY

The major physical and chemical processes occurring in the free-space reactor include: (1) homogeneous gas-phase decomposition of the silane gas, generating condensible poly-silanes and silicon; (2) homogeneous nucleation of these vapors to produce very small particles; (3) heterogeneous decomposition of silane on the surface of the particles; (4) particle growth by heterogeneous condensation of the products of the homogeneous silane decomposition reactions; (5) increase in the particle size and decrease in the number concentration due to coagulation. The chemistry of the pyrolytic decomposition of silane is not completely understood. Purnell and Walsh (1966) studied the homogeneous reactions in the temperature range 375-430°C, which is considerably lower than the temperatures at which the previous free-space reactors have been operated. The activation energy for the silane pyrolysis reaction was found to be about 55.9 Kcal/mole. The rate of silane decomposition in the free space reactor is, thus, highly sensitive to temperature. In both the JPL and Union Carbide systems, operating temperatures have been in the range from 580 to 900°C. At the upper end of this range, the silane pyrolysis reactions are very rapid by comparison with the residence time of the reactants in the reactor, i.e., reaction times are much less than a few seconds. Assuming that silicon is produced directly by the pyrolysis of silane, the vapor can be expected to condense homogeneously to form very small particles. The critical radius for particles, i.e., the minimum size of particle which is thermodynamically stable, is a function of the surface tension of the material,  $\sigma$ , and the saturation ratio,  $S = P_v/P_{sat}$ , viz.,

$$r^* = \frac{2\sigma v_m}{kT \ln S} \quad (1)$$

For silicon at the relatively low temperatures of the free-space reactors, the critical radius is less than about 4 Å, i.e., less than about 40 silicon atoms. Substantial growth must occur to produce the observed 0.1 to 1.0  $\mu\text{m}$  particles. We shall, therefore, first examine the growth of nucleation generated silicon particles, assuming, for the present, that nucleation occurs as fast as silane pyrolyzes.

### 2.1 Sectional Model Calculations

The dynamics of the particle size distribution of an aerosol evolving due to condensation and coagulation is described by an integro-differential conservation equation known in the general dynamic equation for aerosols. A preliminary examination of the evolution of the silicon aerosol was undertaken using the sectional representation of the general dynamic equation developed by Gelbard and Seinfeld (1979). The original code has been modified to allow for variable gas temperature and the influence of interparticle dispersion forces on the coagulation rate coefficients in the manner of Graham and Homer (1973). The JPL free space reactor operated at 580°C, 50 psig, and with a feed gas containing 50 percent silane was considered in these calculations, in order to simulate the experimental conditions of Levin (1980). We assumed that the silane reacted slowly, at a constant rate.

The results of these sectional model calculations are illustrated in Figure 1. The particles formed initially by homogeneous nucleation grow primarily by coagulation. Early in the reaction process, 0.1 sec., a broad distribution of particle sizes is generated. Brownian coagulation rapidly narrows this broad distribution, producing a sharp peak in the 0.1 to 1.0 micron size range. Because of the low volatility of silicon, new particles continue to be formed as additional silane is reacted. These particles are, however, rapidly scavenged by the larger particles. Thus, even though molecular clusters or very small particles continue to be formed, the number concentration of silicon particles stabilizes and even decreases due to coagulation among the larger particles. Little change in the qualitative nature of the particle size distribution can be expected after the particles have grown into the 0.1 to 1.0 micron size range, because the coagulation rate decreases rapidly as the number concentration of particles decreases. Growing particles out of the submicron size range would require increasing the residence time of the particles to several hours, thereby eliminating much of the anticipated benefit of the compact free-space reactor for silicon production.

## 2.2 Maximum Particle Size

The ultimate size of particles required from the free space reactor depends upon the way in which the subsequent processing of the silicon particles will be conducted. For example, if the particles produced in the free space reactor are to be used as seed particles for a fluidized bed reactor, the particles should be in the 50 to 200 micron size range. If, on the other hand, the particles are to be deposited directly into a melt, either inertially or through gravitational settling, smaller particles can be tolerated, perhaps no more than 10 microns in diameter. The particles produced in the Union Carbide or JPL free-space reactors are in the 0.2 to 1.0 micron size range. Assuming that the reactant gas was pure silane and the reaction was complete, there are approximately  $10^8$ - $10^{10}$  particles per cubic centimeter in the gases leaving the reactor. Approximately 90 percent of the mass in the system at that point is in the form of silicon particles. Growth of the particles to 10 microns in size will require an increase in the mass of each particle by about a factor of 1000. For larger particles, the required mass addition increases as the cube of the diameter of the product particles.

Since the coagulation time for this growth is so long, it is more reasonable to introduce additional silane into the reactor and then deposit silicon produced from reaction of the secondary silane on the particles previously generated. The deposition may be in the form of direct condensation of silicon on the particles or the diffusion of small molecular clusters or particles to the surface of the existing aerosol. If, however, additional stable new particles are generated, the increase in the aerosol number concentration may prevent the growth of 10 micron particles.

We see that the major factor limiting the size of particles generated in previous free-space reactors is the very large number concentration of particles produced by nucleation of the silane pyrolysis products. An improved understanding of the factors which govern how many new particles will be formed by nucleation is necessary to the design of free-space reactor

systems for the production of silicon. If nucleation could be suppressed, it might be possible to grow a small number of particles to large size. Because the product of the silane pyrolysis reactions has such low volatility, particles nucleate readily even if the vapor pressure of the product silicon is low, or other particles are present in the system.

### 2.3 Nucleation in the Presence of a Growing Aerosol

In the calculations outlined above, the influence of particles generated early in the reaction process on the nucleation rate at later times has been neglected. Implicit in those calculations is the assumption that the gas composition is uniform at any position along the length of the reactor. Pesthy et al. (1981) have recently shown that the reduction in vapor concentration in the region surrounding a growing particle can substantially reduce the rate of new particle formation. Their analysis involved a number of assumptions which limit its applicability to particles in the continuum size range, i.e., to particles much larger than the mean-free-path of the gas molecules, nevertheless, their results do suggest that it may be possible to inhibit nucleation by judicious control of the aerosol concentration and the rate of reaction of the silane precursor. For this reason, an effort to extend the theory of the influence of a growing aerosol on new particle formation into the free-molecular and transitional size ranges has been undertaken. The details of the extended theoretical analysis have been presented elsewhere (Alam and Flagan, 1982). We shall only briefly summarize the method and relevant results here in order to understand how large silicon particles of silicon can be produced by the homogeneous pyrolysis of silane.

In the presence of an aerosol, some condensible vapor diffuses to the particle surfaces, thereby reducing the vapor concentrations in a region surrounding the growing particle. These local perturbations may have significant effects on the nucleation rate. The particles produced by silicon pyrolysis and nucleation are initially very much smaller than the mean free path, i.e., their Knudsen numbers ( $Kn = 2\lambda/d$ ) are much greater than unity. One objective of the present work is to grow these very small particles to sizes much larger than the mean free path. It is, therefore, necessary to extend the previous theory through the transition and free molecular size ranges.

Consider the diffusion of a vapor to a particle of radius,  $r_0$ . The vapor diffusion is described by the continuum transport equations, i.e.,

$$\frac{\partial x_v}{\partial t} + v^* \frac{\partial x_v}{\partial r} = \frac{D}{r} \frac{\partial}{\partial r} \left( r \frac{\partial x_v}{\partial r} \right) \quad (2)$$

In the continuum limit ( $Kn \ll 1$ ) we generally assume that the vapor is present at the particle surface in its thermodynamic equilibrium concentration. One approximate method for dealing with diffusion to particles too small for the continuum equations to be strictly valid is to use the flux-matching method (Fuchs, 1964; Davis et al., 1978). In this method, the region surrounding the particle is divided into two parts by a spherical surface which is concentric with the particle at a distance from its surface. The fluxes inside the sphere are described according to free molecular gas kinetic theory.

The fluxes in the exterior region are described by the continuum model, Eq. (2). The fluxes are then matched at the boundary sphere. We shall adopt this simple approach and further simplify the analysis by locating the boundary sphere at the particle surface. By this method, the temperature and vapor concentration at the particle surface may be estimated in terms of the values far from the particle surfaces and the particle Knudsen number, viz.,

$$T' = T_o + (T_\infty - T_o) \frac{\gamma Kn}{1 + \gamma Kn} \quad (3)$$

$$X'_v = X_{vo} + (X_{v\infty} - X_{vo}) \frac{\beta Kn}{1 + \beta Kn} \quad (4)$$

Given these boundary conditions, the temperature and vapor concentration in the gas can be calculated using the unsteady continuum transport equations. The details of the solution are presented by Alam and Flagan (1982).

Far from the surface of the growing particle, the nucleation rate,  $J$ , approaches that described by the classical theory of homogeneous nucleation (Springer, 1979). Because the vapor concentrations are reduced in the vicinity of the particle, the total rate of new particle formation in the system is decreased. The reduction of the overall new particle formation rate by a single growing particle is

$$\Delta \dot{N} = \int_{r_o}^{r_a} (J_\infty - J(r)) 4\pi r^2 dr \quad (5)$$

where the limit of integration,  $r_a$ , is a distance sufficiently far from the particle surface that background concentrations are reached. It is convenient to define a clearance volume around the particle as that radius,  $\rho r_o^3$ , for which setting the nucleation rate inside to zero and that outside to  $J_\infty$  would yield the same reduction in the overall nucleation rate as that determined by the exact integration, i.e.,

$$\rho^3 = \frac{3}{4\pi r_o^3} \int_{r_o}^{r_c} \left(1 - \frac{J(r)}{J_\infty}\right) 4\pi r^2 dr \quad (6)$$

As the sum of the clearance volumes associated with all particles in the system approaches unity,

$$\int_c^\infty \rho^3 v n_v(v, t) dv \sim 1 \quad (7)$$

it is apparent that a significant decrease in the nucleation rate may be expected.

The calculated clearance volume for silicon is plotted as a function of  $Kn^{-1}$  (which is proportional to diameter) in Figure 2. For particles in the free-molecular size range, the dimensionless clearance volume is approximately inversely proportional to Knudsen number and therefore, to the diameter. The dimensionless clearance volume decreases to a constant value with decreasing Knudsen number in the continuum size range. Thus the absolute volume in which nucleation is quenched increases rapidly with increasing particle size. The clearance volume also increases with decreasing vapor partial pressure. We see, therefore, that once

nucleation has been quenched, particles may be expected to grow by heterogeneous condensation provided the aerosol number concentration does not decrease too much and the vapor partial pressure does not increase too much.

The behavior of the Union Carbide free space reactor has been modeled by this approach. New particle formation and growth of particles by condensation of vapor have been considered. Coagulation has been neglected in these calculations. The operating conditions for the reactor were taken to be 900 K with pure silane at atmospheric pressure. In these calculations, nucleation quenching occurred after about 70 microseconds of reaction time. The calculated particle size distribution at that time is illustrated in Figure 3. The largest particles grow only to about 1 nm radius and the total number concentration is large, about  $2 \times 10^{11} \text{ cm}^{-3}$ . At this point long before the pyrolysis reactions have ceased, the particles are sufficiently abundant to scavenge the vapor and prevent additional nucleation. Allowing the aerosol to remain in the reactor for 10 sec., coagulation would reduce the number concentration by about a factor of 200. Considering both coagulation and growth due to heterogeneous condensation and assuming that no further nucleation occurs, the particle size at the reactor outlet is estimated to be between 0.1 and 0.5 microns radius. This estimation is in close agreement with the results of the Union Carbide experiments.

### 3.0 CONCLUSIONS

In this paper we have reviewed the roles of nucleation, coagulation, and heterogeneous condensation in the growth of particles in the free space reactor. Because of the low volatility of the silane decomposition products, particles are rapidly formed by homogeneous nucleation once pyrolysis begins. The critical particle of silicon consists of a cluster of less than 50 atoms due to its high surface tension. The initial burst of nucleation produces very large number concentrations of very small particles. Vapor (and small cluster) scavenging by these particles effectively quenches nucleation before a significant fraction of the silane has been converted to aerosol silicon. Further silane pyrolysis leads to particle growth by heterogeneous condensation. Because of the very large number concentrations and the large increase in mass required for particle growth, heterogeneous condensation in the free-space reactors produces particles smaller than a few tenths of a micron in diameter. Coagulation reduces the number concentration and increases particle size somewhat. In spite of the very large number concentrations, Brownian coagulation does not produce particles larger than about one micron within reasonable residence times. The coagulation calculations were based upon spherical particle dynamics. Chain agglomerates might grow more quickly, but would not result in the formation of large, dense particles.

The results of these theoretical calculations clearly indicates how an aerosol reactor should be operated to grow large particles by homogeneous pyrolysis of silane. By reacting a small fraction of the total silane flow, a seed aerosol may be generated. Mixing this seed aerosol with the main silane flow produces a low enough number concentration that large particles may be grown in a second stage of reaction, provided the silane pyrolysis rate is kept low enough that the seed aerosol can efficiently quench

nucleation. A prototype, two-stage silane reactor has been constructed and is now being tested. Operating the reactor as a single-stage isothermal system, i.e., in the free-space reactor mode, number concentrations in the range from  $3 \times 10^7$  to  $4 \times 10^8$  particles per standard cubic centimeter have been produced. These particles are small, in the 0.1 to 1.0  $\mu\text{m}$  size range. Operating the reactor in the two-stage mode outlined above and with the same total flow of silane and nitrogen carrier, particle concentrations have been maintained at about  $2\text{--}8 \times 10^4/\text{cm}^3$ . This reduction in particle number by a factor of  $10^3$  to  $10^4$  corresponds to an increase in the mean particle diameter of a factor of 10 to 20. Particles as large as 20 microns in diameter have been observed in the silicon produced in the aerosol reactor.

#### REFERENCES

- Alam, M. K., and R. C. Flagan (1982) Simultaneous Homogeneous Nucleation and Aerosol Growth, presented at the First Annual Conference of the American Association for Aerosol Research, Santa Monica, California, February 17-19. Submitted for publication.
- Davis, E. J., and A. K. Ray (1978) J. Aerosol Science 9, 411-422.
- Fuchs, N. A. (1964) Mechanics of Aerosols, Pergamon Press.
- Gelbard, F., and J. H. Seinfeld (1980) J. Colloid. Interface Sci. 68, 363.
- Graham, S. C., and J. G. Homer (1973) Faraday Symposia of the Chemical Society, 39, 395.
- Lay, J. R., and S. K. Iya (1981) Silane Pyrolysis in a Free-Space Reactor, Proc. Fifteenth IEEE Photovoltaic Specialists Conference, pp. 565-568.
- Levin, H. (1980) Pyrolysis of Silane in Free Space, Proc. Symp. on Materials and New Processing Technologies for Photovoltaics Electrochem. Soc.
- Pesthy, A. J., R. C. Flagan, and J. H. Seinfeld (1981) J. Colloid. Interface Sci. 82, 465-479.
- Purnell, J. H., and R. Walsh (1966) Proc Royal Soc. 293, 543-561.
- Springer, G. S. (1978) Advances in Heat Transfer 14, 281-346.

ORIGINAL PAGE 11  
OF POOR QUALITY

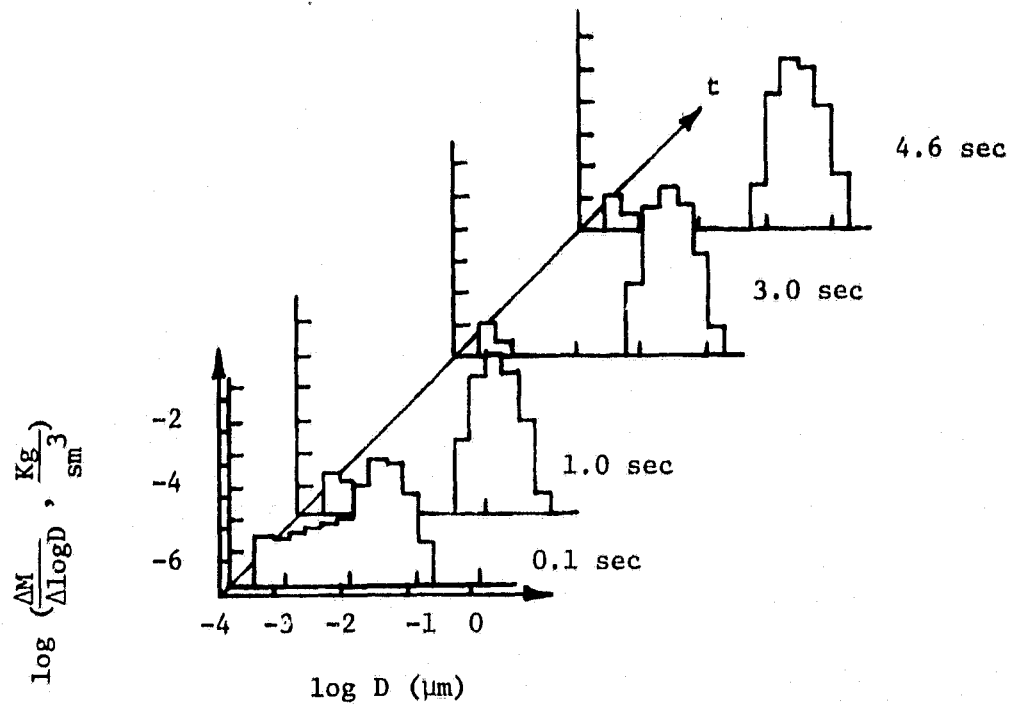


Figure 1. Sectional Model Calculations of Aerosol Evolution in the JPL Free Space Reactor.

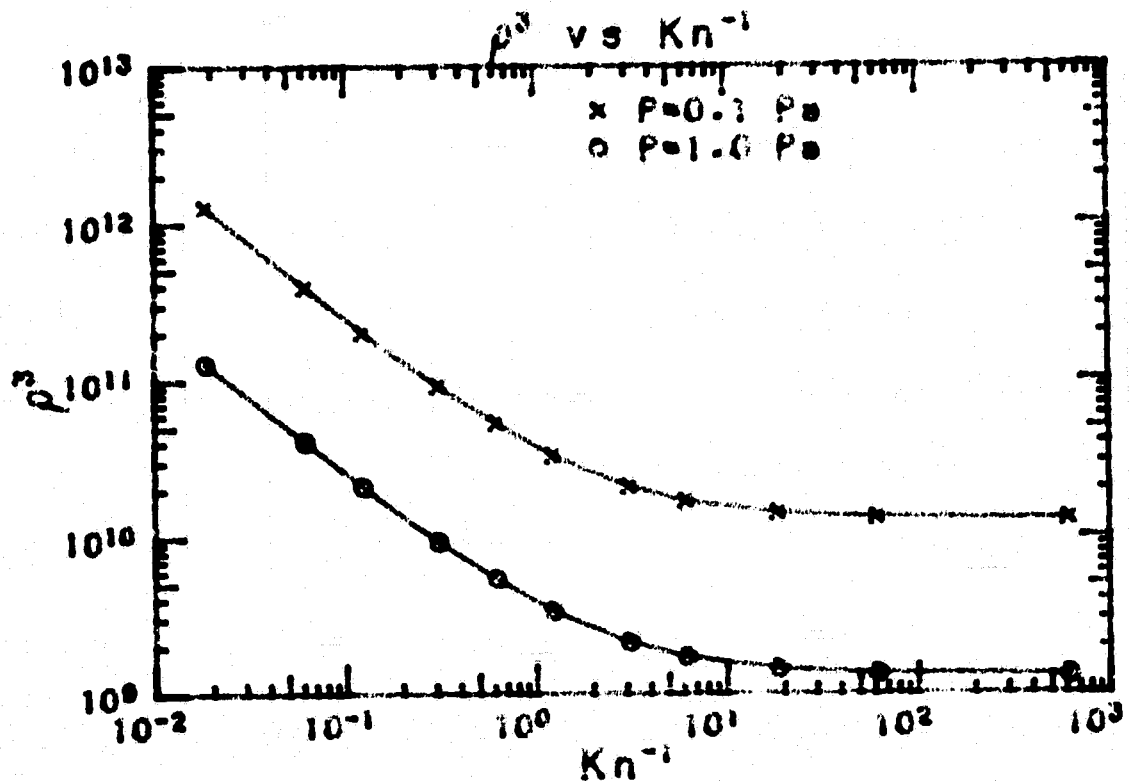


Figure 2. Dimensionless clearance volume for silicon aerosol.

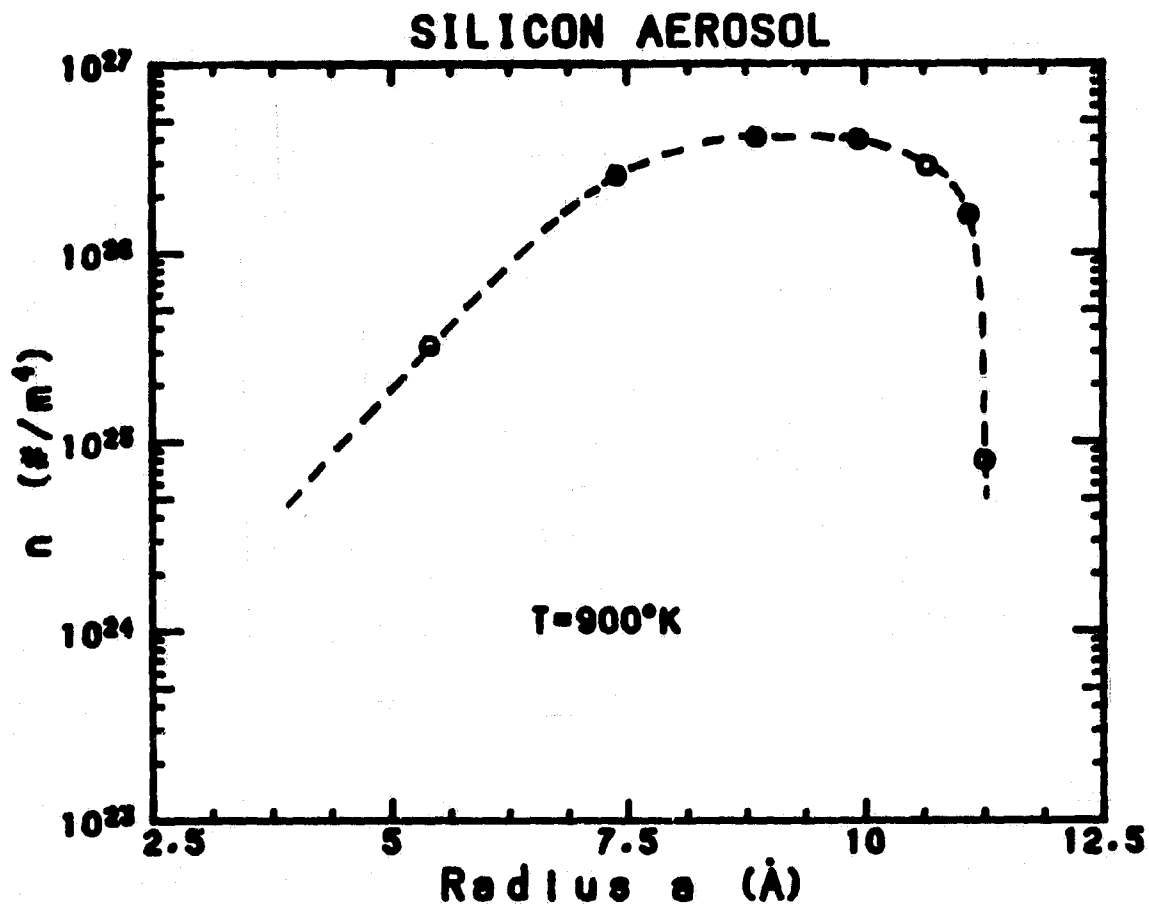


Figure 3. Particle size distribution at time nucleation is quenched in the Union Carbide Free Space Reactor.



## DISCUSSION

PETTIT: The seed particles you are making look like collections of many little tiny particles from the coagulation mechanisms. After you run those through your second stage of particle growth, do they look like nice smooth little spheres?

FLAGAN: I was hoping I would have some pictures for illustration, but I don't.

PETTIT: I am curious to know what they look like.

FLAGAN: The vast majority of experimental work on this system has been recently done, in the last two months, and we simply do not have all the data.

FITZGERALD: What is the residence time in the second reactor and what is the silane concentration in the second reactor?

FLAGAN: The residence time was about 10 seconds and the silane concentration 10% in  $N_2$ .

DUDUKOVIC: I have a comment and then a couple of questions. I think it is very exciting that you have provided a nice analysis for a system of small particles so that essentially now we have a quantitative means for calculations and for characterizing competing heterogeneous and homogeneous processes. The chemical engineers knew that it was necessary to provide some surface for these types of reactions systems, but we were unable to quantify how much surface we needed to enhance the heterogeneous reaction. Since I don't work in this area, I am interested in the real dimension of the sphere of influence that a particle of about .5 micron or 1 micron depletes in the saturation volume around it. Could you give me an indication of what that dimension is?

FLAGAN: That is strongly dependent on the physical and thermodynamic properties of the material with which you are dealing. If we assume that we are dealing with elemental silicon, then the clearance volume at .1 Pascal was on the order of  $10^9$  to  $10^{11}$  times the volume of the particle. That's on the order of 4 magnitudes larger than the particle radius.

DUDUKOVIC: So that would be a pretty large volume even when compared to the possible microstructure of turbulence.

FLAGAN: In many systems, yes.

DUDUKOVIC: Does the theory apply completely for such systems?

FLAGAN: As you get into systems where turbulence becomes important, the microstructure of turbulence would certainly have to be taken into account.

DUDUKOVIC: What kind of measurements are used and how is  $\beta$ , the coagulation coefficient, evaluated?

FLAGAN: We have simply used the rate which has been measured by numerous people. The procedure for the measurements is to produce an aerosol of a known concentration of particles of known sizes and measure the time evolution of that aerosol.

STEINWANDEL: If you are dealing with a classical theory of homogeneous nucleation, what value of surface tension did you introduce, and did you use any corrections which you probably might have to use? When did the particles go to smaller sizes?

FLAGAN: I do not have that value right at my fingertips. I can get it for you. We did not use the corrections, since we were basing our calculations strictly on silicon and do not believe that the condensing species is necessarily elemental silicon at these low temperatures. We were running the reactor at 500 to 600°C over most of its residence time. Since we were working with such low temperatures, I don't know the properties of the material which is condensing. I don't put a tremendous amount of weight on the quantitative results from the present calculations. I would like to be able to do quantitative calculations, but I don't think the data are yet published.

FITZGERALD: I just made a quick order-of-magnitude calculation. You are assuming that a particle goes from about 1 micron to 10 microns in 3 seconds. This means that the diameter is increasing at a rate of around 1 micron  $\text{sec}^{-1}$ . Now 1 micron of deposited silicon gives off about 50 thousand volumes of hydrogen at the same condition and that hydrogen will leave the surface at a velocity of a few  $\text{cm sec}^{-1}$ . Is that going to give a barrier to diffusion? That's going to be coming out at a temperature which is about 300° or so hotter than the rest. I wonder if that particle which grew to 10 microns, in fact, wasn't a particle which spent a lot of time, like a hailstone in a thunderstorm, going around and around before it finally came out?

FLAGAN: Part of the reason we increased the flow velocity was to prevent that effect, because in the early experiments we did see particles sedimenting out. A velocity of a few  $\text{cm sec}^{-1}$  is probably not significant when the diffusion calculations are done on this very small length scale. You will find that the characteristic diffusion velocity will be much shorter than that. We are dealing with the length scale of a micron, or a few microns. I have gone through the detailed calculations looking at that microstructure in the case of coal combustion and that velocity is significant but certainly does not inhibit the reactant from getting to the particle surface and there the problem is equally severe.

IYA: Using your concept of controlled aerosol reactor, do you think you can go grow even larger particles? What is the limitation of this process?

FLAGAN: In our experiments, we have run the reactor first as a single-stage reactor and then we ran it as a two-stage reactor for the seed aerosol generation and the growth of particles. In that system the maximum size is limited to about 10 microns and that is due to the number of particles and the amount of silane in the system. By reducing the number of particles further and by controlling the rate of reaction more carefully we should be able to grow larger particles. Alternatively, by operating this second stage in the mode we have used and then adding additional silane, we should be able to grow larger particles. I don't see any fundamental limits, provided the rate of reaction is controlled such that the scavenging of the reaction products by the growing particles can inhibit nucleation. Problems due to turbulence may arise and there may be other factors which distort the flow field more significantly but as long as the number concentration of particles is large enough nucleation should be inhibited.

IYA: I have another question. In your present system what is the throughput of silane?

FLAGAN: The silicon production rate is about 6 grams per hour.

LEIPOLD: Were you able to get any kind of preliminary mass balance on your reactor?

FLAGAN: No, not yet.

PRATURI: You mentioned the use of some experimental values for the  $\beta$ . I assume these were based on measurements of other aerosols.

FLAGAN: They are both experimental and theoretical. They are well supported in the literature.

PRATURI: If I remember correctly, the  $\beta$  is very much a function of the mechanism of the coagulation, is it not?

FLAGAN: Yes.

PRATURI: So which particular mechanism did you assume?

FLAGAN: Brownian coagulation.

PRATURI: Not gradient coagulation?

FLAGAN: No thermal or electrophoretic effects were involved.

PRATURI: I have one more question. You said that theoretically you don't see any limit to how large you can grow these particles. However, if, for example, you consider 10 microns is the limit now, that is still a particle size where the particles still go with the fluid flow.

FLAGAN: 10 microns is quite large enough to separate from the fluid flow aerodynamically.

PRATURI: It depends on the velocity though, does it not? For example, for 100-micron particles there will be settling out.

FLAGAN: Yes, the design becomes slightly more complicated at that point. But to go to the extreme limit, the particles become a fluidized bed.

PRATURI: Did you happen to measure the density of these 10-micron particles?

FLAGAN: We do not have that much data yet. The particles appear dense enough so that their settling velocities are several  $\text{cm sec}^{-1}$ . We have observed particles with settling velocities of several  $\text{cm sec}^{-1}$ . Those were larger than 10 microns.

HSU: You mentioned 3 seconds for the residence time in the primary section. For that value of 3 seconds, I presume that the flow rate is based upon gas flow rate. In this case you assume the seed introduction is like an aerosol which has the same flow rate as the gas. What happens if later on the particle gets bigger and bigger? The explanation of Tom Fitzgerald may apply here so that the gas velocity and the seed velocity will be different.

FLAGAN: That increases the mass transfer to the particle which should help things along.

HSU: What is the configuration of the flow? Is it an upward flow?

FLAGAN: The first version we built is operating at a very small flow rate. Due to the problems of the thermally induced secondary flows, the flow is vertically upward. We are planning to increase the scale of the reactor somewhat and invert it at the same time. That change is in process now.

PRATURI: I just have one more comment. You said that in the ideal case when the process proceeds to really large-size particles, it becomes a fluidized-bed reactor. Is that correct?

FLAGAN: It could provide a seed for a fluidized bed ultimately. Probably the practical limit for the operation of this system is the approach to a dense bed.

PRATURI: But this same type of analysis would show, would it not, that this is actually what would happen to a fluidized-bed reactor itself?

FLAGAN: In the analysis that we have carried out so far, we have been dealing with very small particles and with a system in which the particles are treated as basically quiescent, or moving, at least, at low Reynolds number. If we consider a fluidized bed, we are dealing with particles at much larger Reynolds number and so the communication between the particles and the free stream drafts is not nearly as good. So you have a boundary layer approximation and there is a region of gas. This will probably limit the ultimate size. There will be a problem at large Reynolds numbers. This is a valid point.

GRIMMETT: In a fluidized bed, breaking up of that boundary will occur because of the collisions between the particles. This will reverse the process.

FLAGAN: Well, that is for the fluidized bed people to answer. That will come tomorrow.

SHANFIELD: A simple question. Why did you have such a low throughput?

FLAGAN: Because we've done the project on a shoestring.

SHANFIELD: Do you see any limitation to scaling this process to a much higher throughput?

FLAGAN: It will require consideration of the role of turbulence. Other than that, no.

## COHERENT DETECTION OF SCATTERED LIGHT FROM SUBMICRON PARTICLES

Donald Pettit

University of Arizona

I discussed the present particle counting technology in the previous talk. Now I will discuss the development at the University of Arizona of a coherent optical particle spectrometer, known as the COPS system. This is an optical technique that uses the coherent properties of light to measure the scattered phase instead of the scattered intensity. In this manner the particles in a size range from .02 to 10 microns can be counted. The .02 micron limit is still based on theoretical calculations. Experimentally we haven't pushed the detection limit down that far, but we have every intention of doing that in the future.

Particle concentrations up to about  $10^9$  particles  $\text{cm}^{-3}$  can be counted because of the small inspection regions that can be achieved with this technique. Since it is an optical technique, there are possibilities for in situ sampling.

Scattered light by particles is incoherent, but there is an optical trick which can be used to make this scattered light appear to be coherent. The sensitivity of coherent detection techniques, such as optical heterodyning, can be used to measure the scattered phase; and this offers a method to optically size the particles. The optical trick consists of using the Van Cittert Zernike conditions in which there is a lens and at the focal point there is a particle scattering light. The wave fronts coming off this particle will be incoherent. If this particle is smaller than the resolution limit of the gathering lens, the scattered wave fronts will not be resolved into a coherent plane wave with average phase shift properties as seen by the solid angle of view. Essentially, incoherent light is imaged into coherent light at the expense of average phase information. This can be used to develop a particle counter in which a laser beam goes into a couple of prisms which constitute a Jamin interferometer. The first prism breaks up the beam into two paths. One is called the subject beam. In its path there are a couple of lenses space one focal length apart so the emerging beam remains collimated. The other path, designated the local oscillator beam, goes directly into the second prism where the two beams are combined and fall on a photo detector.

Consider a collection of particles which pass one at a time through the beam waist region provided by the lenses in the subject beam. The gathering lens will image the scattered light into a coherent plane wave with average phase shift properties and will be coherently superimposed with the local oscillator beam at the surface of a shot noise limited square law detector. The principles of optical heterodyne detection are used to measure the power in the phase modulated side bands. Light scattered out of the beam will cause an attenuation. That will appear as amplitude modulation. Thus, amplitude modulated side bands can occur at the same time as phase modulated side bands. The vector sum of the electric field vectors is measured by the

photodetector. If the relative phase and amplitude of the local oscillator beam is adjusted so that the resultant vector is  $90^\circ$  out of phase from that of the carrier and the subject beam, the phase modulated side-bands on the original carrier now will appear as amplitude modulated side-bands on the resultant, and the amplitude modulated side-bands on the carrier are now phase modulated side-bands on the resultant.

The signal from this device will appear as a string of pulses, the height being the magnitude of the phase modulated side-bands. The power in the phase modulated side-bands can be related to the magnitude of the phase shift, and the magnitude of the phase shift can be related via the scattering mechanisms to the size of the particle. The height of the pulses then is a direct measure of particle size and the means of processing these pulses would not be any different than those from a conventional optical particle counter that uses intensity based measurements. The physics describing these pulses are fundamentally different, because they are based on phase measurements and not intensity measurements.

A primary lens is used to focus the light down to a beam waist. The resolution limited blur spot diameter with its associated depth of focus (the focus from the gathering lens) is submerged inside this beam waist. The phase modulated side-bands can only be measured if there is a coherent signal, and this will only occur when the light is being scattered within this volume. Light being scattered outside this volume will not be imaged as coherent plane waves by the Van Cittert Zernicke conditions and will not contribute to the measurements in the phase modulated side-bands. An optical viewing volume is therefore specified here by the resolution limited blur spot diameter and the depth of focus of the gathering lens. There will be a Gaussian intensity profile throughout this beam waist. If the diameter of this blur spot is made a factor of 10 smaller than the diameter of the beam waist, the intensity distribution across this inspection region will be sufficiently uniform to give path independent signals. Using heterodyning and Rayleigh scattering theory, an estimate of the minimum detectible particle size will be of the order of .02 microns for this technique. The reason this technique has more sensitivity than intensity based techniques is that there is no background scattered phase. The background phase is the propagation of light with a refractive index through the medium. There is no background scattered intensity as in the case with intensity based measurements. The signal to noise ratio is given in terms of the frequency of the light, the electronic bandwidth, and quantum efficiency of the detector, parameters important in optical heterodyning.

In conclusion, then, the coherent properties of light available in the laser beam can be used to measure the scattered phase and an instrument for measuring the scattered phase has some advantages over the present intensity based techniques.

## DISCUSSION

FLAGAN: What volumes were you sampling? What is the number concentration that you can observe?

PETTIT: For the calibration aerosols I was using, I had at least  $10^5$  particles  $\text{cm}^{-3}$  for a calibration aerosol, and I was getting signal rates of the order of maybe 10 or 20 Hertz. The size of my inspection region right now is about 15 microns in diameter and about 50 microns long. That is about the size of the inspection region I am presently using. I have experimented with different size regions, and I have gotten regions down to as small as 2 microns by 5 microns; that is a function of the microscope objective.



#### SESSION IV: Fluidized-Bed Reactor Technology

FITZGERALD (Chairman): This morning's session is on fluidized-bed reactors. There are four papers. The first two deal with different conceptual methods of growing particles of fluidized beds. In the first paper Jim Kaae of General Atomic will describe the work he has been doing with carbon deposition systems, which are a little different from silicon, but there are a number of similarities. He will be pointing those out to us. Then I will discuss a proposed mechanism for silicon deposition from silane in a fluidized bed. Dr. Kayihan's paper deals with a numerical procedure which is very useful to actually calculate what goes on a fluidized bed where the particles are changing size. Finally, Earl Grimmett, who has probably done more experimental fluidization studies than anybody I know, is going to talk about some of the studies he has done on particles in fluidized beds.

Before we start, I should point out for those of you who haven't been following the JPL program for the silane system that particles have been grown in a fluidized bed. When these particles were grown around 700°C, some unusual things happened. In progressing from 5% to 10% to 14% silane as the feed concentration, the amount of dust coming out of the top did not increase as expected. In fact, I believe that the silane concentration was increased above 60% with only a modest amount of dust going out of the top. This came as a surprise when it was first done, because everyone was convinced that you had to use a lot of dilutant and not too much silane if you wanted to get a dense coat. A lot of dust was expected when operating with these high silane concentrations, and these experiments showed it doesn't happen. Now, the fluidization apparently must be done with a high velocity so there is no sticking together or agglomeration of the particles. Under these conditions, the particles appeared to have a dense coat. Further, using BET measurements of the amount of surface that was available, there were attempts to determine whether these particles were just little dense spheres which stuck together. The evidence was that this was not the case and that the apparent surface area was consistent with the overall size of the particle. So, these experimental results at JPL which showed that silane has been used in fluidized bed to yield dense particles should be kept in mind during this session. The first two papers should form a basis for the discussion of the phenomena involved in this reaction.

PRECEDING PAGE BLANK NOT FILMED

J. L. KAAE

GENERAL ATOMIC COMPANY

P. O. BOX 81608, SAN DIEGO, CA 92138

## 1. INTRODUCTION

As the title indicates, this paper concerns the mechanism of chemical vapor deposition of carbon in a fluidized bed of particles. One may ask what relevance this subject has to the preparation of silicon materials. The answer is that there are two ways in which this work is relevant. Firstly, chemical vapor deposition in a bed of fluidized particles can be a very efficient means for conversion of gas into a solid at a high rate. Thus, the process of chemical vapor deposition in a fluidized bed of particles is of interest for low-cost conversion of gaseous compounds of silicon into solid silicon. As an example of the capability of this process, in the deposition of carbon, which has been studied extensively for coating of nuclear fuel particles for the high-temperature gas-cooled reactor, deposition efficiencies greater than 90% can be attained at deposition rates of 4-5  $\mu\text{m}/\text{min}$  on the particles. The rate of total carbon deposition depends on the size of the coater because more particles can be coated in a large coater than in a small coater. Thus the process has a high efficiency and is open ended on the rate of deposition, depending on the size of the coater. Secondly, because carbon and silicon occupy the same column in the periodic table, they are chemically similar, each having four valence electrons. Therefore, one might expect the chemical vapor deposition of carbon to be similar to the chemical vapor deposition of silicon. However, there are differences. The hydrogen-carbon bond is stronger than the hydrogen-silicon bond, and as a result, hydrocarbon compounds are more stable than hydrosilicon compounds. For example chemical vapor deposition of carbon from methane ( $\text{CH}_4$ ) requires deposition temperatures greater than about  $1200^\circ\text{C}$ , while chemical vapor deposition of silicon from silane ( $\text{SiH}_4$ ) can be carried out as low as  $700^\circ\text{C}$ . The major difference between the chemical vapor deposition of carbon and that of silicon, however, is in the crystalline form of the deposited material. One of the crystalline forms of carbon, diamond, is identical to that of silicon, but this is not the form that results from chemical vapor deposition. The crystal structure of chemically vapor deposited carbon is a variation of the graphite crystal and is known as turbostratic carbon. The graphite and turbostratic carbon crystal structures are shown in Fig. 1. In turbostratic carbon, the order between one layer plane and the next has been lost, and in effect, the crystal is two dimensional. Because of the very strong bonding between carbon atoms within the layer planes and the very weak bonding between atoms in adjacent layer planes, the graphite crystal and the turbostratic carbon crystal are very anisotropic, with the optical, electrical, thermal, and mechanical properties all being very directionally dependent. This anisotropic nature of the turbostratic carbon crystal, to some extent, has facilitated the structural studies of the pyrolytic carbons.

## 2. DEPOSITION CONDITIONS

The coater used for these studies consisted of a vertical tube with a conical gas inlet at the bottom end. The tube diameter was 3.5cm. A charge of 50g of nearly spherical  $\text{ZrO}_2$  particles about 400  $\mu\text{m}$  in diameter was employed for each coating run, and the total gas flow rate was 10  $\ell$ /min.

The deposition mechanism described below is based on microstructural observations made on coatings deposited in a series of coating runs where first the deposition rate of carbon was varied by varying the concentration of a hydrocarbon gas in the fluidizing gas stream at a constant deposition temperature of 1300°C. Then, in another series of coating runs the deposition temperature was gradually increased while holding the deposition rate approximately constant at an intermediate rate of 4  $\mu\text{m}/\text{min}$ .

Propylene ( $\text{C}_3\text{H}_6$ ) was used as the hydrocarbon gas. However, it is known that the carbon microstructure is independent of the source hydrocarbon for similar deposition rates and deposition temperatures<sup>(1)</sup>, and therefore the carbon source gas is not considered to be an important variable.

Measurements of the preferred orientation of the carbon crystallites in the deposit on the particles were made using an optical technique developed by Stevens (2). The densities of the carbon coatings were measured by a sink-float technique in a mixture of bromoform and alcohol after coatings were broken off the particles. Optical and scanning electron microscopy was performed on sectioned coated particles. Transmission electron microscopy was carried out on coatings removed from small graphite discs fluidized along with the bed of particles after the coatings were thinned first by grinding and then by argon-ion bombardment.

## 3. CHANGES IN STRUCTURE WITH DEPOSITION RATE AND TEMPERATURE

The density of the deposits in the series of coating runs made at constant deposition temperature did not greatly change with increasing deposition rate, but the preferred orientation of the carbon crystallites did vary, increasing with decreasing deposition rate. The variation of the preferred orientation with deposition rate is shown in Fig. 2, where the preferred orientation is expressed in terms of the Bacon Anisotropy Factor (3), which is a universally employed manner of expressing preferred orientation of carbons and graphites. The Bacon Anisotropy Factor is 1.0 for an isotropic coating and is        for a coating with perfect alignment of the crystallites.

Another change in the deposit that occurred with increasing deposition rate was a strong increase in the porosity in the surface layer of the coating as well as an increase in the number of pores within the coating. (Surface porosity was not included in the density measurement because the sink-float fluid penetrated this porosity.) These changes are shown in the three scanning electron micrographs of cross-sectioned coated particles shown in Fig. 3.

The primary structural change in the series of deposits made with increasing temperature while holding the deposition rate constant was first a decrease in the density of the deposit with increasing temperature up to

about 1600°C and then a subsequent increase in the density at higher temperatures. This density variation is shown in Fig. 4.

Point counts of the pores in scanning electron micrographs showed that the decrease in coating density with increasing deposition temperature in the range 1300°C to 1600°C was not caused by an increase in the volume fraction of the 0.1  $\mu$ m to 1.0  $\mu$ m diameter pores observable in the scanning electron microscope (See Fig. 5).

#### 4. VARIATIONS IN THE MICROSTRUCTURES WITH DEPOSITION RATE

Only with transmission electron microscopy has it been possible to resolve the microstructures of fluidized-bed pyrolytic carbons, and until application of this technique, the nature of this material remained relatively unknown. The type of microstructure that is observed when a 1300°C deposit is viewed parallel to the deposition plane is shown in Fig. 6. The grain-like units making up the carbon will be called growth features. By selected area electron diffraction it was found that the growth features are polycrystalline with the layer planes of the small (30A) carbon crystallite tending to lie parallel to the surface of the growth feature. This arrangement of crystallites is shown schematically in Fig. 7.

When the carbons were viewed perpendicular to the deposition plane, it was found that the shape of the growth features changed with deposition rate, and the manner of the changes suggested a deposition mechanism that was consistent with the structural changes described in the previous section.

A transmission electron micrograph of a 1300°C carbon that had been deposited at a low rate is shown in Fig. 8. The viewing plane is perpendicular to the deposition plane. When viewed in this orientation, it can be seen that the growth features in this carbon are conical with a small sphere at the apex of each cone. No inter-growth-feature pores are present because the cones impinge uniformly on one another.

The microstructure of a 1300°C carbon deposited at a medium rate is shown in Fig. 9, where the viewing plane is again perpendicular to the deposition plane. Here, the growth features are still conical, but the spheres at the apex of the cones are larger, and the cones are shorter than those in the low-deposition-rate carbon. A close examination of the growth features reveals that they are made up of smaller cones which emanate from the center of the sphere at the apex of the growth feature. (See arrows in Fig. 8.) These sub-growth-feature cones are extended in the macroscopic growth direction in order to conform to the shape of the growth feature. Again, no inter-growth-feature pores are present.

The microstructure of a 1300°C carbon deposited at a high rate is shown in Fig. 10. Again, the viewing plane is perpendicular to the deposition plane. In this carbon, the growth features are more polygonal than those in carbons deposited at lower rates, and some inter-growth-feature pores are present. Sub-growth-feature cones are evident in the growth features, a few of which are indicated by arrows in Fig. 10. These small cones emanate from near the center of the growth features, and no extension of the cones in the macroscopic growth direction is apparent.

## ORIGINAL TEXT OF POOR QUALITY

The shapes of the growth features in the carbons deposited at higher temperatures were similar to those described above for the 1300°C carbons when comparisons were made at the same deposition rates. There was, however, a difference in the appearance of the fine structure of the carbon within the growth features. A transmission electron micrograph of a carbon deposited at 1500°C is shown in Fig. 11 with the viewing plane parallel to the deposition plane. This microstructure should be compared with the microstructure of the 1300°C carbon shown in Fig. 6 to see the difference in the fine structure within the growth features. At very high magnification, where the layer planes of the carbon could be imaged under phase contrast conditions, the source of the differences in the structure could be determined. Micrographs showing the imaged layer planes in the two carbons are shown in Figs. 12 and 13. Note that layer planes are imaged in the deposits only when they are perpendicular to the electron beam. Thus, regions where layer planes are not imaged are not necessarily vacant, but they may contain crystallites oriented in other than the perpendicular orientation. In the 1300°C deposit, the small 30Å carbon crystallites are in a very uniform arrangement, with the layer planes of one crystallite oriented very nearly in the same direction as the layer planes of adjacent crystallites. Thus, in this deposit the preferred orientation on a microscopic scale is very high, and there is little microporosity between adjacent crystallites. In the low-density deposit, the crystallites are in a nonuniform arrangement in a structure that can be likened to a collection of tangled fibrils. This structure obviously contains considerable microporosity, and this microporosity is almost certainly the very fine porosity required to explain low density of this deposit. At higher deposition temperatures, the fine structure within the growth features returned to the uniform arrangement observed in the 1300°C, except that the crystallite size was larger.

### 5. DEPOSITION MECHANISM

Because of the very different size scales on which the changes in the shapes of the growth features and the changes of the fine structure occur, the mechanisms of these two structural changes are thought to be separate. Thus, two aspects need to be considered in the deposition mechanism, one to deal with the change in the shape of the growth features, and the other to deal with the change in the crystallite arrangement.

A mechanism to explain the change in the crystallite arrangement will be considered first. Because of the fine scale of the structural changes within the growth features (a crystallite in this material contains only about 1000 atoms) and because the temperature changes that produce the fine structural changes have a strong effect on the molecular species within the decomposing gases, it is likely that the temperature-induced changes in structure are due to changes in the nature of the depositing molecular species. Palmer and Cullis have suggested that the depositing species in carbon deposition from decomposing hydrocarbons are planar molecules with relatively high carbon to hydrogen ratios<sup>(4)</sup>. The uniform arrangement of the crystallites in deposits made at 1300°C suggests that at this temperature the depositing molecules react with molecules on a surface in a preferred way to produce order between one crystallite and the next. To produce the observed crystalline structure, a planar molecule would have a

high reaction probability with the surface only when its plane is parallel to the plane of the surface. This is shown schematically in Fig. 14. Loss of hydrogen would continue after deposition, and indeed, pyrolytic carbons deposited at about 1300°C do contain appreciable hydrogen<sup>(5)</sup>.

At deposition temperatures near 1600°C, the reaction probability of the planar molecules with the surface apparently is changed, perhaps because of the presence of more active bonding sites within the planar molecules within the molecule. These more active molecules would have appreciable reaction probabilities for orientations other than the parallel orientation active at lower temperatures, resulting in deposition of molecules in various orientations, and a structure similar to that of the low-density carbons would be formed. This mechanism is shown schematically in Fig. 14b.

At even higher temperatures there may be sufficient thermal energy for the depositing molecules to migrate and reorient to energetically favored positions, and a uniform arrangement of crystallites would again be formed.

The change in shape of the growth features with changing deposition rate is believed to occur because of a change in the amount of carbon deposited on the substrate directly by molecular deposition and the amount deposited by particles that are nucleated and grow in the gas before deposition on the substrate. At low hydrocarbon concentrations, where deposition rates are low, there is a low probability for the formation of particles, and those that do form will be small. Most of the carbon deposited on the substrate will come from molecular deposition. The few small spherical particles that are formed and deposited influence the structure by acting as nucleation sites for new growth cones. In this deposition sequence, which is shown schematically in Fig. 15, a structure made up of small growth cones will be formed; there will be a high degree of preferred orientation of the crystallites because molecular deposition on the substrate occurs only for a specific orientation of the molecules; and, there will be very little surface porosity.

At higher hydrocarbon concentrations, where the deposition rates are higher, nucleation and growth rates of the gas-born particles are higher, and more and larger particles are incorporated into the deposit. The spherical particles are made up of small cones emanating from the center of the sphere, and these small cones become the sub-growth-feature cones observed in the transmission electron micrographs. The carbon layer planes are oriented preferentially parallel to the surface of the particle, but because of spherical symmetry, each particle is an isotropic entity. As is shown schematically in Fig. 16, once the particles are deposited on the substrate, they continue to grow by molecular deposition in regions that have access to the gas. Because of this post-deposition growth, the sub-growth-feature cones nearest the surface elongate while those nearest the substrate do not. Also, as long as access to the gas is not blocked by the deposition of other particles or by closure of gas paths by molecular deposition, interstices between particles are gradually filled by molecular deposition. In this way, an increased deposition rate, which is caused by an increased hydrocarbon concentration, leads to a more isotropic deposit, an increased number of inter-growth-feature pores, and an increase in the porosity in the surface layer.

# 6. REFERENCES

1. Kaae, J. L., Carbon, **13**, 55 (1975).
2. Stevens, D. W., Surface Science, **96**, 174 (1980).
3. Bacon, G. E., J. Appl. Chem., **6**, 477 (1956).
4. Palmer, H. B., and Cullis, C. F., Chemistry and Physics of Carbon, Vol. 1, (Marcel Dekker Inc., New York, 1965).
5. Kaae, J. L., Carbon, **10**, 691 (1972).

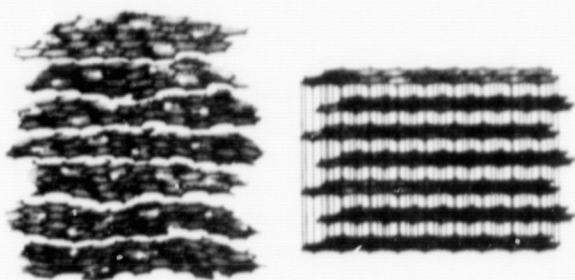


Fig. 1. (a) The crystal structure of graphite.  
(b) The crystal structure of poorly crystalline turbostratic carbon.

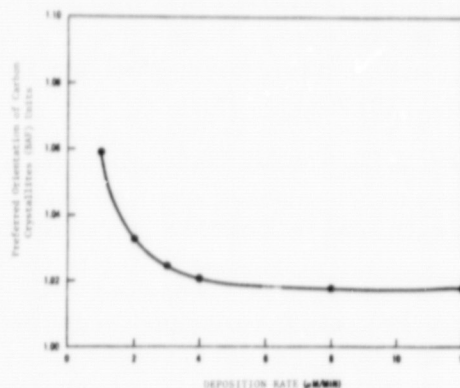


Fig. 2. Change in the preferred orientation of turbostratic carbon crystals in 1300°C deposits as a function of the deposition rate. Preferred orientation is expressed in terms of the Bacon Anisotropy Factor (3)

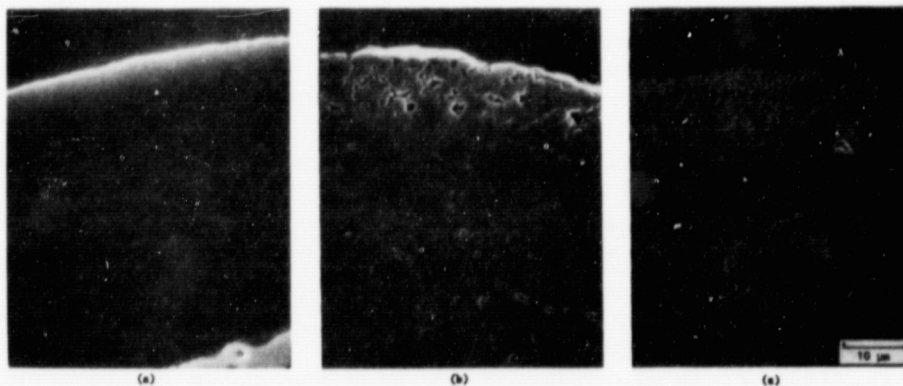


Fig. 3. Scanning electron micrographs showing surface and internal porosity of 1300°C deposits at deposition rates of (a) 1.1 μm/min, (b) 4.1 μm/min, and (c) 8.1 μm/min.



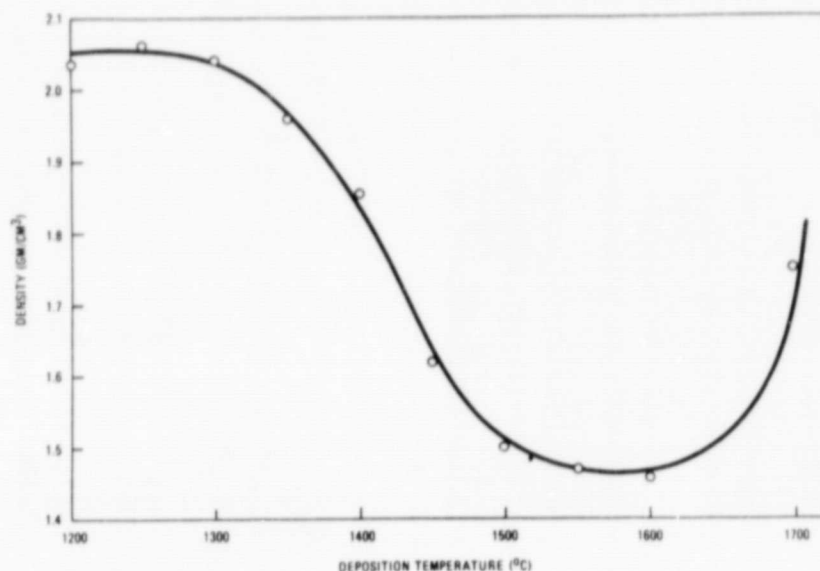


Fig. 4. Variation of the density of pyrolytic carbon with the deposition temperature at a deposition rate of  $4\mu\text{m}/\text{min}$ .

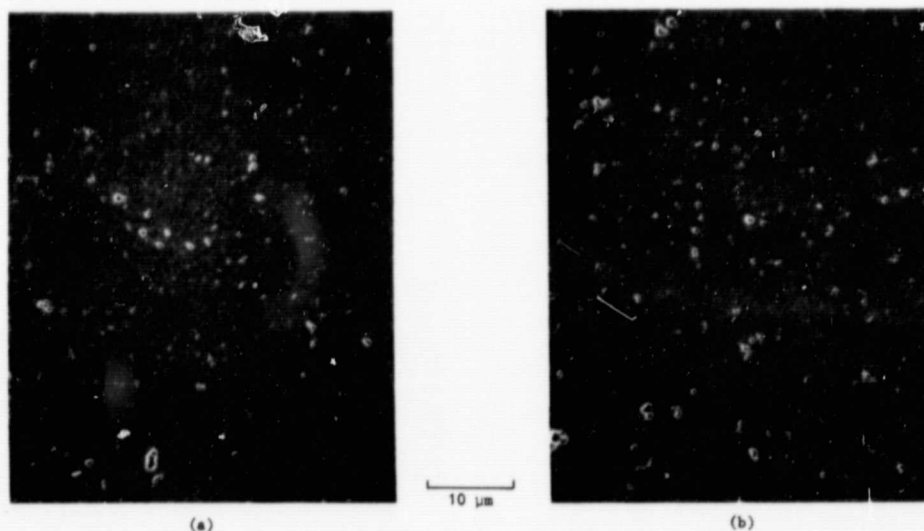


Fig. 5. Scanning electron micrographs of polished sections of (a) a high-density carbon ( $1.95\text{ g/cm}^3$ ) and (b) a low-density carbon ( $1.60\text{ g/cm}^3$ ). Point counts of the pores ranging from about  $0.1\mu\text{m}$  to  $1.0\mu\text{m}$  in diameter showed their volume fractions to be about 3% and 6% for the high- and low-density carbons, respectively. The volume fractions of porosity required to account for the densities are 11% and 25%.



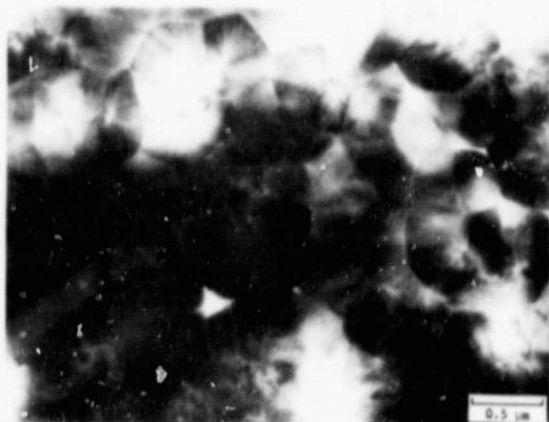


Fig. 6. Growth features observed by transmission electron microscopy of a 1300°C deposit viewing parallel to the deposition plane.

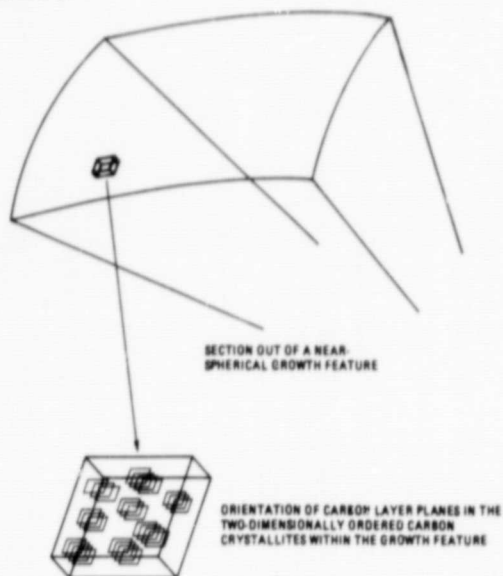


Fig. 7. Schematic diagram of the crystalline arrangement within a growth feature.

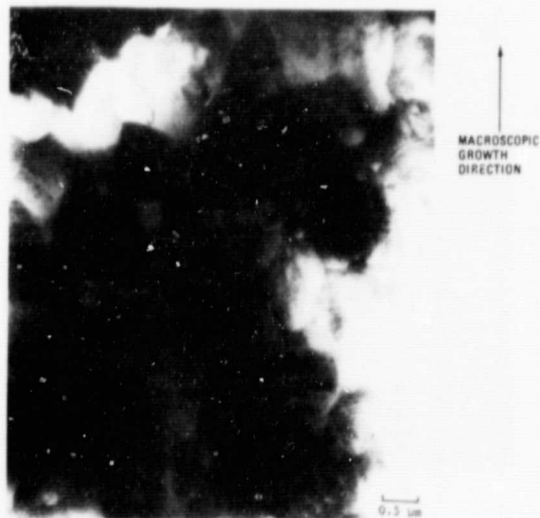


Fig. 8. Transmission electron micrograph viewing perpendicular to the deposition plane of a carbon deposited at a low rate. Note the conical growth.



Fig. 9. Transmission electron micrograph viewing perpendicular to the deposition plane of a carbon deposited at a medium rate. Arrows indicate conical growth features within the larger growth features.

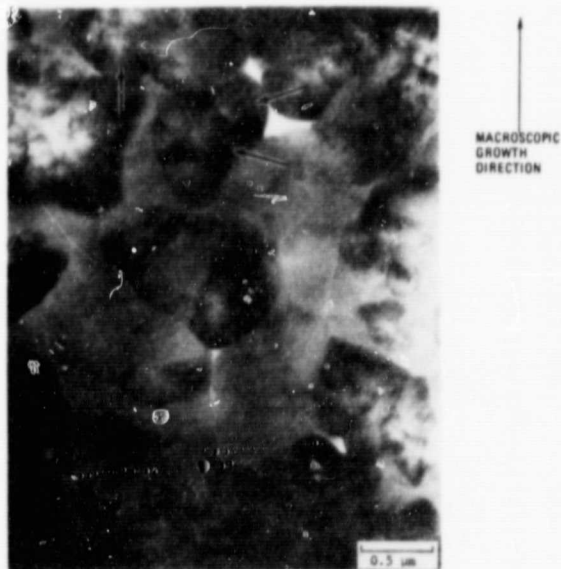


Fig. 10. Transmission electron micrograph viewing perpendicular to the deposition plane of a carbon deposited at a high rate. Arrows indicate conical growth features within the larger growth features.



Fig. 11. Growth features observed by transmission electron microscopy of a 1500°C low-density carbon viewing parallel to the deposition plane. Compare this structure with that of the high-density carbon shown in Fig. 6.

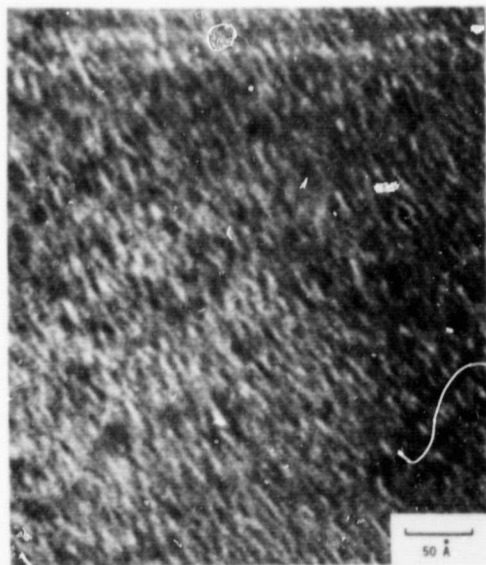


Fig. 12. Phase-contrast transmission electron microscopy showing the carbon atomic planes in a high-density deposit.



Fig. 13. Phase-contrast transmission electron microscopy showing the carbon atomic planes in a low-density deposit.

ORIGINAL PAGE IS  
OF POOR QUALITY

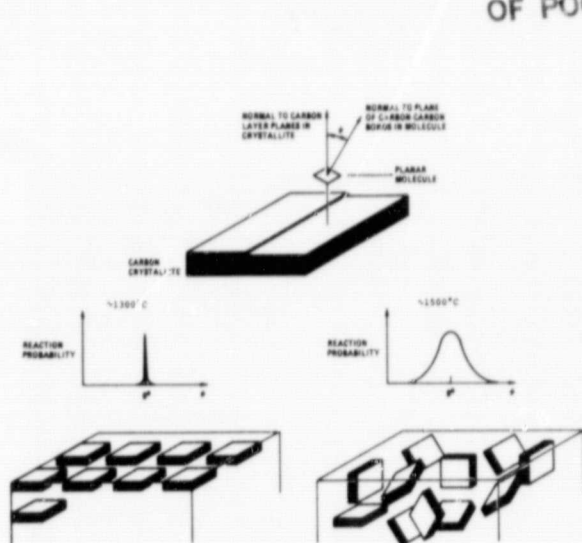


Fig. 14. Proposed temperature-induced changes in reaction probability between planar molecules and the surface which lead to changes in the density of the deposit.

— HYDROCARBON MOLECULAR SPECIES  
① PARTICLES FORMED BEFORE DEPOSITION ON THE SURFACE

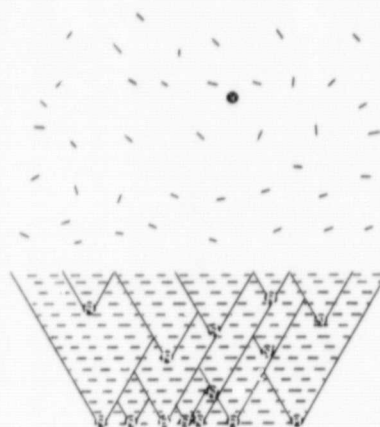


Fig. 15. Schematic diagram of the proposed carbon deposition mechanism at low deposition rates which leads to conical growth features and a high degree of preferred orientation of the carbon crystals in the deposit.

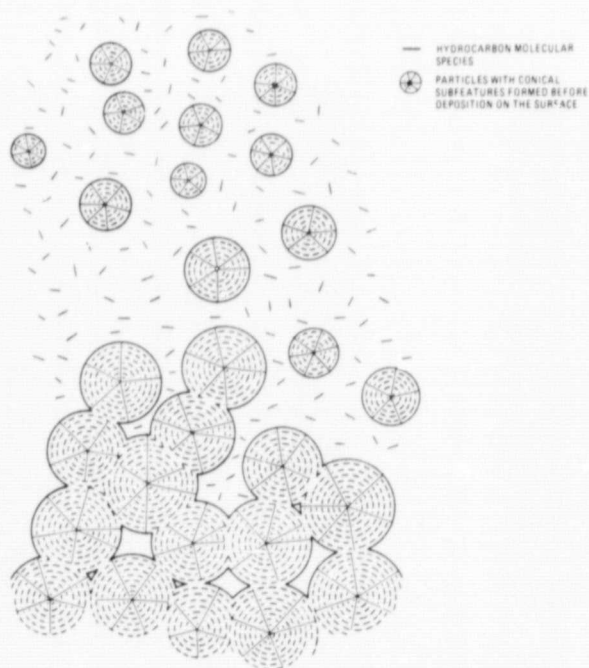


Fig. 16. Schematic diagram of the proposed carbon deposition mechanism at high deposition rates which leads to polygonal growth features, a low degree of preferred orientation of the carbon crystals and inter-growth feature pores.

## DISCUSSION

PRATURI: Do you always find the carbon crystallites to be about 50Å?

KAAE: No. They vary somewhat with deposition temperatures; as the temperature increases, the size increases. For example, at 1300°C, the size is about 30Å and at greater than 1500°C they're about 100Å. It's not a huge change.

HSU: What range of deposition rates did you have?

KAAE: About 0.5 microns minute<sup>-1</sup> at the low end and about 10 microns minute<sup>-1</sup> on the high end.

DeLUCA: Taking account the two different growth mechanisms, one at the low rate and another at the high rate, one would suspect that at the higher rate dust would come out of the reactor, because very large nuclei of crystallites are forming in the gas phase. Did you observe that?

KAAE: Yes. As the conditions are changed from low to higher concentrations, the deposition efficiency, that is the amount of carbon deposited on the bed, decreases somewhat. There are very high efficiencies at low rates in the carbon system -- more than 90%. The efficiency will fall off to about 60% at high rates. Dust is formed by gas-phase nucleation, which forms particles which, for some reason, don't stick to the surfaces.

DeLUCA: Did you do X-ray diffraction of the low-density and high-density carbon as a function of temperature to find a difference in the d 100 lattice parameter?

KAAE: Yes.

DeLUCA: Could that account for the density difference?

KAAE: No. It doesn't. It only increases slightly.

GAUTREAU: Can you describe the fluidized bed you used? Did you have a distribution plate? Was it a conical bottom? What size feed was used? What was the product size?

KAAE: I used very small reactors of about 1-1/2 inches in diameter having a conical bottom, single cone. We used zirconium oxide particles as the substrate. They were about 500 microns in diameter. It was not a slugging bed.

GODDARD: I really don't see any reason to presume that carbon deposition and silicon deposition would be comparable just because they're in the same column in the periodic table. The characteristic difference between carbon and silicon is that carbon makes strong pi bonds. It makes very strong triple bonds, such as in acetylene. It forms conjugated systems

such as benzene and large polycyclic aromatics. On the other hand, silicon just hates to make pi bonds. A pi bond for silicon is maybe 15 kcal and so silicon would tend to want to make single bonds at every opportunity. So you wouldn't expect to get flat, plate-like molecules from silicon. Looking at vapors of carbon and silicon,  $C_3$  is a very prominent species in carbon vapor and  $C_3$ 's can combine to make  $C_6$ 's which may be precursors for making polycyclic molecules, and silicon does not have that property. Silicon and carbon in these respects can be considered as belonging to different parts of the periodic table. Just because each makes four bonds doesn't make them at all similar.

KAAE: I agree with you. I mentioned in my talk that they make different crystalline forms, but I think that the changes in the shapes of the growth features would be common. I think that's probably common to almost all chemical vapor deposition. It's obvious that you are not going to get the same crystalline forms, and that obviously has to do with the bonding between atoms. So you would not find these changes in preferred orientation. You would probably get preferred orientation of some sort in Si. I would be very surprised if you didn't. But it isn't as strong, because the carbon crystal is very anisotropic. So I agree totally with what you said.

BAILEY: I think silicon forms  $Si_3$ 's, to  $Si_6$ 's, to  $Si_{12}$ 's and so forth. They are called polysilanes.

PRATURI: You mentioned that the dust production increases with increase in deposition rate. Is it also a function of the temperature of the deposition?

KAAE: Yes, it is.

PRATURI: Does it increase or decrease with increasing temperature?

KAAE: I'm trying to remember. It's not as strong a function as it is with deposition rate. I think the efficiency goes up. If I remember rightly, the efficiency goes up with increasing temperature somewhat.

ATWATER: You alluded briefly at the end of your talk to the surface mobility of the nuclei at low deposition rates. Related to that, how thin a layer can you grow that is continuous? How uniform is the nucleation at the low deposition rate?

KAAE: Well, it turns out that if you want to get down to that particular aspect, I have seen in some of my TEM studies that at low deposition rates the initial layer that goes down on the substrate is not nucleated by gas-phase nucleated particles, but nucleates right on the surface. So to start out with, right on the surface there is a layer of growth cones that are nucleated and then the next layer of growth cones are probably nucleated by particles that come down. So the initial layer can be quite thin and continuous. I can't answer your question. I would think very thin. Probably 100Å. It's hard to say. But the first layer, you see,

is just direct molecular deposition on the surface; so there's no reason for it to break up. At high deposition rates, I think there probably would be, but at low deposition rates not so.

FLAGAN: Have you looked at the structure of the fume that is carried out of the bath for clues to the source of the microstructure of the deposits that you are seeing and its variation with temperature?

KAAE: We did pull out the soot, or what you would call the dust -- that is, the particles that come out -- and we looked at the particle sizes to see how they compare with the particle sizes that might be presumed from the shapes of the growth features; they are consistent in size. The growth features of these particles are on the order of 0.5 micron in size and the nucleating particle, or particle that comes down and forms those, is somewhat less than that if you look at the shapes of things. That is consistent with the kind of carbon dust that comes off the top of the coater.

FLAGAN: Did you see any variation in the degree of agglomeration of those fine particles with temperature? What I am wondering is whether at the higher temperatures and the higher deposition rates you might be seeing more coagulation of very small nuclei which may provide the seed for the multidirectional growth?

KAAE: No, I didn't. The dust itself tends to be made up of agglomerates. It is very agglomerated. It is hard to say whether that agglomeration occurred as the stuff came out and collected, or whether it came out of the coater that way. It is obviously an agglomeration. The dust is a big mass and you try to disperse it. You can't really say which came first--the chicken or the egg. You can say that those little particles that are in there and form this dust are the same size, but whether they agglomerate within the coater, or out of the coater, I just do not know.

ROGERS: Is there a reason that you did not use chloroform or carbon tetrachloride? I ask that because we have found that the silane mechanism for deposition is perhaps considerably different than the mechanism for deposition for a chlorinated silicon compound. I was wondering if you had explored the differences between a chlorinated compound and a non-chlorinated compound?

KAAE: No, not really. Our technology is first of all economics. The hydrocarbons are cheap, easy to get and easy to put into a coater. They're gaseous. Secondly, we rely upon the fact that a lot of the material we coat would react with the chlorine or HCl that would be formed on decomposition of a molecule containing hydrogen and chlorine. Our technology is not in that direction but is really not oriented toward a different thing. It wasn't really a study of silicon formation, but rather carbon.

ROGERS: Would you have anticipated a different mechanism with etching taking place at the same time there is deposition?

KAAE: There have been studies where people have put in chlorine in combination with hydrocarbons. They have not gone into great detail and there's not a lot of information, but in general I think there was very little effect on the deposition. Chlorine has been introduced to see whether there was enhancement of deposition efficiencies and to see whether the carbon structure changed in a macroscopic sense; they didn't. There were subtle variations, but nothing striking and remarkable.



# A MODEL FOR THE GROWTH OF DENSE SILICON PARTICLES FROM SILANE PYROLYSIS IN A FLUIDIZED BED

by

THOMAS J. FITZGERALD

Senior Staff Process Engineer, Major Programs  
TRW Energy Development Group  
Redondo Beach, CA

This paper attempts to model the decomposition of silane in a fluidized bed. In particular, it seeks to reconcile the observed performance of actual fluidized bed reactors which produce silicon from silane at high concentration, with the generally accepted rates for various physical processes in the bed, notably: heat transfer, particle coalescence, thermophoresis and particle collection. In this model, the chemistry is drastically simplified: the formation of silicon by homogeneous decomposition is considered to be instantaneous, with no intermediates. The silicon will either be present as silane or as silicon metal. It will be seen that reconciling this assumption with reasonable estimates of the various rate processes that occur in the fluidized bed makes it necessary to hypothesize a rather large solid diffusion coefficient in order to produce the dense, coherent plating of silicon onto bed particles which has in fact been observed.

A detailed mathematical treatment with all the appropriate partial differential equations will be avoided; rather the attempt will be to find which rate processes are important and must be considered if a detailed model is to be constructed.

## BED CONDITIONS

For simplicity we will assume a bed temperature of 700°C, a bed particle size of 100 microns, and an inlet gas composition of pure silane. Figure 1 shows silane entering a fluidized bed. By assumption the incoming temperature is 350°C, which is low enough to prevent the spontaneous nucleation of silicon particles. As the gas enters the bed it forms a small jet, and as the gas from the jet moves out through the bed particles it is heated to bed temperature. Before the gas comes all the way to bed temperature, homogeneous nucleation will begin and silicon particles will form in the gas phase. The gas velocity is assumed to be 1 cm per second in the interstitial channels between particles. Thus, the gas will pass over a 100  $\mu$ m particle in 1/100 of a second.

## PARTICLE TO GAS HEAT TRANSFER

Now consider how rapidly the gas will come up to bed temperature. Because of its very low-density compared to the solids, the gas has a very low heat capacity. In fact, the heat capacity of the solids per unit volume is on the order of 10,000 times the heat capacity of the gas per unit volume. The result of this mismatch is that the gas passing over the solids comes to the temperature of the solids, and in the time that it takes for the gas to



pass over a particle the solids temperature hardly changes at all. The only way, in fact, that a sustained temperature gradient in the fluidized bed solids can be obtained, is to restrict the motion of the solids so severely that they will stay in a region of the bed for a rather long time -- on the order of minutes. The heat transfer coefficient from a particle to gas passing over the particle, is given by the formula

$$Nu_p = \frac{hd_p}{k_g} = 2 + 0.6 Pr^{1/3} Re^{1/2} \quad (1)$$

For the low particle Reynolds numbers ( $\frac{d_p u_p \rho_{gas}}{\mu}$ ) which are encountered in typical beds, theory predicts that the Nusselt number ( $hd_p/k_g$ ) should be 2, since that is the limiting value for very small Reynolds numbers. In fact what has been found experimentally is that the Nusselt number approaches 2 as the particle diameter goes to 0, but it does not approach 2.0 as the velocity goes to 0 (both factors would cause the Reynolds number to go to 0). Measured values of the Nusselt number are typically between 0.1 and 0.001. A number of explanations have been proposed for this disagreement but they don't concern us at this point. For our purpose it will be sufficient to assume a Nusselt number of 0.1 as being reasonable for the gas velocity and particle size which we have assumed. Based on this number we now calculate how quickly the silane heats to decomposition temperature.

We consider a very idealized geometry (shown in Figure 2) as representative of an interstitial flow channel between particles. We assume that the channel is rectangular in shape and is 100 microns on a side. The physical properties of the gas will be somewhere between the physical properties of silane and the physical properties of hydrogen which is produced when the silane decomposes. As an easy compromise we pick the physical properties of air -- thus, the heat capacity of the gas is assumed to be  $6 \times 10^5$  calories/cm.s.K. For a particle of 0.01 cm diameter, the heat transfer coefficient is then  $6 \times 10^{-4}$  cal/cm<sup>2</sup> s.K. When the gas moves a short distance into the channel it is heated by heat flux through the walls. The heat flux into the channel in length  $x$  is approximately

$$(6 \times 10^{-4}) (4 \times 0.01) (T_{Particle} - T_{gas}) x$$

and the heat picked up by the gas in the same length is

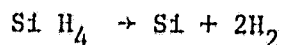
$$\frac{(0.01)^2 (12)}{67000} (T_{gas,out} - T_{gas,in})$$

In the above expression 12 is the heat capacity per mol of the gas and 67000 cm<sup>3</sup> is the gas volume per mol. Equating these two expressions leads to a rough estimate of the length required for the gas to come to particle temperature. The estimated length is three microns; therefore, it is quite reasonable to assume that the gas will come to the particle temperature in a distance less than the length of a particle.

#### ADIABATIC TEMPERATURE RISE FROM REACTION

Now consider what temperature rise occurs when silane decomposes adia-

batically. The stiochiometry is



At approximately 600°C the heat of reaction is 5000 cal/mol. (exothermic) and the heat capacity of hydrogen is approximately 7 cal/mol. K, the heat capacity of silane is approximately 12 cal/mol. K, and the heat capacity of the silicon metal is approximately 6 cal/mol. K. Figure 3 shows a simple control volume into which silane flows at temperature T and from which exits a product gas stream of hydrogen containing silane particles. The exiting gas stream is assumed to be at a uniform temperature. A simple energy balance based on the assumption that the heat of reaction is used to heat the products of reaction to exit temperature, indicates that the temperature rise will be approximately 350°C for complete reaction. Thermodynamics indicates that the reactions are strongly irreversible and hence if there are no major rate inhibiting steps, one can expect that the reaction will occur autothermally; that is, as reaction begins the temperature increases and so does the rate -- which in turn causes more reaction and still higher temperature. The limit of this temperature escalation is a 350 K rise in temperature.

#### AREA OF NEWLY FORMED MICROPARTICLES

When homogeneous silane decomposition occurs, a suspension of microscopic particle or silicon are formed in the gas phase. These particles will rapidly grow by collisions resulting from Brownian motion until the diameter of the microparticles is somewhat greater than 0.01 micron. Consider at this point how the surface area of the microparticles compares with the surface area of the interstitial flow channel through which the particles are moving. The volume of solids produced by one volume of silane is approximately 1/5000. The volume of hydrogen produced by one volume of silane is about 2.0. Therefore, the volume fraction of solids in the product is approximately 0.0001. The volume of a 0.01 micron microparticle is about  $5 \times 10^{-7} \mu\text{m}^3$ . The area of a 0.01 micron particle is approximately  $3 \times 10^{-4} \mu\text{m}^2$ . Therefore, in a cubic volume 100 microns on a side, the total surface of the microparticles is

$$\left[ \begin{array}{l} \text{Surface of} \\ \text{Microparticles} \end{array} \right] = \frac{(3 \times 10^{-4}) (100)^3}{(10000) (5 \times 10^{-7})} = 50,000 \mu\text{m}^2$$

The wall surface of the bed particles in the 100 micron cube is  $4 \times 100 \times 100 = 40,000 \mu\text{m}^2$ . Thus, the surface of the wall and the distributed surface of the particles are comparable. What is important, is that the newly formed particles are dispersed through the gas, and therefore are only a short distance away from any remaining silane molecules which still need to react. Therefore, if there is anymore silicon deposition, it will more than likely occur on the newly formed microparticles, rather than at the walls of the flow chamber (the surface of the existing bed particles).

We must now consider what processes bring the microparticles into contact with the existing bed particles. Thermophoresis is one such process, and to estimate its efficiency we must know the temperature of the particles in the bed.

### BED PARTICLE TEMPERATURE

Consider now how much a bed particle changes temperature in the presence of reacting silane. The particle time constant when there is no external resistance to heat transfer, can be estimated from the thermal diffusivity of silicon. The thermal diffusivity is a ratio of the square of a characteristic distance (in this case the radius) to the time for heat transform over that distance by conduction. For a 100 micron bed particle the time constant is of the order of  $10^{-4}$  seconds. Essentially, this means that the temperature at the inside of the particle will very rapidly track the temperature at the particle surface.

When there is heat transfer resistance at the surface of the particle, then this must be taken into account in estimating the response time of the particle. For this simple case we consider the particle as being isothermal with all the resistance concentrated in the film at the surface of the particle characterized by a heat transfer coefficient  $h$ . The time constant for the particle is now given by

$$T = \frac{MC_p}{hA} = \frac{(2.34)(6/28)(.01)^3 \pi/6}{(6 \times 10^{-4})(.01)^2 \pi/4} \sim 5 \text{ seconds}$$

The heat capacity of silicon is taken to be approximately 0.5 cal/gm.K, and the heat transfer coefficient is the same as was used previously (based on a Nusselt number of .1 for the particle). It is seen that the time constant is approximately 5 seconds -- much longer than when there is no external heat-transfer resistance. Therefore, it is reasonable to assume that the particle temperature is uniform.

Now consider how long the particle will stay at a bubble surface. To estimate the time, we will use a simple surface renewal model and assume that the amount of time that a particle stays at the surface is approximately equal to the diameter of the bubble divided by the velocity by which the bubble rises. Therefore the time at the surface is given by

$$\left[ \text{time at surface} \right] \sim \frac{d_b}{u_b} = \frac{d_b}{.7 \sqrt{g d_b}} = \frac{\sqrt{d_b}}{22}$$

For a two centimeter diameter bubble, the time at the surface is approximately 0.05 seconds. It follows therefore, that a particle does not spend enough time at the surface for it to significantly change its temperature, and we may conclude therefore that all particles throughout the bed are at the same temperature.

### THERMOPHORESIS

Thermophoresis refers to a drift velocity which is caused by different temperatures on opposite sides of microparticles. The resulting difference in momentum flux of colliding molecules pushes microparticles toward the cooler temperature. In this case, it pushes them toward the bed particles. The drift continues so long as the temperature gradient persists. A problem

similar to this, in which particles enter with a uniform distribution across a cylindrical channel, and are then collected by thermophoresis on the walls of the channel, has been solved by Walker (1979). The particles are assumed to move down the cylinder in laminar flow, and heat transfer between the flowing gas and the walls occurs along with the thermophoretic capture of particles. As first order approximation, the fraction of microparticles which are collected by thermophoresis is given by the simple formula

$$\frac{T_{\text{hot}} - T_{\text{cold}}}{T_{\text{cold}}} = \frac{\Delta T}{T_{\text{bed}}}$$

The numerator of this expression is the difference between the incoming gas temperature and the bed particle (wall) temperature. In our case this temperature difference is the adiabatic temperature rise which occurs when silane decomposes to make silicon and hydrogen -- approximately 350°C. The bed temperature is approximately 1000° K, hence, the capturing efficiency is approximately 35%. Thus, when the temperature difference has relaxed, 65% of the microparticles will still remain uncaptured.

#### PARTICLE CAPTURE BY IMPACTION

The particles which have not been captured by thermophoresis must eventually be collected by impaction on the existing bed particles. This must be so, because in experimental runs virtually no dust was seen to emerge from the bed. We have assumed that particles grow to approximately 0.01 micron in diameter. In the remaining time in the bed they may grow as large as .1 micron, but certainly no larger. Brownian motion becomes very slow as particles approach 0.1 micron. 0.1 micron diameter particles essentially travel with gas streamlines. When a streamline comes closer than one particle radius from a wall, then the particle will touch the wall and be captured. The probability of a microparticle being captured as it passes a bed particle is approximately equal to the ratio of the radius of the microparticle to the radius of the bed particle. This number varies between  $10^{-4}$  and  $10^{-3}$  depending on the size of the captured particle. We will assume that the distribution of particles remains essentially uniform across the flow channel, and that as particles are captured from the edges of the flow channel that other particles diffuse toward the edges to keep the distribution approximately uniform.

If one particle in a thousand is captured as the gases flow over a particle, then in a total length of 1,000 particles we would expect approximately 2/3 of the particles to be captured. In a length of 10,000 particles there would be virtually complete capture. For our assumed particle size of .01 centimeter, this length would correspond to a bed depth of 10 cm. If the probability of capture is 1 part in 10,000 as it would be for 0.1 microparticles, then approximately 10 times that bed depth of 100 cm would be required for complete particle capture. Experimental evidence (Hogle 1981) shows that virtually complete capture would be obtained in approximately 20 cm which is consistent with this picture.

Thus far we have explained how silane could decompose to form micro-

particles and how the microparticles could be captured by contacting particles in the bed. But we do not have an explanation for the dense coherent coating which has been observed on silicon particles grown in a fluidized bed. There must be some mechanism by which the captured microparticles, which have diameter between .01 micron and .1 micron smooth out to form a dense layer on the surface.

#### DENSIFICATION OF DEPOSITED SILICON

A dense coat would occur if the time interval between arriving microparticles at a surface is greater than the time required for them to spread by diffusion. With a linear growth rate of 1 micron per minute, which is characteristic of the systems in which smooth coherent coats have been obtained in fluidized beds, one can allow for approximately 5 seconds between the arrival of 0.1 microparticles. In order for bulk diffusion to account for the smoothing of the surface, the diffusivity would have to be greater than  $(10^{-5} \text{ cm})^2 / 5 \text{ seconds}$ ; that is, approximately  $10^{-11} \text{ cm}^2 \text{ per second}$ . Another possible method would be surface diffusion, in which atoms move off the microparticle surface and diffuse to a position in which the radius of curvature is smaller. Now a microparticle approximately 0.1 micron in diameter is approximately 1,000 atom layers thick, and 500 layers would need to diffuse a distance of approximately 0.1 micron in a total time of 5 seconds in order to produce the smoothing indicated in the sketch in Figure . In this case, the surface diffusion coefficient would have to be greater than  $(10^{-5} \text{ cm})^2 \div 10^{-2} \text{ seconds}$ . This would require a surface diffusivity therefore greater than  $10^{-8} \text{ cm}^2 \text{ per second}$ . At the temperature involved (about  $700^\circ\text{C}$ ) the required diffusion coefficients to give a dense coating seem rather large. If the true bulk diffusion coefficient and surface diffusion coefficient are indeed much smaller, then there must be an error in the postulated mechanism.

One possibility is that the amount of silane which is used in the formation of microparticles is relatively small, with most of the silane depositing later by a heterogeneous mechanism on to existing smooth silicon bed particles. Whatever nuclei were formed would be trapped under the heterogeneous deposit. In order to produce a relatively smooth coat, at least 90% of the silane would have to be deposited by the heterogeneous mechanism. Otherwise, the collected microparticles would continue to protrude like warts from the surface. Also, if heterogeneous deposition dominated, then one would expect to find more dust in the effluent gas as the concentration of the feed gas silane is increased. One would expect that homogeneous nucleation would have approximately second order kinetics as compared with first order kinetics for heterogeneous vapor deposition; hence, at very high concentration the homogeneous mechanism would dominate and produce an enormous amount of dust. It doesn't, thus making this mechanism unlikely.

There is another modification of the proposed mechanism which would lead to the kind of results that are observed. Recall that it was assumed that the decomposition of silane to silicon was virtually complete and instantaneous, therefore, the microparticles captured by bed particles would already be pure silicon. Perhaps the formation of pure silicon is a bit slower -- it may take a bit more time for the hydrogen to be eliminated from a polymeric  $(\text{SiH})_x$

compound. Thus, the particles captured at the surface could still be reacting and the silicon contained in them might still be mobile.

The fluidized bed reactor has demonstrated that a very efficient mechanism of growing silicon particles is indeed possible. Scale up of fluidized bed reactors, however, is never direct, and the more one knows about the underlying mechanisms the better is the chance of building a reactor which will work. What seems to be required now is a relatively careful look at the processes involved during the growth of particles in an environment essentially the same as would be found in a fluidized bed pyrolyzer.

#### REFERENCES

Hogle, R., G. Hsu and R. Lutwack, "Dust Formation and Bed Agglomeration in Fluidized Bed Silicon Production from Silane Pyrolysis". JPL Report, California Institute of Technology. 1981.

Walker, K.L., G.M. Homsy and F.T. Geyling, "Thermophoretic Decomposition of Small Particles in Laminar Tube Flow". Journal of Colloid and Interface Science, Vol. 69, No. 1. Mar. 1979.

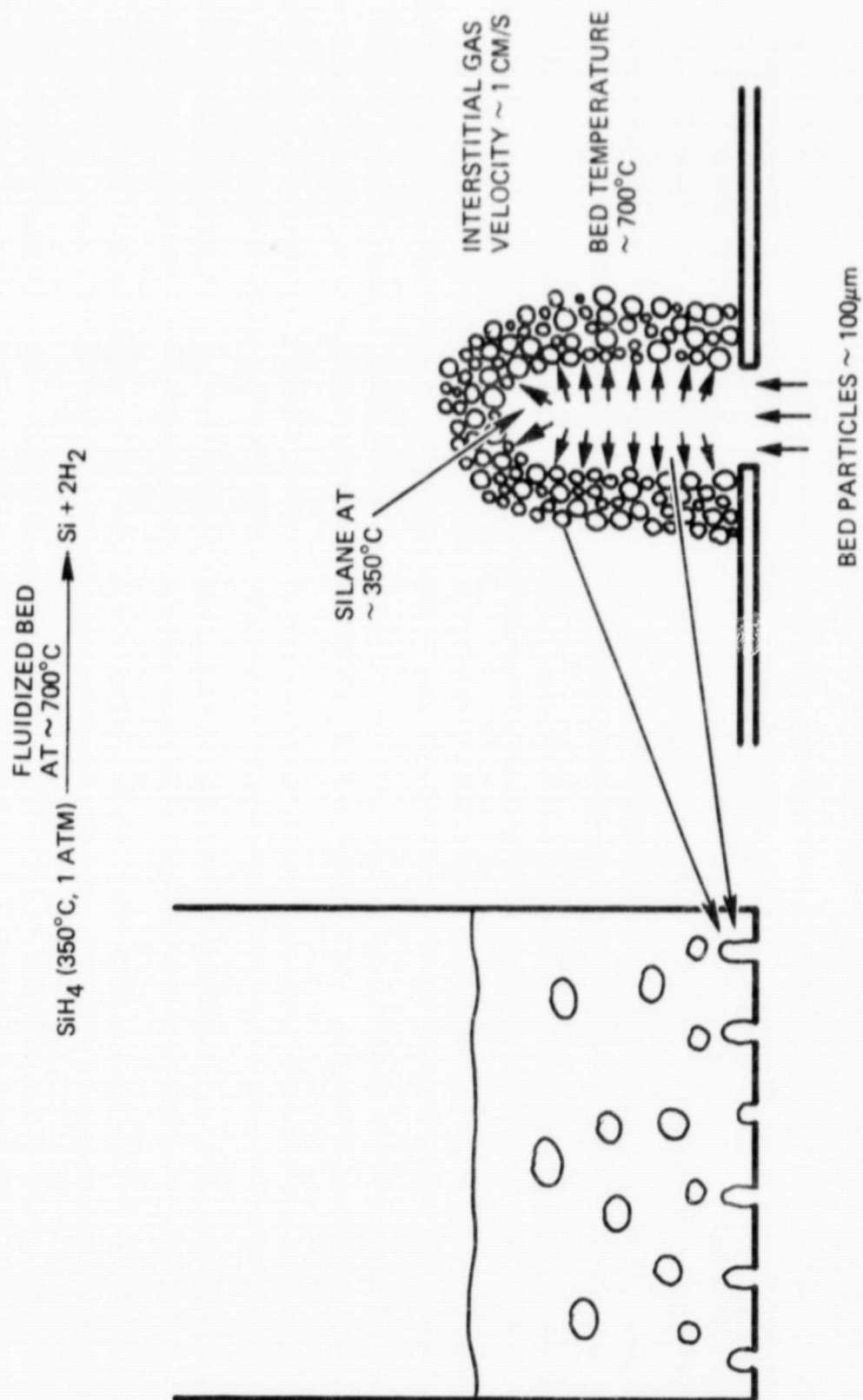


Figure 1.

ORIGINAL PAGE IS  
OF POOR QUALITY

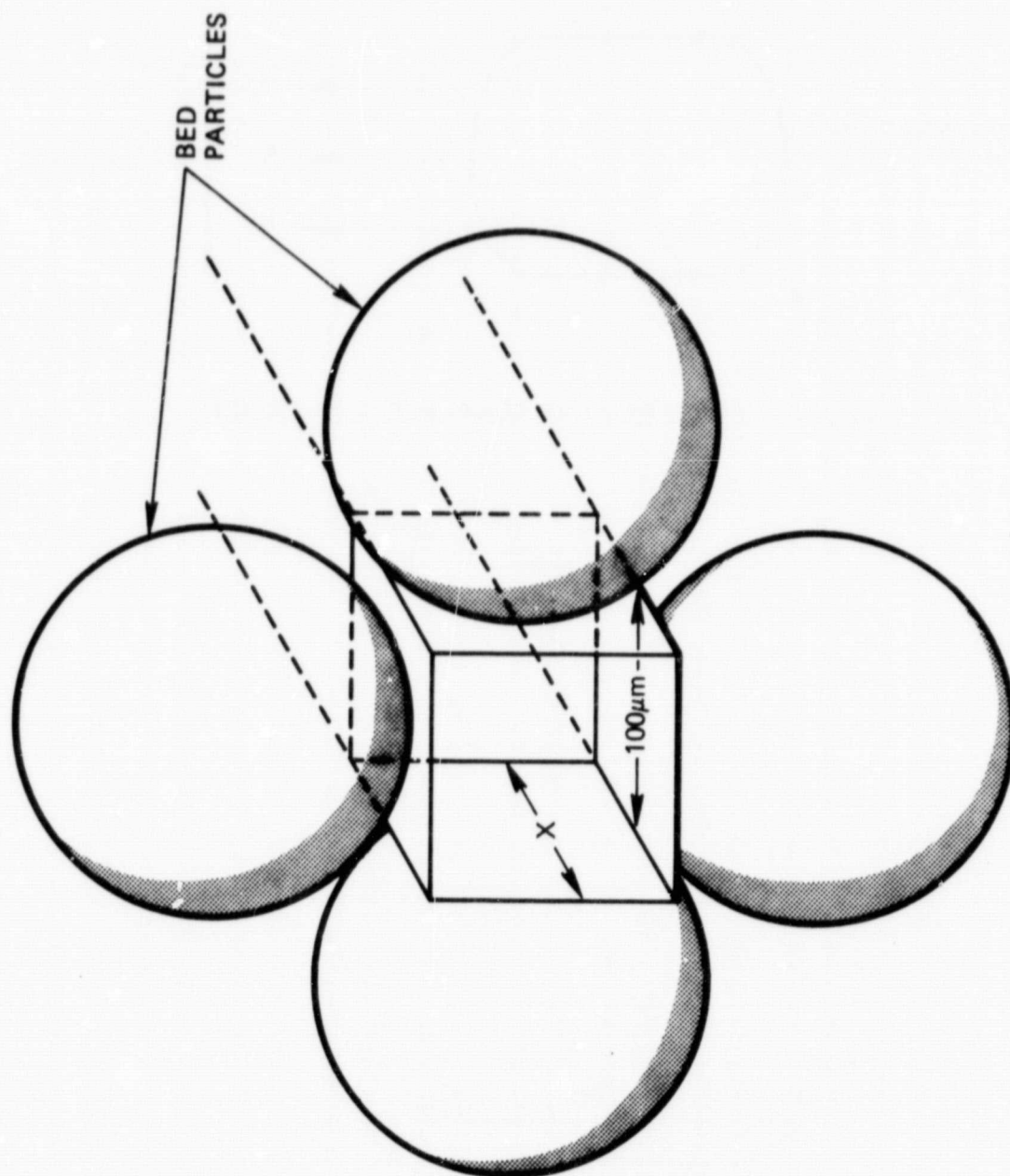
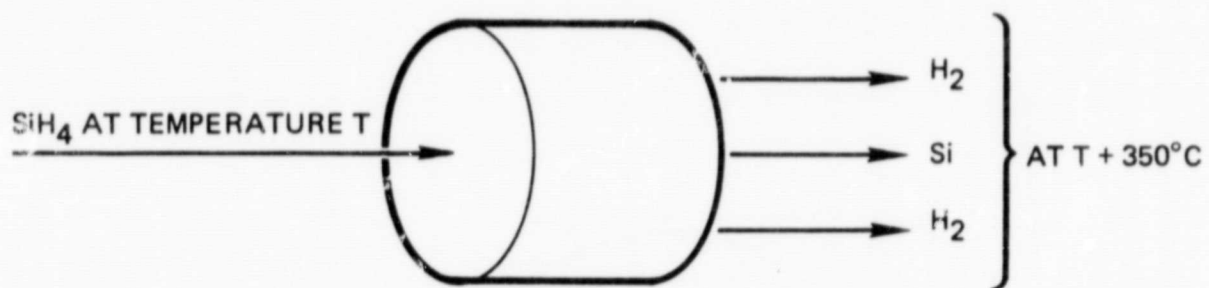


Figure 2.



ORIGINAL PAGE IS  
OF POOR QUALITY



BASED ON PURE SILANE FEED AND COMPLETE CONVERSION

Figure 3.

## DISCUSSION

DUDUKOVIC: I know very little about this mode of growth that you are proposing, but I would suggest that perhaps it is possible. Perhaps the place to look for other information is in the sintering literature. I would say that you shouldn't even look at the parallel between silicon and carbon, because there isn't any. Considering the conditions for forming the small silicon particles at temperatures above 800°C, that's well above the time and temperature for silicon. So sintering or the fusing-in of small particles into big ones will proceed. I understand that the time and temperature conditions for carbon wouldn't allow it to flow and simulate any kind of process which we call sintering. Something else still bothers me about your calculations, and it mainly concerns the heat-transfer coefficient. On one hand, I intuitively agree that the gas heats up fast; we always teach that to students in the course on fluidized-bed technology. On the other hand, if the gas heats the 100-micron particles up to 350°C over a one-particle diameter, then how did we possibly take any measurements on those Nusselt numbers which were taken in beds over many centimeters? That's what the correlation is based on. If profiles are measured in beds 10, 20, or 100-cm long, how can we get the proper heat transfer coefficients if the heating occurred in a regime that's almost nonexistent? So that really is a problem. Experimental evidence, in spite of what we teach students about a mythical bubbling bed, suggests that in highly exothermic, catalytic reactions there are very distinct temperature profiles in the fluid bed.

FITZGERALD: The first question I want to answer is how those temperatures are obtained in the packed bed. The particles don't move and so an indication of what the heat transfer coefficient is can be gotten by looking at the temperature profile in the solids which go through. So that makes a difference. As far as I know, nobody ever has measured it in a fluidized bed. They just assume that it is similar to what exists in a packed bed. Or else, they measure it incorrectly by taking into account the gas that bypasses and bubbles. But that's off the point, I think.

FLAGAN: I think you've considered most of the mechanisms that may be going on here, but I would like to suggest one additional mechanism that you've left out. And that is this: as the large particles are scavenging some of the 0.1 micron particles by impaction they form dendrites, which grow out from the particles and then act as a filter. These would be much more effective in collecting the smaller particles by diffusion than the larger particles would be. The smaller particles coming in would then give a smaller length scale for the subsequent surface diffusion and would reduce the requirement on the surface diffusivity to achieve that smoothing out and densification. Also, on the subject of carbon, carbon does in fact undergo surface diffusion if the carbon is heated to sufficiently high temperatures. Pyrolytic graphite is densified at temperatures approaching 3000°C, but that's a much higher temperature than considered here.

MILSTEIN: SERI supported a program at Case Western done by Professor Hoya to look at the matter of sintering roughly 1-micron silicon particles. He observed that there was essentially no sintering activity whatsoever up to temperatures within perhaps 10 or 20° of the melting point. Now, one thing that occurs in that circumstance is that there may be an oxide layer on the particles and that might not be true in this case. That's a point you might keep in mind. I think that in view of some of the numbers that you presented, one consideration is that these very small particles may not turn out to be in thermal equilibrium in the sense that you have suggested that they might be. For one thing, you pointed out that there is an exothermic heat reaction. That suggests to me that if you have a particle as small as .01 micron or perhaps smaller, then the exothermic reaction heats it up. In the time that it has to impinge on something, it may in fact remain molten. At that point, if it strikes, it's basically getting splat cooled.

FITZGERALD: Well, the fact is that the heat transfer coefficient for those very small particles will bring them down to temperature in .01 second or so. The microparticles have a very quick relaxation time.

MILSTEIN: But if they are moving very close to the surface of a larger particle, they may simply be splat cooled.

FITZGERALD: Yes, some are but there are still the 40% or so left over that grow bigger; it's a point I have to look at. Dr. Flagan's suggestion that the particles may in fact form a net which makes capture efficiency better would also give smaller particles and require a smaller surface diffusion.

SCOTT: There have been some interesting observations recently about the way poly- and epi-silicon grow that might be relevant here. Some recent work reported in Applied Physics Letters by Bloem and his co-workers indicates that at high temperatures during silicon growth from silane, for example, the surface is essentially bare silicon. The surface appears to be hydrogenated below 650°C. Growth on the hydrogenated surface occurs with a fairly high activation energy, and there is a drop in activation energy from about 50 kcal to 35 kcal going into the regime where the surface is bare. I just wonder whether, in part, there might be a very strong heterogenous reaction going on to explain the growth and that this may tell you something about why everything is changing so rapidly going from 600° to 700°C.

FITZGERALD: Let me follow up on this. If there is a strong change at 350°C, the hotter particles are going to be the particles that are just formed as opposed to the bed particles. That means that if there is a heterogenous reaction left, they should be the ones that grow. By the time that they actually consolidate under the bed particles, they should have scavenged most of the silane out of the gas.

BAILEY: A useful experiment might be to warm these small particles in one step and then feed them at various temperatures into a fluidized bed containing silicon.

FITZGERALD: In fact, exactly that experiment was done, and there were some interesting results. George Hsu, could I ask you to describe the results?

HSU: Yes. Recently at JPL we conducted some very crude experiments. The experimental results are by no means conclusive. We first generated powder in a free space reactor; the powder was about 3 microns. The powder was then pneumatically transported into the fluidized bed column. When silane was introduced, there was no scavenging effect. In other words, the kind of coherent, dense deposition we found in our fluidized bed deposition did not take place.

FITZGERALD: But then you found out that as you did put silane into the 700° bed, you got partial capture of the particles going through.

HSU: Yes. We used 4% silane, and we observed a somewhat similar result to what we had previously observed. CVD deposition occurred, sealing the small particles to the big seed particles. However, we have not concluded yet whether this is the same effect we observed in the fluidized-bed silane deposition in which the particles were smaller at the start than the free space particles.

FITZGERALD: The critical thing here is that the time of arrival of the particles and the size of the particles is what determines the result. If a number of particles arrive into the same place at the same time, the time of arrival between particles onto the surface will be shortened; and to go from 0.1 micron up to 0.3 micron is going to require nine times the diffusion coefficient in order to even those out. So about an order of magnitude greater diffusivity is required just for that small change. I don't know if that makes a difference or not.

HSU: Is the self-diffusivity used in your melting effect model theoretically a function of the particle size?

FITZGERALD: I don't know. I don't know enough about it to give you an answer.

HSU: In your calculations for heating the small particles, you have assumed the heat capacity to be nearly the same as for solid silicon. Is that a valid assumption to use? At JPL we have wondered what heat capacity we should use for the very fluffy powder, because we observe that the powder seems to behave entirely different from a solid particle in heating and melting properties.

FITZGERALD: The heat capacity of silane of the deposited silicon is only about 1/4 of the heat capacity of the product mix. Most of it is hydrogen, and the hydrogen has the bigger heat capacity. So even if you perturbed the silane by a factor of two, you are not going to change the temperature rise very much. It isn't going to have that big an effect.

JEWETT: I am uncomfortable with the model. I just can't think of silicon particles hitting at half the melting point and actually spreading out like that with no force pushing them. There is no reason for them to

9  
Y

spread out. I'd rather think in terms of a spongy particle, a particle with lots of arms and legs. The reaction system is very complex with the formation of intermediates and particle reactions taking place at the same time. So that there is no nice, simple sphere of crystalline silicon with the problem of how it changes. Rather, it's something that is still in formation when it hits. I realize that this idea does all sorts of thing to your mathematics; and it becomes very amorphous in concept, but it may relate more to reality.

FITZGERALD: Well, let's consider that very small particles are formed in the vapor deposition of silica in making glass, and these particles sit down on the silica fibers. (This is the kind of thing that you are talking about.) They are tacky and when they touch each other, they become a sponge-like structure instead of retaining the geometry of spheres. Then, the sponge-like structure forms by means of capillary forces and viscosity. Is that the mechanism you are proposing?

JEWETT: No. I am thinking in terms of a system containing a little bit of silicon and maybe some polysilanes; and several reactions are happening at the same time. The mechanism may not be the formation of a particle and then capture. It may be an end process which takes place over an extended period of time. I don't think that a particle of silicon will hit (granted if it is very clean so that you have no oxide, it could possibly stick), but I see no reason for it to slump. I would assume in that case that there would be multiple, very small particles on that particle, and this effect would be observable.

FITZGERALD: There are very strong thermodynamic reasons, by the way, why it should slump. Because the radius of curvature is extreme, metals have very high surface tensions and regardless of the mechanism used for going from Condition A to Condition B, if Condition B has a lower radius of curvature and has a much lower energy level, it will stay there.

JEWETT: Everything that has been done in the area of crystalline silicon says that there is not much flow until the temperature is very close to the melting point. It just does not happen in silicon.

FITZGERALD: There is some evidence contrary to that on the growth of polycrystalline silicon, and it has to do with very clean surfaces. In polycrystalline the rate at which -- would somebody from Monsanto say something about this?

DeLUCA: Well, I can say something about it, but I think it is a little bit in disagreement. In the sintering of covalent or ionic materials there must be very high forces driving toward reduction of the surface area. I don't think your temperature is nearly high enough, even in very pure silicon, to get the kind of atomic movement that is needed for a reduction of the surface area. I would suggest that someone from JPL take these particles and do a cross section optical examination of them under a scanning electron microscope. Then, there might be some kind of evidence to corroborate your theory. Again, I think the temperature is too low.

OLSON: Have you completely ruled out just a simple silicon heterogeneous reaction as a mechanism for forming this surface morphology? I have seen nodules on polycrystalline silicon surfaces which look exactly like the things we have seen in the last 1 1/2 days. Has that completely been ruled out? In other words, that this bumpy surface is formed just by a pure silicon heterogeneous reaction? Do we have to invoke the spreading of these spheres?

FITZGERALD: The question is, when the spheres are formed and a lot of surface is available, why don't the spheres scavenge silane rather than react at the surfaces? If the mechanism is chemical vapor deposition then the mechanism should account for a remainder of some silane. And that's the question. There will have to be slow induction periods and a slow reaction. The real question is, where did that silane come from?

FLAGAN: I'd like to make a very brief comment. Consider the recirculation of the particles going back through the reaction zone at a later time. Surface area is available at that zone where silane is once again available.

OLSON: Yesterday Dr. Flagan described to us a model and an experiment whereby he took a small number of nuclei and injected them into a heated silane gas and invoked depletion in the gas phase as a model for the simple heterogeneous growth of these small particles into large particles with no homogeneous nucleation of further silicon particles. If he is correct, then how can you say that there is homogeneous nucleation in a fluidized bed and therefore the growth of the fluidized bed particles is by conglomeration of smaller homogeneously nucleated particles? Why can't it simply be a growth of fluidized bed particles from the gas phase? Just straight CVD with no homogeneous nucleation?

DUDUKOVIC: Not with 60% silane. Some of the experiments were done at 60%.

KAAE: I want to chide the silicon community somewhat. I think there is an easy answer to all this speculation. You just need to do some structural studies of the deposit. Then the answer will sort itself out. I think you need to do TEM instead of SEM or optical observations, because I think that the structural features are so small. I think the use of TEM to determine the shape of the growth features on coated particles will answer the question.

INGLE: The reaction of silane to form silicon actually occurs in a collision, a collision of the silane molecule with the wall rather than only by silane molecule collisions. The reaction of silane to silicon occurs when that silicon is at the wall. Now I think Ring's mechanism is different, since the reaction at a lower temperature is a fairly complex, slower mechanism. At higher temperatures, between 650° and 700°, there is a much faster reaction involving silane going to silene, then to a silicon hydride, and then to silicon. And since this reaction is only occurring at the wall and not throughout the volume of 100 microns by 100 microns by 100 microns, the reaction is rapidly going from silane to silene to

9  
Y

silicon, and could all occur right there at that wall impact, in one collision at 700°C. At 650°C, it may be going through the step of silane to silyl breaking down in a much slower process, and consequently it could drift away from the wall and maybe not stick. But I see that only occurring at the wall. A collision of silane at the wall giving silicon deposition would account for the fact that we just see heterogeneous nucleation at the wall at 700°C while powders are formed at 650°C, because the reactions do not occur in wall collisions.

SCOTT: I want to go back to what I said before about the observation of a hydrogen-rich interface with growing films and to the comment that was made earlier about further reactions. I think one way of looking at these particles is that they are sort of alive. They are nucleating and growing, and they're growing by some complex mechanism, one which involves a way which the interface always stays hydrogen-rich. When the entities come together, rather than there being any melting, the reactions continue. As they come together, there are cross-linking reactions that connect them with the elimination of hydrogen. This probably occurs at a very, very rapid rate at these temperatures. But it still is not so rapid that there isn't a lot of cross-linking going on, which allows the particles to grow. These clusters are growing as a consequence of cross-linking. It is not necessary that any melting be invoked to give the reduction in the radius of growth of the globules that are there growing together. I think that this is essentially growth involving globs that chemically react with one another. It's the only way I can describe it, and that may be the kind of sintering that is really going on here.

DUDUKOVIC: I want to make one quick comment. In a paper by Hogness, Wilson and Johnson, in the Journal of the American Chemical Society of 1936, there is this statement: "Changing the surface area in the bed for the decomposing silane has no effect on the apparent rates of the decomposition." In other words, putting decomposing silane in an empty tube or in a packed bed with much more surface in it has no effect whatsoever on the apparent rate of decomposition. The point I was making is that the wall or a particle is not at all a necessary precursor for the decomposition of silane. There will never be enough surface there to compete with homogeneous nucleation when the system is in a subsupersaturated region, because the time constant for homogeneous nucleation is milliseconds or microseconds and the time constant for any type of CVD is in the order of seconds or even minutes. So when the reaction takes place in a highly saturated condition, the same rate of decomposition will be observed despite attempts to increase the surface area. The data to confirm this conclusion are available in the chemistry journals.

DeLUCA: Tom, I would like to make a comment about the temperature gradients in a fluid bed. In your model, the temperature is very uniform, and the nominal bed temperature is reached very quickly as the gas comes into the fluid bed. I don't agree with that. I think we have experimental measurements to show that there is a substantial temperature gradient in fluid beds. The mode of fluidization of the bed, the static L/D of the

9  
Y

bed, and also the gas used to fluidize the bed can have dramatic influences on the temperatures that the bed attains ultimately as well as on the temperature gradient from the distributor plate to the exit of the reactor. I don't believe that it is nearly as fast as you have explained.

FITZGERALD: My model does not assume that. It assumes that the gas is at the same temperature as the particles. Now, whether the particles from the bottom of the bed to the top are at the same temperature depends primarily on whether slugging exists in the bed. If it's a slugging bed, there can easily be a 100, a 200, or a 300° difference. Exxon has run a fluidized-bed coal combustor with a 1000° difference in a few feet. So a temperature gradient is quite possible if there is slugging or a poor particle flow. That isn't my point. My point is that the gas is at the same temperature as the particles. And, if the particles are very well mixed, as they would be in a large-scale fluidized bed where slugging doesn't dominate, then, all the particles would not only be uniform in temperature, but also they would be at nearly the same temperature throughout the bed.

GRIMMETT: I agree with Tom. I have run experiments in which I have had a heat source that was running somewhere around 1200°F, a bed that was running somewhere around 900°, and within just inches there was a heat sink in which we were putting a solution at essentially room temperature, evaporating it, and making a deposition. Measurements were taken right above the heat exchanger near the support plate. There was a drop in temperature near the heat sink and within an inch or two above this heat exchanger. No temperature difference was measurable due to the rapid mixing. Now we're talking about a well-fluidized bed, not a slugging bed which I seem to hear quite a bit about. I think that slugging beds are terrible. In my talk, I will show slides to give you an idea how the beds mix.

DUDUKOVIC: Would you care to comment on what the time constant is for the mixing?

GRIMMETT: We made no measurements of that sort. I really don't know.

DeLUCA: If the fluidizing gas is changed in a bubbling fluid bed, do dramatically different temperature gradients arise? If so, I would infer that the gas and the particles are not at the same temperature.

FITZGERALD: No.

DUDUKOVIC: One more comment on fluidized beds. I agree that mixing is very good and fast, but everything has a time constant, and so does every reaction. Surely the temperature is uniform in a bubbling fluid bed if the rate of reaction has a time constant of a few seconds or minutes. If the reaction is highly exothermic and has a time constant on the order of milliseconds, do you maintain that in a well mixed, bubbling fluidized bed the temperature is uniform?



FITZGERALD: Yes.

HSU: Our fluidized bed was operated in essentially an isothermal condition. It is a violently bubbling bed, however; it has a one-foot bed depth. The distributor plate is water-cooled and there is a temperature gradient from 350° to 700°C within the first two inches of the bed. So obviously temperature gradients exist.

FITZGERALD: A further statement on isothermality. Pressurized fluidized-bed combustors, which have an energy density release two orders or maybe three orders of magnitude greater than anything we are talking about here, are isothermal within 10°.

FLAGAN: They may be isothermal in the mean, but care must be taken to distinguish between mean particle temperature and the temperature of individual particles which may differ substantially. In the combustion system they certainly do, and I would suspect that there would be some variations occurring in the system as well.

GRIMMETT: That's very true. All you have to do is look in a coal combustion fluidized bed and you can see these temperature differences. Yet the bulk temperature will be essentially the same no matter where it is taken. To put this in perspective, the fluidized bed I'm describing was two foot square and had a bed depth of about two feet. Right down over the support plate there was a difference. Beyond this there was another four inches and the heat exchanger, which had about a 400-500°F temperature difference. On the top there was the heat sink plus maybe another six inches of bed depth. A difference of 10°F was the most that could be measured away from where we sprayed in.

# STEADY-STATE AND TRANSIENT PARTICLE SIZE DISTRIBUTION CALCULATIONS FOR FLUIDIZED BEDS

by

FERHAN KAYIHAN  
Senior Research Engineer  
Weyerhaeuser Technology Center  
Tacoma, Washington 98477

## INTRODUCTION

Particle size distribution calculation procedures were developed by Levenspiel et al. (1,2) to describe the steady-state behavior of fluidized beds using continuous size density functions. Chen and Saxena (3,4) later modified the suggested equations to describe special reaction cases and attrition problems. Recently, Overturf and Kayihan (5) noted that when the continuous size distribution equations are interpreted for discrete size cut applications, there can be substantial computation errors. They (5) developed a new set of equations specifically for discrete size cut computations which are more reliable and easier to implement. These equations were successfully applied to a variety of design problems (6,7,8).

In what follows the original continuous size distribution functions will be summarized and compared to the corresponding discrete case computation scheme. Reasons for the inherent numerical problems with the continuous case will be suggested. The design equations for the discrete cut size distribution calculations will be extended to cover the attrition problems including the cases when particles either grow or shrink through independent reaction mechanisms. The special case of simultaneously changing particle size and density will also be discussed. Finally, the equations and the analytical solution for the time dependent size distributions for batch and semi-batch fluidized bed reactors will be presented. It is hoped that the development and equations presented here will provide enough information which can be directly adopted or otherwise used as guidelines to derive specific relations.

## STEADY-STATE CONTINUOUS SIZE DISTRIBUTION

Figure 1 shows the steady-state flow of particles through a well mixed fluidized bed reactor where the outflow and bed size distributions are identical. In the fluidized bed, the particle sizes change due to reaction, attrition, and elutriation. Kunii and Levenspiel (2) develop the design equations starting from a material balance for the solids contained in a size cut of width  $\Delta R$  between  $R$  and  $R + \Delta R$  for which the following equality applies:

$$\begin{aligned}
& \left( \begin{array}{l} \text{rate of particle} \\ \text{input in range } \Delta R \\ \text{coming with input} \\ \text{stream } F_0 \end{array} \right) - \left( \begin{array}{l} \text{rate of particle} \\ \text{output in range } \Delta R \\ \text{leaving with output} \\ \text{stream } F_1 \end{array} \right) - \left( \begin{array}{l} \text{rate of particle} \\ \text{output in range} \\ \Delta R \text{ carried in} \\ \text{elutriate } F_2 \end{array} \right) \\
& + \left( \begin{array}{l} \text{rate of particles} \\ \text{entering into} \\ \text{range } \Delta R \text{ due to} \\ \text{size change} \\ \text{caused by reaction} \end{array} \right) - \left( \begin{array}{l} \text{rate of particles} \\ \text{leaving the range} \\ \Delta R \text{ due to size} \\ \text{change caused by} \\ \text{reaction} \end{array} \right) + \left( \begin{array}{l} \text{rate of particle} \\ \text{mass generation} \\ \text{due to reaction} \\ \text{while staying in} \\ \text{size range } \Delta R \end{array} \right) \\
& = 0
\end{aligned} \tag{1}$$

Writing the corresponding finite difference expression and then taking the limit as  $\Delta R$  goes to zero a general expression can be derived as

$$\begin{aligned}
& F_0 p_0(R) - F_1 p_1(R) - W \kappa(R) p_1(R) - W \frac{d}{dR} (R(R) p_1(R)) \\
& + \frac{3W}{R} p_1(R) R(R) = 0
\end{aligned} \tag{2}$$

where  $R(R) = dR/dt$  is the reaction rate and  $\kappa(R)$  is the elutriation constant.

Integrating Eqn. (2) for all  $R$  gives the overall mass balance as

$$F_1 + F_2 - F_0 = 3W \int_{R_{\min}}^{R_{\max}} \frac{p_1(R) R(R)}{R} dR \tag{3}$$

Kunii and Levenspiel (2) show that when attrition fines are ignored the particle size distribution in the bed for a feed of wide size distribution can be computed through two different sets of equations depending on the direction of size change. For growing particles

$$p_1(R) = \frac{F_0 R^3}{WR(R)} I(R, R_{\min}) \int_{R_{\min}}^R \frac{p_0(R_i) dR_i}{R_i^3 I(R_i, R_{\min})} \tag{4}$$

and

$$\frac{W}{F_0} = \int_{R_{\min}}^{R_{\max}} \left( \frac{R^3}{R(R)} I(R, R_{\min}) \int_{R_{\min}}^R \frac{p_0(R_i) dR_i}{R_i^3 I(R_i, R_{\min})} \right) dR \quad (5)$$

with  $I(R_j, R_i) = \exp \left( - \int_{R_i}^{R_j} \frac{F_1/W + \kappa(R)}{R(R)} dR \right)$  (6)

and  $\int_{R_{\min}}^{R_{\max}} p_1(R) dR = 1$  (7)

describe the particle behavior.

On the other hand, for shrinking particles, the corresponding equations are

$$p_1(R) = - \frac{F_0 R^3}{W R(R)} I(R, R_{\max}) \int_R^{R_{\max}} \frac{p_0(R_i) dR_i}{R_i^3 I(R_i, R_{\max})} \quad (8)$$

and

$$\frac{W}{F_0} = \int_{R_{\min}}^{R_{\max}} \left( \frac{R^3}{R(R)} I(R, R_{\max}) \int_R^{R_{\max}} \frac{p_0(R_i) dR_i}{R_i^3 I(R_i, R_{\max})} \right) dR \quad (9)$$

with Eqns. (3), (6), and (7) holding as before.

These equations are usually solved for the unknown particle size distribution function  $p_1(R)$  and the bed weight  $W$  through an iterative scheme. Details are provided in Kunii and Levenspiel (2).

Chen and Saxena (3) observed that these equations need to be modified when, due to the reactions taking place, the minimum or the maximum particle size is reached within finite time. The modification is the addition of a delta function to the size density at the extreme size. In further analysis, Chen and Saxena (4) also worked out the equations necessary to describe the

attrition of particles to a small size for cases when feed consists of a single size input. Their results can be extended to feeds of wide size distribution and summarized for the shrinking particle case as

$$\begin{aligned}
 p_1(R) = & - \frac{F_0}{W} \int_R^{R_{\max}} \frac{R^3/R_i}{R(R)} I(R, R_i) p_0(R_i) \cdot dR_i \\
 & + \delta(R_f) \frac{F_0/W}{F_1/W + \kappa(R_f)} \int_{R_{\min}}^{R_{\max}} \left( \frac{p_0(R_i)}{R_i^3} \int_{R_{\min}}^{R_i} 3R^2 I(R, R_i) dR \right) dR_i \\
 & + \delta(R_{\min}) \frac{F_0/W}{F_1/W + \kappa(R_{\min})} R_{\min}^3 \int_{R_{\min}}^{R_{\max}} \frac{p_0(R_i)}{R_i^3} I(R_{\min}, R_i) dR_i
 \end{aligned} \quad (10)$$

Here  $\delta(R_f)$  and  $\delta(R_{\min})$  are equal to 1 at  $R=R_f$  (fines) and  $R=R_{\min}$  (minimum size reached by reaction) respectively and zero elsewhere. The delta functions do not change the overall balance expressions, Eqns. (3) and (9).

#### DISCRETE CUT PARTICLE SIZE DISTRIBUTION

For most practical applications, the computations are performed for a finite number of size ranges which represent the overall size distribution. Each size range is characterized by a mean size within the range. Implementation of the above equations for discretized size distributions leads to summation formulas. For example, for  $N$  different size cuts represented by ranges  $\Delta R_1, \Delta R_2, \dots, \Delta R_N$  and mean sizes  $R_1, R_2, \dots, R_N$  Eqn. (5) becomes

$$\begin{aligned}
 \frac{W}{F_0} = & \sum_{j=1}^N \frac{R_j^3}{R(R_j)} \exp \left( - \sum_{k=1}^j \frac{F_1/W + \kappa(R_k)}{R(R_k)} \Delta R_k \right) \\
 & \sum_{i=1}^j \frac{p_0(R_i) \Delta R_i}{R_i^3} \exp \left( \sum_{k=1}^i \frac{F_1/W + \kappa(R_k)}{R(R_k)} \Delta R_k \right)
 \end{aligned} \quad (11)$$

Overturf and Kayihan (5) point out that such application of the particle size distribution equations may lead to significant errors in fluidized bed

design and that under certain conditions the computations give unacceptable values for  $W$  and negative values for  $F_2$ . Numerical errors are expected to originate from the inaccuracies of the arguments of the exponential terms and from the fact that the summation expressions may not retain all of the pertinent material balance information established in Eqn. (1).

A new set of equations can be derived which are specifically applicable for the discrete cut particle size distribution problems. For  $N$  discrete size ranges represented by  $\Delta R_1, \Delta R_2, \dots, \Delta R_N$  and mean sizes  $R_1, R_2, \dots, R_N$  Eqn. (1) takes the form for growing particles

$$F_0 p_0(R_i) \Delta R_i - F_1 p_1(R_i) \Delta R_i - W \kappa(R_i) p_1(R_i) \Delta R_i + W R(R_{i-1}) p_1(R_{i-1}) - W R(R_i) p_1(R_i) + \frac{3W}{R_i} p_1(R_i) R(R_i) \Delta R_i = 0 \quad (12)$$

Here  $p_1(R_{i-1}) = 0$  for  $i=1$ .

For shrinking particles only the fourth and the fifth terms change to

$$- W R(R_{i+1}) p_1(R_{i+1}) + W R(R_i) p_1(R_i)$$

where, of course,  $R$  is negative and  $p_1(R_{i+1}) = 0$  for  $i=N$ . Defining the mass fractions in the bed as

$$m_i = p_1(R_i) \Delta R_i \quad (13)$$

Eqn. (12) gives for growing particles

$$m_i = \frac{F_0 m_0 + W R(R_{i-1}) m_{i-1} / \Delta R_{i-1}}{F_1 + W (\kappa(R_i) + R(R_i) (\frac{1}{\Delta R_i} - \frac{3}{R_i}))} \quad (14)$$

The corresponding equation for shrinking particles becomes

$$m_i = \frac{F_0 m_0 - W R(R_{i+1}) m_{i+1} / \Delta R_{i+1}}{F_1 + W (\kappa(R_i) - R(R_i) (\frac{1}{\Delta R_i} + \frac{3}{R_i}))} \quad (15)$$

For both cases the constraints are

$$\sum_{i=1}^N m_i = 1 \quad (16)$$

and the material balance

$$F_1 + F_2 - F_0 = 3W \sum_{i=1}^N \frac{m_i R(R_i)}{R_i} \quad (17)$$

Computation procedures using Eqns. (14) and (15) are discussed by Overturf and Kayihan (5).

# ATTRITION WITH PARTICLE GROWTH OR SHRINKAGE

Above equations cover the special cases discussed by Chen and Saxena (3) where minimum or maximum size is reached in finite time. For these cases  $R(R_1) = 0$  and  $R(R_N) = 0$  respectively. However, for problems where attrition fines need to be accounted for, the design equations should be modified. Attrition can happen either when particles are growing or shrinking due to the heterogeneous reactions. Let  $R(R) = dR/dt$  be the size change due to reaction (positive for growth, negative for shrinkage) and  $\tilde{R}(R) = dR/dt$  be the size reduction (negative) due to attrition. Assume that the attrition products are of size  $R_1$ .

For particles growing with reaction but shrinking with attrition, a similar material balance as before gives

$$m_1 = \frac{F_0 m_{01} - W R(R_2) m_2 / \Delta R_2 - 3W \sum_{i=2}^N \frac{\tilde{R}(R_i) m_i}{R_i}}{F_1 + W \left( \kappa(R_1) + R(R_1) \left( \frac{1}{\Delta R_1} - \frac{3}{R_1} \right) \right)} \quad (18)$$

and

$$m_i = \frac{F_0 m_{0i} + W \left( R(R_{i-1}) m_{i-1} / \Delta R_{i-1} - \tilde{R}(R_{i+1}) m_{i+1} / \Delta R_{i+1} \right)}{F_1 + W \left( \kappa(R_i) + R(R_i) \left( \frac{1}{\Delta R_i} - \frac{3}{R_i} \right) - \tilde{R}(R_i) \left( \frac{1}{\Delta R_i} - \frac{3}{R_i} \right) \right)} \quad (19)$$

for  $i=2, \dots, N$  where  $m_{N+1} = 0$ .

For particles shrinking due to both reaction and attrition

$$m_1 = \frac{F_0 m_{01} - W m_2 \left( R(R_2) + \tilde{R}(R_2) \right) / \Delta R_2 - 3W \sum_{i=2}^N \frac{\tilde{R}(R_i) m_i}{R_i}}{F_1 + W \left( \kappa(R_1) - R(R_1) \left( \frac{1}{\Delta R_1} + \frac{3}{R_1} \right) \right)} \quad (20)$$

and

$$m_i = \frac{F_0 m_{0i} - W m_{i+1} \left( R(R_{i+1}) + \tilde{R}(R_{i+1}) \right) / \Delta R_{i+1}}{F_1 + W \left( \kappa(R_i) - \left( R(R_i) + \tilde{R}(R_i) \right) \left( \frac{1}{\Delta R_i} + \frac{3}{R_i} \right) \right)} \quad (21)$$

for  $i=2, \dots, N$ . Eqns. (16) and (17) apply as before.

## VARIABLE SIZE AND DENSITY

Overturf et al. (6) showed that for problems where particle size and density change simultaneously, the finite difference expressions for size distributions can be extended to reflect the two dimensional behavior.

ORIGINAL PAGE IS  
OF POOR QUALITY

Assume that  $R(R_i) = dR/dt \text{ } R=R_i \text{ (m/s)}$  and  $\tilde{R}(\rho_j) = dm/dt \text{ } \rho=\rho_j \text{ (kg/s)}$  are the size change and density change reaction rates, respectively. Particle size distribution or mass fractions are now defined in terms of a two dimensional grid system where  $\Delta R_1, \dots, \Delta R_N$  define the size ranges and  $\Delta \rho_1, \dots, \Delta \rho_M$  define the density ranges. The corresponding mean sizes and densities are  $R_1, \dots, R_N$  and  $\rho_1, \dots, \rho_N$ .

$$\text{Let } m_{ij} = p_i (R_i, \rho_j) \Delta R_i \Delta \rho_j \quad (22)$$

In this problem a particle may change its characterization by changing its size and/or density. For growing particles with increasing density (without attrition) the expression for  $m_{ij}$  is

$$m_{ij} = \frac{F_0 m_{0ij} - W (m_{i-1,j} R(R_{i-1})/\Delta R_{i-1} - m_{i,j-1} \tilde{R}(\rho_{j-1})/3 \pi R_i^3 \Delta \rho_{j-1})}{F_1 + W \left( \kappa_{ij} + R(R_i) \left( \frac{1}{\Delta R_i} - \frac{3}{R_i} \right) + \tilde{R}(\rho_j) \left( \frac{1}{\Delta \rho_j} - \frac{1}{\rho_j} \right) / 3 \pi R_i^3 \right)} \quad (23)$$

The corresponding expressions for other combinations of size and density changes with attrition can be developed through similar steps established thus far.

#### TIME DEPENDENT PARTICLE SIZE DISTRIBUTION COMPUTATIONS FOR BATCH FLUIDIZED BEDS

Consider the batch fluidized bed shown in Figure 2. Here, original seed particles with a known distribution grow in time through reactions with gas. Attrition and density changes are neglected but elutriation is included in the development.

A transient mass balance in a size range  $\Delta R_i$  gives

$$\begin{aligned} \frac{d}{dt} (W p_i (R_i) \Delta R_i) &= W p_i (R_{i-1}) R(R_{i-1}) - W p_i (R_i) R(R_i) \\ &- W \kappa (R_i) p_i (R_i) \Delta R_i + \frac{3W}{R_i} p_i (R_i) R(R_i) \Delta R_i \end{aligned} \quad (24)$$

where  $p_i (R_{i-1}) = 0$  for  $i=1$ .

By defining  $w_i = W p_i (R_i) \Delta R_i$  as the bed weight belonging to size range  $\Delta R_i$  Eqn. (24) becomes

$$\frac{dw_i}{dt} = w_{i-1} \frac{R(R_{i-1})}{\Delta R_{i-1}} - w_i \left( \kappa(R_i) + R(R_i) \left( \frac{1}{\Delta R_i} - \frac{3}{R_i} \right) \right) \quad (25)$$

If elutriation and reaction rates are dependent on particle size only as assumed here, then there are  $N$  ordinary differential equations of the form



ORIGINAL PAGE IS  
OF POOR QUALITY

$$\frac{dw_1}{dt} + a_1 w_1 = 0 \quad w_1(0) = w_{10} \quad (26)$$

$$\frac{dw_i}{dt} + a_i w_i = b_{i-1} w_{i-1} \quad w_i(0) = w_{i0} \quad (27)$$

for  $i=2, \dots, N$ .

$a_i$  and  $b_i$  are constants defined as

$$a_i = \kappa(R_i) + R(R_i) (1/\Delta R_i - 3/R_i) \quad (28)$$

and  $b_i = R(R_i)/\Delta R_i$

The solution is

$$w_i(t) = \sum_{j=1}^i C_{ij} e^{-a_j t} \quad i=1,2,\dots,N \quad (29)$$

$$\text{where } C_{11} = w_{10} \quad (30)$$

$$\text{and } C_{ij} = \frac{b_{i-1}}{a_i - a_j} C_{i-1,j} \quad j=1,\dots,i-1 \quad (31)$$

$$\text{with } C_{ii} = w_{i0} - \sum_{j=1}^{i-1} C_{ij} \quad (32)$$

Particle size distributions can be constructed as

$$m_i(t) = w_i(t) / \sum_{i=1}^N w_i(t) \quad (33)$$

#### SEMI-BATCH FLUIDIZED BED REACTOR

For the special case of semi-batch operations where there is a continuous constant feed of the minimum size,  $F_{01}$  kg/s, as shown in Figure 3, the time dependent discrete bed weights become

$$w_i(t) = C_{i0} + \sum_{j=1}^i C_{ij} e^{-a_j t} \quad i=1,\dots,N \quad (34)$$

$$\text{where } C_{10} = F_{01}/a_1 \quad (35)$$

$$C_{11} = w_{10} - C_{10} \quad (36)$$

and for  $i=2, \dots, N$

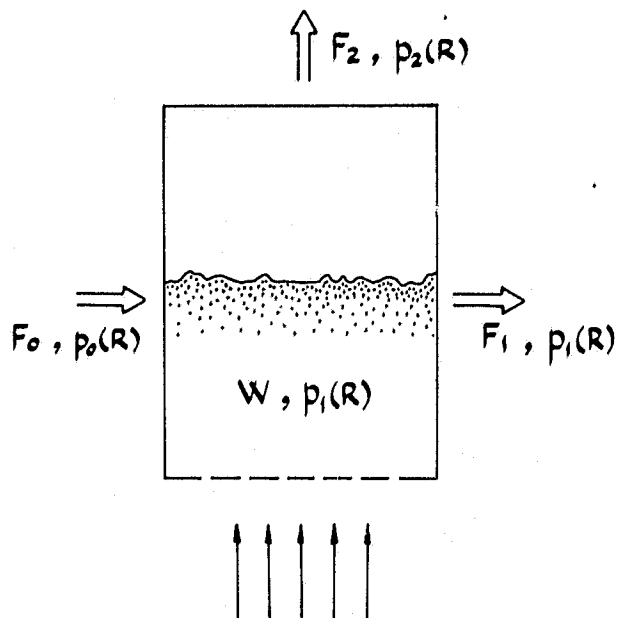


Figure 1.  
Steady-state flow of particles  
through a well mixed fluidized  
bed reactor.

Figure 2.  
A well mixed batch fluidized bed reactor.

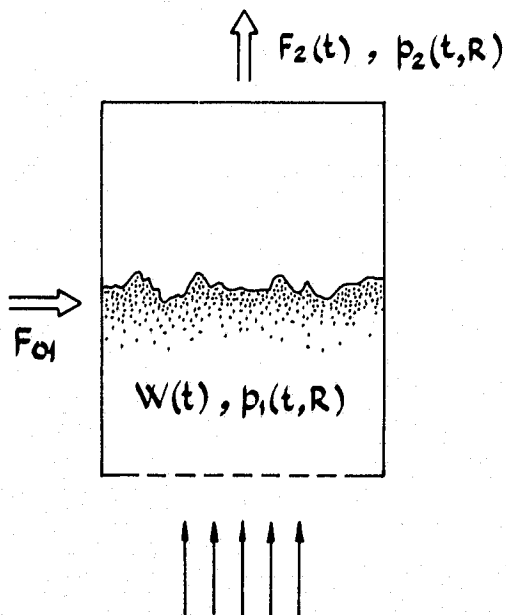
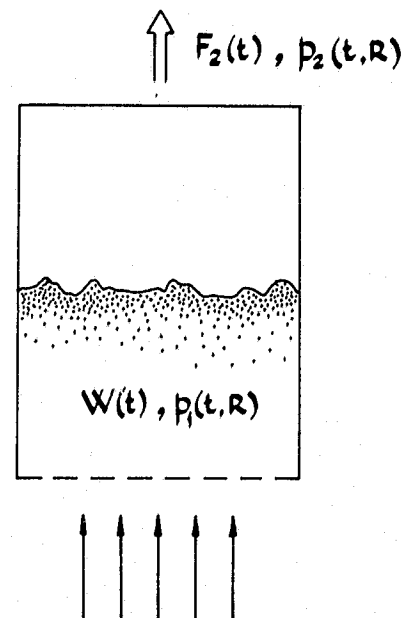


Figure 3.  
A semi-batch fluidized bed reactor  
with continuous constant feed of  
smallest size particles.

$$C_{i0} = \frac{b_{i-1}}{a_i} C_{i-1,0} \quad (37)$$

$$\text{and } C_{ij} = \frac{b_{i-1}}{a_i - a_j} C_{i-1,j} \quad j=1, \dots, i-1 \quad (38)$$

$$\text{with } C_{ii} = w_{i0} - \sum_{j=1}^{i-1} C_{ij} \quad (39)$$

## CONCLUSIONS

Equations are developed for finite cut particle size distribution calculations in fluidized beds. Steady-state equations are presented for growing and shrinking particles with and without attrition. Alterations in the formulas for simultaneous size and density changes for two dimensional distributions are also presented. The transient size distribution equations for batch and semi-batch fluidized beds are developed and shown to have easy analytical solutions for reactions that depend on size only. It is hoped that the results established here can be directly used for design applications or else that the variations in the formulations to match specific needs can be worked out simply by following the guidelines provided through the development.

## REFERENCES

1. O. Levenspiel, D. Kunii, and T. J. Fitzgerald, Powder Technology, 2 (1968/69), 87.
2. D. Kunii and O. Levenspiel, "Fluidization Engineering," Wiley, New York (1969).
3. T. P. Chen and S. C. Saxena, Powder Technology, 15 (1976), 283.
4. T. P. Chen and S. C. Saxena, Powder Technology, 18 (1977), 279.
5. B. W. Overturf and F. Kayihan, Powder Technology, 23 (1979), 143.
6. B. W. Overturf, F. Kayihan, and G. V. Reklaitis, "Modeling and Analysis of an Integrated Coal Pyrolysis, Gasification and Combustion Reactor System," paper presented in 71st Annual AIChE Meeting, Miami Beach, Florida (1978).
7. B. W. Overturf, "Towards a General Description of Gas Solid Reactions in a Fluidized Bed Reactor," PhD Thesis, Purdue University (1980).
8. D. Park, O. Levenspiel, and T. J. Fitzgerald, "A Model for Large Scale Atmospheric Fluidized Bed Combustions," paper presented in 72nd Annual AIChE Meeting, San Francisco, California (1979).

## DISCUSSION

FLAGAN: It seems to me that you are not actually representing particle size distribution as a histogram but rather as a set of delta functions. Is that correct?

KAYIHAN: Eventually, I do get a histogram.

FLAGAN: But do you actually integrate all of these processes over the intervals of the histogram, or are you assigning the values for any processes to the mean size in that interval?

KAYIHAN: I am assigning processes to that mean value. We have interpreted the original continuous equations in terms of an exact solution at which time we use numerical integration techniques, quadratures, where we continuously integrated the rate functions. We used those as our basis to compare the approximations.

FLAGAN: In systems where you have processes which are strongly dependent upon particle size, the approach of evaluating rate-of-change coefficients at the mean particle size can lead to substantial errors. That problem can be overcome without complicating the ultimate analysis significantly by evaluating those coefficients as integrals over the interval of the histogram. For that I would refer you to the work of Galbart and Steinfeldt who have carried this quite a ways on a number of studies dealing with aerosol systems but not with fluidized-bed systems.

DUDUKOVIC: I think, Ferhan, that you should defend your procedure and say that in the processes that you are looking at the growth rate, if it is kinetically controlled, is a constant and is independent of particle size. And if, at worst, it is mass-transfer-controlled, then the dependence of particle size may be reduced to the  $-1/2$  or perhaps  $-1$ . So it's true that by averaging it you lose something, but the dependence, I think, is not as serious as you observe in aerosol systems. Would that be correct?

FLAGAN: Yes, that is probably true. I was simply making a point in terms of precision. I think the model is a good step forward.

KAYIHAN: I think the major difference between what Rick (Flagan) is saying and what I presented is that Rick actually uses a quadrature or suggests the use of a continuous integration procedure which keeps the original equations exact but simply presents the final form of the results in terms of histograms instead of a continuous function.

FLAGAN: No. What I am suggesting is that the histogram approach is quite convenient for computational reasons. To do the quadrature becomes an extremely expensive computation. This is particularly true if you deal with a stiff reaction system. What I was suggesting was using a quadrature to evaluate the growth terms, not basing it on the mean particle size but the size distribution as a histogram, and computing

exactly how that histogram should grow, how it should contribute to the next size interval, and how much of the growth should be attributed to its own size interval. Representing the size distribution as a histogram, you can evaluate those integrals once before you ever go to your detailed modeling. For example, if you have diameter to the  $1/2$  to  $-1/2$  power dependence, you can integrate that analytically and plug that result in and get a more accurate representation of the contributions of growth of particles within one interval to that particular and subsequent intervals.

KAYIHAN: We may be talking about a slightly different approach. All of those integrals have an unknown in them. So you really don't have the pleasure of integrating once and for all beforehand.

FLAGAN: You scale those, take that outside the interval, and deal with the dimensionless particle size distribution in evaluating the coefficient. Let's discuss this more later.

AN UPDATE ON A MATHEMATICAL MODEL WHICH PREDICTS  
THE PARTICLE SIZE DISTRIBUTION  
IN  
A FLUIDIZED-BED PROCESS

by

Earl S. Grimmett  
G. & R. Technology  
1085 Syringa Drive, Idaho Falls, Idaho 83401

INTRODUCTION

A major problem when operating processes using fluidized beds is that of controlling bed particle size or size distribution. The consequence of not achieving control can be disastrous. If particles in the bed become too large, fluidization may cease; if particles become too small elutriation takes place and the required bed level cannot be maintained. Product specifications may require that a certain particle size be maintained. Particle size distribution determines the type of off-gas cleaning system required as well as the effectiveness of this system.

This paper concerns fluidized-bed processes where particles grow or decrease in size. Control of particle size (particle size distribution) in such processes cannot be achieved without having a thorough understanding of the factors which affect these changes. These factors include imposed operating conditions as well as the physical attributes of the material from which particles are made. Properties of the feed material may have a pronounced effect on the physical properties of the particles, and this in turn affects particle size distribution.

Grimmett(1) proposed a mathematical model for predicting the particle size distribution in a fluidized bed as a function of time. This model includes most, if not all, the rate processes taking place when particles grow in a fluidized bed. In another paper(2), the growth rate of particles were studied in a process where aluminum nitrate solutions were calcined to form aluminum oxide. One of the weak parts of this model is the lack of a good method of mathematically expressing the rate of attrition. At that time a suggestion was made that attrition could be considered a "negative growth rate". In a sense it is, but it does not answer many questions about the basic mechanisms of attrition, nor how to express these mechanisms in a manageable mathematical form.

The purpose of this discussion is to up-date the previously described model. A new technique for managing attrition is presented.

#### ATTRITION

Attrition occurs because forces act on particles in a bed. How should this attrition rate be determined? Particles of all sizes break into smaller ones during attrition. These particles may break in half, or into four pieces, or into dozens of pieces. No piece is the same size. In turn these same particles break into still smaller ones. Every particle has its own "breakage rate", and therefore individual rates for every particle would be impossible to determine and impossible to use in a model.

Vaux(3) analyzed the factors that cause attrition of particles in a fluidized bed steam generating system. He concluded that attrition is caused by the following:

1. particle characteristics (shape, angularity, strength, chemical composition),
2. heating rate and cooling rate of particles,
3. moisture in particle cracks,
4. pressure fluctuations (puffed rice process),
5. fluidizing gas flow rate,
6. gas composition and reactivity with particles,
7. system temperature, and
8. sorbent pretreatment.

Of course not all of these apply to every system where particles undergo attrition. He further relates attrition with operating conditions in a fluidized bed system such as:

- a. bubbling bed,
- b. grid or gas distributor plate,
- c. thermal shock,
- d. chemical reaction,

- e. transfer lines and cyclones
- f. internal gas pressure,
- g. and ejection from surface of bed.

Factors that cause attrition vary from system-to-system, but in any case the problem of determining an attrition function that can be used in a model is not an easy one to solve. He suggests that the main cause of attrition must be primarily due to the energy put into the system, and this energy acts on particles in the several ways described above. This is born out by studies conducted at the Idaho Chemical Processing Plant(4). He concludes that when particles are initially subjected to forces which cause attrition, the rate is high and then decreases to a constant value.

In a second paper Vaux and Fellers(5) describe a method of measuring the tendency of particles to attrite. They used an apparatus which consists of a heated vessel with a support plate having three holes. Pressure drop across the holes is measured as well as the amount of air put through them. Air flow, pressure drop, bed height, and temperature are fixed. A sample of material whose size distribution is known is put into the vessel. Air is put into the bed through these holes, and the material allowed to fluidize for a specified length of time. The results of these tests show that limestone samples have characteristic resistance to attrition.

A report by Brown, Legler, Wheeler, Grimmett, and Buckham(6) describes a similar apparatus. It was used to measure the attrition resistance of calcined aluminum oxide particles. It had only one hole and was not heated. A given weight and screen size (50 grams of -28 + 35 Tyler mesh) of calcined material was put into the apparatus and air at a given pressure allowed to pass through it for one hour. The percent remaining of the original size was defined as the attrition index. The relationship between alpha aluminum oxide in the particle and its attrition index (resistance) is shown in Figure 1. These two test methods do not give values for attrition rates, but do show that such an apparatus can be used to determine the relative attrition resistance between different types of material (particles). Each apparatus used different amounts of kinetic energy, but the amount used in each remained constant from test to test.



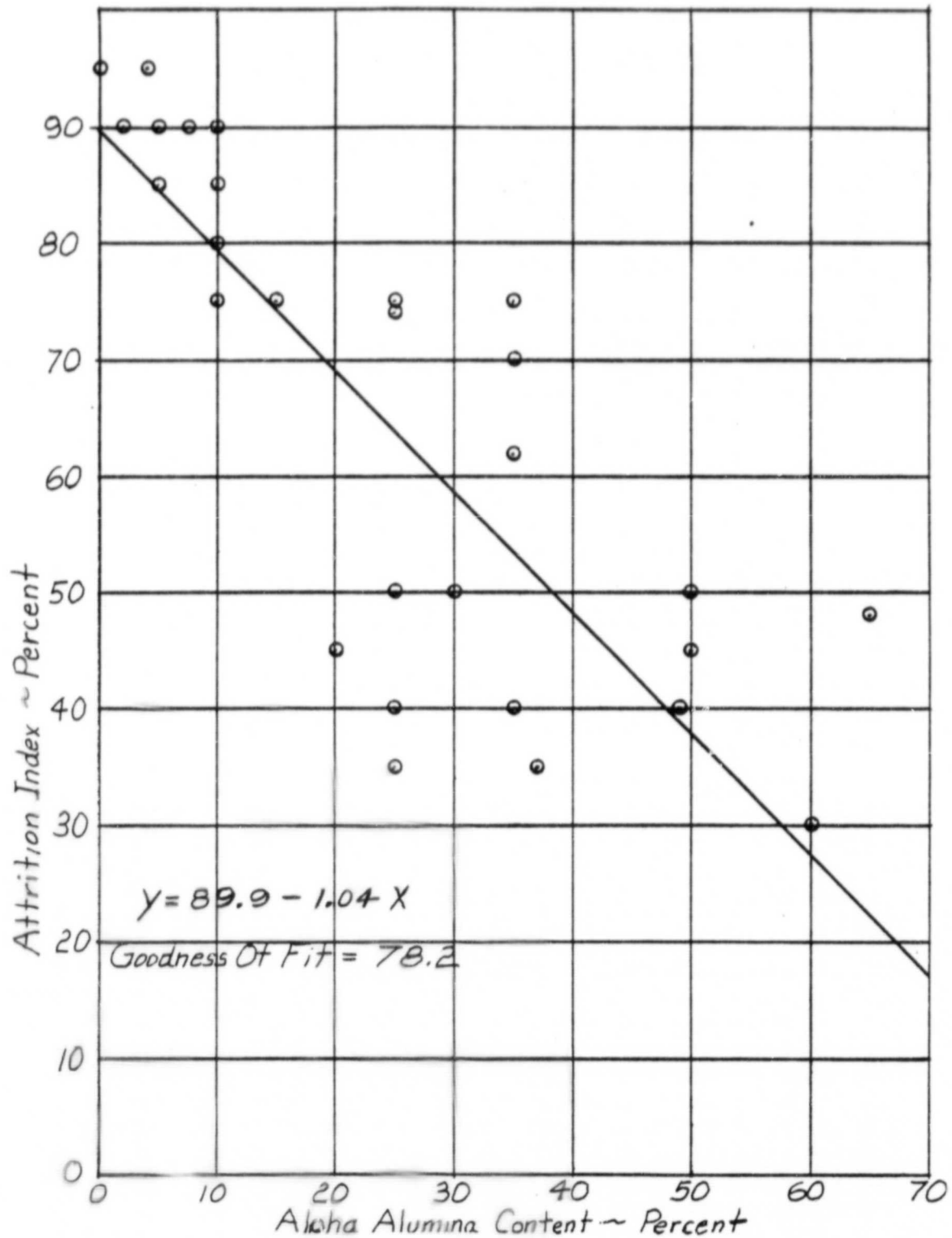


Figure 1. The Relationship between Alpha Aluminum Oxide Produced in a Calciner and its Attrition Resistance.

Can this information be used in a model? It appears so. Attrition rate data can be obtained for a given type or size of particle using either method if elutriated fines are sized and measured. The results must be correlated with the energy (and heat for Vaux's apparatus) put into the system. Even without knowing attrition rates, this information can be used to give relative values.

The effect of attrition on the particle size distribution of a sample of particles is shown in Figure 2. This is typical of data obtained by using the apparatus of Vaux or Brown. Fines that are elutriated from the apparatus are not included in the particle size distribution analysis. Notice that chips or fines formed from larger particles end in the smaller particle size range, just as expected. If the material is not attrition resistant a noticeable bulge occurs on the curve in the smaller particle sizes. If the material is attrition resistant little change is noted in the size distribution of the original sample. How information from these curves can be used is demonstrated in the following sections.

#### DESCRIPTION OF MATHEMATICAL MODEL

The model for determining particle size distribution in a fluidized bed where material is deposited, or growth takes place is described in detail elsewhere(1). What follows is a description of the basis upon which the model is formulated. Figure 3 shows a pictorial illustration of particles in a fluidized bed arranged side-by-side in order of increasing diameter. Vertical lines  $L$  and  $L + \Delta L$  are boundaries of a small differential weight of particles between this size interval.

An arrow pointing to the left of line  $L$  represents particles that leave and end up in an increment containing smaller particles. An arrow pointing toward line  $L$  shows the weight of particles entering because of particle growth. Likewise particles enter the boundary at  $L + \Delta L$  because of large particle attrition. Particles in the increment grow past the boundary and become larger because of growth. If seeds, usually small particles, are brought into the system from an external source, the arrow pointing down represents this rate. Shown also entering the size interval is the feed deposited on the particles. Leaving the interval from the top is an arrow representing the rate at which particles elutriate, and from the bottom an arrow representing the rate particles leave as product. All of these rate processes may occur in any size interval in the bed.

## TYPICAL PARTICLE SIZE CHANGE DURING ATTRITION TEST

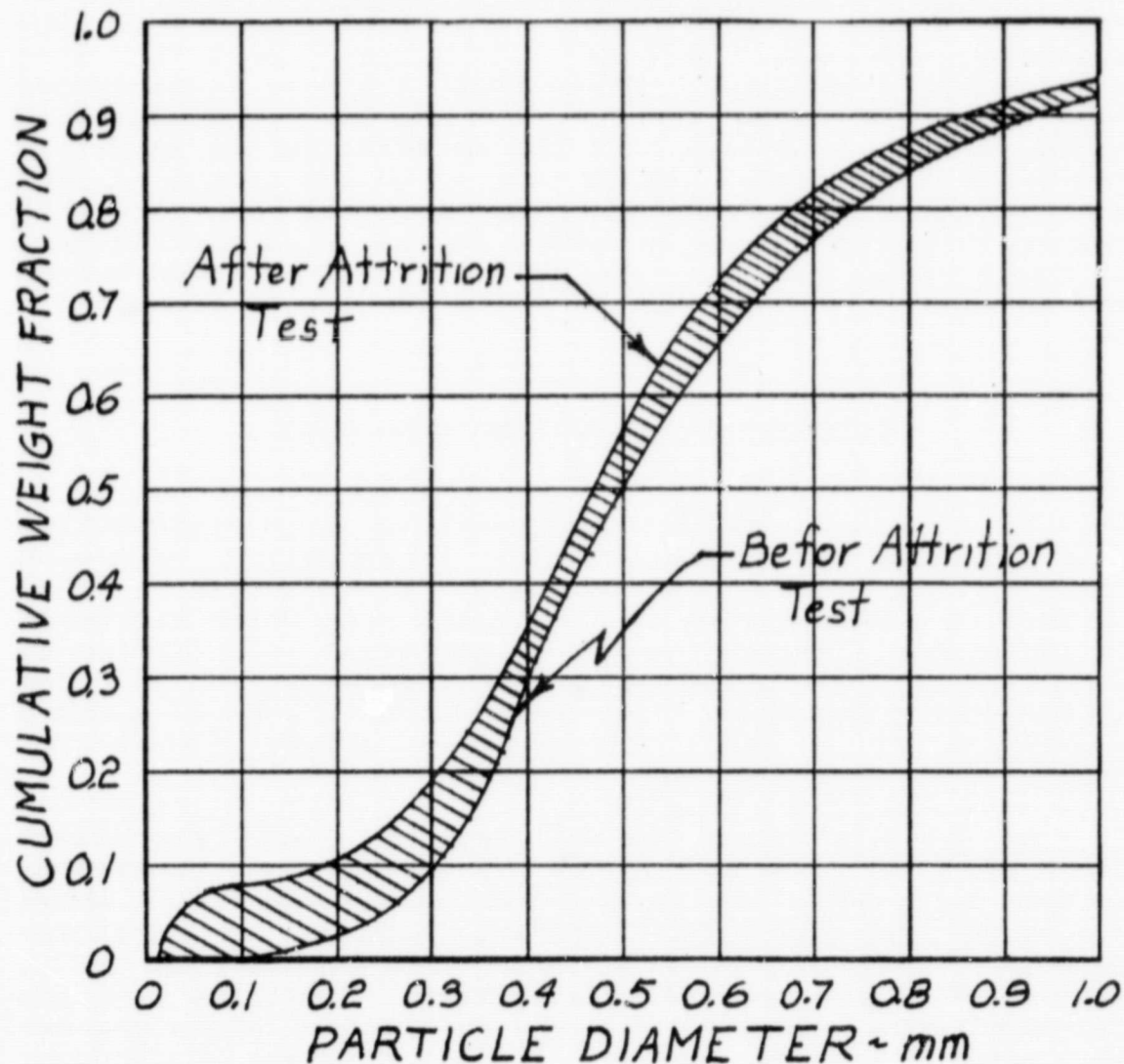


Figure 2. Typical Changes observe when a Sample of Particles has been tested in an Attrition Apparatus.

ORIGINAL PAGE IS  
OF POOR QUALITY

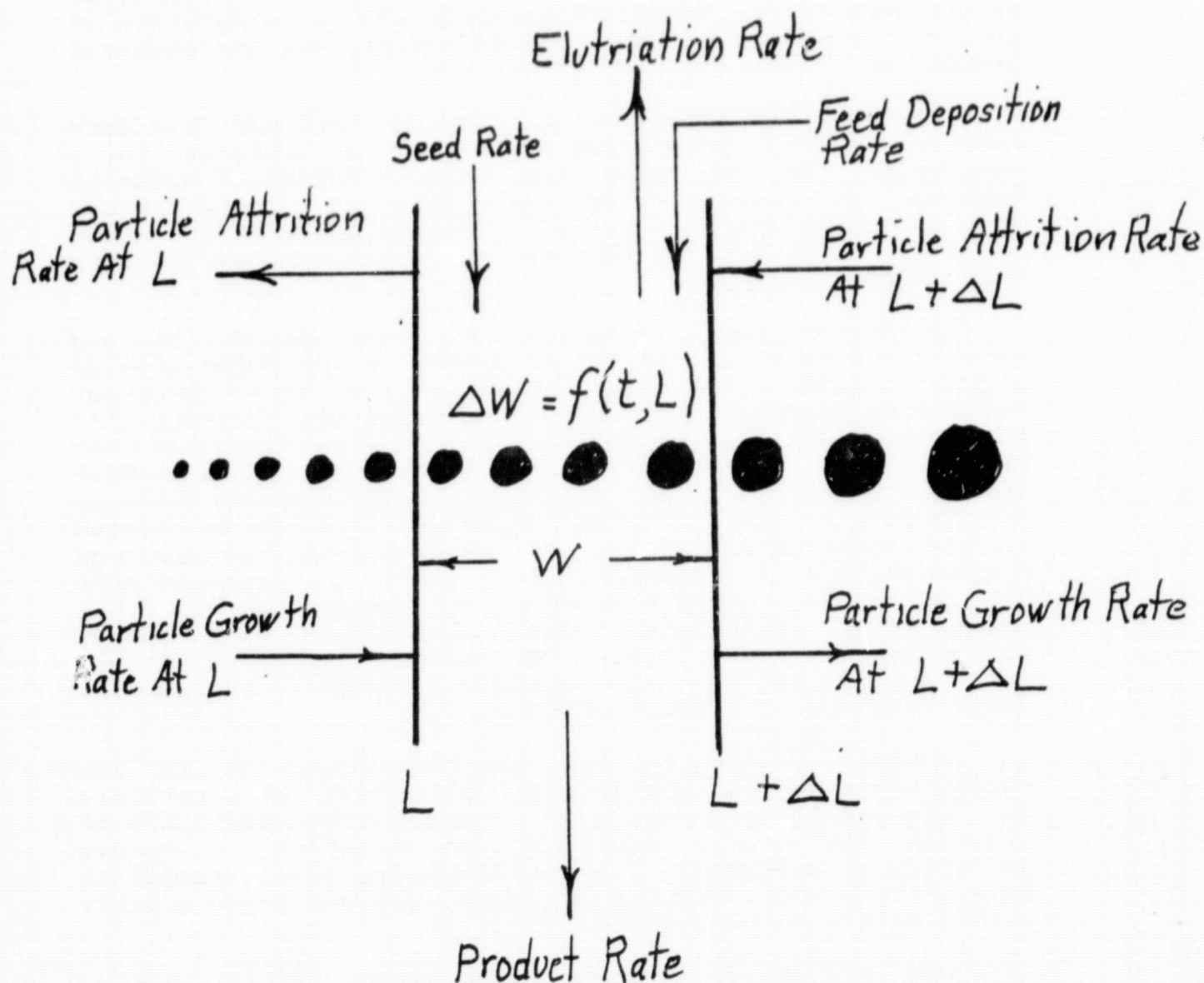


Figure 3. Pictorial Illustration of Particles in a Fluidized Bed Arranged in order of Increasing Size.

SUGGESTED METHOD OF INCORPORATING ATTRITION RATE  
INTO MODEL

Figure 4 illustrates the concept used to incorporate attritions rates into the model. Instead of trying to describe attrition by using rates from each particles size going into every other smaller size in the bed, the total rate leaving each particle size is used. It is expressed in the form of an empirical equation and is a function of particle diameter, energy input to the system, and physical properties of the material in the bed.

The amount of material leaving each particle size interval during some time interval, accumulates in a reservoir. At the same time, the fraction of material leaving the reservoir is calculated and redistributed among appropriate increments. This is accomplished using a set of redistribution factors. The sum of these factors must always equal one.

Attrition tests conducted by both Vaux(4)(5) and Kono(7) indicate little or no effect of particle size on attrition rate. Tests conducted at the Idaho Chemical Processing Plant(6) indicate a particle size effect. In any case an empirical equation can be formulated so that particle size is included. There is general agreement that the rate of attrition in a bed increases with an increase of energy put into it. The largest contributor is related to the amount of fluidizing air used, to the pressure drop across the air distributor system, and to the pressure drop across the bed. Feed nozzles which use air to atomize a liquid feed contribute significant quantities of energy which results in attrition. Of course "jet grinders" are put into a bed for the express purpose of introducing kinetic energy to promote attrition.

Another factor in the attrition function is the relationship between the physical properties of a particle and its attrition resistance. For example particles of aluminum are highly resistant to attrition, whereas particles of amorphous aluminum oxide are fairly resistant to attrition, and particles of alpha aluminum oxide exhibit little attrition resistance.

How are these factors formulated into a working equation that is useful? First, one must know something about the attrition characteristics of the material in question.



ORIGINAL PAGE IS  
OF POOR QUALITY

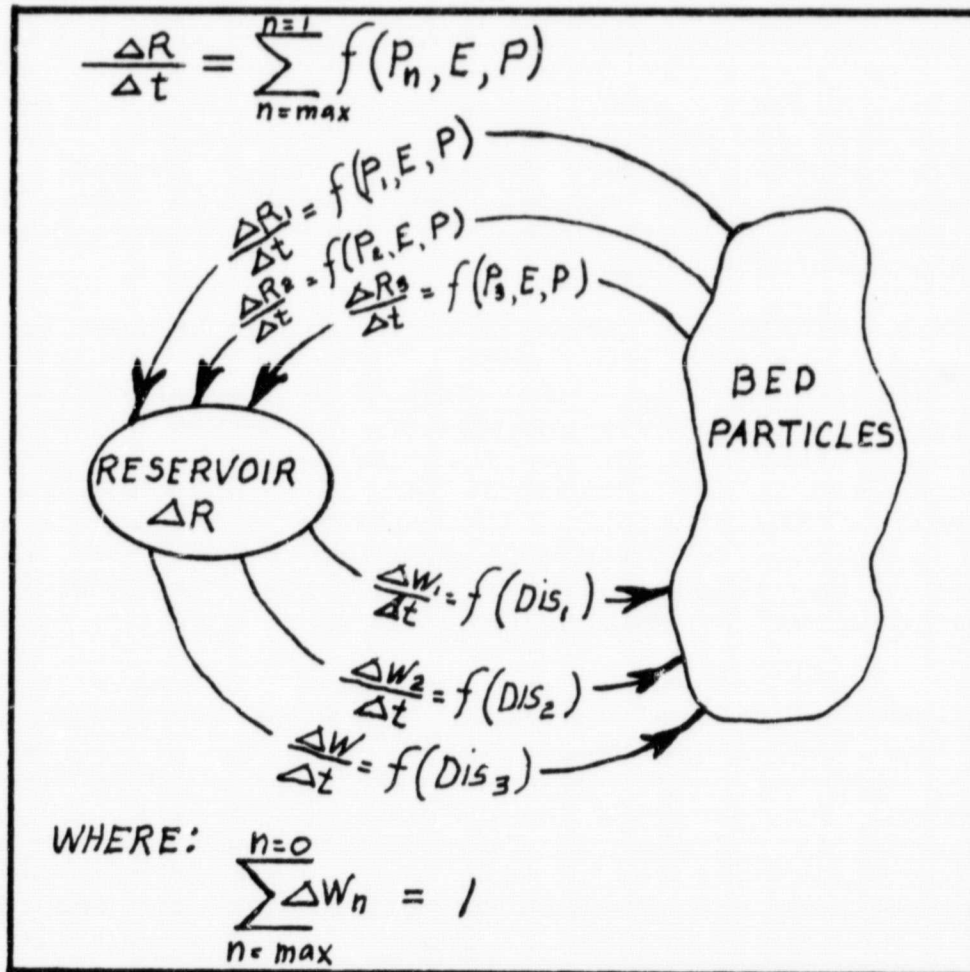


Figure 4. Sketch Illustrating Concept of Attrition Function(s) and Redistribution Functions

This can be done by running an attrition test on it, using an apparatus similar to the ones described above. A weight fraction curve typical of a material before and after such a test was shown previously in Figure 2. These curves, as expected, show that material is broken away from larger particles and becomes smaller ones.

An attrition test made at the Idaho Chemical Processing Plant gave some indication of the way large particles broke into smaller ones. Minus 10 + 14 mesh particles were fluidized in a fluidized bed at 6.5 feet per second over a time of 80 hours. About 20 percent of the particles formed by attrition was -16 + 14 mesh, 73 percent was less than 150 mesh in size, and the remaining 7 percent was distributed between these two size ranges. This phenomenon no doubt caused the bulge in the "after attrition test" size distribution curve in Figure 2 and in curves presented by Vaux.

Such information prompted this writer to test various functions representing both attrition rates and redistribution factors. At this time the attrition rate function is a logarithmic expression. It gives the attrition rate as a function of particle diameter. The particle diameter used is the arithmetic mean of each particle size increment. The attrition function contains also a value which is related to the energy put into the system. At the present time this value is calculated external to the program and must be entered before a simulated run is made.

A micro-computer can be used to help convert experimental attrition data into a useful expression. The model has been programed in basic so that it can be used with a computer, and with it attrition tests can be simulated. To do this a particle size distribution is chosen that is the same as that used in the attrition test. This represents the bed at time zero. A feed rate of zero is entered and the program started. At the end of a specified time the program is stopped and the particle size in the bed noted. The investigator then "forces" the computer to simulate the results of an experimental run. Mathematical expressions for both the attrition function and the redistribution factors can be established by such a trial and error procedure. No doubt a program can be devised which would "home in" on the correct expressions and factors with little operator attention. So far this has not been done.

Figure 5 shows the results of one such study. A logarithmic expression is used for the attrition function. Ten redistribution factors redistribute the material from the reservoir to each of ten intervals containing the

ORIGINAL PAGE IS  
OF POOR QUALITY

## DISTRIBUTION FACTORS

.001	.250
.004	.150
.045	.045
.150	.060
.250	.040

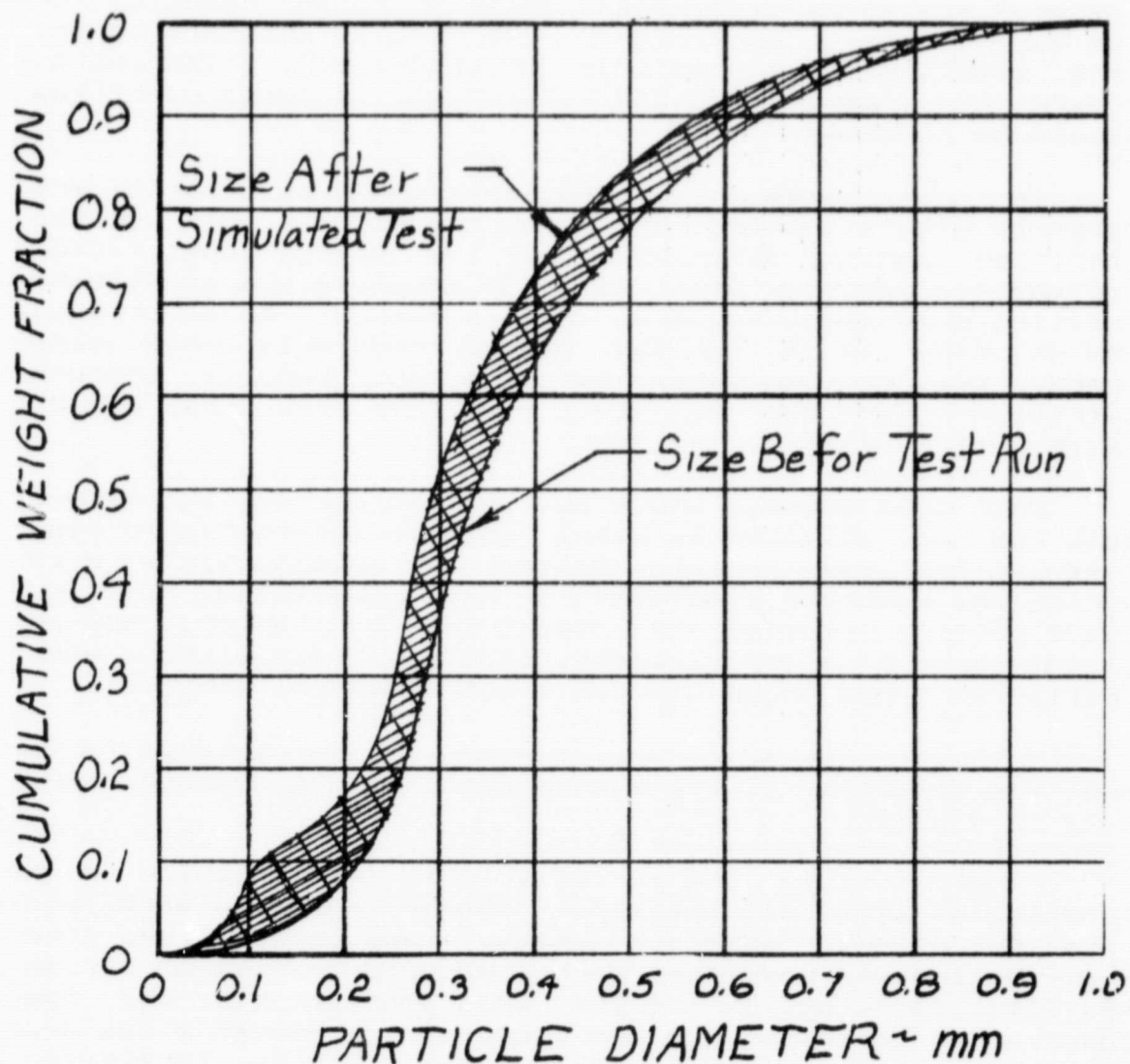


Figure 5. Plot of Attrition Test Simulated by using a Zero Feed Rate in the Model.



smallest particles in a fictitious bed. The particle sizes in the initial bed are shown as well as the size distribution after the test. The redistribution factors used are shown on the figure also.

#### HAS THIS APPROACH IMPROVED THE ORIGINAL MODEL?

Has the model been improved by using the concept of an attrition function and redistribution factors? Can the particle size distribution in a fluidized bed be predicted? The only way to answer these questions is to compare, for the same operating conditions, the results obtained by the model with those obtained from an actual run. The system should grow particles, and attrition of these particles should be possible.

Two runs made in a two-foot-square calciner(6) are compared with simulated runs using the model. Both use the attrition concept described, but the energy input factor for one run was very small so as to simulate the conditions existing when amorphous alumina was formed. An amorphous bed was used again for the second run, only this time energy was deliberately put into the bed to promote attrition. For the run that simulated it, the energy factor was increased.

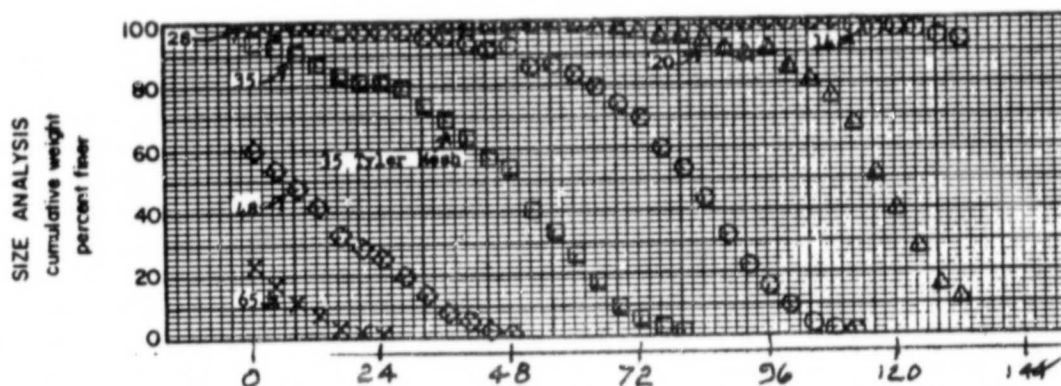
Increased energy input to the bed during the second test run was obtained by using a large air-to-liquid feed ratio in the feed nozzle. Control of bed particle size during the computer simulated run was accomplished by using the attrition function, ten redistribution factors, and as stated earlier a large energy factor. These factors were similar to those shown for the simulated attrition test.

A third simulated run is shown. Its purpose is to show the effect on particle size distribution when the feed rate is doubled.

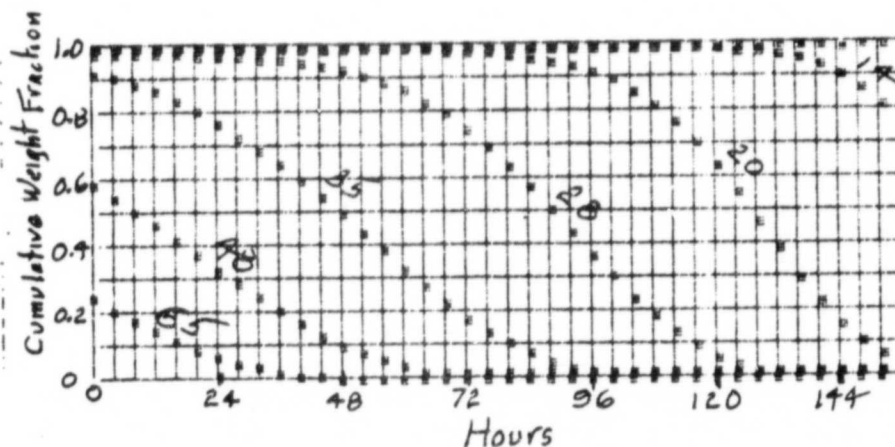
Figure 6 shows the particle size distribution as a function of time for the first comparison. The same feed rate, bed weight, particle density, and initial bed size distribution was used for each. The upper series of curves are data generated during the experimental run, and the lower ones generated by the computer. Screen sizes are Tyler mesh. The experimental run had to be terminated because the particles in the bed were too large to fluidize.

The shape of the computer generated curves for each screen cut compare extremely well with curves obtained from the experiment. Time-wise the simulated curves do not

ORIGINAL PAGE IS  
OF POOR QUALITY



Run Made In Calcliner.



Simulated Run Using Model.

Figure 6. Plot of Particle Size Distribution as a Function of Time for an Actual Calcliner Run and a Simulated Run Using A Mathematical Model. Upper Set of Curves Were Generated By Experiment. Energy Factor for this run was Close to Zero.

follow the actual curves as close. In the simulated run most of the size cuts do not disappear as soon as in the actual one. Even so the model does an admirable job in predicting both the size distribution expected and the time it takes to reach it.

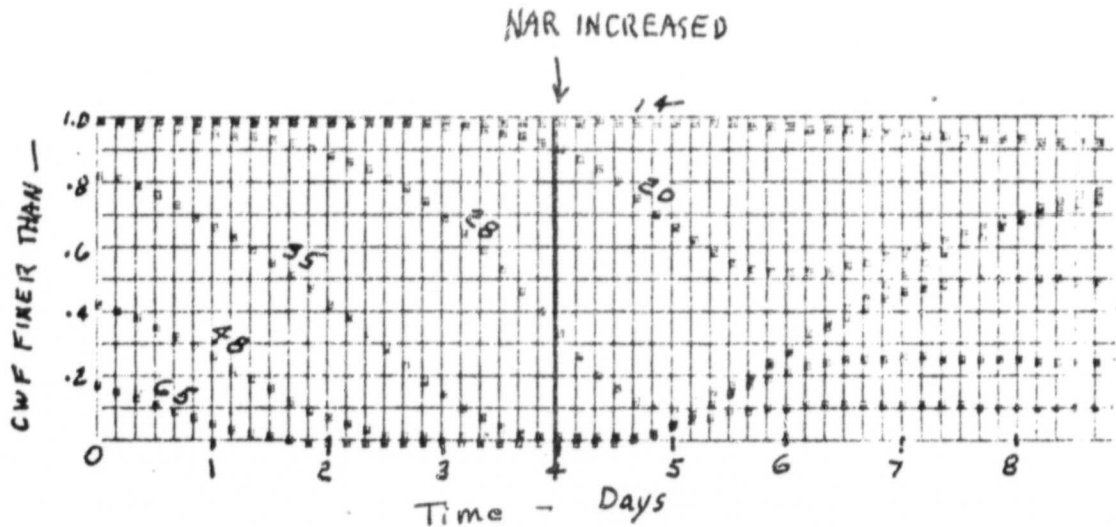
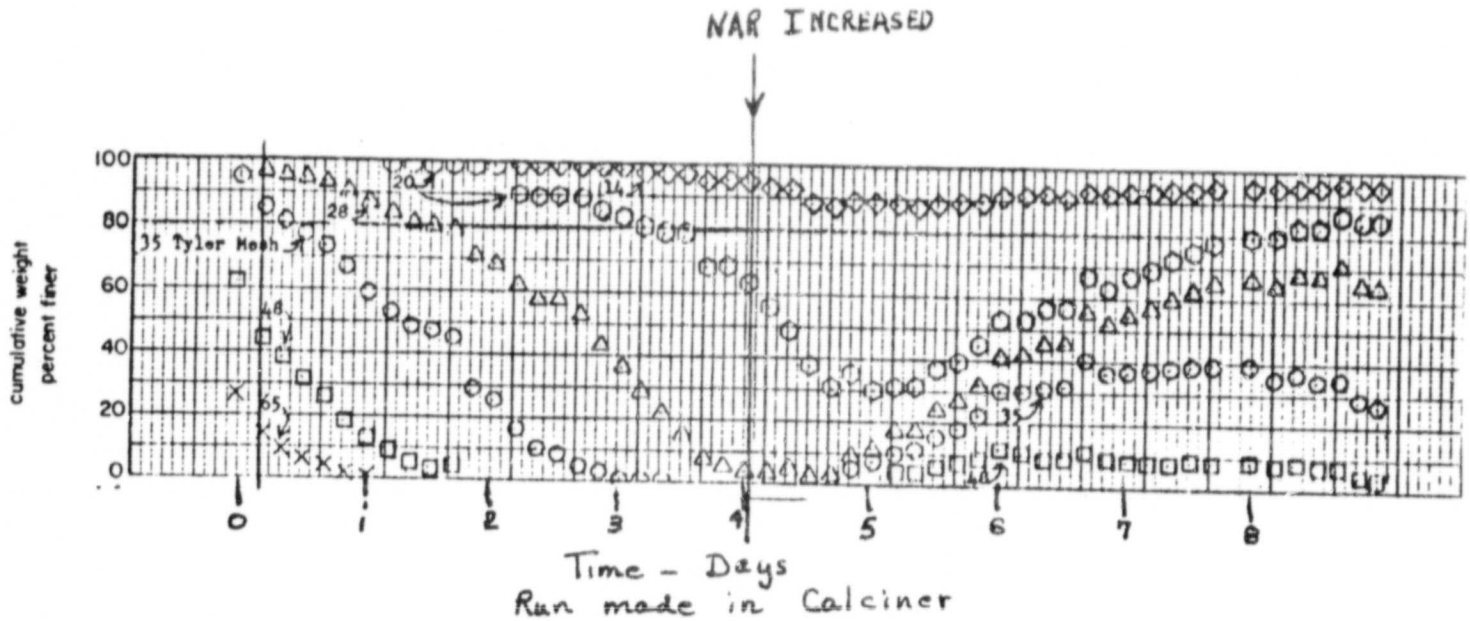
Figure 7 show a data comparison from the second experimental and simulated runs. The initial conditions for this run were much the same as those represented by the first comparison. In this run the particle size in the bed was not allowed to increase to the point where fluidization could not be maintained. After operating for four days the NAR was increased. The term NAR is used to represent the nozzle air-to-liquid throughput ratio. When this is increased, such as in this experiment, a great deal of kinetic energy is released into the bed in the form of a high velocity stream of air. In effect it acts as a jet grinder, causing particle attrition and new small seed particles which are necessary for particle size control of the bed. This example shows how particle size in a bed can be controled if no new seeds are generated because the bed material is attrition resistant.

Until the NAR was increased, the curves generated by the experiment and computer had almost identical shapes. The time lag in the computer data is evident again. After four days of simulated operation the energy function (NAR) was arbitrarily increased. Just as in the actual run seeds are generated and smaller particles begin to appear in the bed. Some of the general characteristic curve shapes are simulated but they are not very accurate. The time lag is also noticeable, but the bed particle size distribution begins to stabilize somewhat near that shown by the actual run.

It is instructive to show a simulated run where the particle size distribution has reached steady state, and then a variable changed such as feed rate. Figure 8 shows such a run. The bed weight used was 200,000 grams, the particle density 1.57 grams per cubic centimeter, and the feed rate 20,000 grams per hour. Though in practice the feed is a liquid, it must be entered into the model as an equivalent solid feed rate. Values for the attrition function and the redistribution factors are nearly the same as for the example above. The energy factor was less. The results of this run are shown in Figure 8.

There are two important things about this run besides the expected change in particle size distribution. First, reaching steady state requires a long time. Second, large fluctuations in particle size are observed. Without changing a single operating variable the particles in the bed changed from small ones to fairly large ones, then back to a size somewhere in between the two.

ORIGINAL PAGE IS  
OF POOR QUALITY



Simulated Run Using Model

Figure 7. Comparison of Actual and Computer Generated Data for a Run in which Seeds were Generated to Control Particle Size in a Bed. Energy in the Form of Feed Nozzle Air was Used in the Experiment, but the Energy Factor was Increased when Simulating the Run with the Model.

ORIGINAL PAGE IS  
OF POOR QUALITY

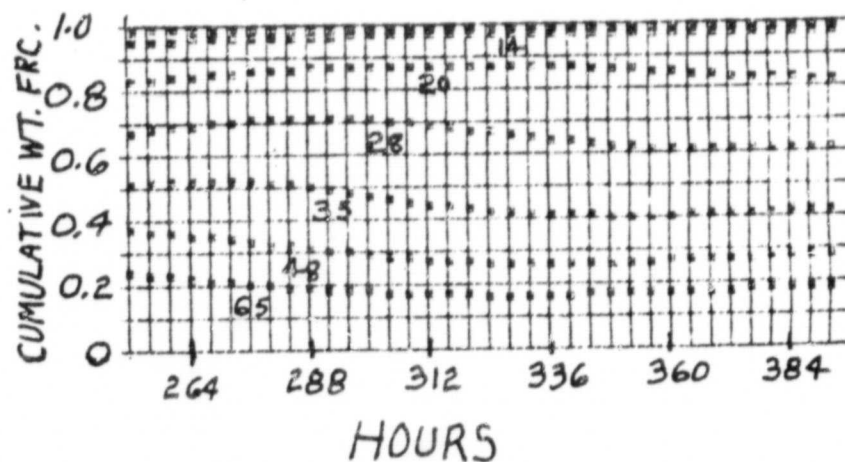
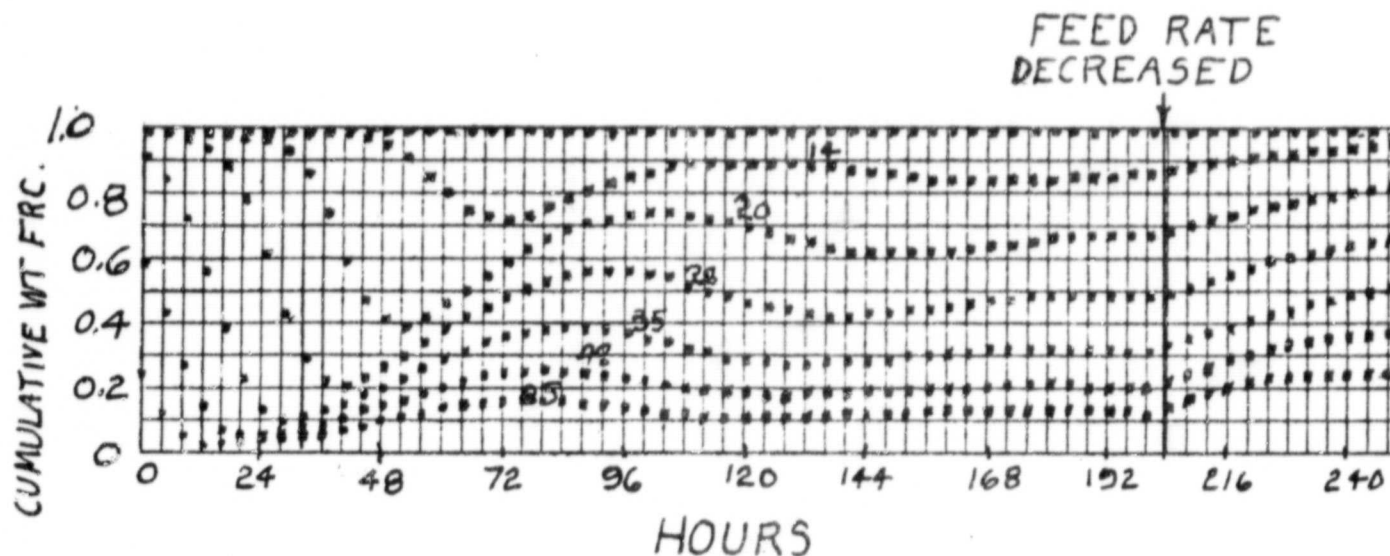


Figure 8. This Set of Curves Show the Effect of Changing the Feed Rate. The Experimental Run and Data Generated by the Model are Shown.

Imagine, it took over 200 hours of operating time for the bed to reach steady state conditions! And then after the feed rate was reduced, an additional 200 hours were required before the bed again reached a stable particle size distribution.

These facts are not appreciated by many who operate fluidized-bed systems. The fluctuations noted at the beginning of the run are in effect "built into the system" by the initial particle size distribution of the bed. It is the road map for future particle size fluctuations until other operating conditions come into play. It should be noted that this characteristic was observed during many runs made in the calciner at the Idaho Chemical Processing Plant(1)(6). These unexplained changes when operating variables remained constant, led to the studies which resulted in the original model.

#### CONCLUSIONS

A mathematical model for predicting the particle size distribution as a function of time was suggested several years ago by Grimmett. This model accounted for most, if not all, rate processes taking place in a fluidized-bed system where particle growth, attrition, and elutriation take place. At that time two parts of the model were not too useful; good rate expressions were not available for elutriation and attrition.

Since that time several good correlations have been proposed for calculating elutriation rates taking place in fluidized beds. However until studies began on the development of atmospheric fluidized-bed combustion of coal, little was done in the area of attrition. In these units limestone must be added to the bed when burning high sulfur coal. Limestone converted in the bed to calcium oxide acts both as a bed media and a material that reacts with the oxides of sulfur to prevent their release to the atmosphere.

Knowing the attrition resistance of various types of limestone has become necessary. Serious problems arise if the bed cannot be stabilized because of attrition. This has resulted in several recent studies concerning attrition, and particularly attrition of limestone. These studies plus those conducted by this author have led to a method of using an attrition function(s) and redistribution functions in the model.



Simulated runs have been compared with runs made in an actual calciner. These functions have been put into the model. A comparison of data from each indicates this method is a promising one. Further, simulated attrition runs have been conducted using the model. Attrition rate functions and redistribution functions can be manipulated so that computer data matches that from an actual attrition test. This gives one the ability to characterize, for a given system, the type of functions to use. The effect of changing various operating conditions can then be studied. The changes in particle size distribution of a bed can be predicted as a function of time.

One final conclusion. No model is better than the information built into it. A process as complex as a fluidized-bed system has to use empirical relationships when using a model. This is true even if it is based on theoretical concepts. No model will be better than the effort put into developing required empirical relationships that go hand-in-glove with theory. They must be based on laboratory and pilot plant studies. My request to you is — put laboratory and theoretical studies together. The micro-computer available to almost anyone today, is a tool that makes this possible.

REFERENCES

- (1) Grimmett, E. S., "Particle Growth and Size Distribution in Fluidized-Bed Process: A Mathematical Model with Computer Solutions", Chem. Eng. Prog. Symp. Ser., 62 (67); (1966).
- (2) Grimmett, E. S., "Kinetics of Particle Growth in the Fluidized-Bed Calcination Process," AIChE J., 717-22 (1964).
- (3) Vaux, W. G., "Attrition of Particles in the Bubbling Zone of a Fluidized Bed", Proceedings of the American Power Conference, Vol 40, 1978.
- (4) Grimmett, E. S. Private Papers
- (5) Vaux, W. G., A. W. Fellers, "Measurement of Attrition Tendency in Fluidization", paper presented at 72 Annual Meeting of American Institute of Chemical Engineers, San Francisco, Ca., Nov. 1979.
- (6) Brown, B. P., B. M. Legler, B. R. Wheeler, E. S. Grimmett, J. A. Buckham, "Development of a Fluidized-Bed Calcination Process for Aluminum Nitrate Wastes in a Two-Foot-Square Pilot Plant Calciner, Part III. Intermediate Process Studies - Runs 11 through 22," IDO-14618 (February 1964).
- (7) Kono H., "Attrition Rates of Relatively Coarse Solid Particles in the fluidized Beds of Various Types", paper presented at the 72 Annual Meeting of American Institute of Chemical Engineers, San Francisco, Ca., Nov. 1979.



## DISCUSSION

None.

SESSION IV GENERAL DISCUSSION

RING: I would like to comment on the question of whether in the decomposition of silane the reaction proceeds immediately to silicon or, as Bruce Scott suggested, silylenes form and dimerize before particles are formed. I did some very quick calculations, and since I really don't know the conditions, I used 1000°K. At 0.1 atmosphere (I really don't know what kind of pressures they use in a fluid bed) the decomposition of silane to give silylene and hydrogen would have a first-order rate constant of about 30 second<sup>-1</sup>. We don't know what the decomposition rate constant for SiH<sub>2</sub> would be, but if it did decompose, it would undoubtedly have to go to silicon and hydrogen. It should be much slower than the silane decomposition with the reaction path degeneracy down by a factor of 6. It is a very small molecule and all of these are in the fall-off so that is at least another factor of 10 which gets you to 60. Also, the SiH bonds in silylene should be stronger than in silane. So if the activation energy is increased a little, the first-order rate constant would be decreased compared to silane by maybe 10<sup>2</sup> or 10<sup>3</sup>. Certainly at 700°C, then, silylene, which is very reactive substance, would not decompose but would react in some way. It might insert into silane to give disilane; but disilane is less stable than silane so it would decompose. So the most likely reaction is for the silylene to dimerize to give Si<sub>2</sub>H<sub>4</sub>. This would be followed by a rearrangement and then either a further polymerization or a rejection of hydrogen. So I would guess that if you are talking about homogeneous reactions at 700°C, a sort of polymerization of polysilicon species that are silylenes or double bonded species occurs and then these would grow. Certainly these would eject hydrogen, and eventually particles that were mostly silicon with a few hydrogens would be formed. This path is different than that of going from silane to silicon and two hydrogens, and then for the silicon atoms to polymerize. There was a question of what would happen at 1200°C. I'll make a calculation and give you an answer in five minutes.

MILSTEIN: I realize there are two considerations that go into the topic that we have been discussing for three days. On one hand, we are talking about the science of silicon preparation and on the other hand is the realization that there is the particular function of being able to make silicon. In that sense, considering the last couple of talks, although it is not clear what mechanisms may be going on in these reactors, one wonders if a stable distribution of particles can be predicted for a fluidized-bed reactor. If so, could one initiate a reaction by inserting that stable circumstance (in other words, those fractional cuts of particles pre-chosen to be the stable circumstance) and simply observe the reaction at that point? The other point, of course, is that it would be very nice to understand the chemistry and physics taking place in this reactor. From that point of view, it seems to me that looking at a fluidized bed is essentially a transfer function, since the reactants and the products are known. However, it is by no means clear what, in fact, is taking place internally. Speaking purely from the chemical point of view, it seems to me that the reactant molecules are typically

tetrahedral. Techniques such as spectroscopy, for observing these molecules, give little information regarding the reactions here. But if you consider some of the reactive entities that might be present in the reactor, such as free radicals, dimers, trimers, tetramers, or whatever, those entities might in fact be materials that you can observe spectroscopically even if they are only present in a steady state as opposed to stable circumstances. The entities are not stable, but they have a steady-state existence and they might be observed from that point of view. So I think both of those questions are things people might consider.

HSU: I would like to describe again what we at JPL have observed for the silane-silicon deposition system. We have seen experimentally a kind of incorporation of small particles by seed particles, a situation described by Tom Fitzgerald. Using SEM pictures, the observation was made that there is a definite incorporation leading to small nodules on the surface. There is no doubt, at least in the way we conduct our experiments, that some sort of homogeneous nucleation takes place. We also believe that the classical interpretation is correct -- that simultaneous CVD and homogeneous reactions occur. The particular operating conditions and distributor plate we used tended to favor the condition for the scavenging of fines onto the seed particles. In all our experiments there is evidence for simultaneous CVD and homogeneous nucleation processes.

FLAGAN: Based upon the rate numbers that Morey (Ring) just quoted for the 700°C condition, it would seem that the initial time constant for the reaction is relatively long compared to the transit through those bubbles in the fluidized-bed conditions that Tom (Fitzgerald) considered earlier today. The initial reaction is relatively slow, and so George's (Hsu) comments that the chemical vapor deposition may be taking place appear to be reasonable. At the higher temperature limits, that Morey (Ring) is now calculating, I think we will find that that is probably not the case.

FITZGERALD: It seems that if the reaction rate to form the homogeneous materials doesn't happen very quickly, say within a order of a few particle diameters, then in fact the picture that emerges is that you might form some nuclei and there may be some material left around. When I did this originally, I must concede that I had assumed that the nucleation was essentially instantaneous which may not have been appropriate for this temperature. Maybe the model will point out that there is in fact a distinct possibility that the alternative mechanism is likely if the reaction rates do turn out to be spread out over a fraction of a second or tens of seconds, or at least a substantial fraction of a second.

PRATURI: I would like to make one comment with regard to the points Tom (Fitzgerald) and Mike (Dudukovic) have made. What is happening is really not a competition between homogeneous nucleation and heterogeneous CVD. Rather, it really is a competition between the homogeneous reaction and the heterogeneous reaction. The homogeneous nucleation, of course, is instantaneous for most of the temperatures of interest. We should

9  
Y

actually compare the time constant for the homogeneous reaction versus the time constant for the heterogeneous reaction. That's what really determines whether we have small particles or have a deposit.

DUDUKOVIC: While I tend to agree, I am a little bit taken aback by the calculation that I just heard; because based on the material that I have read, I also assumed that for homogeneous nucleation the time constant is always of the order of milliseconds. Of course, that time constant will depend dramatically on temperature, and I would hope that the calculation being done now (by Ring) will show that at very much higher temperatures the precursor can be formed fast enough so that it will allow the homogeneous nucleation to be essentially instantaneous while at lower temperatures that may not be the case. Maybe then things will start falling a little more into place.

FLAGAN: Carrying the last point a little bit further. Does anyone who has done fluid-bed reactor experiments have any comments on the structure of the particles which are produced at temperatures significantly higher than 700°C for bed temperatures? That would give some very interesting insight in conjunction with the kinetic calculations.

HSU: I can only comment on the morphology of the deposition. The configuration seems to be very similar. We did some early feasibility experiments operating the reactor up to 900 and 930°C. The morphology changes as the temperature goes up. As expected, the deposition becomes more and more coherent as well as more and more dense. However, in terms of the configuration, the deposits are still pretty much nodular in shape.

DUDUKOVIC: I would like to remind you of some of the old papers in the Journal of American Chemical Society. I will try to quote to the best of my recollection. The studies of the pyrolysis of silane were done from 350 to 490°C because anywhere above 500°C the rate was too fast to follow. Of course, those comments were made in 1936 when the instrumentation was not as capable as present-day instruments. At that time the words "too fast to follow" meant that observations could not be made of conversions of the order of minutes and tenths of minutes on the time scale. So it is indeed possible then that even at temperatures of 500°C perhaps it takes a finite time for the precursor to form.

RING: I have done part of the calculations for 1200°C and one atmosphere pressure of silane. As I said, the rate constant is pressure-dependent. At one atmosphere and 1500°K, the silane decomposition rates goes up to about  $10^7$  second<sup>-1</sup>. Then, if a  $10^3$  lowering for silylene is assumed, its decomposition rate goes up. It could be  $10^4$ , maybe even  $10^5$  second<sup>-1</sup>. Maybe at those temperatures and those pressures the reaction will go all the way. I think it could be very pressure-dependent, because the rate constants themselves are quite pressure-dependent. It may well be that at those temperatures, that is, at 1200°C, you do get just silicon, I think that at 1000°K, or thereabouts, there would probably still be a lot of insertion.

SCOTT: Let me propose another way that these particles can form. Morey Ring and others have shown very nicely that silylene is the main precursor when you decompose silane. At least on a short time scale it's the  $\text{SiH}_2$  that's coming out and reacting further. All the products of reaction of silylene with silane are very easy to describe. You get disilane which is even less thermally stable than silane so that silane is kicked back out again. Now suppose that at high pressure and high temperature a lot of silylene is produced causing a lot of insertions that make higher silanes, such as disilanes and trisilanes. Even though these are less stable, so many of them are forming so rapidly that the chains are growing very rapidly. Now the reverse reaction may occur reforming free silane. This reaction may not really occur fast enough relative to dehydrogenation reactions that are taking place on these growing chains. As a result, there is chain formation with simultaneous dehydrogenation that leaves a particle growing very, very rapidly and dehydrogenating very rapidly so the reverse reactions to smaller and smaller intermediates can't occur. This mechanism can explain the production of silicon without having to invoke the idea of breaking down the silane itself. As the chains grow the reverse reactions can't occur fast enough relative to dehydrogenation reactions that crosslink the chains and create the silicon framework. This mechanism is a description of how to eliminate the necessity of breaking up  $\text{SiH}_2$  to even smaller units like  $\text{SiH}$  and  $\text{Si}$  at these low temperatures.

KAAE: The discussion is very similar to discussions concerning carbon deposition that have gone on in the carbon literature over the years. One of the mechanisms proposed for carbon deposition is that the decomposition of the hydrocarbon molecules occurs through a polymerization in which larger and larger molecules are formed so that the carbon to hydrogen ratio increases. One situation is that in which the particle that is forming is actually a liquid rather than a solid, and the liquid droplet comes down upon the surface, intersects the surface, and then flows on the surface; this is another mechanism that has been proposed. I think that the work that I showed demonstrated that this does not happen in carbon, but I bring it up as a possible mechanism that may apply to silicon.

RING: It would be nice to have a computer fit of the data and the answer depends on the assumptions. At any rate, if the silane decomposition rate is  $10^7$ , which can be taken as being instantaneous, and if the silylene decomposition rate is  $10^4$  (and of course that is a guess, maybe it's  $10^5$ ) then if you compare silylene decomposition, the first order rate constants would be say,  $10^4$  times the silylene concentration (which can be taken as essentially equal to the initial silylene concentration). The silylene dimerization which is a bimolecular process, would be about  $10^{10}$  times a silylene squared and so if silylenes are crossed out, the decomposition to dimerization is  $10^4$  divided by  $10^{10}$  times the silylene concentration. At one atmosphere that is about  $10^{-2}$  moles per liter; so that means that the dimerization rate is about  $10^4$  faster than the decomposition. So it would seem that at  $1500^\circ\text{K}$  the dimerization should be faster than decomposition. Of course, I have just had to assume that the silane decomposes immediately and that the only reactions are decomposition and dimerization. The simple model, then, indicates that

9  
Y

dimerization ought to be faster, because dimerization should be a very, very fast process.  $\text{Si}_2\text{H}_4$  would be formed, which might dimerize ejecting hydrogen. That may well be what is happening.

BAILEY: The literature is sprinkled with references to compounds having the formula  $\text{SiH}$  taken from 1 to 1.6-1.7. These are solids and they are reasonably stable under lower temperature conditions. I don't know at what temperature  $\text{SiH}$  polymers come apart. It may be around  $650^\circ\text{C}$ . What is needed is some research with these solids to find out how much  $\text{SiH}$  they contain.

FITZGERALD: I want to point out that I do have some photographs from JPL reports which show the SEM of surfaces grown in a fluidized bed at 600, 650, and  $700^\circ\text{C}$ . At  $600^\circ\text{C}$  there were particles which were  $1/8$  inch (in the scale of the photograph) in diameter and at  $700^\circ\text{C}$  there were mounds which were about  $1/2$  inch in diameter. These mounds, which look like they were parts of spheres, were always relatively small portions of a sphere, never a full hemisphere and certainly never more than a hemisphere. Using a model of a small particle sitting down on a surface and enough growth of material around it so that just a mound and not a hemisphere is formed, it follows that the initial particle grows perhaps by a factor of 3 in diameter before the surface becomes smooth. Now a factor of 3 in diameter is a factor of 27 in terms of mass. What that would mean is that the deposition of particles takes place first and then a chemical deposition process follows. About 95% of the silane must remain unreacted for a fraction of the time up to a 0.1 second, and we have direct data taken showing that there is no possibility of that happening. The silane disappears in 40 milliseconds in the actual runs. So the concept of incompletely formed particles, perhaps a polymer, on the surface, ejecting hydrogen, rearranging, and forming a dense form is an alternate intermediate mechanism. A number of mechanisms could be invoked. I hope this consideration will lead to additional research. I should point out also this is not a trivial problem, because although you can certainly grow particles and there are models to describe the formation as well as the size and the attrition can perhaps be controlled, the problems with wall deposition, purity, sintering, and plugging of the distributor remain to be solved. If the operating window for concentrations, temperature, and pressure is not well defined, the bed operation will not be stable. So it is important to pin down, at least in a superficial way, the range in which the mechanisms occur and what kinds of deposition give rise to these particles.

SESSION V: Chemical Vapor Deposition

DUDUKOVIC (Chairman): This sessions deals with the factors involved in CVD processing for silicon. In the first paper of the session, I will review reactor models for CVD technology and try to present the review from a chemical engineering point of view. Then Dr. Bruce Scott of the IBM Thomas J. Watson Research Center will describe his very interesting work on the deposition of low defect density amorphous semiconductor grade silicon by homogeneous CVD. The third paper will be given by Dr. Sarma of Solavolt International, and it will be on the mechanisms of plasma-enhanced silicon deposition. Rafael Reif of MIT will then discuss the CVD of epitaxial silicon under transient and steady-state conditions. The final paper of the session will be presented by Dr. Jacobson of the University of Arizona, and he will describe the CVD of silicon for optical uses. I believe that this session will be very interesting and will provide additional information to help us in understanding the mechanisms involved in silicon preparation.

PRECEDING PAGE BLANK NOT FILMED

# REACTOR MODELS FOR CVD OF SILICON

MILORAD P. DUDUKOVIĆ

Professor of Chemical Engineering, Washington University  
St. Louis, Missouri

## ABSTRACT

This paper reviews the currently used reactor models for CVD of silicon and the key features of the thermodynamics and kinetics of the Si-H and Si-H-Cl system. A simple model for bell-jar decomposers is suggested and some problems related to fluidized bed modeling outlined.

## INTRODUCTION

Silicon, for a variety of electronic and solar devices, is mainly produced by chemical vapor deposition (CVD). Two reaction systems are used: i) pyrolysis of silane and ii) hydrogen reduction of chlorosilanes such as  $\text{SiCl}_4$ ,  $\text{SiHCl}_3$ ,  $\text{SiH}_2\text{Cl}_2$ , or a mixture thereof. The form of silicon, depending on its final use, resulting from CVD, varies and can be: a submicron film or a multimicron layer of amorphous, polycrystalline or single crystal material on a substrate (epitaxial films), bulk polycrystalline or single crystal material (silicon rods) or granules of polycrystalline material. The reactors, in which some of these forms of silicon can be produced, are summarized in Table I and Figure 1. The objective here is to review this broad area of silicon CVD from the chemical reaction engineering (CRE) point of view. The emphasis is on evaluation of the current reactor models and identification of parameters which are needed for improved reactor modeling. Equation (1) can be written for any reactor and it applies also to CVD reactors.

Reactor Performance = f (Thermodynamics, Kinetics, Hydrodynamics) (1)  
Various measures of reactor performance may be used such as crystal growth rate, silicon yield, total production rate etc.. In any event, the desired measure of reactor performance can only be related quantitatively to input (T, P, composition, flow rate) and operating variables (T, P, cooling or heating rate, etc.) through a reactor model if the thermodynamics and kinetics of the reaction system and hydrodynamics (which dictates mass and heat transfer rates) of the reactor are understood. These three areas are now considered.

## THERMODYNAMICS, KINETICS AND MECHANISM

### $\text{SiH}_4\text{-H}_2$ ( $\text{SiH}_4$ -Inert gas) System

Pyrolysis of silane can be described by a single overall reaction.  
 $\text{SiH}_4(\text{g}) \rightarrow \text{Si}(\text{s}) + 2\text{H}_2(\text{g}); \Delta H^\circ = -7.8 \text{ kcal/mol}; \Delta G^\circ = -13.2 \text{ kcal/mol}$  (i). Some times at higher pressures and/or at lower temperatures, traces of polysilanes (silicon polymers) are detected also. The reaction is practically com-



plete at all temperatures above 500°C. The main questions are: in what manner does the reaction proceed through the active intermediate silylene ( $\text{SiH}_2$ ), when does homogeneous nucleation of Si start, what are the rates of homogeneous and heterogeneous reaction? A representative sample of the findings reported in the literature (1-19) is given in Table II. Most of the investigators studied the growth of poly or single crystal films on silicon, silicon oxide or silicon nitride substrates at very low pressures in hydrogen or inert gas atmosphere. There is no generally accepted mechanism of homogeneous or heterogeneous reaction but a unified picture of the system is starting to emerge. At fixed pressure amorphous films are formed at the lowest temperatures, polycrystalline films at intermediate ones and single crystal at the highest temperatures. The temperatures separating these regions depend on the pressure of the system and mole fraction of silane, they go up as pressure and partial pressure of silane are increased. Monocrystal can only be formed when there is no homogeneous nucleation and when the temperature is high enough to keep the mobility of ad-molecules of the active intermediate very high on the surface while keeping their concentration low and thus preventing heterogeneous nucleation. Conflicting arguments are advanced with regard to the role of adsorbed atomic hydrogen (12-15). Large surface coverage of hydrogen is reported (14) as well as negligible coverage (12-13). There seems to be an agreement, however, that at lower temperatures ( $< 850^\circ\text{C}$  but depending upon P) surface reaction of the active intermediate at the step (kink) site is the rate controlling step (RLS) (12, 13, 15). At higher temperatures it is argued that mass transfer controls the rate (15). To investigate the effect of mass transfer one can consider a CVD number (16) which is really the Damkohler number of CRE and is given by eq. (2) where

$$\text{CVD} = \frac{(G'/C^\circ\text{SiH}_4) \delta}{D_{12}} \quad (2)$$

$G'$  is the growth rate in ( $\text{mol}/\text{cm}^2\text{s}$ );  $\delta$  (cm) is the mean BL thickness,  $C^\circ\text{SiH}_4$  ( $\text{mol}/\text{cm}^3$ ) is the bulk concentration of silane and  $D_{12}$  ( $\text{cm}^2/\text{s}$ ) is the diffusivity of silane in the carrier gas. Observed growth rates, or those calculated from the model, can be used. When  $\text{CVD} < 10^{-1}$  no appreciable mass transfer effects are present, when  $\text{CVD} \rightarrow 1$  mass transfer is becoming the RLS. The problem with eq. (2) is that mean B L thickness is difficult to assess in CVD reactors with even 50% accuracy. Nevertheless, the above approach was used well, at least in a qualitative sense, by Claassen and Bloem (13) to explain the shift in transition temperature from kinetic to mass transfer control as a function of carrier gas ( $\text{H}_2$  vs inert) and of total pressure. The behavior of the system is given in Figure 2. The assumption is that the growth rate is:

$$G = \frac{k_o e^{-E/RT} P_{\text{SiH}_4}}{1 + K_o e^{-\Delta H/RT} P_{\text{H}_2}} \quad (3)$$

In inert gas and in  $\text{H}_2$  at high T,  $1 > K_o e^{-\Delta H/RT} P_{\text{H}_2}$ . In hydrogen at higher pressure  $1 < K_o e^{-\Delta H/RT} P_{\text{H}_2}$ . Under the experimental conditions analyzed

$\delta = \text{const}$ ,  $D_{12} \propto P^{-1}$  so that the CVD number reaches a critical value indicative of mass transfer control at lower temperature at higher pressure in inert gas. At the fixed pressure the transition temperature is lower

in an inert gas than in  $H_2$  because in  $H_2$  the values of  $G'$  are smaller due to the existence of the denominator in eq. (3) i.e.  $(CVD)_{\text{inert gas}} = (CVD)_{H_2} \cdot (1 + K_o e^{-\Delta H/RT} P_{H_2}) > (CVD)_{H_2}$ .

It is clear from Table II that most kinetic work with the Si-H system investigated the conditions typical of epitaxial growth at low pressure. Due to different reactor configurations used and the inability to completely characterize the reactor hydrodynamics it is difficult to coherently tie all the data presented in the literature. Often it is not clear whether one dealt with differential reactors (infinitesimal conversion of gas phase per pass) or integral reactors (substantial change in gas composition) and when the latter was the case, whether variation in gas phase composition was properly analyzed for. For that reason a generally accepted rate form has not been found yet. Rate forms of the type given by eq. (3) or more general Langmuir-Hinshelwood forms as reviewed by Praturi et al (17,18) are suggested. The diagram (Figure 3) for the onset of homogeneous nucleation (3) is also quite useful. Recently, while this paper was in preparation, some new but still inconclusive information on heterogeneous vs homogeneous nucleation in silane pyrolysis became available (78). Nucleation rates (both homogeneous and heterogeneous) can be predicted by classical theory as previously reviewed (17,18) provided some data are available for determination of a few constants that cannot be calculated. This has not been done yet for silane pyrolysis. The currently used nucleation expressions are given in Table III (19). Most importantly, from the point of view of producing bulk silicon in fluidized beds or free space reactors, there are no quantitative models of simultaneous homogeneous nucleation, particle growth by CVD and particle growth by particle-particle interaction.

In summary, it seems that a simple (or general) Langmuir-Hinshelwood rate form should be used for epitaxial growth rate at lower temperatures and low or intermediate pressures. At high pressures and temperatures a first order process such as mass transfer can be used. The parameters for the rate form used should be extracted from experimental work on the same reactor type. There is no information at present on particle-particle and particle-nuclei interactions which are of interest in fluidized beds.

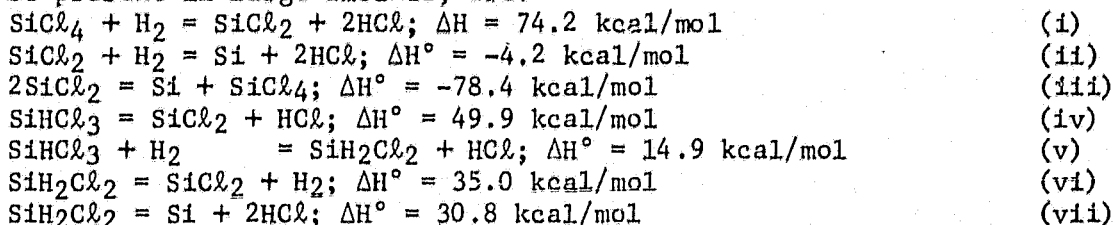
#### Si-H-Cl System

The thermodynamics of this system is well understood (20-22). This is a three component system with two degrees of freedom. At fixed pressure,  $P$ , and temperature,  $T$ , the inlet molar ratio  $(Cl/H)$ , which is the invariant of the system and can be calculated from inlet flow rates of hydrogen and chlorosilanes, determine the equilibrium composition i.e.  $(Si/Cl)_{eq}$ . Algorithms can readily be written for evaluation of complete equilibrium composition (23). The nonlinear behavior of the system is well illustrated by the number of charts in published papers (20-22). It is important to note that differences in data bases for free energies of formation still exist which lead to different predictions of equilibrium composition as shown in Figure 4 (23). Thermodynamics also reveals that the seven species present at temperatures between  $700^\circ C$  and  $1300^\circ C$  are:  $SiCl_4$ ,  $SiHCl_3$ ,  $SiH_2Cl_2$ ,  $SiCl_2$ ,  $SiH_3Cl$ ,  $HCl$  and  $H_2$ . Equilibrium conversion (yield)  $\eta = [(Si)_{in} - (Si)_{eq}] / (Si)_{in}$  is a strong function of  $(Cl/H)$  and  $T$  and a weaker function of pressure. At fixed  $(Cl/H)$  ratio  $\eta$  exhibits a maximum at a certain temperature,  $T_{max}$  as seen in Figure 5. This has an important

ORIGINAL PAGE IS  
OF POOR QUALITY

ramification for fluidized bed or epitaxial reactor operation. If equilibrium is reached at  $T_{\max}$  in a fluid-bed then a potential for etching (negative growth) will exist in the freeboard irrespective whether this is kept at temperature higher or lower than  $T_{\max}$ . In epitaxial reactors, or tubular decomposers, operation above  $T_{\max}$  may lead to potential instabilities and dendritic crystal growth since existing protuberances on the surface, which are cooler than the flat portion due to improved heat transfer, have a better potential for growth. At a fixed temperature equilibrium yield shows a maximum at a certain chlorosilane mole fraction, Figure 6. Pressure in general tends to somewhat reduce the yield. However, it should be remembered in production of bulk silicon that the equilibrium amount of silicon deposited per unit reactor volume rises rapidly with pressure.

Kinetics of hydrogen reduction of chlorosilanes has been studied extensively (24-43). Representative findings are given in Table IV. Possible reactions in the system, excluding radicals which at temperatures of interest are not present in large amounts, are:



Many additional reactions can be postulated and written. However, in the reactor effluent one always detects in measurable amounts only  $\text{SiCl}_4$ ,  $\text{SiHCl}_3$ ,  $\text{HCl}$ ,  $\text{H}_2$ . This implies that in a differential reactor one can monitor only the change in composition of these four species. Any postulated set of overall reactions must contain only those species using the well established CRE technique (44), the rank of the system can be found, the invariants of the system calculated and point rates of all postulated overall reactions determined. This has not been done yet for Si CVD.

Many investigations summarized in Table IV addressed the following two questions: i) What is the prevailing reaction mechanism and what seems to be the rate limiting step (RLS) and the rate determining active intermediate; ii) When is the observed crystal growth rate determined by transport effects? With regard to the first question there is no universally accepted answer. It is generally assumed that reactions (i), (v) and (vi) occur in the gas phase. Possible adsorption-desorption processes are listed in Table V. Calculations of Chernov (57) provided the surface coverage expected by all reactants, identified reaction intermediates and hydrogen and chlorine radicals. They suggest a large coverage by hydrogen radicals ( $> 0.6$ ) but these findings have not been documented either directly experimentally or indirectly by kinetic data. It seems more likely that  $\text{SiH}_2^*$  and  $\text{SiCl}_2^*$  are the dominant surface species in Si-H and Si-H-Cl system, respectively. For various surface reactions, mechanisms suggested by Claassen and Bloem (37, 38, 42) and by Nishizawa and Saito (41) seem best documented. Crystal growth is thought to occur via either a step-flow mechanism for single crystals or by heterogeneous nucleation and radial growth for polycrystalline material. Langmuir-Hinshelwood type of rate form again seems in order for describing the reaction rate but the rate is now clearly reversible, as opposed to the silane pyrolysis system, and the

etching term must be included.

With regard to the second question much has been written on mass transfer-kinetic interactions in the Si-H-Cl system but almost exclusively as it applies to the epitaxial reactors. Two main observations are advanced as evidence that crystal deposition rate is limited by mass transfer at temperatures above 1100 to 1200°C. One is that the general shape of the deposition rate curve against temperature takes the form shown in Figure 7 i.e. that an apparent high activation energy at low temperatures (steep slope) becomes a very low apparent activation energy (low slope) at high temperatures (21, 22, 28, 43) or even can become a negative activation energy (43). Mass transfer rates which are supposed to be rate limiting at high temperature have a very weak dependence on temperature. The other observation is that the growth rate shows a square-root dependence on velocity (45-49) and on the distance along the reactor (35, 45, 48). The mass transfer coefficient in laminar flow has a square root dependence on the Reynolds number i.e. velocity, and boundary layer thickness increases with the square root of distance. Conclusive evidence would be if at high temperature at fixed bulk composition in a differential reactor one could show that velocity past the surface has no effect on growth rate. This has not been demonstrated for silicon CVD from chlorosilanes. It is true that mass transfer limiting rate i.e. equilibrium conditions at the surface has been used successfully to model some CVD results but this only proves that the results conformed to a first order process. Although it is almost universally accepted that mass transfer rates control silicon CVD at high temperatures one should use such a generalization with caution since the following results still challenge this assertion. The differences in rates at high temperature (Figure 7b) among various chlorosilanes have not been explained quantitatively. Since equal mole fractions are used in all runs, if approximately the same boundary layer thickness is assumed, the ratio of mass transfer rates of SiH<sub>4</sub> and SiCl<sub>4</sub> should be equal to the ratio of their diffusivities in hydrogen and hence given by the  $\sqrt{D_{SiCl_4}/D_{SiH_4}} = 2.3$ . The ratio of the rates is at least five. On the other hand a simplest, single reactant-single site Langmuir-Hinshelwood rate based on a two-step mechanism can be represented by:

$$r = \frac{k_o K_o e^{-(E + \Delta H_{ad})/RT} P_1}{K_o e^{-\Delta H_{ad}/RT} P_1 + 1} \quad (4)$$

Since  $\Delta H_{ad} < 0$  at low temperatures one may have  $K_o e^{-\Delta H_{ad}/RT} P_1 > 1$  and the apparent activation energy is then equal to the true activation energy of the surface reaction which may be fairly high,  $E_{app} = E$ . At high temperature  $K_o e^{-\Delta H_{ad}/RT} P_1 < 1$  and  $E_{app} \approx E + \Delta H_{ad} < E$ . When  $|\Delta H_{ad}| > E$ ,  $E_{app} < 0$ . Hence weak temperature dependence or even negative activation energy can be seen at high temperatures for plots of  $\ln r$  vs  $1/T$  at fixed  $P_1$  (such as Figure 7a) without mass transfer control.

Sugawara (39) performed a set of runs on a rotating disk susceptor under well controlled conditions. At 1200°C, where the rate is presumably mass transfer controlled, the change in rotation speed from 50 to 1000 rpm had hardly any effect on the rate. The rate varied as  $\omega^{1/20}$  instead of the  $\omega^{1/2}$  dependence for mass transfer control. Moreover considering the

# ORIGINAL PAGE 1, OF POOR QUALITY

margin of experimental error it is fair to say that the growth rate was independently of  $\omega$ . At 1200°C and  $(Cl/H) = 0.01$  Sugawara (39) found a growth rate of 4.1  $\mu/min$ . In a tubular decomposer run at a low yield per pass at 1210°C and at the same  $(Cl/H)$  ratio using the same starting material ( $SiCl_4$ ) a rate of 4.2  $\mu$  was detected (50). The same growth rate from two different reactor types, where the velocity past the surface varied widely, is hardly convincing evidence for mass transfer control. Finally, the question of the square-root dependence of the deposition rate,  $R_d$ , on flow rate at fixed T, P,  $Cl/H$  can be addressed. In a laboratory rod type decomposer such a square root dependence was also suspected in a set of runs (50). Following Sedgwick (51) one can write eq. (5) for the deposition rate  $R_d$  (mol/min) where

$$R_d = \beta F_{Si} \eta = \beta Q C_{Si} \eta \quad (5)$$

$F_{Si}$  (mol/min) feed rate of silicon carrying species,  $\eta$  thermodynamic yield,  $\beta$  efficiency coefficient for the reactor,  $Q$  (lit/min) total volumetric feed rate, and  $C_{Si}$  (mol/lit) total inlet chlorosilanes concentration. Under the conditions of the above experiment  $\eta = \text{const}$ ,  $C_{Si} = \text{const}$  and  $\beta Q \eta \propto k_m A_c$  where  $k_m$  (cm/min) is the mass transfer coefficient and  $A_c$  (cm<sup>2</sup>) is the area of crystal growth. Since  $k_m \propto Q^{1/2}$  then  $\beta \propto Q^{1/2}$ . This, however, is not the case as seen from Figure 8. It will be shown later that if we model the reactor as a 2-phase CSTR (stirred tank reactor) we find, when surface kinetics controls the rate for a pseudo-first order reaction, that  $\beta^{-1} = 1 + (k_s A_c)^{-1} Q$  where  $k_s$  (cm/min) is the surface reaction rate constant. A plot of  $1/\beta$  vs  $Q$  should give a straight line and it does as shown in Figure 8. Thus, it seems that at high temperatures the deposition process can be modeled by a first order process of low activation energy. This may indicate mass transfer control in some epi-reactors but it would not be prudent to extrapolate this column to other reactor types, especially fluidized beds where mass transfer rates may be an order of magnitude larger.

In summary, CVD by hydrogen reduction of chlorosilanes is an activated process at lower temperatures (30 - 50 kcal/mol) and temperature insensitive at higher temperatures ( $> 1100^\circ C$ ). The mechanism proposed by Bloem and Claassen (38, 42) assumes that hydrogen reduction of  $SiCl_2$  on step sites is the RLS for  $SiHCl_3$  or  $SiH_2Cl_2$  reactants when  $SiCl_2$  is formed by gas phase reaction. The rate form based on such a mechanism exhibits the experimentally observed dependence on reactant partial pressure (first order except at higher concentrations where saturation occurs) and hydrogen partial pressure (which has an inhibitory effect). Effects of inert gas and  $HCl$  can also be explained. For  $SiCl_4$  reaction (42) it is suggested that the attack of  $SiCl_4$  on Si at step sites is the RLS. At very high temperatures the gaseous reduction reaction producing  $SiCl_2$  which can adsorb on the surface becomes also important. This implies that a general Langmuir-Hinshelwood form should be tried as a rate form. The values of various constants still need to be evaluated by experimental work. Due to difficulties in obtaining quality experimental data there is a scarcity of such data. An experimental program based on factorial design of experiments (52, 53) should be conducted in order to evaluate the proper rate expression among the competing ones and in order to quantify all kinetic parameters of the accepted rate form. Such a program can only be conducted in a reactor with an exponential residence time distribution for the gas (CSTR) with well defined (calculable or measurable) gradients between the bulk and crystal surface. High RPM double-rotary disk reactor presents such a possibility.

## ORIGINAL PAGE IS OF POOR QUALITY

At high temperature there is a possibility that in some reactor types the process is mass transfer controlled since the apparent activation energy is low, growth rate is inversely proportional to total pressure and increases with the square root of flow rate. However, in studies specifically designed to prove mass transfer control by examining the effect of gas velocity close to the surface of a rotating disk susceptor this conclusion was contrary to experimental evidence (39, 40). Square-root dependence of growth rate on flow rate and low activation energy can be the result of other phenomena e.g surface kinetics and reactor flow pattern as shown earlier. At high temperatures a proof of mass transfer control should be obtained for the reactor type to be used through evaluation of its CVD number. However, the importance of thermal diffusion in mass transfer, due to gradients in excess of several hundred degrees per centimeter found in epitaxial reactors, seems undisputable (13) and it allows prediction of experimental growth curves as shown in Figure 6.

### CRYSTAL GROWTH AND GROWTH OF PARTICULATES

#### Crystal Growth

Traditionally, silicon is grown in epitaxial reactors in form of films or in bell-jar decomposers as bulk polycrystalline material. In either case well established concepts of heterogeneous nucleation and lateral growth of nuclei, as described in texts on crystal growth (54, 55), seem to apply. Some novel concepts on nucleation were introduced by Walton (56) and used in silicon CVD. The theory developed by Chernov (57) on dense adsorption layer (resembling that of a thin liquid film) and his calculation on surface coverage by various species was later effectively utilized by Claassen and Bloem (37, 38) in developing the models for silicon CVD by hydrogen reduction of chlorosilanes and by Hottier and Cadoret (14) in CVD by silane pyrolysis. The general theory of layered growth of crystals developed by Kaschchiev (58) was also utilized in CVD by silane pyrolysis (14). It is beyond the scope of this paper to review this vast area extensively. From the practical point of view an empirical finding of Bloem (59) is of interest. He shows, based on experimental evidence, that single crystal will be formed provided the inequality given by eq. (6)

$$G \text{ (}\mu\text{/min)} < 4 \times 10^{19} e^{-115,000/RT} \quad (6)$$

is satisfied, where  $R = 1.987$  (cal/mol K). The energy of the separation line of 115 kcal can be thought of as the activation energy for silicon diffusion in silicon since the slow stage in monocrystalline growth is the diffusion of free silicon which is looking for a crystalline step site on the surface. Indeed, the calculated activation energy for self diffusion of silicon is 110 kcal.

#### Growth of Particulates

In reactors under development for production of bulk silicon in granular form such as fluidized bed or free space reactors (60) one encounters the problem of particle growth. In a fluidized bed for hydrogen reduction of chlorosilanes as in TI silicon to silicon process (61) the existing particles of Si grow by CVD alone because homogeneous nucleation does not occur in this system and the temperatures are below silicon

softening temperature so that growth by particle-particle interaction in the size range used (100  $\mu$  m to 2000  $\mu$  m) is not possible. Particles may grow by CVD in a kinetically controlled regime when

$$G = k f(C, T) \quad (7)$$

where  $f(C, T)$  is the concentration and temperature dependence of the reaction rate. At fixed temperature and composition, all particles grow at the same rate irrespective of size. In mass transfer control regime:

$$G = k' \Delta C / d^\alpha \quad (8)$$

where  $k'$  is proportional to the mass transfer coefficient which is a weak function of temperature ( $T^{3/2}$ ),  $\Delta C$  is the concentration driving force (i.e. bulk concentration of the limiting reactant and  $d$  is particle diameter. Parameter  $\alpha = 1$  for small particles ( $Re < 1$ ) and  $\alpha = 1/2$  for large particles. At fixed set of temperature and composition larger particles grow slower.

In case of a fluidized bed or free space reactor for silane pyrolysis (60) some new modes of growth of particles may be encountered. Here, nuclei and submicron size particles are formed by nucleation, Brownian motion, coalescence caused by shear flow, CVD and impaction. The dependence of particle linear growth rate on the diameter varies from  $d^{-3}$  for coagulation,  $d^{-1}$  for coalescence by turbulent eddies,  $d^{-1}$  or  $d^{-1/2}$  for mass transfer control CVD,  $d^0$  for growth of large particles by impaction of small ones (62). Much more work is needed in this area to understand the interplay of all these competing processes in a nonuniform temperature and concentration field. Good starting points may be found in the literature on the dynamics of aerosols (63, 64). The effect of growing particles on homogeneous nucleation have been examined (65). From the CRE point of view it is essential to be able to estimate the characteristic times for nucleation, coagulation, coalescence, CVD and impaction so that by comparison at these resistances a dominant step can be selected. It is expected that silane pyrolysis will show some similarities to deposition of pyrolytic carbons also (66).

#### REACTOR MODELS

From the CRE viewpoint reactor models are needed to solve one of the following three basic types of problems:

I. Given the kinetics of the reaction system, the desired production rate and a set of input conditions find the required reactor type and size and set of operating conditions.

II. Given the kinetics, input and operating conditions, reactor type and size, relate them and find the set of operating and input conditions necessary to maximize production rate or yield.

III. Given the input, operating conditions, output conditions, and reactor type and size, find the kinetics.

The first problem is the one encountered by the design engineer, the second is of interest to plant and process development engineers, the last one is always encountered by experimentalists in R&D. In silicon CVD most of the time was spent on problems of type II and III. As a reminder Figure 9 illustrates ideal reactor types (PFR and CSTR) and reactors with

well defined velocity profiles in which analysis of kinetic data can readily be accomplished. The problem with CVD data discussed in the previous sections is that it was collected in nonideal reactors of unknown gas residence time distribution, unreported conversion of gas per pass and where temperature and concentration profiles between solid and bulk gas are hard to estimate. This is why quantitative evaluation of kinetic rate forms has eluded us so far.

### Epitaxial Reactors

Modeling of horizontal (45, 46, 47, 67, 68, 69, 70, 72-75) and vertical (48, 71) epitaxial reactors has produced a number of papers in the published literature. Representative models are summarized in Table VI. The flow patterns and mass and heat transfer phenomena in epitaxial reactors are complex, they do not fit neatly into the idealized reactor schemes given in Figure 9, and their modeling is difficult. Literature (73-75) shows that in typical operation the range of dimensionless numbers is:  $25 \leq Re \leq 200$ ;  $100 \leq Gr \leq 1000$ ;  $0.4 \leq Pr \leq 0.9$ ;  $40 \leq Ra \leq 800$ . This means that the conditions for fully developed temperature profile  $x > 0.05 d$  and velocity profile  $x > 0.029 d$  are often not satisfied over most of the susceptor length. Due to temperature gradients normal to the susceptor surface of up to  $500^\circ\text{C}/\text{cm}$  thermal diffusion may be important and when  $Gr/Re^2 > 0.3$  free convection should be accounted for. Exact modeling of such a hydrodynamic situation coupled with possible homogeneous reactions and the multicomponent diffusion problem would require excessive computer time and storage. All the solutions presented in Table VI are in some way approximate. Equilibrium or zero reactant concentration at susceptor surface i.e. the mass transfer control assumption is made by all investigators except Pollard and Newman (40) who used the law of mass action to describe the kinetics of five postulated reactions. The models can further be divided into two categories. In one group a constant thickness of stagnant layer is assumed with fully laminar or turbulent velocity profile above it (47, 67, 68). In the other group a developing boundary layer is considered (45, 46, 70). From the CRE viewpoint the models with stagnant layer are equivalent to assuming CSTR (67) or PFR (68) behavior for the bulk gas phase and a mass transfer resistance between bulk gas and surface. This resistance is evaluated based on the diffusion equation using either experimental or theoretical predictions for the thickness of the layer. Most appropriately this resistance could be determined from experimental results for a desired reactor type. The developing B L models conform to experimental reality that the mass transfer resistance between gas and solid changes along the direction of flow.

It is interesting to note that in epitaxial horizontal reactors both stagnant layer and developing layer models are in reasonable agreement with selected experimental data in spite of the fact that the assumptions that entered their development are often quite different, as shown in Table VI. This confirms a recognized fact that when type II problems are considered in CRE it is often better not to start from the most general description of the system but to construct the simplest model that incorporates the key features of the system and add further terms as required by comparison of model predictions and experimental data.



### Bell-Jar Decomposers

No models to my knowledge have appeared in the open literature that deal with the classical Siemens decomposer. A typical decomposer, shown in Figure 1, has a diameter D and height H. A set of N silicon rods of height L and diameter D are heated electrically. Chlorosilanes ( $\text{SiCl}_4$ ,  $\text{SiHCl}_3$  or  $\text{SiH}_4$ ) and hydrogen are injected into the bell-jar via one or several nozzles. Gas jets cause good mixing in the chamber. Complete modeling of the decomposer is very difficult due to the complex hydrodynamics of the system. Instead, it can be shown that a simple model can match the observed experimental data and can be used to adjust operating conditions in order to insure desired deposition rates.

The model is based on the following assumptions: i) gas phase is well mixed (CSTR); ii) a single reaction stoichiometry of a pseudo-species (silicon carrying components) can describe the system  $x \text{SiHCl}_3 + y \text{SiCl}_4 + z \text{H}_2 = \text{Si} + w \text{HCl}$ ; iii) a single mass transfer resistance,  $k_m^{-1}$ , and a single pseudo first order surface rate constant  $k_d$  can be used; iv) species mass balance and energy balance can be decoupled; v) reaction driving force is the difference between surface and equilibrium concentration; vi) pseudo-steady state exists. Species mass and energy balance mass at the crystal surface are:

$$k_m (C_g - C_s) = k_d e^{-E/RT_s} (C_s - C_e) = k_{ds} (C_s - C_e) = r_s \quad (9)$$

$$h(T_s - T_g) = (-\Delta H_r) r_s + q_s \quad (10)$$

subscripts g, s denote bulk gas and surface conditions, C is the concentration of the silicon carrying species,  $r_s$  is the molar deposition rate per unit surface, h is heat transfer coefficient and  $q_s$  is heat generated by electric current in the rods per unit external surface. Total mass deposition rate,  $\bar{R}$ , is obtained from the mass balance on the reactor:

$$\bar{R} = N \pi D_c r_s M_{\text{Si}} = A_c r_s M_{\text{Si}} = Q(C_g^0 - C_g) M_{\text{Si}} \quad (11)$$

Here  $A_c$  is the total crystal growth area at time t,  $M_{\text{Si}}$  molecular weight of silicon,  $C_g^0$  - inlet concentration of pseudospecies based at bulk gas temperature, Q - gas flow rate at bulk gas temperature. This gives

$$\bar{R} = \frac{Q M_{\text{Si}} (C_g^0 - C_e)}{1 + \frac{Q}{k_d A_c} + \frac{Q}{k_m A_c}} = \frac{M F_{\text{Cl}} (\text{Si/Cl})_0 \eta}{1 + \frac{Q}{k_d A_c} + \frac{Q}{k_m A_c}} \quad (12)$$

where  $F_{\text{Cl}}$  is total molar flow rate of chlorine (invariant),  $(\text{Si/Cl})_0$  - silicon/chlorine molar ratio at the inlet;  $\eta$  - thermodynamic efficiency (21, 22) to be evaluated at the  $(\text{Cl/H})$  ratio of the system. Comparison of eq (12) with the deposition rate defined by Sedgwick (51) shows that the reactor efficiency coefficient  $\beta = (1 + Q/k_m A_c + Q/k_d A_c)^{-1}$  as used earlier in this paper. Only under flow limited conditions  $Q/k_m A_c \ll 1$ ,  $Q/k_d A_c \ll 1$ ,  $\beta \rightarrow 1$ . For kinetic and mass transfer control regime  $\beta < 1$ .

Mass balance on the crystalline material gives

$$\frac{\rho_{\text{Si}} A_c}{2 \pi N L_c} \frac{d A_c}{dt} = \bar{R} \quad (13)$$

$$t = 0 \quad A_c = A_{c0} \quad (14)$$

This leads to the following quadratic equation for the  $A_c$  at time t.

# ORIGINAL PAGE 13 OF POOR QUALITY

$$A_c^2 + 2 Q \left( \frac{1}{k_d} + \frac{1}{k_m} \right) A_c - \{ A_{c0}^2 + 2 Q \left( \frac{1}{k_s} + \frac{1}{k_m} \right) A_{c0} + \frac{4 \pi N L_c M_{Si} F_{Cl} (Si/Cl)_o \eta}{\rho_{Si}} t \} = 0 \quad (15)$$

Deposition rate  $G$  ( $\mu/\text{min}$ ) is:

$$G = \frac{10^6 \bar{R}}{60 \rho_{Si} A_c} = \frac{(\frac{10^6}{20}) F_{Cl} (Si/Cl)_o \eta}{\rho_{Si} \sqrt{Q^2 \left( \frac{1}{k_s} + \frac{1}{k_m} \right)^2 + A_{c0}^2 + 2 Q \left( \frac{1}{k_s} + \frac{1}{k_m} \right) A_{c0} + B t}} \quad (16)$$

where  $B = 4 \pi N L_c M_{Si} F_{Cl} (Si/Cl)_o \eta / \rho_{Si}$  ( $\text{m}^4/\text{h}$ ) and  $\bar{R}$  ( $\text{kg}/\text{h}$ ),  $A_c$  ( $\text{m}^2$ ),  $\rho_{Si}$  ( $\text{kg}/\text{m}^3$ ),  $t$  ( $\text{h}$ ). This assumes that the flow rate of the gas was kept constant and rod temperature was constant by keeping  $q_s$  constant through adjustment of the current with growth rate ( $q_s = i^2 \rho D_c / 4 = \text{const.}$  where  $i = 4I / \pi D_c^2$  is current density and  $\rho$  resistivity). Under a set of conditions (of proprietary nature) when the growth was assumed to be kinetically controlled one gets:  $G = 4 / \sqrt{0.02 + 0.01t}$  which is given in Figure 10. For comparison an actual set of experimental pilot plant data is also presented.

It is clear that such a simple model is adequate to examine the effects of operating conditions,  $Q$ ,  $T_o$ ,  $(Cl/H)_o$ ,  $(Si/Cl)_o$ ,  $i$  etc on deposition rate. For example, if constant growth rate is required the flow rate would have to be increased so as to keep the ratio  $Q/A_c = \text{const.}$  Flow rate, as an explicit function of time, can be obtained by solution of the simple quadratic eq (15). Thus, this simple model based on CSTR behavior of the gas and a single pseudo reversible linear surface reaction is of value for estimation of certain operating variables.

## FLUIDIZED BEDS

Modeling of fluidized beds with growing particles in a uniform gas environment under mass transfer or kinetically controlled conditions has been treated extensively (62, 76). When dealing with feeds with wide particle size distribution care has to be taken to overcome computational problems (77). However, in CVD from chlorosilanes it is of economic interest to achieve substantial yields of the gas phase and hence gas composition changes in the reactor. This complicates computations further by coupling of the gas and solid mass balance. A problem with a pseudo-first order reversible reaction can be treated. No comprehensive model has appeared in the literature.

In case of silane pyrolysis additional difficulties created by new modes of particle growth arise as discussed previously. No general model has been reported.

## SUMMARY

No general quantitative models for silane pyrolysis and hydrogen reduction of chlorosilanes have been accepted. The reactions seem to follow a Langmuir-Hinshelwood rate form and become temperature insensitive at high ( $\approx 1000^\circ\text{C}$ ) temperatures.

Modeling of epitaxial reactors seems fairly advanced while that of fluidized beds and bell-jar decomposers is in its infancy.

ORIGINAL PAGE IS  
OF POOR QUALITY

#### REFERENCES

1. T. R. Hogness, T. L. Wilson and W. C. Johnson, J. Am. Chem. Soc., 58, 108 (1936).
2. B. A. Joyce and R. R. Bradley, J. Electrochem. Soc., 110 (12), 1235 (1963).
3. F. C. Eversteijn, Philips Res. Repts., 26, 134 (1971).
4. R. F. C. Farrow and J. D. Filby, J. Electrochem. Soc., 119 (1), 149 (1971).
5. R. C. Henderson and R. F. Helm, Surf. Sci., 30, 310 (1972).
6. F. C. Eversteijn and B. H. Put, J. Electrochem. Soc., 120 (1), 106 (1973).
7. R. F. C. Farrow, J. Electrochem. Soc., 121 (7), 899 (1974).
8. J. Y. W. Seto, J. Electrochem. Soc., 122 (5), 701 (1975).
9. M. Ogirima, H. Saida, M. Suzuki and M. Maki, J. Electrochem. Soc., 124 (6), 903 (1977).
10. T. I. Kamins, M. M. Mandurah and K. C. Saraswat, J. Electrochem. Soc., 125 (6), 927 (1978).
11. M. J. P. Duchemin, M. M. Bonnet and M. F. Koelsch, J. Electrochem. Soc., 125 (4), 637 (1978).
12. W. A. P. Claassen and J. Bloem, J. Crystal Growth, 51, 443 (1981).
13. W. A. P. Claassen and J. Bloem, Philips J. Res., 36, 124 (1981).
14. F. Hottier and R. Cadoret, J. Crystal Growth, 52, 199 (1981).
15. C. H. J. van der Brekel and L. J. M. Bollen, J. Crystal Growth, 54, 310 (1981).
16. C. H. J. van der Brekel, Mass Transport and Morphology in Chemical Vapor Deposition Processes, D.Sc. Thesis, University of Nijmegen, 1978.
17. A. K. Praturi, R. Lutwack, and G. Hsu, JPL Publication 77-38, (1977).
18. A. K. Praturi, Proc. Sixth Int. Conf., CVD, Vol. 77-5, 20 (1977).
19. J. P. Hirth and G. M. Pound, "Condensation and Evaporation", Progress in Materials Science (B. Chalmers, ed.), Vol. 77, N.Y. (1963).
20. R. F. Lever, IBM Journal, 460 (1964).
21. L. P. Hunt and E. Sirtl, J. Electrochem. Soc., 119 (72), 1741 (1972).
22. E. Sirtl, L. P. Hunt and D. M. Sawyer, J. Electrochem. Soc., 121 (7), 916 (1974).
23. H. F. Erk, The Science of Silicon Material Preparation Workshop, Phoenix; August 23-25, 1982.
24. D. J. Ashen, G. C. Bromberger and T. J. Lewis, J. Appl. Chem., 18, 348 (1968).
25. H. C. Theuerer, J. Electrochem. Soc., 108 (7), 649 (1961).
26. E. G. Bylander, J. Electrochem. Soc., 109 (12), 1171 (1962).
27. P. Van der Putte, L. J. Gilling and J. Bloem, J. Crystal Growth, 31, 299 (1975).
28. J. Bloem, J. Crystal Growth, 31, 256 (1975).
29. V. S. Ban and S. L. Gilbert, J. Electrochem. Soc., 122 (10), 1382 (1975).
30. V. S. Ban, J. Electrochem. Soc., 122 (10), 1389 (1975).
31. T. O. Sedgwick, J. E. Smith, Jr., R. Ghez and M. E. Cowher, J. Crystal Growth, 31, 264 (1975).
32. T. O. Sedgwick, G. V. Arbach and R. Ghez, Proc. Sixth Intern. CVD Conference, p. 79 (1977).
33. P. Van der Putte, L. G. Giling and J. Bloem, J. Crystal Growth, 41, 133 (1977).

**ORIGINAL PAGE IS  
OF POOR QUALITY**

34. J. Bloem, Proc. Electrochem. Soc. Semiconductor Silicon, Vol. 77-2, 201 (1977).
35. J. Nishizawa and H. Nihira, J. Crystal Growth, 45, 82 (1978).
36. T. O. Sedtewick and G. V. Arbach, J. Japan Assoc. Crystal Growth, 5, 93 (1978).
37. J. Bloem and W. A. P. Claassen, J. Crystal Growth, 49, 435 (1980).
38. W. A. P. Claassen and J. Bloem, J. Crystal Growth, 50, 807 (1980).
39. K. Sugawara, J. Electrochem. Soc., 119 (12), 1749 (1972).
40. R. Pollard and J. Newman, J. Electrochem. Soc., 127 (3), 744 (1980).
41. J. Nishizawa and M. Saito, J. Crystal Growth, 52, 213 (1981).
42. J. Bloem, W. A. P. Claassen and W. G. J. N. Valkenburg, J. Crystal Growth, 57, 177 (1982).
43. F. Langlais, F. Hottier and R. Cadoret, J. Crystal Growth, 56, 659 (1982).
44. R. Aris, Introduction to the Analysis of Chemical Reactors, Prentice-Hall, N.J., 1965.
45. S. E. Bradshaw, Int. J. Electronics, 21 (3), 205 (1966).
46. S. E. Bradshaw, Int. J. Electronics, 23 (4), 381 (1967).
47. F. C. Eversteyn, P. J. W. Severin, C. H. J. Van der Brekel, and H. L. Peek, J. Electrochem. Soc., 117 (7), 925 (1970).
48. C. W. Manke and L. F. Donaghey, J. Electrochem. Soc., 124 (4), 561 (1977).
49. F. C. Eversteyn, Philips Res. Repts., 29, 45 (1974).
50. H. Gutsche, Monsanto Co., private communication.
51. T. O. Sedgwick, J. Electrochem. Soc., 111 (12), 1381 (1964).
52. W. G. Hunter and M. E. Hoff, Ind. Eng. Chem. 59 (3), 43 (1967).
53. G. E. P. Box and W. G. Hunter, Technometrics, 7 (1), 23 (1965).
54. E. Kaldis, in Crystal Growth and Characterization (R. Veda and J. B. Mullen, eds.), North Holland, Amsterdam, 1975.
55. C. H. L. Goodman, ed. Crystal Growth, Plenum Press, N.Y., 1974.
56. D. Walton, J. Chem. Physics, 37 (10), 2182 (1963).
57. A. A. Chernov, J. Crystal Growth, 42, 55 (1977).
58. D. Kaschier, J. Crystal Growth, 40, 29 (1977).
59. J. Bloem, J. Crystal Growth, 18, 70 (1973).
60. Union Carbide Final Report, JPL Contract 954334, June, (1979).
61. F. A. Padovani et. al., U.S. Patent 4,092,446, May, (1978).
62. O. Levenspiel, The Chemical Reactor Omnibook, OSV Book Stores, Inc., Corvallis, Oregon (1979).
63. J. H. Seinfeld, "Dynamics of Aerosols" in Dynamics and Modelling of Reactive Systems, Academic Press, N. Y., 1980.
64. S. K. Friedlander, "The Behavior of Constant Rate Aerosol Reactors", AIChE Annual Meeting, New Orleans, November (1981).
65. M. K. Alam and R. C. Flagan, The Science of Silicon Material Operation Workshop, Phoenix, Arizona, August (1982).
66. J. L. Kaae, General Atomic Project 9152, January, (1978).
67. W. H. Shepherd, J. Electrochem. Soc., 112 (10), 988 (1965).
68. F. C. Eversteijn and H. L. Peek, Philips Res. Repts., 25, 472 (1970).
69. R. Takahashi, Y. Koga and K. Sugawara, J. Electrochem. Soc., 119 (10), 1406 (1972).
70. V. S. Ban and S. L. Gilbert, J. Crystal Growth, 31, 284 (1975).
71. C. W. Manke and L. F. Donaghey, Proc. Sixth Intern. CVD Conference, Electrochem. Soc., Princeton, 151 (1977).

- 9  
Y
72. V. S. Ban and E. A. Miller, Sixth CVD Conference, 102 (1977).
  73. V. S. Ban, J. Electrochem. Soc., 125 (2), 317 (1978).
  74. V. S. Ban, J. Crystal Growth, 45, 97 (1978).
  75. V. S. Ban, J. Japan Assoc. Crystal Growth 5, 119 (1978).
  76. D. Kunii and O. Levenspiel, Fluidization Engineering, Wiley, N.Y., (1969).
  77. F. Kayihan, The Science of Silicon Material Preparation Workshop, Phoenix, Arizona, August (1982).
  78. S. K. Iya, R. N. Flagella and F. S. DiPaolo, J. Electrochem. Soc., 129(7), 1531 (1982).

**ORIGINAL PAGE IS  
OF POOR QUALITY**

ORIGINAL PAGE IS  
OF POOR QUALITY

TABLE I. SILICON FORMS FOR SEMICONDUCTOR AND SOLAR DEVICES AND REACTORS USED

<u>Form of Product</u>		
amorphous film	polycrystalline film	epitaxial
submicron		
multimicron		
single crystal film		
bulk polycrystal		decomposer
bulk single crystal		decomposer - tubular
polycrystalline granules		fluidized bed
powder		free space reactor

TABLE III. NUCLEATION RATES

Rate of homogeneous nucleation of critical size clusters ( $\text{cm}^{-3} \text{s}^{-1}$ )

$$I = \left(\frac{\pi}{6}\right)^{1/2} \left[ \frac{4\pi}{3v_m} \left( \frac{2\sigma v_m}{kT \ln s} \right)^3 \right]^{1/6} (\ln s)^{1/2} s^2 s^{-g^*/2}$$

k - Boltzmann's constant; T - absolute temperature  
s - saturation ratio;  $v_m$  - monomer molecular volume  
 $\sigma$  - surface tension;  $g^*$  - number of monomer molecules in critical cluster

$$d_p^* = \frac{4\sigma v_m}{kT \ln s} \quad (2) - \text{diameter of critical size}$$

Rate of condensation per unit surface ( $\text{cm}^{-2} \text{s}$ )

$$I_c = \frac{\alpha_c P}{\sqrt{2\pi m k T}} \quad (3)$$

P - monomer partial pressure, m - monomer molecular mass

$\alpha_c$  - condensation coefficient

$\alpha_c = 1$  - Hertz - Knudsen equation,  $I_c = I_H$

Rate of heterogeneous nucleation ( $\text{cm}^{-2} \text{s}^{-1}$ )

$$I = I_H \frac{\sigma^*}{a} \left( \frac{I_H a^2}{v} \right)^{n^*} \exp\{[(n^* + 1)Q_{ad} + E_{n^*} - Q_D] (1/kT)\}$$

$\sigma^*$  - capture width of critical nucleus

a - separation between adsorption sites

$n^*$  - number of atoms in nucleus, v - attempt frequency

$Q_{ad}$  - binding energy to surface;  $Q_D$  - surface diffusion activation energy

$E_{n^*}$  - binding energy of the cluster

**ORIGINAL PAGE 13  
OF POOR QUALITY**

TABLE II. SILANE PYROLYSIS - KINETIC STUDIES

Investigator	Conditions	Rate Form	Activation Energy(kcal)	Comments
Hogness et al (1)	380-490°C 85-570 mm Hg pure SiH <sub>4</sub>	$r_{SiH_4} = \frac{k_1(SiH_4)}{1 + \frac{k_2}{k_1}(H_2)}$	51.7±2	Homogeneous, High T, low P no H <sub>2</sub> inhibition Low T, high P marked (H <sub>2</sub> ) inhibition => E <sub>-1</sub> > E <sub>2</sub> . No H <sub>2</sub> ads. detected. SiH <sub>4</sub> → SiH <sub>2</sub> + H <sub>2</sub> ; SiH <sub>2</sub> → Si + H <sub>2</sub>
Joyce and Bradley (2)	920 to 1260°C 0.1 to 1.5 mm Hg	$G = k \frac{P_{SiH_4}^2}{P_{H_2}}$	37 T < 1100°C	Heterogeneous reaction. Epitaxial growth of single crystal. RLS surface reaction (T < 1100°C), RLS gas diffusion (T > 1100). High growth 29 μ/min.
Eversteijn (3)	1000-1100°C P = 1 atm P <sub>SiH<sub>2</sub></sub> = 28 mm Hg	$r_{SiH_4} = k P_{SiH_4}$	30	Homogeneous nucleation observed. Diagram given for onset of nucleation.
Farrow and Filby (4)		$r_{SiH_4} = k P_{SiH_4}$	10	Growth rate of arsenic doped epitaxial layer.
Henderson and Helm (5)	823-983°C 0.02 to 0.15 mm Hg	$r_{SiH_4} = k P_{SiH_4}$ $G \propto k P_{SiH_4}$ $G \propto k \frac{2 \lambda_{Si}}{\lambda} P_{SiH_4}$	E <sub>d</sub> = 20±5 E <sub>sd</sub> = 24	Epitaxial growth of single crystalline films T = 800°C. Efficiency 10 <sup>-3</sup> to 10 <sup>-4</sup> . BCF theory of flow-step growth used to explain differences in E <sub>d</sub> , E <sub>g</sub> .
Eversteijn and Put (6)	550 to 1160°C 1 atm, 5% SiH <sub>4</sub>	$G \propto P_{SiH_4}$	37(< 830°C) 0(> 830°C)	Growth of polycrystalline films. Much rougher films at T > 700°C.
Farrow (7)	200 to 1200°C 10 <sup>-5</sup> to 0.1 mm Hg	$r_{SiH_4} = \frac{k P_{SiH_4}}{1 + K P_{SiH_4}}$	E = 17 E <sub>sd</sub> = 36±6	Mass spectrometry. Single crystal deposits T > 800°C. 800 to 750°C lower quality. T < 750°C polycrystalline layer. Weak adsorption of SiH <sub>4</sub> and sparse surface coverage. Surface reaction efficiency (prob of SiH <sub>4</sub> molecules decomposing upon striking the Si surface) low α = 5.45 e <sup>-17000/RT</sup> . Condens. coeff. (fraction of Si atoms produced which are incorporated into silicon crystal) low σ = 0.232 x 10 <sup>-2</sup> $\frac{G}{\alpha} < 0.3$ Step flow model of growth (BCF).
Seto (8)	650-800°C P = 1 atm, 0.1 to 1.2% silane	$G = \frac{M_{Si}}{P_{Si}} \times \frac{k_2 K_1 (SiH_4)}{K_1 (SiH_4) + K_3 (H_2) + 1}$	E = 12	Polycrystalline films. Negligible effect of H <sub>2</sub> .
Kamins et al (10)	580 to 640°C 0.35 to 0.55 mm Hg			Growth of silicon films. Amorphous films < 600°C and polycrystalline above.
Duchemin et al (11)	900 to 1100°C 10 to 760 mm Hg	$G \propto P_{SiH_4}$ , low P $G \propto \frac{P_{SiH_4}}{P_{H_2}^\alpha}$ , high P	P = 10 torr E=15 kcal/mol P = 70 torr only up to 800°C P = 500 torr E = 0	Mechanism: * + SiH <sub>4</sub> → SiH <sub>4</sub> * 2* + H <sub>2</sub> → H <sub>2</sub> * * + HCl → HCl*
Ogirima et al (9)	1050°C 80 to 760 mm Hg 0.2 to 0.3% silane		43 at 80 mm Hg 11 at 760 mm Hg	Growth of polycrystalline film. Homogeneous nucleation RLS at low P, diffusion at high P.

<p>Claassen and Bloem (12, 13)</p>	<p>700°C P = 1 atm (H<sub>2</sub>+N<sub>2</sub>) 0.1% to 0.9% SiH<sub>4</sub></p>	$G_{exp} = \frac{A P_{SiH_4}^{in}}{1 + B P_{H_2}}$ $C = \frac{K_1^0 K_2^0 K_3^0 K_4^0 P_{SiH_4}^a}{P_{H_2} + k_2/k_{-1}}$ $-(\Delta H_1 + \Delta H_2 + \Delta H_3 + E_4)$	<p>Polycrystalline film. Mechanism proposed:</p> <ol style="list-style-type: none"> <li>(1) SiH<sub>4</sub>(g) ⇌ SiH<sub>2</sub>(g) + H<sub>2</sub>(g); 52 kcal/mol</li> <li>(2) SiH<sub>2</sub>(g) + * ⇌ SiH<sub>2</sub>*; -73 kcal/mol</li> <li>(3) SiH<sub>2</sub>* + s* ⇌ SiH<sub>2</sub>s*; -73 kcal/mol</li> <li>(4) SiH<sub>2</sub>s* ⇌ Si + H<sub>2</sub> + * + s* E=130 kcal/mol</li> <li>(5) 1/2 H<sub>2</sub> + * ⇌ H*</li> <li>(6) 1/2 H<sub>2</sub> + s* ⇌ H<sub>s</sub>*</li> </ol>
<p>Hottier and Candoret (14)</p>	<p>900 to 1300°C 1 to 100 mm Hg</p>	$G_{mono} \propto \frac{P_{SiH_4} e^{-12000/RT}}{P_{H_2}^{1/2}} > 1000^\circ C$ $G_{poly} \propto \frac{P_{SiH_4}^{1/4} e^{-40000/RT}}{P_{H_2}} < 1000^\circ C$	<p>Single and poly silicon films. Hydrogen coverage reported E<sub>H</sub> = 94. Step flow theory with SiH<sub>4</sub> dominant was used to explain single crystal results. Nucleation theory of film growth used to explain polycrystalline results. Lateral extension of clusters and cluster number RLS.</p>
<p>Van der Broek and Bollen (15)</p>	<p>625°C 0.5 to 1 mm Hg 5 to 30% SiH<sub>4</sub></p>	$G_{exp} \propto \frac{A x_{SiH_4}}{1 + B x_{SiH_4}}$ $C = \frac{k_3 K_2 \alpha P_{SiH_4}^{in}}{(1 + K_2 \alpha P_{SiH_4}^{in} + K_4 P_{H_2})^{1/2} (1 + K_4 P_{H_2})^{1/2}}$ $\alpha = \frac{K_1}{K_1 + P_{H_2}}$	<p>Same mechanism as Claassen and Bloem proposed</p> <ol style="list-style-type: none"> <li>(1) SiH<sub>4</sub>(g) ⇌ SiH<sub>2</sub>(g) + H<sub>2</sub></li> <li>(2) SiH<sub>2</sub> + * ⇌ SiH<sub>2</sub>*</li> <li>(3) SiH<sub>2</sub>* + s* ⇌ Si + 2H* RLS</li> <li>(4) 1/2 H<sub>2</sub> + s* ⇌ H*</li> </ol> <p>K<sub>4</sub> P<sub>H<sub>2</sub></sub><sup>1/2</sup> small</p> <p>Also homogeneous nucleation observed</p> <p>SiH<sub>2</sub>(g) + SiH<sub>2</sub>(g) → Si<sub>2</sub>H<sub>2</sub> + H<sub>2</sub></p> <p>SiH<sub>2</sub> + Si<sub>j</sub>H<sub>2</sub> <math>\xrightarrow{k_{ij}}</math> Si<sub>j+1</sub>H<sub>2</sub> + H<sub>2</sub></p> <p>Si<sub>i</sub>H<sub>2</sub> + Si<sub>j</sub>H<sub>2</sub> <math>\xrightarrow{k_{ji}}</math> Si<sub>i+j</sub>H<sub>2</sub> + H<sub>2</sub></p>



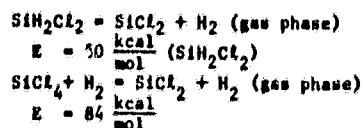
ORIGINAL PAGE IS  
OF POOR QUALITY

TABLE IV. HYDROGEN REDUCTION OF CHLOROSILANES - KINETICS

HOMOGENEOUS REACTIONS		Findings	Comments
Investigator	Conditions		
Ashen et al (24)	530-930°C P = 1 atm	$\text{SiCl}_4 + \text{H}_2 = \text{SiHCl}_3 + \text{HCl}$ $r = 7.8 \times 10^{10} (\text{SiCl}_4)(\text{H}_2)^{1/2} e^{-\frac{55000}{RT}} \left( \frac{\text{mol}}{\text{lit s}} \right)$ $\text{SiHCl}_3 + \text{H}_2 = \text{SiH}_2\text{Cl}_2 + \text{HCl}$ $r = 2 \times 10^{10} (\text{SiHCl}_3) e^{-\frac{51000}{RT}} \left( \frac{\text{mol}}{\text{lit s}} \right)$	Homogeneous gas phase reaction. Plausible reaction mechanism through propagation of hydrogen radical proposed.
HETEROGENEOUS REACTIONS			
Theuerer (25)	$\text{SiCl}_4$ ; (Cl/H) = 0.04 900 to 1300°C	$G \propto \sqrt{F_{\text{H}_2}}$ $E_{\text{app}} = 37 \frac{\text{kcal}}{\text{mol}}$	> 1270° perfect single crystal 895 to 1270° terraced structure < 875°C polycrystalline deposit
Bylander (26)	$\text{SiCl}_4$ ; (Cl/H) > 0.12 900 to 1300°C	$E_{\text{app}} = 37 \frac{\text{kcal}}{\text{mol}}$ (950 to 1100°C)	Surface reaction control postulated for 950 < T <sub>p</sub> < 1100°C. Mass transfer control at T > 1100 °C for x <sub>SiCl<sub>4</sub></sub> > 1.2%.
Van der Putte et al (27)	$\text{SiCl}_4$ data of others		General shape of growth-etch curve (Figure 6) explained based on mass transfer effect, including thermal diffusion, on surface (Cl/H) ratio thus affecting surface equilibrium.
Bloom (28)	chlorosilanes		Importance of thermal diffusion stressed. Kinetics and equilibria reviewed.
Ban and Gilbert (29)	$\text{SiH}_2\text{Cl}_2$ $0.01 \leq \left( \frac{\text{Cl}}{\text{H}} \right) \leq 1$ 750 to 1230°C		Compared experimental partial pressures of all species (mass spectrometry) to equilibrium calculations. HCl, SiCl <sub>2</sub> , SiH <sub>2</sub> Cl <sub>2</sub> higher than equilibrium values. At higher T better agreement. Proposed mechanism $\begin{array}{c} \text{SiCl}_4 + \text{H}_2 \\ \swarrow \searrow \\ \text{SiH}_2\text{Cl}_2 \quad \text{Si} + 2 \text{HCl} \\ \swarrow \searrow \\ \text{SiCl}_4, \text{SiHCl}_3, \text{SiCl}_2 \end{array}$
Ban (30)	$\text{SiHCl}_3$ ; $\text{SiCl}_4$ Cl/H = 0.1 780 < T < 1130°C		Mass spectroscopy used for species identification. SiCl <sub>4</sub> below equilibrium levels. Deposition efficiency decreases from SiH <sub>2</sub> Cl <sub>2</sub> to SiHCl <sub>3</sub> to SiCl <sub>4</sub> .

ORIGINAL PAGE IS  
OF POOR QUALITY

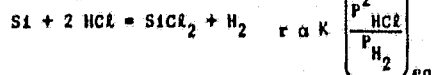
Sedgwick  
et al (31,32) chlorosilanes  
500 < T < 1300°C



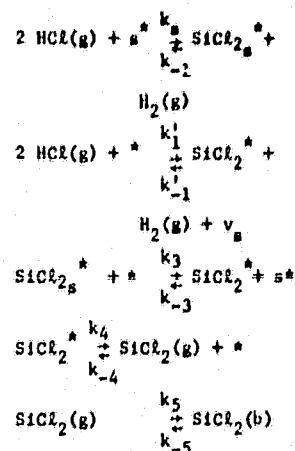
Species identified by Raman and resonance fluorescence spectra. Boundary layer thickness of 0.8 cm seen.  $\text{SiCl}_x$  identified (x=2 most likely). All rates become less T dependent above  $T^*$  when  $\text{SiCl}_x$  seems to be saturated,  $T^* = 1200^\circ\text{C}$  for  $\text{SiCl}_4$  input and  $T^* = 1000^\circ\text{C}$  for  $\text{SiH}_2\text{Cl}_2$  input.  $\text{SiCl}_2$  is formed in gas phase. No strong correlation between  $(\text{SiCl}_2)$  and growth rate.

Van der Putte  
et al (33)

etching reaction



Mechanism proposed.

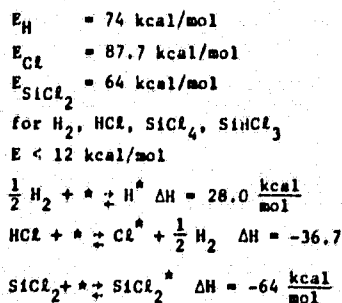


It is concluded that any of the last 3 steps can be RLS. Smooth etching is governed by one of the two last steps-desorption or diffusion. Pitted etching is dictated by surface diffusion of adsorbed  $\text{SiCl}_2$ .

Bloem (34)

$\text{SiH}_4$  pyrolysis  
chlorosilanes +  $\text{H}_2$

Adsorption energies



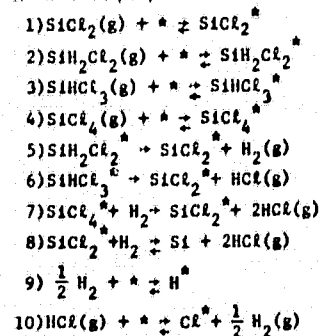
$$r = k_2 P_{\text{H}_2} (\text{SiCl}_2^*) - k_2 P_{\text{HCl}}^2$$

when  $\text{H}^*$  is the dominant surface species

$$r = \frac{k_4 P_{\text{SiCl}_4}}{1 + K_{\text{H}} P_{\text{H}_2}^{1/2}} - k_2 P_{\text{HCl}}^2$$

similar for other chlorosilanes

Mechanism proposed



RLS step (8)

Nishizawa and  
Nihira (35)

$\text{SiCl}_4$   
950 to 1200°C

ORIGINAL PAGE IS  
OF POOR QUALITY

Direct IR spectroscopy  
identified  $\text{SiHCl}_3$ ,  $\text{SiH}_2\text{Cl}_2$ ,  
 $\text{HCl}$ ,  $\text{SiCl}_2$ ,  $\text{SiCl}_4$  and  $\text{H}_2$ .  
Postulated reactions  
 $\text{SiCl}_4 + \text{H}_2 \rightleftharpoons \text{SiHCl}_3 + \text{HCl}$   
 $\text{SiHCl}_3 \rightleftharpoons \text{SiCl}_2 + \text{HCl}$   
 $\text{SiHCl}_3 + \text{H}_2 \rightleftharpoons \text{SiH}_2\text{Cl}_2 + \text{HCl}$   
 $\text{SiH}_2\text{Cl}_2 \rightleftharpoons \text{SiCl}_2 + \text{H}_2$   
 $\text{SiCl}_4 + \text{H}_2 \rightleftharpoons \text{SiCl}_2 + 2\text{HCl}$   
 $\text{SiCl}_2 + \text{H}_2 \rightleftharpoons \text{Si} + 2\text{HCl}$

Sedgwick and  
Arbach (36)

$\text{SiH}_2\text{Cl}_2$ ;  $\text{SiCl}_4$   
1050 to 1200°C

Fluorescence spectroscopy  
used to get  $\text{SiCl}_2$  gradient  
and show its proportion-  
ality to the growth rate.  
Reactions postulated,  
 $\text{SiCl}_4 + \text{Si} \rightleftharpoons 2\text{SiCl}_2(\text{surface})$   
 $\text{SiH}_2\text{Cl}_2 \rightleftharpoons \text{SiCl}_2 + \text{H}_2(\text{gas})$   
 $\text{SiCl}_2 + \text{H}_2 \rightleftharpoons \text{Si} + 2\text{HCl}(\text{surface})$

Duchemin  
et al (11)

all chlorosilanes  
10 mm Hg  $\leq P \leq$  1 atm  
900 to 1100°C

$$r = \frac{k_1 K_1 P_{\text{source}}}{1 + (K_2 P_{\text{H}_2})^{1/2}}$$

At low P kinetics on the  
surface controls the rate  
at high T, P  
 $r \propto \frac{1}{P}$  and mass transfer  
controls the rate.

Bloem and  
Claussen (37)

$\text{SiH}_4 + \text{HCl}$   
0.1% 0.9%  
800 to 1100°C

$$r = k_1 P_{\text{SiH}_4} - k_2 P_{\text{HCl}}^2$$

no T dependence T > 900°C

In presence of  $\text{HCl}$   $\text{SiCl}_2$  is  
the dominant species on the  
surface. Surface diffusion  
and reaction of  $\text{SiCl}_2^*$  is  
RLS.  $\text{SiCl}_2^*$  is incorporated  
at steps after which  $\text{Cl}$  de-  
sorbs. At T > 1000°C surface  
process is rapid and gas  
phase diffusion is RLS.

Claussen and  
Bloem (38)

$\text{SiH}_2\text{Cl}_2/\text{H}_2/\text{N}_2$   
800°C to 1000°C

$$r = \frac{k_3 k_6 k_7 P_{\text{H}_2} P_{\text{SiH}_2\text{Cl}_2}^\alpha \theta}{(k_3 + k_6)(k_3 + k_7 P_{\text{H}_2})} - K \frac{P_{\text{HCl}}^2}{P_{\text{H}_2}}$$

$$\alpha = \frac{K_1}{K_1 + P_{\text{H}_2}}$$

$$\theta = \frac{1}{1 + K_3 \alpha P_{\text{SiH}_2\text{Cl}_2} + K_4 \frac{P_{\text{HCl}}}{P_{\text{H}_2}}^{1/2}}$$

Proposed mechanism  
1)  $\text{SiH}_2\text{Cl}_2(\text{g}) \rightleftharpoons \text{SiCl}_2(\text{g}) + \text{H}_2(\text{g})$   
2)  $\text{SiCl}_2(\text{g}) + \text{HCl}(\text{g}) \rightleftharpoons \text{SiHCl}_3(\text{g})$   
3)  $\text{SiCl}_2(\text{g}) + * \rightleftharpoons \text{SiCl}_2^* *$   
4)  $\text{HCl}(\text{g}) + * \rightleftharpoons \text{Cl}^* + \frac{1}{2} \text{H}_2(\text{g})$   
5)  $\frac{1}{2} \text{H}_2(\text{g}) + * \rightleftharpoons \text{H}^*$   
6)  $\text{SiCl}_2^* \rightleftharpoons \text{SiCl}_{2\text{a}}^*$   
7)  $\text{SiCl}_{2\text{a}}^* + \text{H}_2(\text{g}) \rightleftharpoons$   
 $\text{Si} + 2\text{HCl}(\text{g}) + *$   
Diffusion of  $\text{SiCl}_2^*$  or  
reaction on steps is the  
RLS

Sugawara (39)  
Pollard and  
Newman (40)

$\text{SiCl}_4/\text{H}_2$   
900 to 1200°C

Rotating Disk Reactor.  
No conclusive evidence  
for mass transfer control  
found at T > 1100°C.  
Extensive modeling based  
on mass transfer but  
without thermal diffusion.

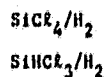
Nishizawa and  
Saito (41)

$\text{SiCl}_4/\text{H}_2$   
950 to 1150°C

IR direct spectroscopy  
identified  $\text{SiCl}_4$ ,  $\text{SiHCl}_3$ ,  
 $\text{SiH}_2\text{Cl}_2$ ,  $\text{HCl}$ ,  $\text{SiCl}_3$  and  
 $\text{SiCl}_2$ . Main reactions  
postulated:  
 $\text{SiCl}_4 + \text{H}_2 = \text{SiHCl}_3 + \text{HCl}$   
 $\text{SiHCl}_3 = \text{SiCl}_2 + \text{HCl}$   
 $\text{SiCl}_2 + \text{H}_2 = \text{Si} + 2\text{HCl}$   
Complete mechanism  
 $\text{SiH}_2\text{Cl}_2$   
 $\uparrow \downarrow$   
 $\text{SiCl}_4 \rightleftharpoons \text{SiHCl}_3 \rightleftharpoons \text{SiCl}_2 \rightleftharpoons \text{Si}$   
 $\uparrow \downarrow$   
 $\text{SiCl}_3$

ORIGINAL PAGE IS  
OF POOR QUALITY

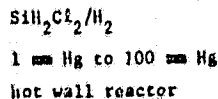
Bloem et al  
(42)



$$E_{\text{app}} = 40 \text{ to } 50 \frac{\text{kcal}}{\text{mol}}$$

Mechanism for  $\text{SiHCl}_3$  parallels that for  $\text{SiH}_2\text{Cl}_2$  with  $\text{SiCl}_2$  production in gas phase. For  $\text{SiCl}_4$ :  
 $\text{SiCl}_4(\text{g}) + \text{H}_2(\text{g}) = \text{SiCl}_2(\text{g}) + \text{HCl}(\text{g})$   
 $\text{SiCl}_4(\text{g}) + 2\text{H}^* = \text{SiCl}_2(\text{g}) + 2\text{HCl}^*$   
 $\text{Si} + 2\text{Cl}^* = \text{SiCl}_2(\text{g}) + 2\text{H}^*$   
 $\text{SiCl}_2(\text{g}) + 2\text{H}^* = \text{SiCl}_2^*$   
 $\text{SiCl}_2^* + \text{H}_2 = \text{Si} + 2\text{HCl} + 2\text{H}^*$   
 First step dominates at high T, second at low T.  
 RLS from  $\text{SiCl}_4$  is the attack of  $\text{SiCl}_4$  on Si. RLS from  $\text{SiHCl}_3$  or  $\text{SiH}_2\text{Cl}_2$  is hydrogen reduction of  $\text{SiCl}_2^*$  adsorbed at step sites. At high T processes may be mass transfer controlled.

Langlais et al  
(43)



$$E_{\text{app}} = 40 \frac{\text{kcal}}{\text{mol}}$$

$$T < 1000^\circ\text{C}$$

$$E_{\text{app}} < 0$$

$$T > 1000^\circ\text{C}$$

$$r \propto P_{\text{SiCl}_2}$$

Homogeneous equilibrium is calculated to represent the gas phase composition. Comparison with heterogeneous equilibrium shows that supersaturation is large  $10^2$  to  $10^5$ .

TABLE V. ADSORPTION-DESORPTION PROCESSES ON SILICON

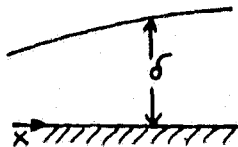
$\text{SiCl}_2 \rightleftharpoons \text{SiCl}_2^*$	;	$E_{\text{ad}} = 64 \text{ kcal/mol}$
$\text{SiCl}_4 \rightleftharpoons \text{SiCl}_4^*$	;	$E_{\text{ad}} = 12 \text{ kcal/mol}$
$\text{SiHCl}_3 \rightleftharpoons \text{SiHCl}_3^*$	;	$E_{\text{ad}} = 12 \text{ kcal/mol}$
$\text{HCl} \rightleftharpoons \text{HCl}^*$	;	$E_{\text{ad}} = 10 \text{ kcal/mol}$
$\text{H}_2 \rightleftharpoons \text{H}_2^*$	;	$E_{\text{ad}} = 8 \text{ kcal/mol}$
$\text{HCl} \rightleftharpoons \text{Cl}^* + \frac{1}{2} \text{H}_2$	;	$E_{\text{ad}} = 88 \text{ kcal/mol}$
$\frac{1}{2} \text{H}_2 \rightleftharpoons \text{H}^*$	;	$E_{\text{ad}} = 74 \text{ kcal/mol}$
$\text{Si} \rightleftharpoons \text{Si}^*$	;	$E_{\text{ad}} = 54 \text{ kcal/mol}$

taken from Chernov (57)

TABLE VI. MODELS FOR EPITAXIAL REACTORS

Horizontal Reactors

Bradshaw  
(45, 46)



$$G = 100 \left( \frac{u P}{M X} \right)^{1/2} S$$

$$\bar{G} = 200 \left( \frac{u P}{M L} \right)^{1/2} S$$

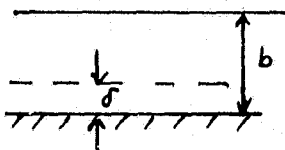
$u$  - gas mean velocity  
 $P$  - pressure  
 $M$  - mean molecular weight  
 $L$  - total length of susceptor  
 $S$  - thermodynamic parameter  
 $X$  - distance from loading edge  
 $\text{SiCl}_4$  or  $\text{SiHCl}_3$  reactant.

Key Assumptions

- isothermal boundary layer thickness over a flat plate
- concentration product gases in bulk core zero
- concentration of reactants in bulk equal to feed
- constant velocity and temperature in bulk gas
- constant surface temperature
- three reactions in Si-H-Cl system
- equilibrium established at the surface at surface temperature
- no thermal diffusion
- equal diffusivities
- no natural convection

Comments: Reasonable agreement in terms of trends with experimental data with  $\text{SiCl}_4$  and  $\text{SiHCl}_3$

Shepherd  
(67)



$$R_D = \psi_1 P_{\text{SiCl}_4}^0 - \frac{\psi_2^2}{16K\mu} \left[ \left( 1 + \frac{32K\psi_1}{\psi_2^2} \right)^{1/2} - 1 \right]^2$$

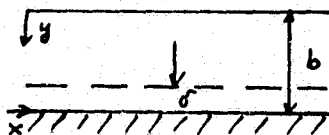
$K^*$  - equilibrium constant for  $2\text{HCl} + \text{Si} = \text{SiCl}_2 + \text{H}_2$   
 $\psi_1, \psi_2$  - mass transfer coefficients for  $\text{SiCl}_4$  and  $\text{HCl}$ , calculable in terms of known quantities. Equations given in the paper.  
 $\mu$  - product mass transfer coefficient. Contains an unknown parameter  $\text{SiCl}_4$  reactant

Key Assumptions

- layer of uniform thickness  $\delta$
- bulk gas well mixed (CSTR)
- no convection through stagnant layer
- no thermal diffusion
- linear temperature gradient,  $\beta$ , in the layer
- constant diffusion flux through the layer
- fully developed parabolic velocity profile between parallel plates
- equilibrium concentrations on the surface
- no natural convection

Comments: Qualitative agreement between theory and experiments obtained.

Eversteijn et al  
(47, 48)



$$G \left( \frac{\mu}{\text{min}} \right) = 7.23 \times 10^6 \frac{D_o T_s P_o}{RT_o^2 \delta} \exp \left( - \frac{D_o T_s x}{T_o V_o b \delta} \right)$$

$D_o$  - diffusion coefficient of silane at 300K  
 $T_s$  - surface temperature  
 $T_o = 300^\circ\text{K}$   
 $P_o$  - inlet partial pressure of silane

Key Assumptions

- constant velocity and temperature with vertical position in the bulk region  $b-\delta$
- constant temperature in the bulk with  $x$
- linear temperature profile in the stagnant layer
- zero axial velocity in stagnant layer
- zero silane concentration on the surface
- no thermal diffusion
- binary diffusion only in stagnant layer
- no natural convection

Comments: Tilt of 2% suggested over 22 cm length for almost uniform growth. Experimental evidence supplied via  $\text{TiO}_2$  tracing for good gas mixing in the bulk.

ORIGINAL PAGE  
OF POOR QUALITY

$$V_o = \frac{Q_o}{A} - \text{mean gas velocity}$$

b - free height above susceptor

$\delta$  - thickness of the stagnant layer

$$R = 8.31 \times 10^7 \text{ erg/K}$$

For tilted susceptor at angle  $\phi$

$$G = 7.23 \times 10^6 \frac{D_o T_s P_o}{K T_o^2 \delta} \exp - \frac{2D_o T_x T_m}{49 T_o^2 \tan \phi} \left( \delta(o) - \delta(x) + 0.2 \ln \frac{\delta(o)}{\delta(x)} \right)$$

$$\delta(x) = \frac{7}{\sqrt{V_T}} - 0.2$$

$$V_T = \frac{V_o b T_m}{(b - x \tan \phi) T_o}$$

$T_m$  - bulk temperature

Takahashi et al  
(69)

rectangular  
tube  
semi-circular

- three dimensional diffusion equation with forced convection ( $Gr/Re^2 < 0.3$ ) and fully developed laminar flow
- three dimensional diffusion equation with combined flow + momentum + continuity + energy equation

Gr - Grashof number

Re - Reynolds number

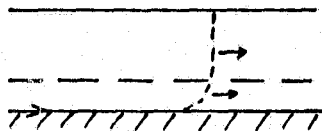
Numerical solution

Key Assumptions

- for forced convection model fully developed laminar velocity profile
- zero reactant concentration at the surface
- single component diffusion
- isothermal
- no thermal diffusion
- no gas phase reactions for combined flow
- combined momentum, mass, species mass and energy balance solved for velocity, temperature and concentration

Comments: Experimentally transition between two flow modes observed in the range  $0.4 \leq Gr/Re^2 \leq 4.1$

Ban and Gilbert  
(70, 72, 75)



Key Assumptions

- developing boundary layer
- developing flow
- turbulent central core
- only reaction at the surface
- reactant concentration at the surface at zero
- thermal diffusion included
- linear T profile assumed

Comments: Experimentally concentrated importance of free convection. Reaction operated for developing this region.

$$G = 1.76 \times 10^5 \frac{(\alpha + 0.33) D_o}{R T_o^{1.67}} \frac{\Delta T(x)}{\delta(x)} Z_x P(x)$$

$$P = P_o \exp \left[ - \frac{(\alpha + 0.33) D_o}{b_o V_o T_o^{0.67}} \int_0^x \frac{\Delta T(x)}{\delta(x)} Z_x P(x) dx \right]$$

$$Z_x = T_g^\alpha / [T_s^{\alpha + 0.33} - T_g^{\alpha + 0.33}]$$

x - distance down the susceptor, P - reactant partial pressure

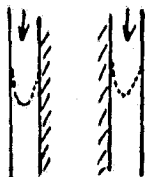
$\alpha$  - coefficient of thermal diffusion,  $D_o$  - reactant diffusivity at  $T_o$

$b_o$  - channel height at  $x = 0$ ,  $V_o$  - gas velocity at  $T_o$ ,  $\Delta T = T_s - T_g$

$T_s$  - solid temperature (constant);  $T_g$  - gas temperature,  $\delta$  - B. L. thickness

### Vertical Reactors

Manke and Donaghey  
(48, 71)



#### Key Assumptions

- fully developed laminar flow in the annulus
- constant wall temperatures
- zero reactant concentration of the susceptor
- deposition efficiency (thermodynamic) yield used to obtain growth rate from Si flux at the susceptor
- no thermal diffusion

- axial momentum balance
- axial energy balance
- continuity equation
- mass balance for  $\text{SiCl}_4$ ,  $\text{HCl}$

$$G = 6 \times 10^5 \frac{M_{\text{Si}}}{\rho_{\text{Si}}} \frac{p}{RT_m} \frac{Sh D \eta}{d_h} X_0 \exp \left( - \frac{2\pi p}{\dot{M} R} \int_0^Z \frac{r_i Sh D}{d_h T_m} dz \right)$$

$M_{\text{Si}}$ ,  $\rho_{\text{Si}}$  - molecular weight and density of silicon

$D$  - diffusivity ;  $p$  - pressure ;  $R = 82.06 \text{ atm cm}^3/\text{mol K}$

$T_m$  - mean cross sectional gas temperature ;  $X_0$  - inlet  $\text{SiCl}_4$  mole fraction

$d_h$  - hydraulic radius ;  $\eta$  - thermodynamic yield

$r_i$  - inner radius ;  $\dot{M}$  - total molar flow rate of gas

$Sh$  - Sherwood number,  $Z$  - axial distance

$Sh$ ,  $T_m$  - calculated numerically

### Rotating Disc Reactors

Sugawara  
(39)

Numerical solution of momentum, continuity, energy and species ( $\text{SiCl}_4$ ) mass balance equations in cylindrical coordinates

#### Key Assumptions

- no natural convection
- equilibrium at disk surface
- no thermal diffusion

Pollard and  
Newman (40)

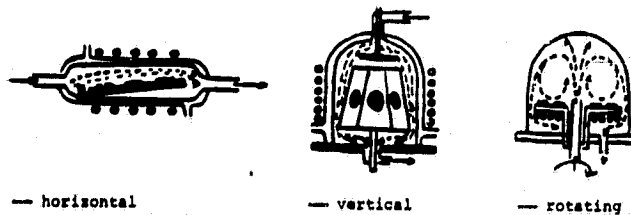
Numerical solution of momentum, continuity, energy and five species mass balance equations

- no natural convection
- no thermal diffusion
- varying physical properties
- two homogeneous and three surface reactions
- law of mass action describes kinetics
- rate constants related through equilibrium constants
- finite normal velocity at disk surface
- gas mixture at equilibrium at bulk temperature

Comments: Model has five kinetic parameters. Nevertheless fit with experimental data is not too good. Demonstrated that viscosity and conductivity change by a factor of three due to variation in temperature and density by a factor of six.

ORIGINAL PAGE IS  
OF POOR QUALITY

#### A. Epitaxial Reactors



#### B. Decomposers

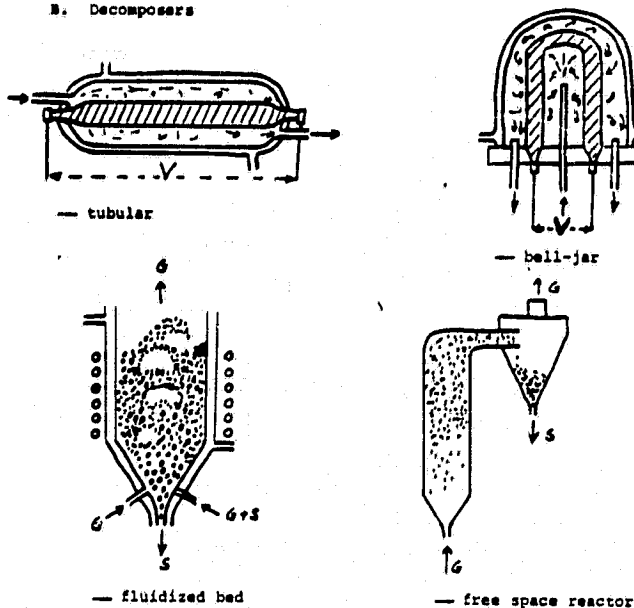


Figure 1. REACTORS FOR CVD OF SILICON

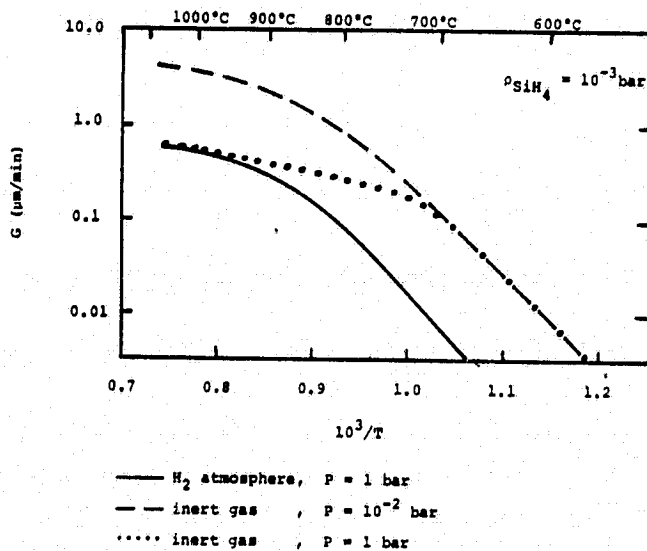


Figure 2. EFFECT OF GAS CARRIER AND PRESSURE ON DEPOSITION RATE  
(Adopted from Claassen and Bloem (13))



ORIGINAL PAGE 19  
OF POOR QUALITY

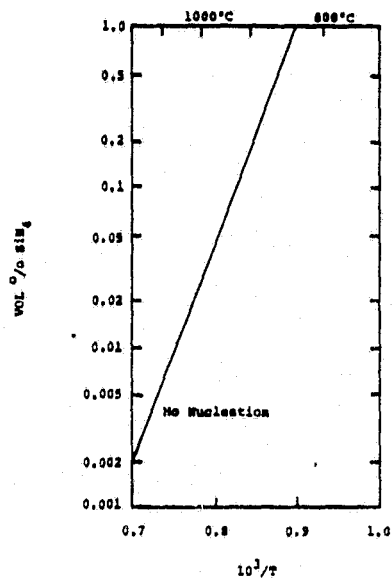


Figure 3. ONSET OF HOMOGENEOUS NUCLEATION  
(From Everstijn (3))

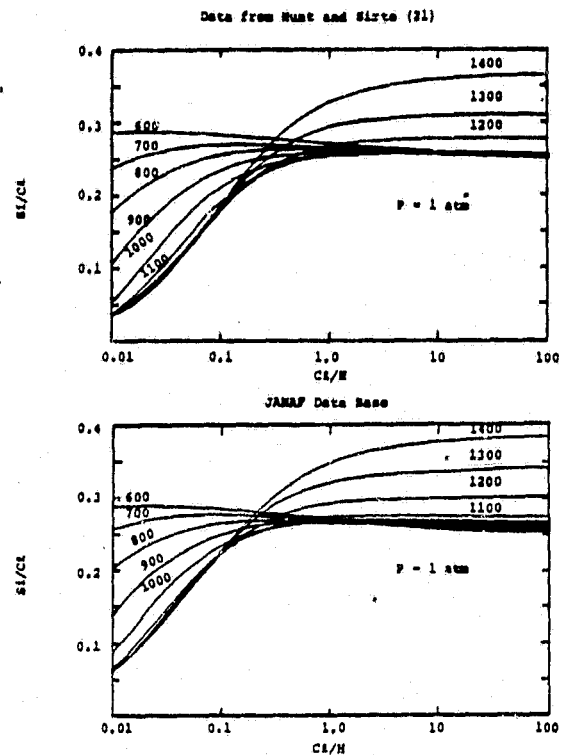


Figure 4. THERMODYNAMICS CHARTS  
(From Erk (23))

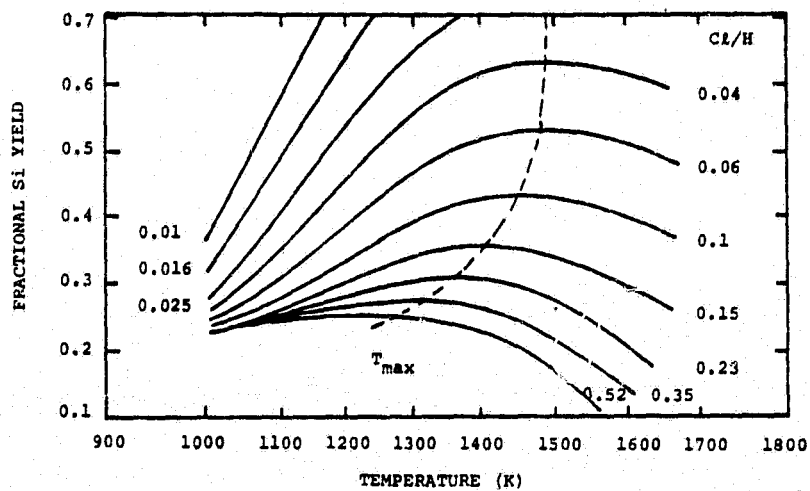


Figure 5. MAXIMUM SILICON YIELD AS A FUNCTION OF TEMPERATURE  
(Adapted from Lever (20))

ORIGINAL PAGE IS  
OF POOR QUALITY

9  
Y

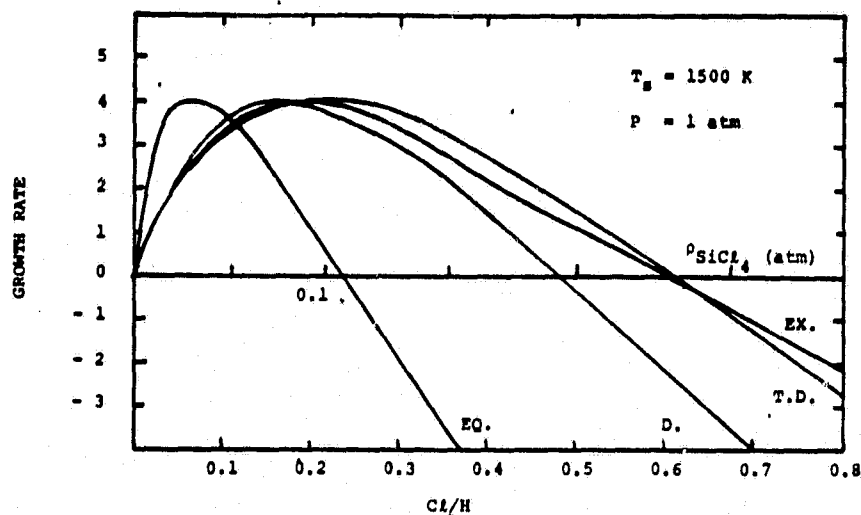


Figure 6. GROWTH RATE AS A FUNCTION OF CHLORINE TO HYDROGEN RATIO  
(Adapted from Van der Putte et al. (27); exper. curve from Bylander (26))

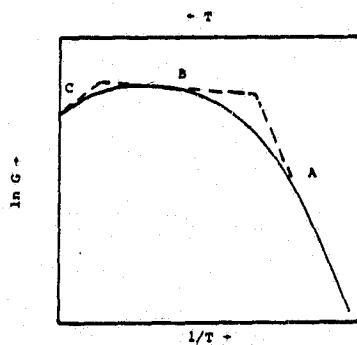


Figure 7a. GROWTH RATE AS FUNCTION OF TEMPERATURE

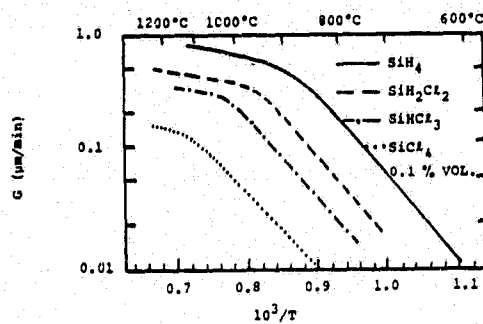


Figure 7b. DATA OF S. G. KROON  
(Philips Development Center, Nijmegen (34))

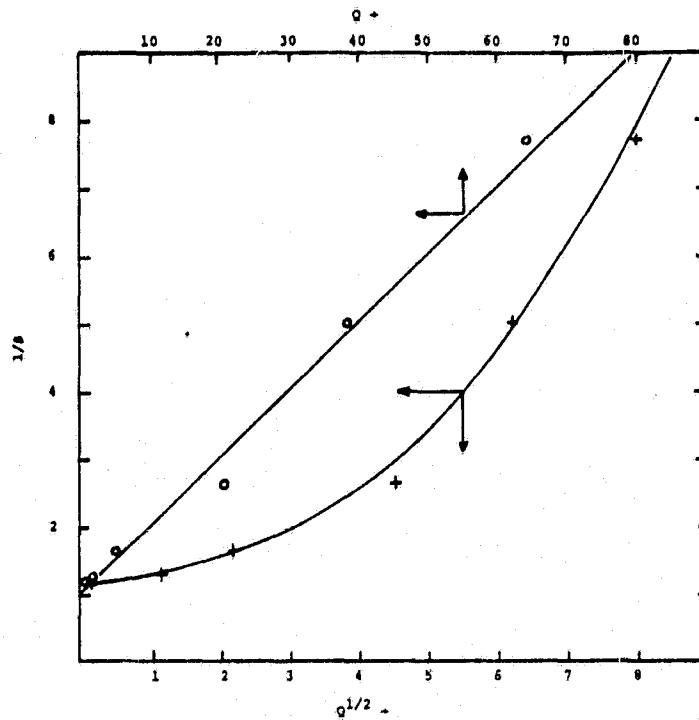


Figure 8. THE RECIPROCAL OF THE REACTOR EFFICIENCY AS FUNCTION OF FLOW RATE AND ITS SQUARE ROOT

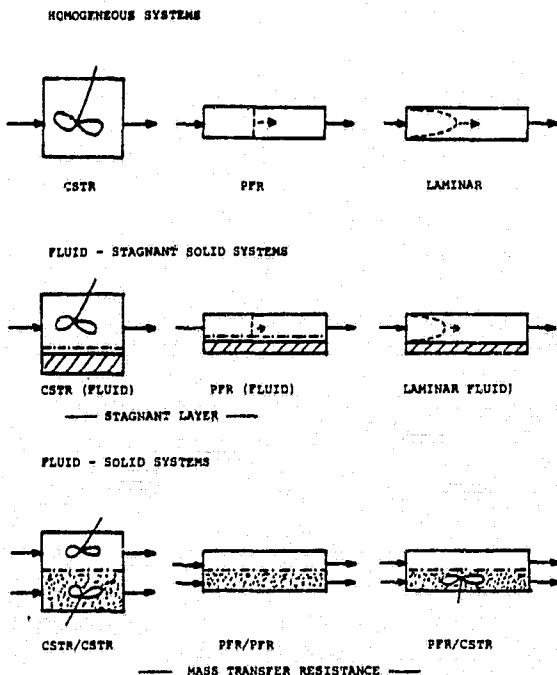


Figure 9. IDEAL REACTORS

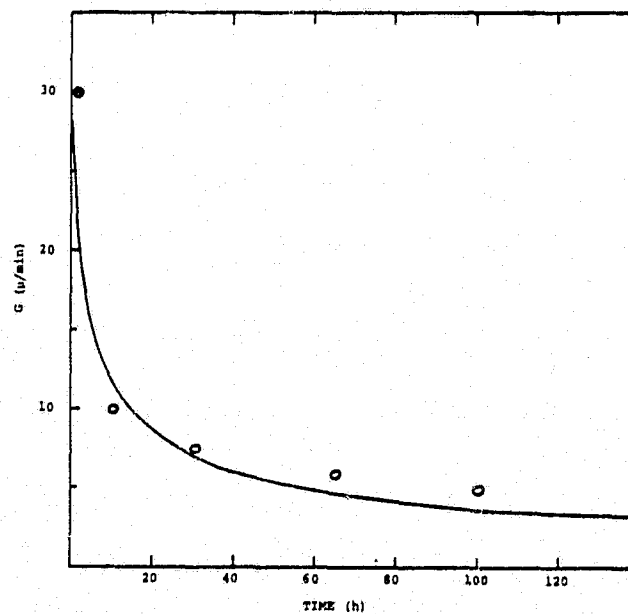


Figure 10. FALL-OFF FOR THE GROWTH RATE IN A BELL-JAR DECOMPOSER

## DISCUSSION

REIF: I just want to do justice to some CVD researchers who are not here in the audience, and I want to make just three quick comments. One has to do with hydrogen coverage on the surface. There are many people who disagree with the notion that hydrogen coverage is negligible; I am one. Probably one of the most striking evidences that hydrogen is important is that as the hydrogen pressure is reduced in a CVD system, the transition temperatures go down. That is probably one of the most striking observations. The second comment concerns  $\text{SiH}_2$ . I am among those who believe that  $\text{SiH}_2$  is important at relatively low temperatures. However, at 800-900°C there are many models that describe the kinetic data which are not based on the assumption of the existence of  $\text{SiH}_2$ . The third thing is about stagnant layers. The Eversteijn model (which involves a stagnant layer) has been around a long time but a couple of years ago Giling, who works with Bloem, showed convincingly that there is no such a thing as a stagnant layer.

DUDUKOVIC: I thank you for the comments and I certainly agree. I mention again that I am not defending that particular mechanism. What I am saying is that the mechanism feeds the kind of data that I am interested in as a chemical engineer. I don't mean to offend anybody by saying that I really don't care anything about hydrogen coverage. All I want is a rate form that will work in the temperature and pressure region that I have an interest. If that rate form works and fits the kind of data that I want to use, I'll be very happy to take it and go from there to design my reactor. In my tables you will find credit given to people who do claim and who do show some evidence for hydrogen coverage as well as others who claim that there is no hydrogen coverage at temperatures above 900 or 1000°C. But I agree with you, that could be the case. As for your comment on the term "stagnant layer," perhaps this is the wrong phrase. As a chemical engineer, I know very well that such a thing does not exist. What the concept of a stagnant layer represents to me is that there is a jump in composition. This means that there exists some additional resistance between the composition in the bulk phase and the composition measured on the surface; it's just a modeling tool which has limited value. It would be much better to be able to solve the complete set equations and not use that parameter. Sometimes, however, this model is useful for limited applications.

BAILEY: With regard to the boundary layer you mentioned, do you have any feeling of how thick that would be and how it is affected by a temperature differential?

DUDUKOVIC: Well, the boundary layer thickness will, of course, depend on the velocity and the pressure. There are some indications that there is a very substantial temperature gradient with a boundary layer. Because of the large temperature gradient, the boundary layer is destroyed eventually. I don't think the concept of the fully developed or developing boundary layer is really very valid.

9  
Y  
BAILEY: I saw a description of a boundary layer that indicated that it might be as thick as 2 inches and that seems rather thick to me.

DUDUKOVIC: I have seen estimates of up to several cm in the papers I've read. Those are just estimates based on a particular interpretation of reality.

# THE DEPOSITION OF LOW DEFECT DENSITY AMORPHOUS SEMICONDUCTORS BY HOMOGENEOUS CHEMICAL VAPOR DEPOSITION

*B. A. Scott, B. S. Meyerson, J. A. Reimer, D. J. Wolford and R. M. Plecenik  
I.B.M. Thomas J. Watson Research Center  
Yorktown Heights, NY 10598*

## INTRODUCTION

Amorphous hydrogenated silicon (a-Si:H) has received considerable recent attention because of its possible use in thin film solar cells. Power efficiencies exceeding 8% have been reported in exploratory devices,<sup>1,2</sup> and commercialization of such arrays in consumer products has already occurred.<sup>3</sup> The improved electronic properties of this material are due to the incorporation of considerable quantities of hydrogen, which tie up the dangling (unconnected) Si bonds. When amorphous silicon is prepared by conventional evaporation or sputtering in the absence of hydrogen, a large density ( $N_s \geq 10^{19} \text{ cm}^{-3}$ ) of dangling bond states<sup>4</sup> appear within the mobility gap, pinning the Fermi level and making the films highly conductive and virtually impossible to dope. Growth of a-Si:H by plasma decomposition of  $\text{SiH}_4$  occurs in such a way that few dangling bonds are formed ( $\leq 10^{16} \text{ cm}^{-3}$ ), and considerable quantities of hydrogen are incorporated as (SiH and/or  $\text{SiH}_2$ ).<sup>5</sup> As shown in Fig. 1, the "optimum" amount of hydrogen required to fabricate most devices lies between 5-20 at.%. This range, corresponding to compositions within the "electronic region", is obtained by preparing films at substrate temperatures in the range  $150 \leq T_s \leq 350^\circ\text{C}$ . Plasma-prepared films containing less hydrogen than  $\sim 5$  at. %, or more than  $\sim 20$  at. %, generally show an increase in the dangling bond density.<sup>6,7</sup> This can be attributed to either the effect of temperature, or to interactions of plasma species with the surface during film growth, resulting in the severing of Si-H and Si-Si bonds.<sup>8-10</sup> In any case, the hydrogen content at both the upper and lower "electronic region" boundaries in Fig 1 is minimally two orders of magnitude greater than required to remove  $N_s \sim 10^{19} \text{ cm}^{-3}$  typical of unhydrogenated a-Si. This suggests that hydrogen incorporation and dangling bond elimination, under most conditions of film growth, are not always simply connected events.<sup>8-12</sup>

## THE HOMOCVD EXPERIMENT

Figure 2(a) shows a conventional reactor such as that used to prepare a-Si:H from a silane plasma. The gas is pumped through the reactor at pressures  $\sim 0.1$  Torr and the plasma created by capacitive coupling to an rf or dc power source. The important point is that although film growth is obviously a heterogeneous process, the rate determining reaction is homogeneous, i.e., the plasma creates highly reactive intermediates (difficult step) which then deposit on the substrate

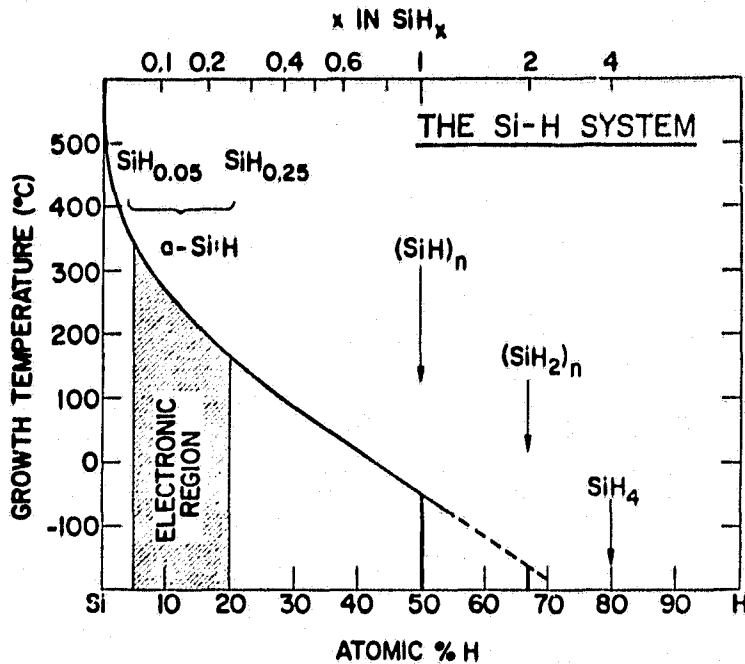


Fig. 1 Relationship between hydrogen content and growth temperature in amorphous  $\text{SiH}_x$ . The "electronic region" corresponds to compositions from which most solar cells are prepared.

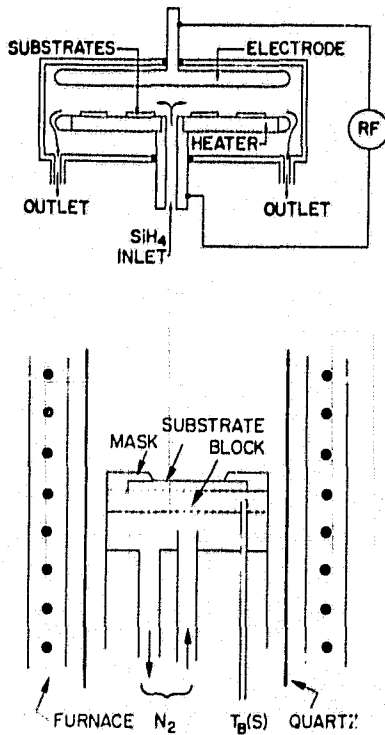


Fig. 2 (a) Top: capacitively-coupled r.f. plasma reactor (b) Bottom: homogeneous chemical vapor deposition experiment.

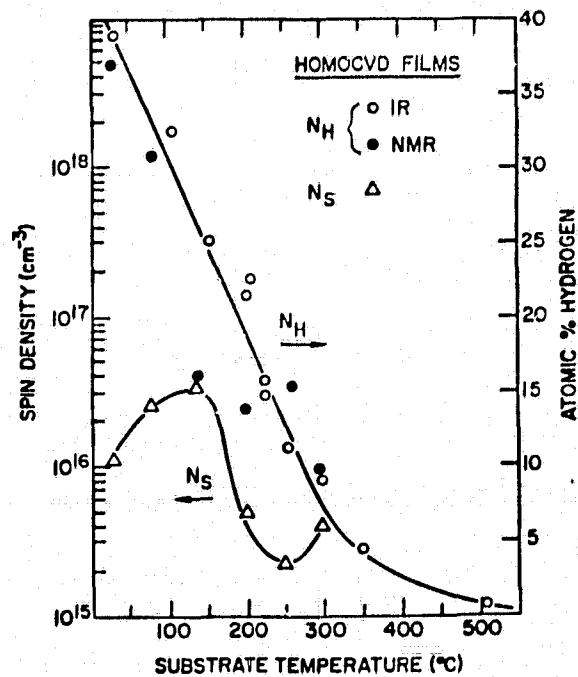


Fig. 3 Hydrogen content (right) and spin density (left) for HOMOCVD films prepared at different substrate temperatures.  $N_H$  was measured by nuclear magnetic resonance and IR absorption (ref. 8),  $N_S$  by electron spin resonance.

to form the film (low activation energy, easy step). We have carried out a number of experiments in an effort to understand the mechanism of this process.<sup>8,9,11,13-15</sup> On the basis of early plasma deposition experiments using higher silane compounds, we hypothesized that the (neutral)  $\text{SiH}_2$  diradical could be the primary plasma intermediate,<sup>13,15</sup> and so the experiment shown in Fig. 2(b) was devised to test this idea. It is now well established that the first step in the homogeneous pyrolysis of monosilane (and also the higher silanes) involves the formation of this highly reactive diradical.<sup>16-18</sup> Also, homogeneous decomposition proceeds in the pressure fall-off regime with a rate proportional<sup>17</sup> to  $p^{3/2}$  and an activation energy  $\Delta E_{\text{act}}(\text{gas}) = 54 \text{ kcal/mole}$ . By pumping  $\text{SiH}_4$  through the reactor of Fig. 2(b) at relatively high pressure and temperature, the homogeneous formation of  $\text{SiH}_2$  intermediates can be made to occur at fairly high rate. Further, if the substrate is heat sunk to a cooled metal block, as shown, it is possible to completely quench the heterogeneous decomposition of  $\text{SiH}_4$ . This occurs with  $\Delta E_{\text{act}}(\text{surface}) = 25\text{-}35 \text{ kcal/mole}$ <sup>19</sup> (accounting for the rapid deposition of a silicon film on the inner wall of the quartz reactor). In practice, we use  $p(\text{SiH}_4) = 5 \text{ Torr}$ , a gas temperature  $T_g \sim 650^\circ\text{C}$ , and substrate temperatures  $T_B(\text{S}) < 400^\circ\text{C}$ . Under these conditions the heterogeneous reaction does not occur on the substrate, and film is formed from precursor  $\text{SiH}_2$  molecules originating in the homogeneous decomposition. If the substrate is not cooled, so that its temperature is the same as that of the gas, the heterogeneous  $\text{SiH}_4$  reaction dominates, producing films containing very little hydrogen and exhibiting considerably poorer electrical properties.<sup>11,20</sup>

In our kinetic studies of the above experiment, which we have called homogeneous chemical vapor deposition (HOMOCVD), it was indeed shown that the a-Si:H deposition rate depends only on gas temperature, occurring with an activation energy of  $54 \text{ kcal/mole}$ -- precisely that measured for the gas phase thermal decomposition of  $\text{SiH}_4$ .<sup>11,14,17</sup> Consistent with this result, the absence of a substrate temperature-dependent growth rate for  $T_B(\text{S}) \leq 400^\circ\text{C}$  (i.e., below the heterogeneous regime) indicates that the film forming reactions of the  $\text{SiH}_2$  intermediate occur with very little activation energy.<sup>11</sup> We subsequently review a simple film growth model<sup>11,14</sup> compatible with these observations. Therefore, unlike plasma deposition where many different atomic and ionic species are present in the discharge, HOMOCVD is simpler because only  $\text{SiH}_2$  diradicals can deposit to form a-Si:H. The other gas phase products of monosilane pyrolysis are  $\text{H}_2$  and small quantities of higher silanes. HOMOCVD is a viable method, because as will be discussed, these gases are thermodynamically and kinetically less stable than  $\text{SiH}_4$ , initially decomposing to a lower silane and the  $\text{SiH}_2$  film forming precursor.<sup>14,16-18</sup> We also note that only a small amount of  $\text{H}_2$  is produced from the homogeneous decomposition of  $\text{SiH}_4$  in our experiment. Most of it is generated on the furnace tube walls, where  $\text{SiH}_4$  depletion of  $\sim 15\%$  is occurring in the reactor.



## FILM PROPERTIES

If the experiment depicted in Fig. 2(b) is properly carried out to avoid homogeneous nucleation, then  $\text{SiH}_2$  intermediates will deposit to form a-Si:H. As shown in Fig. 3, such films exhibit compositions which depend strongly on substrate temperature. The hydrogen content is 38 at.% for room temperature depositions, decreasing to  $\sim 4$  at.% for  $T_B(S) = 350^\circ\text{C}$ . Recalling that a-Si:H films deposit from species containing 67 at.% H, it is clear that  $T_B(S)$  affects only the hydrogen content, since  $T_B$  ( $625^\circ\text{C}$ ), and therefore the growth rate, was held invariant to obtain the data of Fig. 3.<sup>11</sup> Hence, as will be discussed, a-Si:H composition is determined by a sequence of rapid, temperature-dependent, surface reactions.

The film-forming surface reactions appear to create very few dangling bond defects, as shown by the low ESR spin densities (also plotted in Fig. 3). We find  $N_s \leq 4 \times 10^{16} \text{ cm}^{-3}$  for the range of substrate temperatures  $T_B(S) < 350^\circ\text{C}$ . The dangling bond concentration of plasma-deposited films, like those of HOMOCVD material, exhibits a minimum  $N_s \sim 3 \times 10^{15}$  at growth temperatures  $\sim 250^\circ\text{C}$ . But unlike HOMOCVD films, plasma-prepared a-Si:H shows  $N_s$  increasing toward  $10^{19} \text{ cm}^{-3}$  as the growth temperature is lowered.<sup>6-8</sup> The implication of these results has been considered elsewhere.<sup>8</sup>

One of the important manifestations of low defect densities in HOMOCVD material is that the composition range of the electronically interesting phase has now been extended beyond the 20 atomic % boundary shown in Fig. 1. As the hydrogen content increases above this value, a new photoluminescence (PL) band emerges from the usual low temperature 1.3 eV emission line.<sup>21,22</sup> The emission energy follows the optical gap variation with composition, reaching 2.0 eV for room temperature-deposited films (38 at.% H). Moreover, the PL band persists to room temperature, where it is visible with high intensity. The low temperature PL results are shown in Fig. 4, and compared to r.f. plasma-deposited films. For the latter, efficient PL is obtained at  $\sim 1.3$  eV only in the high substrate temperature sample ( $T_s = 300^\circ\text{C}$ ). Because of its high defect density, room temperature-deposited plasma material shows a band drastically reduced in intensity and shifted below 1.3 eV.<sup>22</sup>

The dark d.c electrical conductivity ( $\sigma_d$ ) of HOMOCVD films is shown in Fig. 5 for samples prepared at substrate temperatures  $222 \leq T_B(S) \leq 450^\circ\text{C}$ . At the upper and lower temperature limits, deviation from strictly linear  $\log \sigma_d$  vs  $T^{-1}$  behavior is observed.<sup>8</sup> Like plasma films deposited over the same substrate temperature range, a minimum dark activation energy of  $\Delta E_d \sim 0.6$  eV can be deduced from the linear portions of such plots.<sup>8</sup> Moreover, maximum photoconductivity  $\sigma_p \sim 10^{-4} (\text{ohm-cm})^{-1}$  is obtained for  $T_B(S) \sim 275^\circ\text{C}$  -- similar again to results measured on plasma-deposited a-Si:H.<sup>8,11</sup> However, unlike the latter films, HOMOCVD material displays more photostability when subjected to high

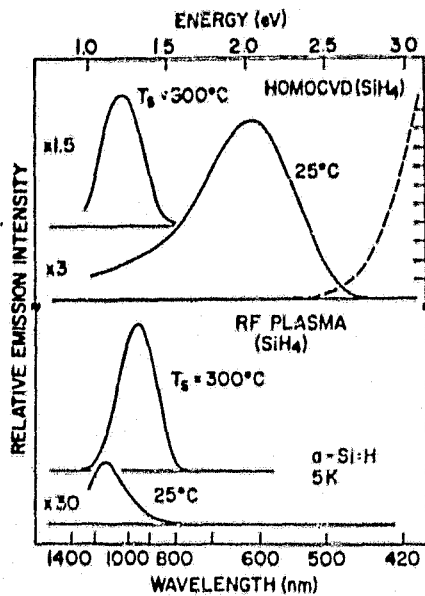


**Fig.4** Photoluminescence excited by 3.01 eV laser light in HOMOCVD and  $\text{SiH}_4$  plasma films deposited at 25 and 300°C. Data taken at 5°K. Dotted line corresponds to optical absorption edge of 25°C HOMOCVD film.

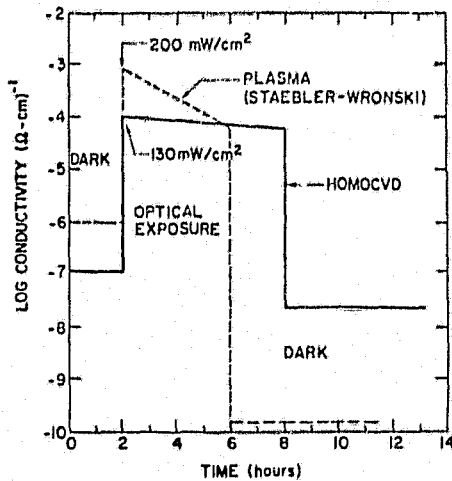


**Fig.6** Effect of light soaking on HOMOCVD and plasma (ref.24) films. The change in dark conductivity after exposure reflects the degree of transformation to the light-induced metastable state.

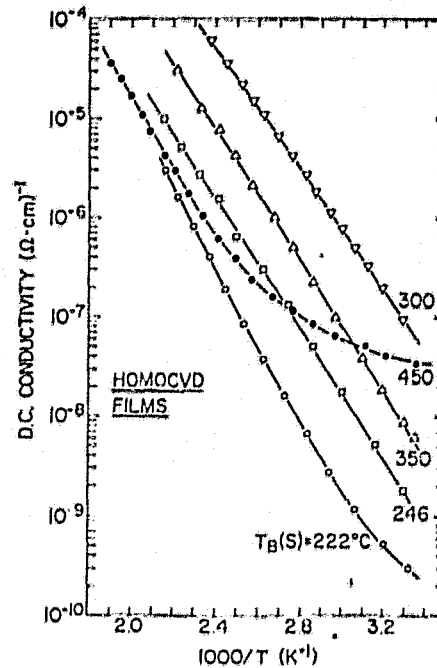


**Fig.5** D.C. electrical conductivity for HOMOCVD a-Si:H deposited at the substrate temperatures indicated.

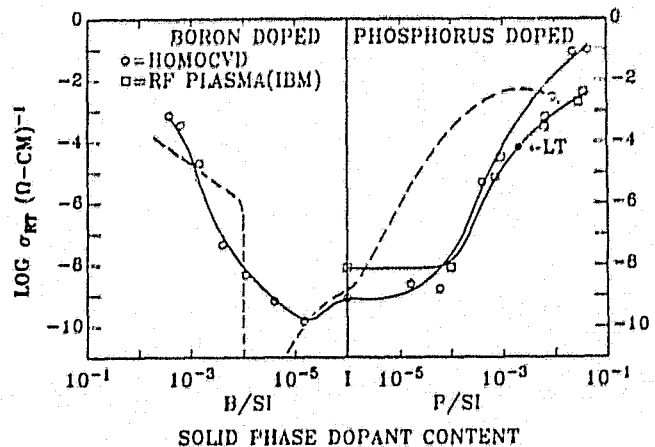


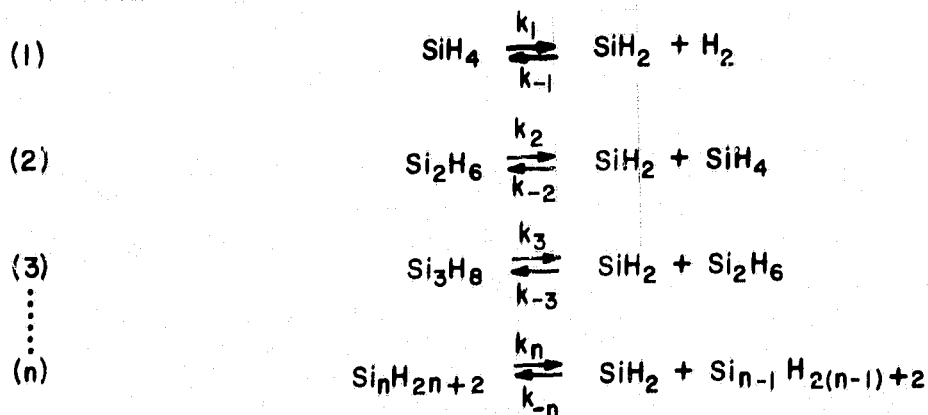
**Fig.7** Effect of p-type (boron) and n-type (phosphorus) doping on the room temperature conductivity of HOMOCVD and plasma a-Si:H films deposited at 275°C. The dotted curve corresponds to literature values for plasma a-Si:H, and LT to a result obtained from a HOMOCVD film prepared at 75°C.

intensity light. This is shown in Fig. 6, where  $\sigma_d$  changes by only a factor of two following illumination, while plasma films are photo-transformed into a metastable state having  $\sigma_d$  reduced by four orders of magnitude. Details of this experiment and its significance are discussed elsewhere.<sup>8,24</sup>

Results of doping experiments on HOMOCVD films are shown in Fig. 7, and compared to those obtained from  $\text{SiH}_4$  r.f. plasma-deposited films. The experiment was carried out using  $\text{B}_2\text{H}_6/\text{SiH}_4$  and  $\text{PH}_3/\text{SiH}_4$  mixtures for p-type and n-type depositions, respectively. Doped conductivities which exceed those of plasma films are clearly obtained in the HOMOCVD material; moreover, such films can be doped to higher  $\sigma_d$  at lower deposition temperatures (Fig. 7-LT) than is possible using the plasma method.<sup>23</sup>

## DEPOSITION CHEMISTRY

The gas phase chemistry of HOMOCVD is simple compared to that occurring in  $\text{SiH}_4$  plasma deposition of a-Si:H. The general set of reactions taking place can be written:



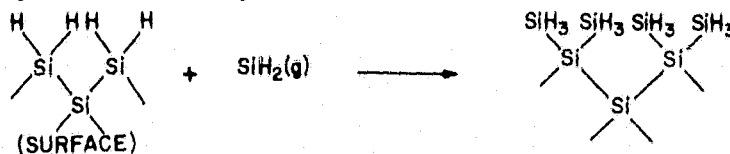
The presence of higher silanes in the reaction mixture<sup>17</sup> is due to the insertion reaction of  $\text{SiH}_2$  intermediates into their parent silanes, i.e., to the reverse reactions shown above (rate constants,  $k$ , with negative subscripts). Although few of the rate constants are known for these reactions,<sup>16</sup> it is possible to make a reasonable estimate of the  $\text{SiH}_2$  concentration under the conditions of our HOMOCVD experiment.<sup>14</sup> For  $T_g \sim 650^\circ\text{C}$  and  $p(\text{SiH}_4) \sim 5$  Torr we find  $(\text{SiH}_2) \sim 10^{13} \text{ cm}^{-3}$ . This requires that the hot gas mixture reach a steady state where higher silanes ( $n \geq 2$ ) are formed and decomposed; i.e., the bath of  $\text{SiH}_4$  provides  $\text{SiH}_2$  radicals which react at collisional velocities with parent molecules to create vibrationally excited  $\text{Si}_2\text{H}_6^*$ . Since the gas is hot, reaction (2) occurs and only a very small fraction of  $\text{Si}_2\text{H}_6^*$  relaxes to the ground state. These can suffer further reaction to  $\text{Si}_3\text{H}_8$  through collisions with  $\text{SiH}_2$ , be removed by decomposition at the hot reactor wall, or be pumped out. Indeed, higher silanes are observed as reaction products in monosilane pyrolysis,<sup>16,17</sup> and we have detected appreciable quantities in our HOMOCVD reactor effluent using GC/MS techniques.<sup>25</sup> Because the gas is hot and the higher silanes less stable

than  $\text{SiH}_4$ , large amounts of higher hydrides are not formed. Thus, the  $\text{SiH}_2$  concentration is always sufficient to sustain film growth.

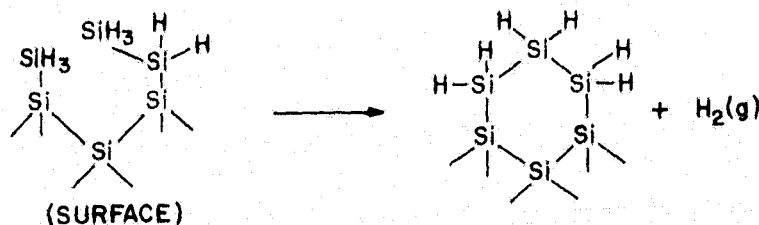
Since the  $\text{SiH}_2$  film precursor which diffuses to the substrate in HOMOCVD contains 67 at.% hydrogen, the attainment of considerably lower film compositions remains to be explained.<sup>11</sup> The fact that the hydrogen content depends on substrate temperature (Fig.3), taken with IR structural and morphological data on HOMOCVD<sup>11,14</sup> and plasma<sup>26-29</sup> films, led us to the following model for film growth.<sup>11</sup> At very low growth temperature ( $\ll \text{RT}$ ),  $\text{SiH}_2$  vapor species simply polymerize on deposition, i.e.,



forming "polysilylene," the silicon analog of polyethylene, in which the hydrogen content is ~67 at.%. Now, as the substrate temperature is raised toward room temperature, silylenes can insert into surface Si-H bonds, a reaction well known in gas phase silicon hydride chemistry:<sup>30</sup>



Each newly formed surface silyl group ( $\text{SiH}_3$ ) contains three Si-H bonds and these can undergo further insertions by incoming  $\text{SiH}_2$  radicals. Clearly the structure can not grow continuously in this manner because of steric factors. Further, the hydrogen content is diminishing with increasing substrate temperature. Hence, elimination and cross-linking reactions must also be occurring to create the 5-, 6- and 7- membered rings of the a-Si:H network:



The insertion and initial hydrogen elimination reactions are probably concurrent. A reaction scheme based on the deactivation of surface silyl-silylene groups (formed, as in our model, by  $\text{SiH}_2$  insertions) has also been proposed to explain the hydrogen elimination reactions which occur during film growth.<sup>12</sup> Although the detailed surface and near-surface reaction mechanisms are not yet even vaguely understood, we note that they are sufficiently rapid and complete to reduce the hydrogen content in HOMOCVD films to below 5 at.% at  $350^\circ\text{C}$ . Also, the relative stability of a-Si:H films grown at low substrate temperature ( $\sim \text{RT}$ ) by both HOMOCVD and plasma<sup>31</sup> methods further suggests that the film growth reactions are highly efficient at hydrogen removal. For example, films

can be heated typically 50-100° hotter than their deposition temperatures before H-evolution becomes measurable.

The presence of secondary reactions in SiH<sub>4</sub> plasma deposition necessarily modifies the local structure and hydrogen content in important ways.<sup>8-10</sup> Nevertheless, the manner in which hydrogen incorporation/elimination occurs in the plasma process is probably very similar to that in HOMOCVD-- following primarily from the surface chemistry of the SiH<sub>2</sub> species. Further studies of SiH<sub>4</sub> plasma decomposition and the consequent surface reactions will be required, however, before definitive conclusions can be drawn.

## ACKNOWLEDGEMENT

This work was partially supported by SERI subcontract ZZ-0-9319 and ONR contract N00014-80-C-0376.

1. Y. Tawada, M. Kondo, H. Okamoto and Y. Hamakawa, *Solar Energy Mat.*, **6**, 299 (1982).
2. Y. Kuwano, M. Ohnishi, T. Fukatsu and S. Tsuda, *J. Electrochem. Soc.*, **129**, 92C (1982).
3. Y. Kuwano and M. Ohnishi, *Jour. de Physique*, **42**, C4-1155 (1981).
4. M. H. Brodsky and R. S. Title, *Phys. Rev. Lett.*, **23**, 581 (1969).
5. See, for example, Amorphous Semiconductors, M. H. Brodsky, Ed., (Springer, Heidelberg, 1979).
6. H. Fritsche, C. C. Tsai and P. Persans, *Solid State Tech.*, **21**, 55 (1978).
7. J. C. Knights, G. Lucovsky and R. J. Nemanich, *J. Non. Cryst. Solids*, **32**, 393 (1979).
8. B. A. Scott, J. A. Reimer, R. M. Plecenik, E. E. Simonyi and W. Reuter, *Appl. Phys. Lett.*, **40**, 973 (1982).
9. J. A. Reimer, B. A. Scott and D. J. Wolford, to be published.
10. F. J. Kampas, to be published.
11. B. A. Scott, R. M. Plecenik and E. E. Simonyi, *Appl. Phys. Lett.*, **39**, 73 (1981).
12. F. J. Kampas and R. W. Griffith, *Appl. Phys. Lett.*, **39**, 407 (1981).
13. B. A. Scott, M. H. Brodsky, D. C. Green, P. B. Kirby, R. M. Plecenik, and E. E. Simonyi, *Appl. Phys. Lett.*, **37**, 725 (1980).

14. B. A. Scott, R. M. Plecenik and E. E. Simonyi, *Jour. de Physique*, **42**, C4-635 (1981).
15. B. A. Scott, M. H. Brodsky, D. C. Green, R. M. Plecenik, E. E. Simonyi and R. Serino, *Am. Inst. Phys. Conf. Proc.*, **73**, 6, (1981).
16. M. A. Ring, "Kinetics of Polysilane Decompositions" in Homoatomic Rings, Chains and Macromolecules of Main Group Elements, edited by A. Rheingold (Elsevier, New York, 1977).
17. J. H. Purnell and R. Walsh, *Proc. Royal Soc. A*, **293**, 543 (1966).
18. C. G. Newman, H. E. O'Neal, M. A. Ring, F. Leska, and N. Shipley, *Int. J. Chem. Kinetics* **XI**, 1167 (1979).
19. W. A. Bryant, *Thin Solid Films*, **60**, 19, (1979).
20. P. Hey, N. Raouf, D. C. Booth and B. O. Seraphin, *Am. Inst. Phys. Conf. Proc.*, **73**, 58 (1981).
21. D. J. Wolford, B. A. Scott, J. A. Reimer, R. M. Plecenik and J. A. Bradley, *Bull. Am. Phys. Soc.*, **27**, 145 (1982).
22. D. J. Wolford, B. A. Scott, J. A. Reimer and J. A. Bradley, *Proc. 16th Inter. Conf. Phys. of Semicond.*, Montpellier, France, 1982 (to be published).
23. B. Meyerson, B. A. Scott and D. J. Wolford, submitted to *J. Appl. Physics*.
24. D. L. Staebler and C. R. Wronski, *J. Appl. Phys.*, **51**, 3262 (1980).
25. B. A. Scott and R. M. Plecenik, unpublished results.
26. J. C. Knights, G. Lucovsky and R. J. Nemanich, *Phil. Mag. B.*, **37** 467 (1978).
27. J. C. Knights, *Jpn. J. Appl. Phys.*, **18**, Suppl. 18-1, 101-8 (1979).
28. J. Reimer, R. W. Vaughan, and J. C. Knights, *Phys. Rev. Lett.*, **44**, 193 (1980).
29. J. Reimer, R. W. Vaughan, and J. C. Knights, *Phys. Rev. B.*, **24**, (1980).
30. W. H. Atwell and D. R. Weyenberg, *Angew. Chemie (Internat. Ed.)*, **8**, 469 (1969).
31. D. K. Biegelsen, R. A. Street, C. C. Tsai and J. C. Knights, *Phys. Rev. B.*, **20**, 4839 (1979).

## DISCUSSION

INGLE: I have made kilograms of  $\text{SiF}_2$  polymers, and they don't look much different from the  $\text{SiH}_2$  polymers. We found that initially the products were white polymeric materials which looked like Teflon materials. We heated them up to about 350 or 400°C and looked at the NMRs. Although no NMR readings have even been reported for the  $\text{SiF}_2$  cyclic systems, there were indications of three-membered, four-membered, and five-membered cyclic  $\text{SiF}_2$  with branch chains on these systems right where we expected to see strong signals. This system looks identical to what we saw with the  $\text{SiF}_2$ . The NMR readings were not obtained unless we heated these polymeric materials. I would warn you to be very careful heating  $\text{SiH}_2$ , because there may be a critical temperature at which fairly large quantities of gases are given off and that can be dangerous in an enclosed system.

SCOTT: What temperature did you deposit the  $\text{SiF}_2$ ?

INGLE: It will deposit at any temperature from about 500°C and below. We went down to liquid-nitrogen temperatures. Our best films were made at -78°C. That gave us the most dense material. At lower temperatures we got incorporation of  $\text{SiF}_4$  in with the  $\text{SiF}_2$  and a spongy material resulted. At about -78 there was no  $\text{SiF}_4$  and that is where we got our most dense materials.

SCOTT: I might mention that if the deposits are made at low temperatures, the products contain a lot of hydrogen as both infrared and NMR data showed. An annealing process will eliminate the hydrogen and restructure the material altogether. Films made at room temperature and annealed at 300°C are not the same as those made directly at 300°C.

INGLE: The materials discussed today should be an excellent source of  $\text{SiH}_2$ . In our system, if we really wanted good clean  $\text{SiF}_2$ , we would make the  $\text{SiF}_2$  cyclic systems and then we would heat those up. They were excellent sources for  $\text{SiF}_2$  without the presence of excess  $\text{SiF}_4$ .

SCOTT:  $\text{SiF}_2$  is a lot more stable. It stays around for minutes, or at least many seconds. If you heat this film, it is not likely to eliminate  $\text{SiH}_2$ ; it's likely the solid will be restructured along with the elimination of  $\text{H}_2$ .

INGLE: You get cyclic materials that are liquids, and if these are heated,  $\text{SiF}_2$  is released.

SETTY: What happens to these hydrogen and silicon bonds in high-temperature processing? At 900°C?

SCOTT: We are operating at temperatures much lower than 900°C. Our temperatures are around 650 to 750°C, and the surfaces are much colder. I don't believe the mechanism in which  $\text{SiH}_2$  collides with the surface,

sticks and moves around is correct. I believe that  $\text{SiH}_2$  is so reactive that if there is any hydrogen on the surface it will insert into it. If there isn't any hydrogen, the bare silicon atoms on the surface will insert into the  $\text{SiH}_2$ . So the incest can go either way, but it is going to happen. Now once that happens and hydrogen is eliminated, some surface mobility of silicon will take place at these very high temperatures, I believe. Under our conditions the  $\text{SiH}_2$  comes down and sticks by reacting. It has just got to stick by inserting or reacting onto those surface bonds.

DUDUKOVIC: Considering the growth rates, it seems that there is an indication that  $\text{SiH}_2$  is an important intermediate, both at high temperatures and at low temperatures. When you consider the case of classical CVD, the temperature is the hottest at the surface and in the chlorosilane system  $\text{SiH}_2$  is abundant in the vicinity of the surface, as was determined with in situ measurements. By analogy,  $\text{SiH}_2$  is abundant at the surface and the instantaneous type of reaction cannot scavenge efficiently at high temperature. Hence, it becomes academic for me as a chemical engineer whether a Si atom migrates and first gets stripped of hydrogen or  $\text{SiH}_2$  migrates on that surface. The rates are orders of magnitude lower. In that system the growth rates are a tenth of a micron a minute or maybe a micron a minute while in this system they are angstroms a minute. That cannot just be explained by the difference in diffusion, because there is a favorable temperature gradient for diffusion in this case and in the other case it is an unfavorable one. So the explanation must be that an intermediate is created, and before it can reach a cold surface, this incestuous reaction acts as a very efficient scavenger under the experimental conditions. This causes the concentration to be reduced by the time it can get to the surface. That is the way I would interpret the situation and, as a matter of fact, that is how you interpreted it, I think.

SCOTT: At higher temperatures there is something else going on. The  $\text{SiH}_4$  can absorb and decompose on the surface. There is probably a regime in which it is homogeneously controlled. In that region the intermediate is a homogeneous intermediate at low temperatures. As the surface is heated there is a change into this heterogeneous regime in which the  $\text{SiH}_4$  is decomposing in a similar way on the surface. It's not clear how this occurs. I think there is a lot of very interesting surface chemistry associated with this system. The reactions do not occur in the regime described for classical CVD. I may mention that you showed an interesting slide in your talk. In it you showed that regardless of whether the CVD films were made in a kinetically controlled regime of silane, or tetrachlorosilane, or dichlorosilane, and I'll add disilane itself because we have worked with it, the slopes are identical. Thus, the activation energies for these surface controlled processes are all identical. So somehow the rate-determining step involves the same kind of intermediate regardless of what the initial reacting object is.



ORIGINAL PAGE IS  
OF POOR QUALITY

KALLURI R. SARMA

SOLAVOLT INTERNATIONAL

P. O. BOX 2934, PHOENIX, ARIZONA 85062

#### ABSTRACT

Polycrystalline silicon ribbons have been deposited by a high pressure plasma (HPP) enhanced deposition process. The HPP deposition process has been characterized for the silicon sources  $\text{SiH}_4$ ,  $\text{SiH}_2\text{Cl}_2$ ,  $\text{SiHCl}_3$  and  $\text{SiCl}_4$  under a variety of process parameters to determine the deposition mechanisms. The observed results were discussed in terms of thermodynamics, silicon deposition modes, and kinetic and mass transport processes for gaseous and particle species. Possible mechanisms responsible for deposition enhancement by HPP compared to a conventional CVD process have been presented.

#### INTRODUCTION

Glow discharge plasmas are increasingly being used for deposition and etching of various inorganic materials in the semiconductor industry. Most of these plasmas operate at low pressures (around one torr). The low pressure plasmas will be in a highly non-equilibrium state with electron temperatures in the range of tens of thousands degrees Kelvin and ion and neutral species temperatures in the range of few hundred degrees Kelvin. Chemical reaction enhancement in this case is due to the presence of free radicals. With increase in pressure, the mean free path between collision of species decreases, collision frequency increases, and the plasma approaches equilibrium. Thermal equilibrium can be assumed when the plasma pressure is about one atmosphere and above. In high pressure plasmas, enhancement of chemical reactions can be due to high gas temperatures in addition to the presence of free radicals.

In this paper, we will discuss the mechanisms in a high pressure plasma (HPP) enhanced deposition process used for producing polycrystalline silicon ribbons. The basic HPP deposition process and the method of depositing silicon films with it have been described earlier (1, 2). Briefly, this HPP plasma operates at a pressure of around one atmosphere and is driven by a 13.56 MHz rf generator with an impedance matching module. The impedance matching module is essentially a Pi network with a tubular inductor and two variable vacuum capacitors. The tubular inductor terminates with the plasma nozzle containing a tungsten electrode. Gases of interest for silicon deposition are introduced into the HPP system at the low potential side of the tubular inductor. When the matching network is tuned for resonance, a plasma jet is created at the tip of the electrode. The size of the plasma jet is typically in the range of 3-8 cm in length and several mm in diameter. However, the plasma beam size is dependent on the gases being used, and the gas flow rates and the rf power levels employed. Temperatures in the range

of 4000°C were estimated to be present in the plasma jet by emission spectroscopic measurements.

Polycrystalline silicon films of desired thickness are deposited by introducing the HPP nozzle in the silicon deposition reactor. The deposition reactor is essentially a square cross-section quartz tube, the walls of which are covered by molybdenum substrates. A resistance furnace placed around the quartz tube provides for control of the substrate temperature. The effluent gases from the HPP deposition reactor are exhausted through a burn-off box and scrubber.

#### EXPERIMENTAL AND RESULTS

Silicon depositions were conducted by the hydrogen reduction of chlorosilanes -  $\text{SiH}_4$ ,  $\text{SiH}_2\text{Cl}_2$  and  $\text{SiCl}_4$  - in the HPP plasma. Silicon deposition process efficiency was characterized by on-line gas chromatographic (GC) analysis of the reactor effluent gases. For comparative purposes deposition experiments were also conducted by the conventional chemical deposition (CVD) process under otherwise identical conditions. The deposition process parameters investigated were - rf power of the HPP plasma, concentration and flow rate of reactant gases, deposition substrate temperatures and orientation (horizontal or vertical) of the reactor. The deposited silicon films were characterized for surface morphology and grain size in some cases.

Deposition efficiencies calculated from GC measurements were found to be repeatable to within  $\pm 0.5\%$ . Under certain deposition conditions, gas phase nucleation was excessive and led to powder growth instead of dense film growth. Also, some of this powder was found to leave the deposition reactor with the effluent gas stream, resulting in a difference between deposition efficiencies determined by the GC analysis and weight gain measurements. (Silicon particles in the effluent gas stream were filtered out before going into the GC column.). Deposition efficiencies determined by weight gain measurements and GC analysis were found to be in good agreement when powder growth was absent.

#### RF Power

RF power requirement for stable operation of the HPP plasma was found to increase as concentration and flow rate of the reactant gases are increased. However, once a stable plasma is established, at a particular rf power, further increase in power level is not found to influence the deposition efficiency.

#### Silane

When silane was used as the silicon source, gas phase nucleation and powder growth are observed with both HPP and CVD processes under all conditions of practical interest that result in reasonable film growth rates. Brown powdery deposits were observed on the substrate surfaces as well as in the exhaust pipe of the deposition reactor. While dense silicon films could

## ORIGINAL PAGE IS OF POOR QUALITY

be deposited by CVD process, with low silane concentrations ( $<0.5\%$   $\text{SiH}_4$  in  $\text{H}_2$ ), substrate temperatures ( $\sim 600\text{--}700^\circ\text{C}$ ), and film growth rates ( $<0.1\ \mu\text{m}/\text{min.}$ ), HPP process always led to powdery deposits.

### Dichlorosilane

Figure 1 shows the deposition efficiencies observed with  $\text{SiH}_2\text{Cl}_2$  source under HPP and CVD modes of operation as a function of substrate temperature and input reactant concentration (expressed as  $\text{Cl}/\text{H}$ ). Deposition efficiencies can be seen to be higher with HPP compared to CVD. With  $\text{SiH}_2\text{Cl}_2$  gas phase nucleation leading to powder growth was found to be a severe problem when using high reactant concentrations and flow rates and high substrate temperatures ( $T_s > 1050^\circ\text{C}$ ) for both HPP and CVD modes of operation.

### Trichlorosilane

Table 1 shows the summary of the results obtained with  $\text{SiHCl}_3$  as the silicon source. Reactant concentration has a major effect on deposition efficiency both for CVD and HPP modes of operation. In the case of CVD, in general, the effect of increasing flow rate is to decrease the deposition efficiency except for depositions with  $\text{Cl}/\text{H} = 0.4$  and with substrate temperatures in the range of  $1100\text{--}1200^\circ\text{C}$ . In the case of HPP, changing the flow rate from 15 to 30 liters/min. seemed to improve the deposition efficiency in many cases and in some cases substantially. Figure 2 shows the effect of reactant concentration on the deposition efficiency for a substrate temperature of  $1100^\circ\text{C}$  and reactant flow rate of 30 liters/min. For comparison, efficiencies calculated (3) from thermodynamic equilibrium are also plotted in Figure 2. Deposition enhancement by HPP is highest at low reactant concentrations. Also, while CVD efficiencies are consistently lower than equilibrium efficiencies, HPP efficiencies are found to be higher than equilibrium values for  $\text{Cl}/\text{H} < 0.12$ . Figure 3 shows the effect of substrate temperatures and deposition efficiency. A maxima in concentration can be seen both for CVD and HPP.

### Silicon Tetrachloride

Results obtained with  $\text{SiCl}_4$  are summarized in Table 2. Reactant concentration has a major effect on deposition efficiency both for CVD and HPP modes of operation similar to  $\text{SiHCl}_3$ . In general, the effect of increased flow rate is to decrease the deposition efficiency. One major exception to this is the case for  $1100^\circ\text{C}$ ,  $\text{Cl}/\text{H} = 0.4$  deposition, where increased flow rate increased efficiency. For HPP, flow rate seems to have a similar but smaller effect. Deposition enhancement by HPP was found to occur for low reactant concentrations ( $\text{Cl}/\text{H} = 0.04$ ). Figure 4 shows the effect of concentration,  $\text{Cl}/\text{H}$ , on efficiency for a substrate temperature of  $1100^\circ\text{C}$ , and reactant flow rate of 30 liters/min. For comparison calculated thermodynamic equilibrium efficiencies (3) for  $1100^\circ\text{C}$  deposition are also plotted in this figure. Both CVD and HPP efficiencies are higher than the equilibrium predictions at high concentrations. This is discussed in the section on Transport Processes.

### Reactor Orientation

To examine the effect of gravity on the HPP process some deposition

experiments were conducted using horizontal and vertical reactor configurations under otherwise identical conditions. In the horizontal configuration, the quartz deposition reactor and the substrates covering its walls were parallel to the horizontal axis while in the vertical configuration they were parallel to the vertical axis. However, in each configuration the plasma beam was parallel to the substrate surfaces. The HPP deposition efficiencies were found to be consistently higher by a few percent with the horizontal configuration compared to vertical, when the efficiency was determined by the weight gain measurements. However, efficiencies determined by GC analysis of effluent gases were similar for both horizontal and vertical configurations. For example with  $\text{SiHCl}_3$  as silicon source, the deposition efficiencies determined by weight gain measurements were 31.7% and 26.0% for the horizontal and vertical configurations respectively - when rf power = 2.5 KW,  $\text{Cl}/\text{H} = 0.1$  and flow rate = 30 liters/min. Under CVD mode of deposition, efficiencies for horizontal and vertical reactor configurations were found to be similar, when  $\text{SiHCl}_3$  and  $\text{SiCl}_4$  were used as silicon sources. Note, that the results presented in previous sections were obtained by GC analysis with horizontal reactor configuration.

#### Grain Size and Morphology

The deposited silicon ribbons were characterized for grain size and growth surface Morphologies. This analysis was done for ribbons deposited from  $\text{SiCl}_4$  and  $\text{SiHCl}_3$  only. Grain size was found to significantly different between the HPP and CVD deposited films under otherwise identical conditions. Substrate temperature employed was also found to influence the grain size. However, substrate temperature had a greater effect on grain size under CVD mode than HPP mode. As an example, for a  $1100^\circ\text{C}$  deposition, CVD ribbons had a grain size in the range of 1-5  $\mu\text{m}$ , while HPP ribbon grain size was around 0.1  $\mu\text{m}$ .

Growth surface morphologies included - macroscopically smooth surfaces and surfaces with nodules and whiskers. High substrate temperatures, and low reactant concentrations and flow rates were found to result in ribbon surfaces with nodules and whiskers. Similar dependence was also observed for CVD mode of deposition also. However, we have not yet established the limits to the growth parameters for growth of ribbons with smooth surface morphologies, for CVD and HPP modes of operation.

#### DISCUSSION

From the experimental results, deposition efficiency can be seen to be higher for the HPP deposition mode than CVD, under cases of practical interest. Furthermore, under several cases of practical interest, HPP deposition efficiency is found to be higher than the equilibrium value calculated by assuming chemical equilibrium in the reactor at the substrate temperature. For an economic process, both deposition efficiency and deposition rate have to be high. While the efficiencies are high for lower reactant concentrations, the deposition rate will be low for a given flow rate. Hence, an economic process requires optimization of the concentration, for a given gas flow rate (dictated by reactor geometry), to obtain acceptable deposition efficiency and deposition rate. High deposition efficiencies reduce the gas

recovery costs and high deposition rates reduce the ribbon deposition costs.

In the following we will discuss the observed results in terms of the thermodynamic, kinetic and transport processes to determine the operative mechanisms in the HPP deposition process.

#### Thermodynamics of Si-H-Cl System

While practical silicon deposition reactors do not generally operate under equilibrium conditions, thermodynamic analysis can be used to determine the range of performance that can be expected. Chemical thermodynamic equilibrium of the system Si-H-Cl, relevant to HPP deposition involving temperatures up to 5000K have been calculated (3) using Gordon and McBride's computer program (4). This program is based on a free energy minimization technique. All possible species between Si, H, and Cl for which data existed in JANAF tables (5) were considered in these calculations, namely, Cl, Cl<sup>+</sup>, Cl<sup>-</sup>, Cl<sub>2</sub>, e, H, H<sup>+</sup>, H<sup>-</sup>, HCl, H<sub>2</sub>, Si(s), Si(l), Si(g), Si<sup>+</sup>, SiCl, SiCl<sub>2</sub>, SiCl<sub>3</sub>, SiCl<sub>4</sub>, SiH, SiH<sup>+</sup>, SiH<sub>2</sub>, SiH<sub>3</sub>, SiH<sub>4</sub>, SiH<sub>2</sub>Cl<sub>2</sub>, SiHCl<sub>3</sub>, Si<sub>2</sub> and Si<sub>3</sub>. An example of these calculations is shown in Figure 5, which shows the relative concentrations of various species at equilibrium as a function of temperature, for a reactor pressure of 1 atm. and a reactant input concentration, Cl/H = 0.1. SiH<sub>2</sub>Cl<sub>2</sub>, SiHCl<sub>3</sub> and SiCl<sub>4</sub> have not been shown in the figure for reasons of clarity and their mole fractions are less than 10<sup>-3</sup> above 1700K and decrease rapidly with increasing temperature. With the information in Figure 5 (equilibrium Si/Cl ratio) and input Si/Cl ratio, the deposition efficiency can be calculated. The calculated deposition efficiency as a function of temperature is shown in Figure 6 for SiHCl<sub>3</sub> source, 1 atm reactor pressure and Cl/H = 0.1. Note that in Figure 6, for temperatures above the boiling point of silicon, 2950K, efficiency should be considered as reaction efficiency rather than deposition efficiency.

With increasing temperature from 1100°C, the efficiency can be seen initially to decrease slightly, then increase gradually to around 45% at 1900°C, then decrease somewhat, and finally increase rapidly and saturate around 4000°C at nearly 100%. The rationale for investigating HPP deposition is that by quenching the equilibrium mixture present at the very high plasma temperature where efficiency is extremely high, it should be possible to obtain higher efficiencies than from the equilibrium mixture present under lower temperature CVD conditions. From experimental results, it can be seen that although improvements in efficiencies are not as much as thought possible, useful improvements in efficiencies were obtained. Even higher efficiencies may be obtained from this plasma process by more severe quenching; however, to form dense and smooth films of silicon substrates were heated to over 1000°C.

The relative performance (deposition efficiency) of SiCl<sub>4</sub>, SiHCl<sub>3</sub> and SiH<sub>2</sub>Cl<sub>2</sub> is in agreement with thermodynamic predictions as can be seen in Figure 7 (3) which shows, equilibrium efficiencies as a function of concentration for a 1100°C deposition. While equilibrium calculations predict etching (zero deposition) for a Cl/H of 0.125 at 1100°C for SiCl<sub>4</sub>, it has not been observed, either for CVD or HPP even up to a Cl/H of 0.2. In the case of cold-wall CVD reactors, this has been explained by Van der Putte et al. (7) by taking into account species dependent ordinary diffusion coefficients and

thermal diffusion. We will discuss this further under the section Transport Processes.

### Silicon Deposition Mechanisms

Deposition mechanism in conventional cold-wall CVD reactors generally involves, transport of reactants to the substrate surface, chemical reactions on the substrate surface producing silicon atoms, and incorporation of these atoms into the growing silicon film. However, a second deposition mode involves occurrence of chemical reactions in the gas phase producing free silicon atoms, condensation of these atoms into nuclei in the gas phase, transport of these nuclei to the substrate surface, and their incorporation into the growing silicon film. This latter mode of deposition becomes important in CVD reactors with the use of  $\text{SiH}_2\text{Cl}_2$  and  $\text{SiH}_4$  source gases, higher substrate temperatures and reactant concentrations, and hot wall deposition reactors (7-9). However, with HPP deposition, deposition through gas phase nucleation is found to be important under all conditions regardless of the type of chlorosilane, its concentration, and the substrate temperature employed. One of the consequences of gas phase nucleation can be powder growth; i.e. silicon nuclei, instead of reaching the substrate and contributing to film growth, grow in the vapor phase to a larger size forming a powder. This powder either lands on the substrate surface or exits the deposition reactor along with the effluent gas stream. This deposition mode in the HPP process is inferred from the grain size of the deposited film, differences in actual deposition efficiencies between the horizontal and vertical configurations of the reactor, and from the powdery deposits when the substrate temperature is intentionally kept very low ( $<700^\circ\text{C}$ ). It has not been possible to determine the relative contributions of these deposition mechanisms to the film deposition rate.

### Kinetic Processes

In the following, we discuss the various kinetic processes that could explain the observed results with HPP. In HPP deposition, reactant gases experience temperatures up to  $4000^\circ\text{C}$  in the plasma. Assuming localized chemical equilibrium in the atmospheric pressure plasma, predominant species at  $4000^\circ\text{C}$  are  $\text{H}$ ,  $\text{Cl}$ ,  $\text{Si(g)}$ ,  $\text{H}_2$  and  $\text{HCl}$  (see Fig. 6). As this high temperature gas stream flows through the reactor and impinges on the substrate surfaces, it will be quenched. As the temperature lowers through the boiling ( $2677^\circ\text{C}$ ) and melting ( $1410^\circ\text{C}$ ) points of silicon, there will be a driving force for condensation of silicon vapor. At the same time, as the temperature is lowered, there is a tendency for formation of  $\text{SiCl}_2$  and  $\text{SiCl}_3$  species. However, silicon condensation could occur before the equilibrium concentrations of  $\text{SiCl}_2$  and  $\text{SiCl}_3$  species increase. When this happens, reaction between the condensed phase and  $\text{HCl}$  and  $\text{Cl}$  will be the rate-limiting step in the attainment of equilibrium as the gas mixture is quenched. This sequence of events can qualitatively explain the improvements in deposition efficiency observed with the HPP process.

Incorporation of gas phase nucleated particles into the growing silicon film is another kinetic factor of importance in HPP deposition. Higher substrate temperatures, turbulence in the gas stream and horizontal reactor orientation were found to enhance the incorporation of silicon nuclei into the

growing silicon film. Substrate temperature in excess of  $1000^{\circ}\text{C}$  was found to be sufficient for dense film growth.

### Transport Processes

HPP deposition reactor ambient contains gaseous species as well as gas phase nucleated particles. Sricastava et al. (10) have modelled hot wall silicon deposition reactors containing silicon particles. They have given an excellent account of the silicon particle transport properties and processes, and considered the agglomeration of gas phase nucleated particles in the absence of chemical reactions. However, for an understanding of the HPP process operative mass transport process along with simultaneous chemical reactions should be considered.

Transport of gaseous and particle species can be due to both convective and diffusive processes. Two distinct regions can be identified in the HPP reactor-entry region, where the plasma beam is introduced into the reactor, and isothermal region where substrate temperature is controlled at a desired level using the auxiliary furnace. Gas flow in the reactor was found to be in a turbulent regime for the conditions investigated, which is in agreement with Reynold's number calculations based on reactor dimensions. The HPP deposition model can be schematically illustrated as shown in Figure 8. At the entry region of the reactor, the gas stream from the plasma beam dispenses as it moves through the reactor and impinges on the substrates covering the reactor walls. Within a short distance after the region, a turbulent flow is well established through the rest of the deposition zone. There will be a stagnant region near the reactor walls where the mass transport is by diffusion. Above this region, concentration can be assumed to be uniform at any given length along the reactor due to turbulent mixing.

Concentration (Fick) as well as the thermal (Soret) gradients provide a driving force for diffusion. While Fick diffusion coefficient is positive for all species (i.e. diffusion down the concentration gradient), the Soret diffusion coefficient will be negative for some species (i.e. in a temperature gradient, lighter species tend to move toward high temperatures and heavier species toward low temperatures). Steep radial temperature gradients exist at the entry region of the reactor, where the plasma core gases are much hotter than the substrate temperature. Thermal diffusion is expected to be important in the region. This is fortuitous, since the silicon particles nucleated in the gas phase will be transported to the substrate surfaces by thermophoretic force (Soret effect), due to their higher density, and become incorporated into the growing silicon film. While submicron sized particles deposit by a diffusion process, particles larger than about a micron will deposit by turbulence-induced inertial impactation (10). The higher actual deposition efficiencies observed with horizontal configuration of the reactor could be explained by the greater probability of the particles reaching the substrate surfaces.

Concentration diffusion coefficients of heavier molecules (e.g.  $\text{SiCl}_4$ ,  $\text{SiHCl}_3$ , etc.) are lower than the lighter ones (e.g.  $\text{HCl}$ ). This leads to a condition where the concentration ( $\text{Cl}/\text{H}$ ) near the substrate surface is lower than the bulk ambient gas stream (which is related to reactor input concentration) in the isothermal region of the reactors. As a result experimental

deposition efficiencies can be higher than the thermodynamic predictions since the effective Cl/H at the substrate surface is lower than the input value. This is indeed observed in case of  $\text{SiCl}_4$  input, both for CVD and HPP, at high concentrations (see Figure 4). The reason that deposition enhancement by HPP is greatest for low concentrations, in general, may be due to concentration dependent gas phase nucleation and/or transport properties.

### CONCLUSIONS

Polycrystalline silicon ribbons have been deposited by a high pressure plasma (HPP) enhanced deposition process at a pressure of about 1 atm. The HPP process was characterized to gain an understanding of the deposition mechanisms. Silane was found to be unsuitable for HPP process due to powdery deposits. Deposition enhancement was observed with HPP when using  $\text{SiH}_2\text{Cl}_2$ ,  $\text{SiHCl}_3$  and  $\text{SiCl}_4$  compared to a CVD mode of operation. This deposition enhancement is believed to be due to quenching the gases at high temperature in the plasma on the substrates which were at a lower temperature. HPP deposition mechanisms are found to involve chemical reactions and silicon nucleation in the gas phase, and transport of both reactant species and silicon particles to the substrate surface. Transport of gas phase nucleated silicon particles due to radical temperature gradients at the entry region of the reactor and turbulent convection in the uniform temperature region of the reactor was found to be an important factor in HPP deposition process.

### REFERENCES

1. K. R. Sarma, R. W. Gurtler, and W. C. Ramsey, in "Proceedings of 7th International Conference on Chemical Vapor Deposition", T. Sedgewick et al., Editors, pp 176-189, The Electrochemical Society Softbound Proceedings series, Princeton, NJ (1979).
2. K. R. Sarma and M. J. Rice Jr., J. Electrochem. Soc., 128, 2647 (1981).
3. K. R. Sarma, R. W. Gurtler, A. Baghdadi, M. Cota and W. C. Ramsey, in "Proceedings 13th IEEE Photovoltaic Specialist's Conference", pp 466-471, June 1978.
4. Gordon and McBride, "Chemical Equilibrium Computer Program", NASA - Lewis Research Center.
5. D. R. Stull and H. Prophet, JANAF Thermochemical Tables", National Bureau of Standards, Washington, D.C.
6. P. Van der Putte, L. J. Giling and J. Bloem, J. Crystal Growth, 31, 299 (1975).
7. T. U. M. S. Murty, N. Miyamoto, M. Shimbo and J. Nishizawa, J. Cryst. Growth, 33, 1 (1976).
8. K. J. Sladek, J. Electrochem. Soc., 118, 654 (1971).
9. F. C. Eversteijn, Philips Res. Rep. 26, 134 (1971).
10. R. Srivastava and R. K. Gould, 7th Quarterly Report, DOE/JPL 954862 (Aug. 1979).



ORIGINAL PAGE 17  
OF PCOR QUALITY

Table 1. Summary of results obtained using  $\text{SiHCl}_3$  as silicon source gas

T (°C)	Mode	Flow rate (liters/ min)	Deposition efficiency (%) for reactant concentration		
			Cl/H = 0.04	Cl/H = 0.08	Cl/H = 0.1
1050	CVD	15	40.5	30.9	26.5
	HPP	15	49.3	35.6	29.8
	CVD	30	39.0	25.0	21.7
	HPP	30	53.5	35.1	32.7
1100	CVD	15	47.3	35.7	32.3
	HPP	15	54.3	38.5	33.5
	CVD	30	48.5	34.0	29.3
	HPP	30	55.1	37.9	34.0
1150	CVD	15	51.9	34.2	30.7
	HPP	15	49.3	35.6	32.3
	CVD	30	53.9	31.7	27.8
	HPP	30	55.7	35.8	31.7
1200	CVD	15	48.0	34.9	30.5
	HPP	15	49.8	37.3	33.2
	CVD	30	51.6	31.4	29.0
	HPP	30	68.4	39.0	33.5

Table 2. Summary of results obtained using  $\text{SiCl}_4$  as silicon source gas

T (°C)	Mode	Flow rate (liters/ min)	Deposition efficiency (%) for reactant concentration		
			Cl/H = 0.04	Cl/H = 0.8	Cl/H = 0.1
1050	CVD	15	43.6	18.8	11.9
	HPP	15	41.8	19.1	10.6
	CVD	30	33.8	13.9	10.1
	HPP	30	42.6	14.4	9.5
1100	CVD	15	40.9	19.2	12.9
	HPP	15	43.1	19.6	11.9
	CVD	30	46.0	17.1	12.0
	HPP	30	50.0	18.2	11.0
1150	CVD	15	54.0	20.3	13.0
	HPP	15	54.4	20.6	11.8
	CVD	30	50.8	19.6	13.7
	HPP	30	55.1	19.9	11.5

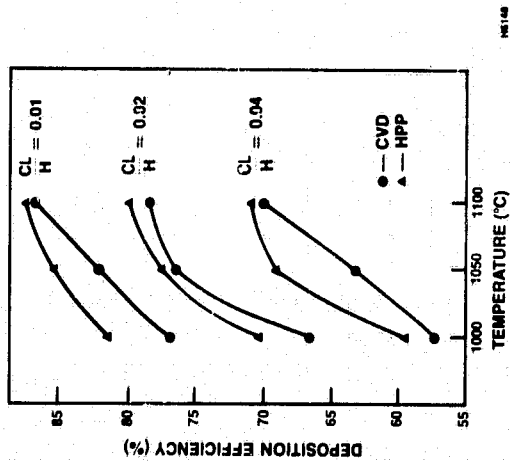


FIG. 1: DEPOSITION EFFICIENCY WITH  $\text{SiH}_2\text{Cl}_2$  SOURCE. TOTAL REACTANT FLOW RATE = 15 LIT./MIN.

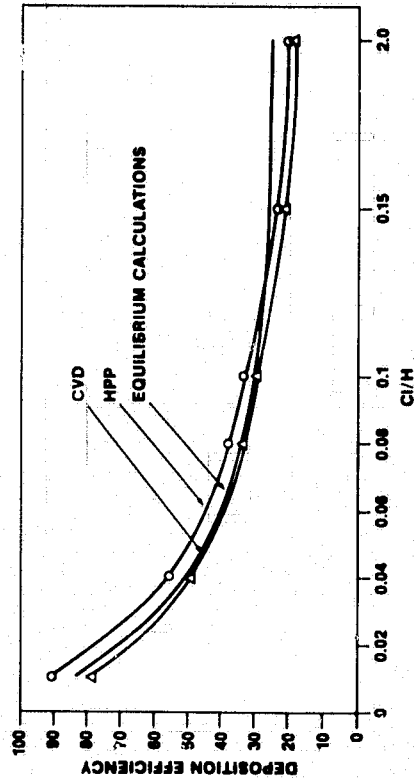


FIG. 2: DEPOSITION EFFICIENCY WITH  $\text{SiHCl}_3$  SOURCE. (FLOW RATE = 30 LIT./MIN.,  $T_s = 1100^\circ\text{C}$ ).

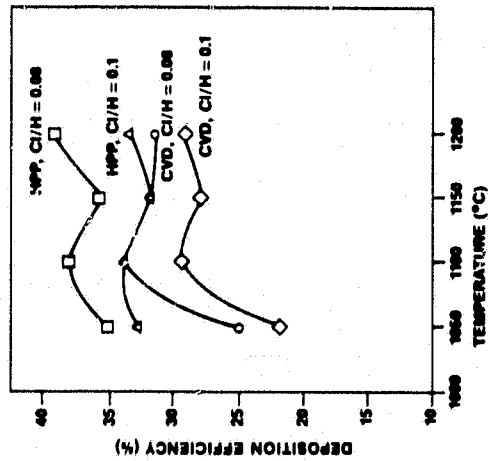


FIG. 3: DEPOSITION EFFICIENCY VS.  $T_s$  FOR  $\text{SiHCl}_3$ . (FLOW RATE = 30 LIT./MIN.)

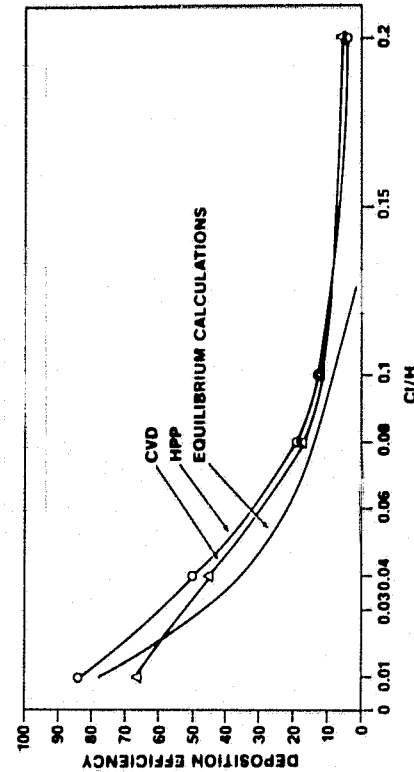


FIG. 4: DEPOSITION EFFICIENCY WITH  $\text{SiCl}_4$ . (FLOW RATE = 30 LIT./MIN.,  $T_s = 1100^\circ\text{C}$ ).

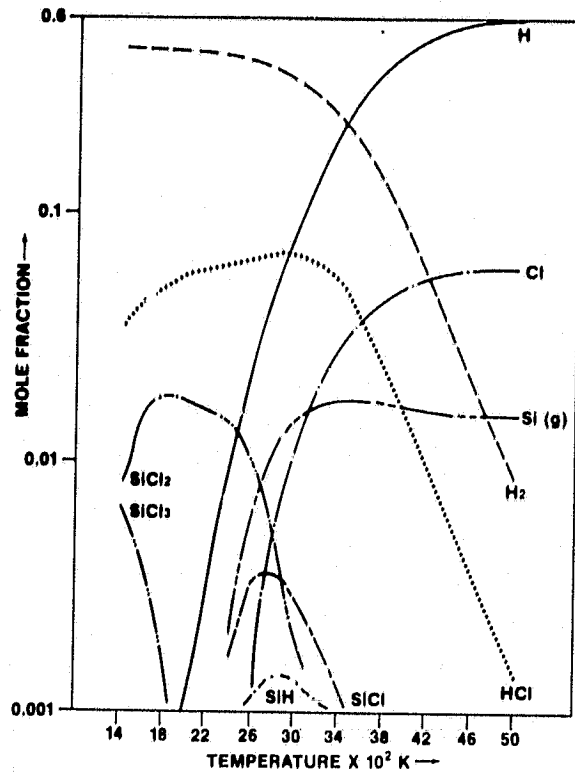


FIG. 5: EQUILIBRIUM CONCENTRATIONS  
FOR  $P = 1$  ATM, AND  $Cl/H = 0.1$ .

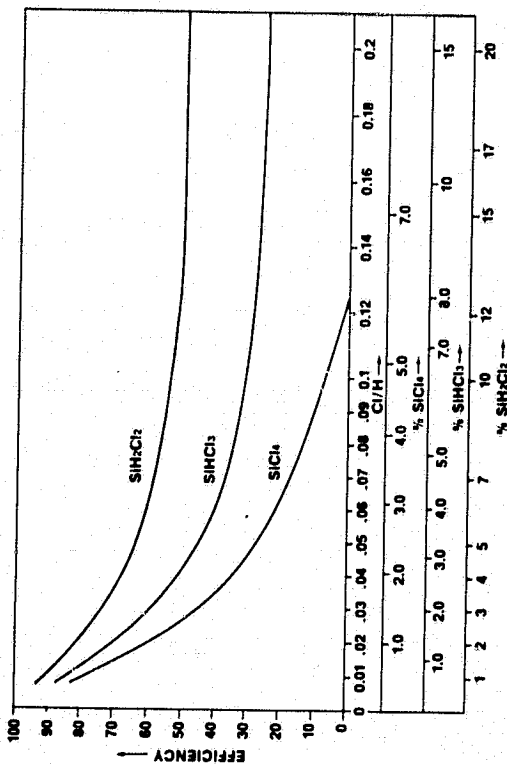


FIG. 7: EQUILIBRIUM EFFICIENCIES FOR  
CHLOROSILANES WHEN  $T_s = 1100^\circ C$ .

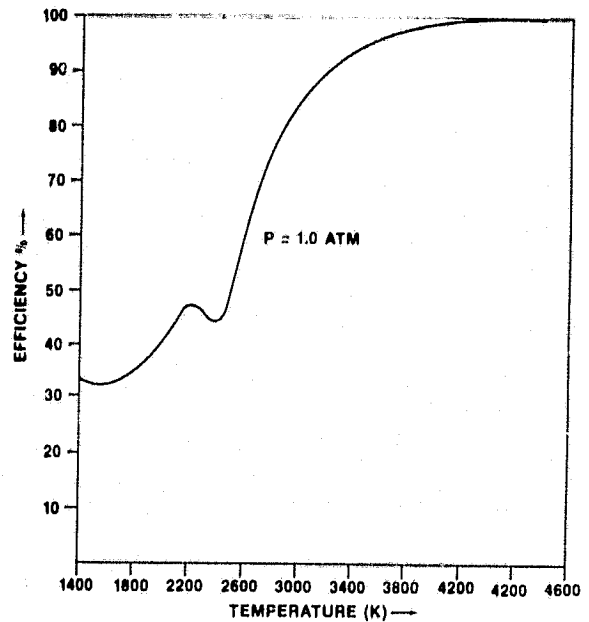


FIG. 6: EQUILIBRIUM EFFICIENCY  
FOR  $SiHCl_3$ .

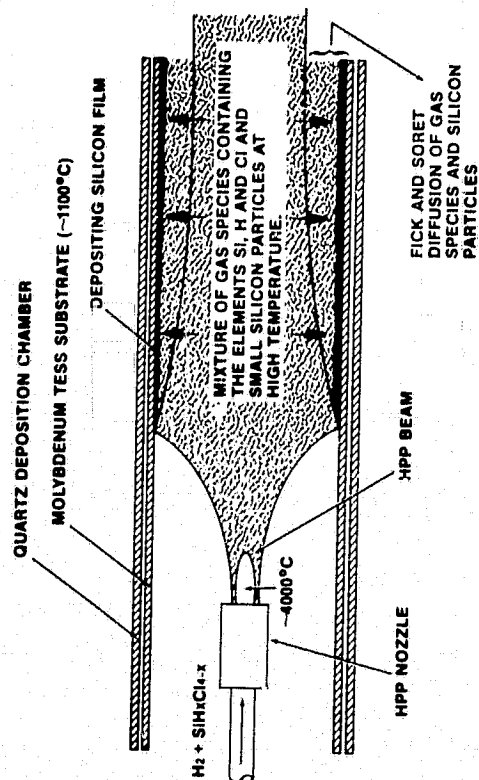


FIG. 8: SCHEMATIC ILLUSTRATION OF HPP MODEL.

## DISCUSSION

SHANFIELD: You mentioned small silicon particles in your plasma system. What size were the particles?

SARMA: We didn't do any extensive analyses. But for the limited analysis we did, they were all submicron size, typically. If we didn't keep the susceptor temperatures high, the deposited particles were loose brown powder about 0.1 of a micron or smaller.

SHANFIELD: Was that brown powder silicon?

SARMA: Yes, it was silicon, and we determined that it was crystalline silicon based on the X-ray diffraction data.

SHANFIELD: Couldn't you use that as a silicon product directly without a heated substrate?

SARMA: Our objective was to deposit silicon as polycrystalline ribbons that could be later recrystallized with an increase in the grain size and make solar cells.

SHANFIELD: I was a little surprised you found that when you increased your RF power the efficiency of material deposition did not increase.

SARMA: We were surprised too, and I think that the result may have been due to the importance of the reverse reactions which limit the efficiency as the gases are brought down to the substrate temperature.

# CHEMICAL VAPOR DEPOSITION OF EPITAXIAL SILICON

RAFAEL REIF

Massachusetts Institute of Technology

Cambridge, MA 02139

## ABSTRACT

This paper reviews the Chemical Vapor Deposition of epitaxial silicon under steady-state and transient conditions. This review will cover the incorporation of arsenic and phosphorus during silicon epitaxial growth, and the transients associated with the establishment of a steady-state silicon deposition process. A physical-chemical model that simulates the behavior of an epitaxial reactor under a variety of transient and steady-state conditions is also discussed.

## 1. INTRODUCTION

Chemical Vapor Deposition (CVD) of epitaxial silicon is one of the most important processes in the fabrication of microelectronic devices and circuits. Chemical vapor-deposited silicon is used in the fabrication of power, information, microwave, imaging, and solar-energy-conversion devices. Silicon epitaxial films are also used in such integrated-circuit technologies as bipolar, I<sup>2</sup>L, CMOS, DMOS, VMOS, and silicon-on-sapphire.

This paper reviews experimental and theoretical studies of the fundamentals of silicon CVD and the doping of chemical vapor-deposited silicon under steady-state as well as transient conditions. The term steady-state is used here to describe deposition conditions for which the gas phase composition has remained unchanged for a relatively long time. The transient experiments consisted of studying the response of the reactor to abrupt variations in gas phase composition. These transient studies are useful because they reveal the importance of various mechanisms that are not apparent in steady-state analyses.

## 2. EXPERIMENTAL DETAILS

The experiments described here were carried out in two different horizontal, rf-heated epitaxial systems (Unipak VI, Sola Basic-Tempress, and Hugle Model HIER II) that operate at atmospheric pressure [1,2]. Silane, phosphine, and arsine were used as the silicon, phosphorus, and arsenic sources, respectively. Hydrogen was used as the carrier gas. The corrected wafer surface temperature during deposition was 1050°C when using arsine and 1040°C when using phosphine. The substrates were (100)-oriented silicon wafers, either boron doped (1-10  $\Omega$ -cm) or phosphorus doped (0.1-0.9  $\Omega$ -cm). The thicknesses of the epitaxial films were measured by a groove-and-stain technique. In the steady-state study, the resistivity of the layers was determined by the four-point probe technique. In the transient study, the dopant profiles in the epitaxial films were determined by capacitance-voltage

(C-V) measurements on planar p-n junctions, mesa p-n junctions, and deep-depletion MOS structures.

### 3. EXPERIMENTS AND RESULTS

#### 3.1 Steady-State Study

The steady-state experiments consisted of studying the effect of variables such as silicon deposition rate, hydrogen flow rate, deposition temperature, and substrate crystallographic orientation on the dopant concentration of uniformly doped epitaxial films. Only the influence of silicon deposition rate is discussed here. Three substrates were used in each experiment to study the wafer-to-wafer uniformity (see Fig. 1).

Figure 2 shows a plot of epitaxial phosphorus concentration as a function of silicon deposition rate for different phosphine partial pressures [3]. The effect of substrate position on the susceptor is indicated by F(front), M(middle), and B(back) (see Fig. 1). The data in Fig. 2 suggest that the epitaxial phosphorus concentration is fairly independent of silicon deposition rate in the range studied. The epitaxial growth rate and phosphorus concentration at position B are appreciably lower than those at positions F and M at growth rates of 0.6-0.7  $\mu\text{m}/\text{min}$ . (see Fig. 2). This loss of uniformity may be the result of gas-phase depletion and/or a parasitic decomposition of silane in the gas phase.

Figure 3 shows the results of a similar set of experiments using arsine [1,3]. These data show a definite growth-rate dependence, in contrast with the data in Fig. 2. The same growth-rate dependence was observed in two different epitaxial systems, i.e., Unipak and Hugle. The loss of wafer-to-wafer uniformity at deposition rates of 0.6-0.7  $\mu\text{m}/\text{min}$  is worse for arsine than it is for phosphine.

#### 3.2 Transient Study

The transient study investigated the response of the epitaxial system to abrupt variations in silane and/or dopant gas flows during the deposition of silicon.

Figure 4 shows measured majority carrier concentrations as a function of depth in the epitaxial film for the decreasing step change in arsine gas flow shown in the inset [1]. This experiment was repeated at four different growth rates: 0.14, 0.32, 0.6, and 1.3  $\mu\text{m}/\text{min}$ . The arsine partial pressure was adjusted each time to compensate for the different growth rates and to achieve the two doping levels of approximately  $1 \times 10^{15}$  and  $3 \times 10^{15} \text{ cm}^{-3}$  in each experiment. The different values of  $T_0$  and  $T_D$  (see table in Fig. 4) were chosen to compensate for growth rate differences. The measured profile obtained for growth rates of 0.6 and 1.3  $\mu\text{m}/\text{min}$  are indistinguishable (solid curve) and differ strongly from that obtained at 0.14  $\mu\text{m}/\text{min}$  (dashed curve) which changes much more abruptly with distance. The dopant profile corresponding to 0.32  $\mu\text{m}/\text{min}$  fell between the two shown in Fig. 4.

Figure 5 shows the influence of dopant species on the transient response

**ORIGINAL PAGE IS  
OF POOR QUALITY**

of the epitaxial system [3]. The dotted line corresponds to phosphine used as the dopant source, and the dashed line corresponds to arsine. These experiments were carried out at  $0.6\mu\text{m}/\text{min}$ . As the figure indicates, the phosphorus profile is more abrupt than the arsenic profile. The transition region between the two uniform doping levels is approximately  $1\mu\text{m}$  for phosphorus and almost twice as much for arsenic.

The two experiments above studied the transient response of the dopant incorporation process. The next experiments studied the transient response of the silicon deposition process, and they are described with the aid of Fig. 6 [4]. Figure 6a shows the silane and arsine flows as functions of time in this experiment, and Fig. 6b shows schematically the variation of epitaxial arsenic concentration with silicon growth rate for two different arsine flows. At  $t=0$  silane and arsine were injected into the reactor tube and their flows were adjusted to produce a silicon growth rate  $g_L$  and an arsine flow  $f_L$ . This deposition condition is indicated by L in Fig. 6b. The epitaxial system was then allowed to reach steady state and establish a uniform epitaxial arsenic concentration  $\bar{N}$  (see Fig. 6b). At  $t=t_0$  both the silane and arsine flows were abruptly increased and adjusted to produce a growth rate  $g_H$  and a flow rate  $f_H$ , respectively. The new deposition condition H (see Fig. 6b) was designed to yield the same epitaxial arsenic concentration  $\bar{N}$ . The epitaxial system was expected to change its steady-state operating condition from L to H following path 1, 2, or 3 in Fig. 6b. Path 2 was expected if the duration of the transient period was negligible, while path 1 or 3 was expected if the transient time was non-negligible. In order to determine which path was followed the dopant profile in the resulting epitaxial film was measured. A peak or dip in the otherwise uniform dopant profile would indicate whether path 1 or 3, respectively, was followed. Figure 7 shows the measured arsenic concentration (solid line) as a function of distance from the surface of the epitaxial film for this experiment, in which  $t_0=15$  min (see Fig. 6a) and the total deposition time was 23 min [4]. The profile shows a definite peak, indicating that the epitaxial system went from L to H via path 1 (Fig. 6b). This peak confirms the existence of non-negligible transients in the silicon epitaxial system.

An experiment similar to that described in Fig. 6 except that the silane and arsine flows were abruptly decreased rather than increased at  $t=t_0$  was also carried out. In this case, the operating condition of the epitaxial system was initially at H and was then changed to L (see Fig. 6b). Figure 8 shows the measured epitaxial dopant profile for this experiment ( $t_0=8$  min, total deposition time = 23 min) [4]. The profile shows a definite dip, indicating that the epitaxial system went from H to L following path 3 (see Fig. 6b) and confirming the presence of significant transients in the silicon epitaxial system. The magnitudes of the dip and peak differ slightly, probably due to artifacts in the measurement technique.

#### 4. PHYSICAL MODEL

The dopant incorporation model used here to describe the results discussed above can be summarized with the aid of Fig. 9 as follows [4]. When a dopant-containing species in the gas phase is in the vicinity of the silicon surface (see Fig. 9a) it undergoes an adsorption process. The adsorbed

dopant species diffuses on the surface until it finds an incorporation site to which it can attach. This incorporated dopant atom is then quickly covered by subsequently arriving silicon atoms.  $r_1$  (Fig. 9) is the rate at which dopant species are adsorbed on the silicon surface, and is given by

$$r_1(t) = k_{mf} \left[ P_D^0(t) - \frac{N_S \theta_D(t)}{K_A K_P} \right] \quad (1)$$

where  $k_{mf}$  is a kinetic coefficient associated with the rate-limiting step of the dopant incorporation process,  $P_D^0$  is the input dopant partial pressure,  $N_S$  is the surface density of adsorption sites per unit area,  $\theta_D$  is the fraction of adsorption sites occupied by dopant species, and  $K_A$  and  $K_P$  are thermodynamic constants relating the epitaxial arsenic concentration to the concentration of dopant species in the adsorbed layer and gas phase, respectively.  $r_2$  (Fig. 9) is the rate at which dopant atoms are covered by silicon atoms and is given by

$$r_2(t) = g(t) \frac{N_S \theta_D(t)}{K_A} \quad (2)$$

where  $g$  is the silicon growth rate. The adsorbed layer plays an important role in this model. It consists of a population of hydrogen, silicon, and dopant species occupying adsorption sites and capable of moving on the solid surface. The model assumes that the concentration of dopant atoms in the growing epitaxial film ( $N$ ) is proportional to the concentration of dopant species in the adsorbed layer, i.e.

$$N = \frac{N_S \theta_D}{K_A} \quad (3)$$

This model views  $r_1$  as the rate at which the adsorbed layer increases its population of dopant species. Similarly,  $r_2$  is viewed as the rate at which the adsorbed layer decreases its population of dopant species due to the silicon-covering step. In steady state, i.e., when the silane and dopant flows entering the reactor have remained unchanged for a "long" time,  $r_1 = r_2$ . Consequently,  $\theta_D$  remains unchanged (see Eq. (1) and (2)) and so does  $N$  (see Eq. (3)). However, when the silane and/or dopant flows vary with time  $r_1$  and  $r_2$  may not be equal and, as a result,  $\theta_D$  and  $N$  may also vary with time. In this case, the rate of change of  $\theta_D$  (and  $N$ ) can be calculated from

$$r_1(t) - r_2(t) = N_S \frac{d\theta_D(t)}{dt} \quad (4)$$

By using Eq. (1), (2), and (3), Eq. (4) can be rewritten as

$$k_{mf} \left[ P_D^0(t) - \frac{N(t)}{K_P} \right] - g(t)N(t) = K_A \frac{dN(t)}{dt} \quad (5)$$

Equation (5) summarizes the dopant incorporation model and relates  $P_D^0(t)$ ,  $g(t)$ , and  $N(t)$ .

Figure 9b shows an equivalent circuit representing the dopant incorpora-



**ORIGINAL PAGE IS  
OF POOR QUALITY**

tion model described above. The "current" in the circuit represents the net flow of dopant species.  $R_1$  represents the limitation imposed by the rate-limiting mechanism on the flow of dopant species.  $R_2$  represents the step by which silicon atoms cover dopant atoms during growth.  $P_D^0$  represents the "voltage" which drives the current, i.e., the driving force for the dopant incorporation process. The capacitor accounts for the accumulation of dopant species in the adsorbed layer. In the equivalent circuit of Fig. 9b,  $R_1 \equiv (k_{mf})^{-1}$ ,  $R_2(t) \equiv [g(t)K_p]^{-1}$ , and  $C \equiv K_A K_p$ , and the voltage across the capacitor is proportional to  $\theta_D$  and  $N$ . Notice that  $R_2$  is proportional to the reciprocal of the silicon growth rate.

During steady-state conditions, the right-hand side of Eq. (5) can be set to zero, and an expression relating the steady-state epitaxial dopant concentration to the epitaxial growth rate and the dopant partial pressure can be obtained, i.e.

$$N = \frac{k_{mf}}{g + \frac{k_{mf}}{K_p}} P_D^0 \quad (6)$$

## 5. DISCUSSION

### 5.1 Steady-State

The growth rate independence observed in Fig. 2 suggests that the phosphorus incorporation process occurs near thermodynamic equilibrium. By assuming that  $g \ll k_{mf}/K_p$  in the range studied, Eq. (6) can be simplified to

$$N \approx K_p P_D^0 \quad (7)$$

From the data in Fig. 2, a value of  $K_p = 2 \times 10^{25}/\text{cm}^3\text{-atm}$  is obtained for the phosphine/silane system at a deposition temperature of  $1040^\circ\text{C}$  [3].

The arsenic data in Fig. 3 show a definite growth-rate dependence, in contrast with that of phosphorus. An equation analogous to Eq. (7) is adequate to describe the arsenic incorporation process at relatively low growth rates. At growth rates such that  $g \gg k_{mf}/K_p$ , however, Eq. (6) simplifies to

$$N \approx \frac{k_{mf}}{g} P_D^0 \quad (8)$$

which describes the growth-rate dependence observed in Fig. 3 at higher growth rates. Equation (8) indicates that the arsenic incorporation rate is controlled by kinetics when  $g \gg k_{mf}/K_p$ . By fitting Eq. (6) to the experimental data in Fig. 3 the following values were obtained for the arsine/silane (Unipak) system at a deposition temperature of  $1050^\circ\text{C}$ :  $k_{mf} = 4.85 \times 10^{19}/\text{cm}^2\text{-sec-atm}$  and  $K_p = 1.05 \times 10^{26}/\text{cm}^3 \text{ atm}$  [2].

## 5.2 Transient Study

Because all experiments can be explained analogously, only that described in Fig. 6 is discussed here with the help of Fig. 10 [4]. In that experiment the arsine and silane flows were both adjusted, before and after  $t=t_0$ , to produce the same epitaxial arsenic concentration  $\bar{N}$  in steady state. The abrupt increase in arsine flow at  $t=t_0$  results in an abrupt increase in the rate  $r_1$  at which arsenic species adsorb on the silicon surface (see Eq. (1)). Similarly, the abrupt increase in silane flow at  $t=t_0$  increases the silicon growth rate thereby increasing the rate  $r_2$  at which arsenic species in the adsorbed layer are covered by silicon atoms (see Eq. (2), Fig. 10a). If the silicon growth rate reaches the new steady-state rate "instantaneously", then both  $r_1$  and  $r_2$  increase by the same amount and reach the new steady-state rates instantaneously. Consequently,  $\theta_D$  remains unchanged during the transition (see Eq. (4)) and so does  $N$ . This situation corresponds to the epitaxial system moving from L to H via path 2 in Fig. 6. However, if the silicon growth rate requires some non-negligible time to reach the new steady-state rate, then  $r_1 > r_2$  for a brief period of time which results in an increase in  $\theta_D$  (see Eq. (4)) and, consequently, an increase in  $N$ . Both  $\theta_D$  and  $N$  gradually fall back to their steady-state levels as the silicon growth rate approaches the new steady-state rate. The end result is a "peak" in the resulting epitaxial arsenic profile, in agreement with the experimental observation in Fig. 7. Note that, according to this model, path 3 is not physically possible in this experiment.

The equivalent circuit in Fig. 10 can also be used to explain the experiment. Figure 10b shows the situation that exists when the silicon growth rate reaches the new steady-state rate instantaneously. In this case,  $R_2$  decreases abruptly and, consequently,  $r_2$  increases abruptly compensating the abrupt increase in  $r_1$ . The amount of charge in the capacitor (which corresponds to  $\theta_D$  in the model) remains unchanged. Figure 10c shows the situation that exists when the silicon growth rate approaches the new steady-state gradually. In this case,  $R_2$  decreases gradually and  $r_1 > r_2$  for a brief period of time, which increases the amount of charge stored in the capacitor. As  $R_2$  reaches its steady-state value, the charge in the capacitor falls back to the steady-state level.

By fitting Eq. (5) to profiles such as those shown in Fig. 4, a value of  $K_A = 5.7 \times 10^{-5} \text{ cm}$  (Unipak) was obtained [2]. The values of  $k_{mf}$  and  $K_p$  were already determined from the steady-state study. Equation (5) can now be used to simulate profiles such as those in Fig. 7 and 8. The dotted and dashed lines in Fig. 7 and 8 are simulations obtained by assuming that the silicon growth rate responds exponentially (with time constant  $\tau_s$ ) to abrupt changes in silane flow. The best fit to the measured profile was obtained with  $\tau_s = 30 \text{ sec}$  (Fig. 7) and  $\tau_s = 20 \text{ sec}$  (Fig. 8). The disagreement in the  $\tau_s$  values is caused by the discrepancy in the magnitudes of the peak and the dip. As mentioned earlier, this discrepancy is believed to be due to limitations in the technique used to measure the profiles.

## 6. SUMMARY

The arsenic and phosphorus incorporation processes during silicon epi-

9  
Y

taxial growth were investigated by studying the steady-state and the transient response of a CVD epitaxial system. The transients associated with the silicon deposition process were also investigated. The most important experimental results discussed here may be summarized as follows:

- (i) The epitaxial phosphorus concentration is independent of the silicon deposition rate in the range studied.
- (ii) The epitaxial arsenic concentration decreases with increasing growth rate.
- (iii) The epitaxial system responds faster to perturbations in phosphine gas flow than it does to those in arsine gas flow.
- (iv) The time constant of the silicon deposition process in a CVD epitaxial system is in the 20-30 sec range.

A physical model capable of simulating the behavior of the epitaxial system was also discussed. The phosphorus results from the steady-state study were consistent with those expected from a process dominated by thermodynamics. The arsenic results were consistent with those expected from a process dominated by a rate-limiting mechanism. The physical mechanisms dominating the transient response of the dopant incorporation process are related to the time needed by the adsorbed layer to reach the new steady-state population of dopant species. The phosphorus incorporation process responds faster than arsenic to abrupt perturbations in dopant gas flow because of the absence of a rate-limiting mechanism.

#### ACKNOWLEDGMENTS

This work was supported by the U.S. Army Research Office through Contract No. DAAG-29-81-K-0087.

#### REFERENCES

1. R. Reif, T.I. Kamins and K.C. Saraswat, "Transient and Steady-State Response of the Dopant System of a Silicon Epitaxial Reactor: Transfer-Function Approach", J. Electrochem. Soc., 125 (1978) 1860-1866.
2. R. Reif and R.W. Dutton, "Computer Simulation in Silicon Epitaxy", J. Electrochem. Soc., 128 (1981) 909-918.
3. R. Reif, "Phosphorus Incorporation during Silicon Epitaxial Growth in a CVD Reactor", 129 (1982) 1122-1128.
4. R. Reif and M. Vanzi, "Transients in the Deposition of Silicon Epitaxial Films in a CVD Reactor", 128 (1981) 2187-2193.

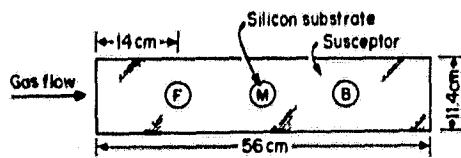


Fig. 1 Location of substrates along the length of the susceptor. F: front, M: middle, B: back. (Dimensions correspond to Unipak system)

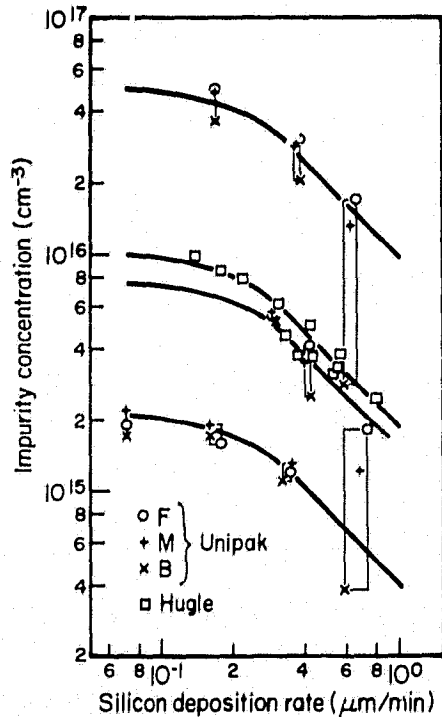


Fig. 3 Arsenic concentration of uniformly doped epitaxial layers as a function of growth rate.

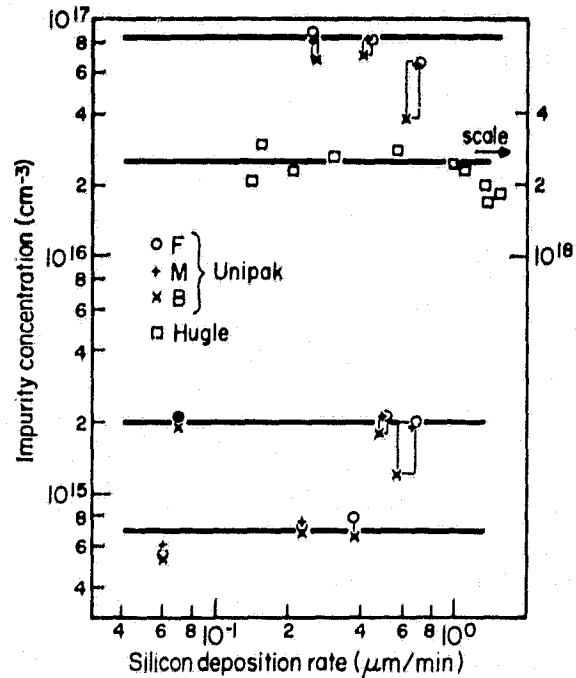


Fig. 2 Phosphorus concentration of uniformly doped epitaxial layers as a function of growth rate.

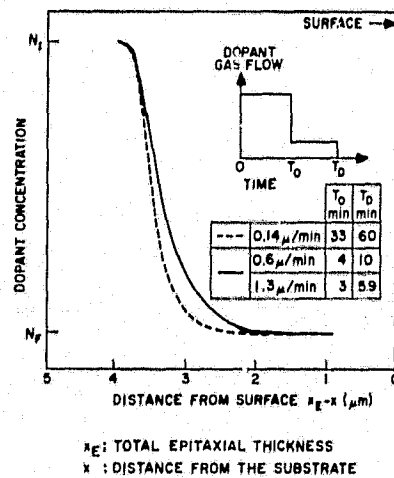


Fig. 4 Measured arsenic profiles for different epitaxial growth rates.

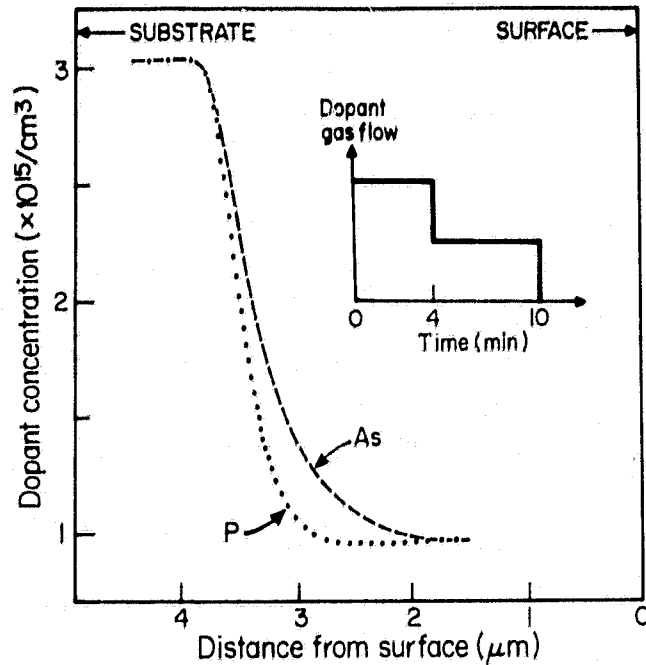


Fig. 5 Measured dopant profiles for the decreasing step change in dopant gas flow shown in the inset. P:phosphorus, As:arsenic.

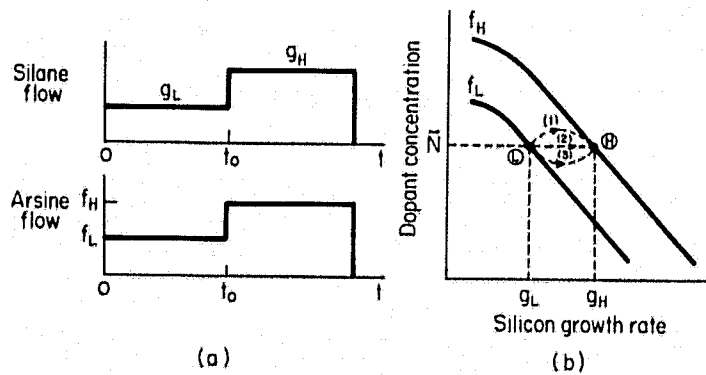


Fig. 6 Experiment to study the transient response of the silicon epitaxial process (see text).

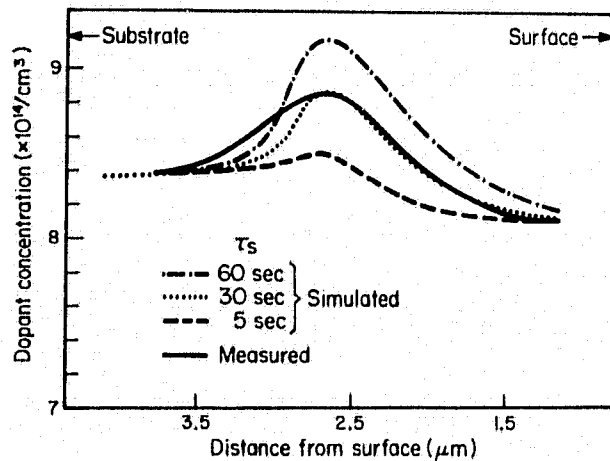


Fig. 7 Solid: experimental dopant profile. Dashed and dotted lines: simulated dopant profiles for different values of  $\tau_s$ .

ORIGINAL PAGE IS  
OF POOR QUALITY

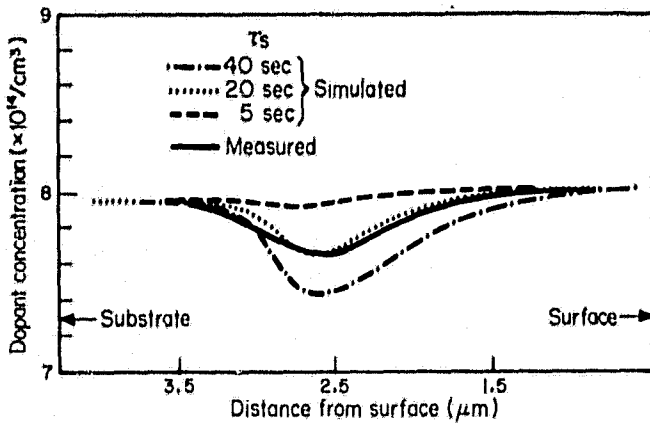


Fig. 8 Solid line: experimental dopant profile. Dashed and dotted lines: simulated dopant profiles for different values of  $\tau_s$ .

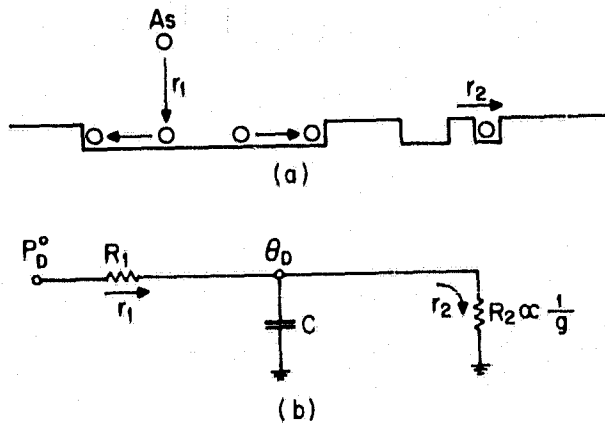


Fig. 9 Model for dopant incorporation into growing silicon epitaxial films: (a) steps taking part in the doping process; (b) equivalent circuit representing the doping process.

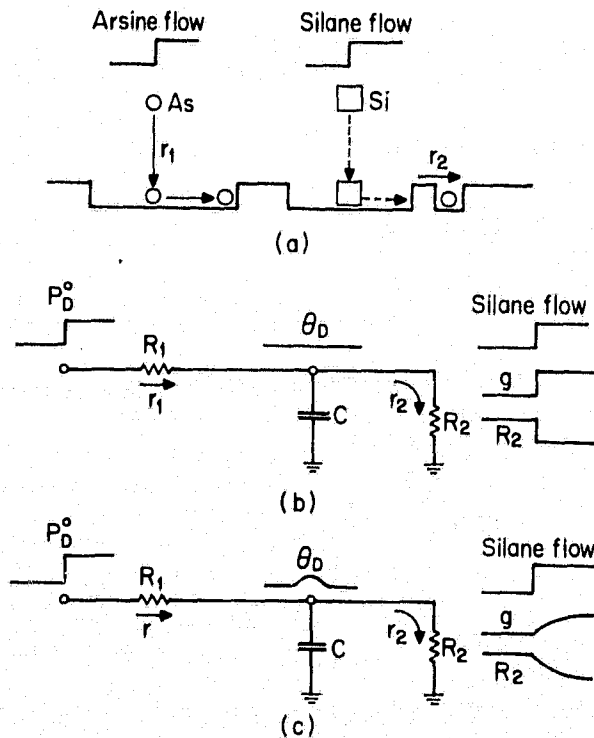


Fig. 10 Physical model used to explain the behavior of the epitaxial system: (a) steps taking part in the doping process and silicon growth; (b) equivalent circuit with  $R_2$  changing "instantaneously"; (c) equivalent circuit with  $R_2$  changing gradually.

## DISCUSSION

LUTWACK: Does your model take into account surface saturation, that is, saturating the capacity of your electrical analog? If it does not, what would happen if you did saturate in view of the time constants which you have found? Would you get competition or inhibition?

REIF: When you saturate, you reach the equilibrium condition. This is as much as you can take and that's it. It doesn't affect the value of the time constant per se, but saturation in this model means just reaching thermodynamic equilibrium.

OLSON: How do you account for mixing in the gas phase of your dopant or your silane concentration? In other words, you apply a step function, I suppose, in the flow controller but that does not mean that the surface is going to see a step function in the arsenic or arsine concentration.

REIF: That is a very good question. I hope I have a good answer. If you estimate how long that delay can be, it is very negligible compared to 40 seconds. There will not be a perfect step function due to the diffusion of species or some other effect. But if you calculate how much distortion there will be, it won't be distorted by anything appreciable compared to 40 seconds.

OLSON: This is interesting for the people who grow gallium aluminum arsenide. Gallium aluminum arsenide has super lattices with lattice spacings on the order of 100 to 200 Å. What they found in that study was that if a commercial CVD reactor with the large tube diameters and the long entrance lengths was used, there was no way to grow those lattices.

REIF: But how do you know that that is a gas-phase problem?

OLSON: They were able to show that it was a gas-phase problem basically by reducing the entrance length and preventing the mixing in the gas phase. Because what is needed is a step function in order to grow the superlattice.

REIF: It depends on the system. For instance, that's why I emphasize the horizontal system that I used. If you consider a pancake vertical system, and Professor Dudukovic showed one, for instance, in his talk, there's a problem with the gas-phase mixing, and it will cause the addition of another sort of time constant. It will be very appreciable. So it depends on what kind of dead part there is in a particular system. In a horizontal system there are very small dead parts in which gas-phase mixing and non-moving gas storage can occur. For instance, in a pancake reactor with silicon that type of thing happens. I wouldn't be surprised, although I haven't done the experiment, that you would see even more gradual transitions than you see here, because you have this effect plus that other you are talking about.

MILSTEIN: It would appear from your last couple of graphs that your time constant is not the same on both sides of the bump. In other words, it fits on one side and it does not fit on the other.

REIF: You mean the left and right side?

MILSTEIN: That's right. It's an asymmetric bump, and the implication of that is that there has to be something very strange going on.

REIF: Well, are you familiar with the capacitor voltage techniques for measuring? Let's look at the figure again just to get a feeling of the kind of errors we could be talking about here. Look, this is  $7 \times 10^{14}$ ; this is  $8 \times 10^{14}$ ; we are talking about  $2 \times 10^{13}$  or so. That difference should not be bothersome if you understand the nature of the measurements. I am very happy to see a bump and a dip. If you try to estimate, you know that it's not about 5 seconds; it's not that short. It is not like the phosphorus or arsenic transitions which were long and you can measure them on the peaks very nicely. These are very, very shallow dips and peaks and the limitations of these are --

MILSTEIN: Your point is well made.

DUDUKOVIC: Are there a lot of possible transients to consider when you calculate the time constants for your system? Would you calculate the time constants for other possible transients in your system? Certainly, the transient for the flow would not be a problem but what about the diffusion transients and others?

REIF: We did that, and it is in the literature. It's a fraction of a second to a second. So it's really quite negligible compared to what we measured.



# CHEMICAL VAPOR DEPOSITION OF SILICON FOR OPTICAL USES

M.R. Jacobson, D.C. Booth\*, and P. Hey  
Optical Sciences Center, University of Arizona  
Tucson, Arizona 85721

\* Present Address: 38 Durand Place, Irvington, N.J. 07111

## I. INTRODUCTION

### 1. History of CVD; CVD of Silicon

Since 1880, when first applied in the incandescent lamp industry, chemical vapor deposition (CVD) has been employed in a diverse group of technologies. At present, CVD plays vital roles in microelectronic, wear- and radiation-resistant coatings, fiber optics, and the purification and fabrication of exotic materials, from ultra-low expansion glasses to high-purity refractory metals. With the notable exception of fiber optics, the application of CVD to optical, and to "macroelectronic," problems has been much more limited. This is unfortunate, since the advantages of the technology have been demonstrated in the areas just listed.

The challenge of photovoltaic conversion is necessarily "macroelectronic," in that relatively large areas must be exposed to the sun, even with concentrating optics, to collect sufficient energy. At the same time, the tight control over composition and structure with depth characteristic of microelectronics production must be maintained. CVD silicon is a proven material in microelectronics; we are exploring CVD amorphous silicon (a-Si) as a photovoltaic material, and hope to develop the technology to produce uniform, efficient a-Si films over sufficiently large areas.

CVD silicon was deposited from the hydrogen reduction of  $\text{SiCl}_4$  on several occasions during the first three decades of this century. (1) During the 1960's, the stringent requirements of the electronics industry led to the development of new CVD technologies for integrated circuits; the pyrolysis of silane and chlorosilanes began on a large scale during this period. (2) During the 1970's, the technology broadened to include glow-discharge assisted CVD.

### 2. Physical Fundamentals of CVD

Picture a mixture of gases, a chemical vapor, flowing through a vessel. This chemical vapor can be mixed so that a chemical reaction, resulting in both solid and gaseous products, is possible. The possibility of chemical reactions depends on the availability of a certain activation energy, or trigger. If we place a substrate in the vessel and heat it to the proper temperature, the hot substrate can trigger the desired chemical reaction and serve as the foundation for the solid reaction products. The gaseous reaction products are entrained in the gas stream and exhausted from the cavity. The reaction normally takes place below or at atmospheric pressure, and the substrate can be heated by optical, infrared, or radio frequency radiation. We have, then, deposition from a chemical vapor, or CVD. This term distinguishes the process

from the commonly employed processes of physical vapor deposition, or PVD, which includes evaporation and sputtering. PVD processes normally do not involve chemical reactions; rather, they exploit changes in the physical state to transform material from a bulk source into a thin film.

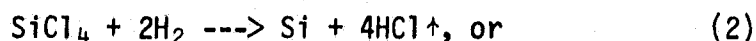
CVD has three major advantages over most other thin film deposition techniques. First, the process allows tight control over gas stream flowrate and composition, which leads to predictable and repeatable film composition and to graded structures, if desired. Second, the thermal activation of the reaction establishes thermal equilibrium at the site of film deposition, producing tight, highly coordinated structures. Third, the throwing power of CVD is excellent. (3,4)

The pyrolysis of silicon is dominated by three reactions:

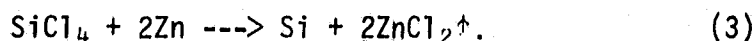
1. The pyrolysis of silane,



2. The hydrogen reduction of  $\text{SiH}_4\text{Cl}_2$ ,  $\text{SiHCl}_3$ , or  $\text{SiCl}_4$ ; for example,



3. The metal vapor reduction of  $\text{SiH}_2\text{Cl}_2$ ,  $\text{SiHCl}_3$ , or  $\text{SiCl}_4$ ; for example,



While the reactions appear simple, it is important to appreciate that the actual chemistry taking place at the surface of the hot substrate is usually rather complex, involving intermediate products and side reactions of unused reactants with reaction products and contaminants.

### 1.3 Engineering Fundamentals of CVD

Uniform heating of the substrate is critical to uniform, controllable coatings. Two strategies can be employed to this end, distinguished by the wall temperature of the reaction or containment vessel. In a hot wall reactor, the vessel has the dual role of containing the reactants and heating the substrates placed inside. Either resistance heaters or radio frequency generators are utilized in hot wall reactors. Cold wall reactor vessels are transparent, so that power from either radio frequency generator coils or from bright lamps is transmitted directly through the walls of the vessel to the susceptor, typically a silicon carbide-coated graphite block, which supports the substrate and acts as a heat reservoir. Other process parameters useful in classifying reactors are the attainable substrate temperatures and the total gas pressure. On this basis, reactors for CVD can be divided into three groups, based on substrate temperature, reactor wall temperature, and total gas pressure: (4)

a) Low temperature, atmospheric pressure reactors, which are used when substrates or adjacent thin film layers cannot withstand high temperatures. Usually, resistance or radiant heating units are employed in either batch or continuous production systems. In batch units, gases either flow through a horizontal tube over horizontal, stationary substrates or flow down to the bottom of a bell jar, where horizontal substrates rotate on a heated plate.

In continuous systems, a belt carries substrates under either premixed or nozzle directed gases.

b) High temperature, atmospheric pressure reactors are either hot- or cold-wall, depending largely on whether the reaction is exothermic or endothermic, respectively. Hot-wall reactors use resistance heaters and are often tubular; the hot walls encourage deposition on the substrate rather than the chamber. Cold-wall reactors rely on either induction or radiant heating in order to direct energy to the substrate where endothermic reactions and deposition will be promoted. Cold-wall systems include horizontal tubes, vertical tubes with descending flow, and bell jar systems with either ascending or descending flow.

c) High temperature, low pressure reactors must employ large capacity roughing pumps to maintain a moderate vacuum. Typical LPCVD systems incorporate horizontal tubes; the samples can be closely spaced vertically, since diffusion lengths are much longer. Resistance heaters produce hot walls, but wall deposits tend to be adherent, and the vertical substrates are less effected by contamination. Unlike the ambient pressure systems, carrier gases are not needed.

## II. CVD a-Si FOR PHOTOTHERMAL APPLICATIONS

Our program for developing amorphous silicon films was originally aimed at high temperature photothermal solar energy conversion. Before describing the preparation, characterization, and properties of CVD a-Si, we will briefly review our photothermal program. Our interest in the high operating temperature range, that is,  $T_0 > 350$  C, sharply reduced the number of available materials. We were further restricted by the need to match the optical properties of the surface to the solar input and thermal reradiation. Figure 1 shows the AM1 solar spectrum for concentration ratios of 1, 10, and 100, and blackbody emittance spectra for operating temperatures of 100, 300, and 500 C. For the 500 C blackbody, the wavelength of minimal overlap of the solar and the thermal spectrum is approximately  $2 \mu\text{m}$ . To perform effective photothermal conversion, it is necessary to find a material that absorbs strongly from 0.35 to  $2 \mu\text{m}$ , and reflects well for wavelengths longer than  $2 \mu\text{m}$ ; such a material is considered spectrally selective. Because no single material exists with a spectral profile suitably close to this ideal step function, we chose to work with a dark mirror design. (5) This consists of a thin film stack with a highly absorbing material in the solar spectral region overlaying a material highly reflective in the infrared. Silicon was chosen for several reasons: it is relatively inexpensive, easily deposited by CVD, and its absorption edge lies in the near infrared. In addition, silicon's melting point is high, suggesting durability at high  $T_0$ .

Of the three groups of CVD furnaces mentioned above, amorphous silicon is usually made in the high temperature, atmospheric pressure environment. Within this group, we can further classify systems by means of heating: radiative (lamps), resistive, and RF inductive. Radiatively heated systems heat primarily the susceptor/substrate combination, leaving the reactor walls and the source gases relatively cool. This prevents coating of the reactor cavity, permitting the use of an optical thickness monitor viewing the growing film through the cavity walls. Such systems also heat and cool in minutes,

allowing sample transfer from the reactor at temperatures low enough to prevent substantial oxidation. Hot wall reactors heat the entire cavity including the walls, resulting in an opaque wall which eliminates optical monitoring. Such furnaces, however, do produce a very stable, uniform temperature profile which produces films with very uniform thicknesses. RF induction furnaces share many of the advantages of the cold wall, radiatively heated systems, but heat substrates much more efficiently. Problems may arise with substrate geometry when coupling the RF field into the susceptor/substrate combination. The RF field can also interfere with the operation of any thermocouples in the cavity. (See Figure 2).

Figure 3 diagrams our silicon deposition system, including the source gases and monitoring system. (6) Because we employed pyrolysis, we chose hydrides for source gases since they decompose more readily at lower substrate temperatures. Representative parameters for preparing a-Si and a-Si:X films are:

Concentrations:

1. Helium as a carrier/diluent gas at 4 l/min;
2. Silane as the silicon source at 0.1 to 0.5% total volume;
3. Alloyant source gases at 1 to 200% of the silane value;

Substrate Temperatures:

1. 525 - 650 C for nonalloyed a-Si;
2. 575 - 850 C for various a-Si:X alloys;

Deposition Times and Rates:

1. Times of 10 to 100 minutes and rates of 50 to 1500 Å/min.

Measurement and characterization techniques were primarily oriented toward optics and structure. Film thickness was measured by using an  $\text{HNO}_3/\text{HF}$  mixture on as-deposited films to etch steps, which were then measured with a Dektak profilometer. Film composition was determined by electron probe microanalysis (EPMA). This method requires standards with well-established compositions which approximate those of the unknown material. Our standards included crystalline silicon, pc-SiC,  $\text{Si}_3\text{N}_4$ , and diamond. The reflectance and transmittance of selected films were measured in the range of 0.35 to  $15\ \mu\text{m}$  using two spectrophotometers. The refractive index was calculated from the film thickness and the location of interference fringes in the spectral region where the films were transparent. The absorption coefficient was computed from thick film formulae considering film thickness, transmittance (averaged where interference occurs), and the previously calculated refractive index. (7) We determined film structure with a General Electric XRD-5 diffractometer operating with Cu K-alpha X-rays and a Ni filter. In general, only the Si(111) diffraction line was detectable (6,9); the appearance and growth of this line monitored the change in structure from amorphous to partially crystalline. Unfortunately, this is essentially a bulk determination and is not capable of resolving the formation of small polycrystalline clusters as they form. In general, at least 10 volume percent of the film must crystallize before an adequate X-ray line can be seen. Crystallization temperatures were determined by annealing films at incrementally longer times at high temperatures, during which optical and structural changes were monitored. A typical annealing temperature was 900 C for films containing 10 to 30 at% C, with annealing times of 15, 30, 60, 120, and 240 minutes.

The silicon used in our selective surface stacks has evolved as we worked to improve their optical efficiency. The first design used pc-Si deposited on stabilized silver reflector layers, resulting in absorptances of 71% and emittances (based on a 500 C blackbody) of 6% (9,10). Because of the predicted advantages of a-Si (11), we determined and achieved the proper process parameters to produce CVD a-Si. At the same time, we began to replace the silver layer with molybdenum, a refractory element easily deposited by CVD with high infrared reflectance and good thermal stability. (12,13) However, long tests, to 1500 hours at 500 C, revealed that the a-Si layer of the stacks on silver or molybdenum crystallized too quickly. Work then began on alloying silicon with small, light elements such as carbon and nitrogen, using the flexibility of CVD. We found that 15-20 at.% carbon resulted in a-Si:C films with a red-shifted absorption coefficient, enhancing their absorptance and in improved structural stability, to 700 C for several decades. (14) Figure 4 shows the absorption coefficient of pc-Si, a-Si, and a-Si:C (20 at.% C) as a function of photon energy.

Having largely stabilized a-Si against crystallization, these a-Si:C films had to be incorporated into existing tandem stack designs. Substituting molybdenum for silver as the reflector layer strongly affected its interaction with the absorber layer. Figure 5 shows the spectral reflectance of three stack designs: silver/a-Si(1.5 $\mu$ m), molybdenum/a-Si (1.5 $\mu$ m), and molybdenum/a-Si:C (700 A). In the first case, the absorber and reflector layer do not interact strongly, so that the stack can be considered as an absorber from 0.35 to 1  $\mu$ m, and a reflector from 1 to 15  $\mu$ m. In the second case, the silicon, both alloyed and unalloyed, produces a strong antireflection effect when deposited on the molybdenum layer, resulting in very deep interference fringes for sufficiently thick a-Si films. Such a stack would emit strongly in the infrared at operating temperatures of 500 C. In the third case, the thickness of the silicon layer has been reduced to eliminate interference fringes in the thermal infrared. At this thickness, the silicon film functions both as an absorber and an antireflection layer. After modeling the performance of such stacks using a multilayer thin film program, and empirically determining an optimal configuration, we were able to produce selective surfaces with a solar absorptance of 77%, an emittance (500 C blackbody) of 4.0%, and an a-Si thickness of 700-800 A covered by a 500 A Si<sub>3</sub>N<sub>4</sub> A film. We projected thermal stability against crystallization for decades at temperatures somewhat above 700 C (6). Further work should improve stack absorptance by at least 10%, while the emittance value represents an upper limit since the 500 C emittance of bare CVD molybdenum is 3.5%. Of course, tradeoffs in emittance will be necessary to reach a larger absorptance value.

### III. CVD a-Si FOR PHOTOVOLTAIC APPLICATIONS

In the course of our photothermal research, especially that involving alloying of the a-Si material, we became interested in its photoelectric properties. It turns out that CVD amorphous silicon is a promising photovoltaic material due to the match of film thickness, penetration depth of light and electronic properties such as carrier diffusion length and space charge layer width. The collection efficiency of a solar cell is influenced by all of these factors. Photons can only be absorbed and converted within the active region of a cell, which is determined by the electronic properties

of the material, i.e., the ability to form space charge layers which can separate photogenerated electron hole pairs. Here we find the potential of a-Si. With an optical absorption ten times higher than its crystalline counterpart, films as thin as  $1\text{ }\mu\text{m}$  are needed, which are easily deposited. The emphasis of our research was consequently put on matching electronic properties to these encouraging optical characteristics.

As deposited CVD a-Si films show a considerable defect density due to broken or strained bonds in the amorphous matrix. ESR measurements of approximately  $10^{19}$  spins per  $\text{cm}^3$  are confirmed by field effect measurements, meaning that approximately 1 in 1000 atoms has an unpaired electron due to an incomplete bond. The defect density was shown to decrease with lower  $T_s$  (Figure 6) (15), while the hydrogen concentration in the films measured by SIMS increases due to the incomplete breakup of silane. These observations confirm the generally accepted model that hydrogen acts as a defect compensator in a-Si. They show in particular that only fractions of an atomic percent of hydrogen can influence the electronic properties of a-Si and that the high (20-30 at.%) hydrogen concentrations in glow-discharge produced films are not needed. (16)

To evaluate further the role of hydrogen in CVD a-Si we have investigated the effects of a postdeposition hydrogen treatment. The high diffusion constant of atomic hydrogen at temperatures well below the crystallization point (675 C) of CVD a-Si was utilized to diffuse additional hydrogen into the amorphous matrix. An RF generator created a weak hydrogen plasma at 0.5 - 1 Torr, while resistive heating of a susceptor decoupled the sample temperature from plasma conditions. Samples were typically treated for 30 minutes at temperatures between 400 and 550 C. A comparison between  $\sigma_d$  and  $\sigma_{ph}$  as functions of  $(1/T)$  before and after postdeposition hydrogenation shows that the additional hydrogen has an extremely beneficial effect on the electronic properties of the material.

We observe that the low temperature branch of the dark conductivity, usually correlated to the hopping conduction mechanism through defect states, is appreciably reduced and its onset (the knee in the curve) is shifted to lower temperatures as the hydrogenation temperature,  $T_H$ , is increased. Moreover, a profound improvement in the photoresponse can be measured. While photoinduced currents in as-deposited silicon can only be detected near liquid nitrogen temperatures we see in Figure 7 that order of magnitude differences between  $\sigma_d$  and  $\sigma_{ph}$  are typical, after postdeposition hydrogenation. These observations can be interpreted as a reduction of defect states in the film due to the hydrogenation.

To distinguish hydrogen remaining from the incomplete breakup of the silane molecule from hydrogen diffused into the film after deposition, we prepared a sample set at  $T_s = 500, 600, 650\text{ C}$ , which consequently underwent the same hydrogenation treatment. As seen in Figure 8, the original variation of electronic properties is still mirrored in the  $\sigma(1/T)$  curves after hydrogenation. We conclude that hydrogen incorporation during film growth determines the overall film structure, while the postdeposition hydrogenation enhances the electronic properties of that original structure. This role can be compared to the "touching up" action of fluorine in a-Si:F:H. (17)

9  
Y

Addition of  $\text{PH}_3$  or  $\text{B}_2\text{H}_6$  to the gas phase produces doped films. Both the activation energy  $E_A$  and the room temperature conductivity  $\sigma_{RT}$  change drastically. Once a certain threshold concentration of dopants is reached (Figure 9), highly conductive films can be prepared. Corresponding field effect measurements indicate that electron (hole) accumulation dominates for phosphorus (boron) doped films, respectively.

Postdeposition hydrogenation of phosphorus-doped films results in the liberation of additional donors, as is evidenced by the earlier onset of the doping action in Figure 10. The defect compensation of phosphorus has been discussed earlier; apparently the hydrogen relieves some of the dopant atoms from their defect compensation, thus enabling them to perform as dopants. Preliminary Schottky barriers, with a molybdenum layer covered by hydrogenated a-Si and covered, in turn, by a semitransparent nickel layer, have shown efficiencies of up to 2.1% without antireflection coatings.

#### IV REFERENCES

- 1) Powell, C.F., Oxley, J.H., Blocher, J.M., Jr., "Vapor Deposition," (John Wiley, New York, 1966) pp. 1, 251-253.
- 2) Weisberg, L.R., and Cullen, G.W., Chemical Vapor Phase Deposition of Electronic Materials, Special Issue of the RCA Review 31,4 Dec. 1970.
- 3) Holzl, R.Z., "Chemical Vapor Deposition," in Bunshah, Ed., Techniques of Metals Research, Vol. 1, Part 3 - Techniques of Materials Preparation and Handling, Chapt. 33 (Wiley, New York, 1968).
- 4) Kern, W., and Ban, V.S., "Chemical Vapor Deposition of Inorganic Thin Films," in Vossen, J.L., and Kern, W., Eds., Thin Film Processes (Academic Press, New York, 1978) p. 258.
- 5) Hahn, R.E., and Seraphin, B.O., "Thick Semiconductor Films for Photo-thermal Solar Energy Research," J. Vac. Sci. Technol. 12 (1975) p.905.
- 6) Booth, D.C., "The Retardation of Crystallization of CVD Amorphous Silicon and the Study of its Structural and Optical Properties," Ph.D. Dissertation, University of Arizona, 1981.
- 7) Connell, G.A.N., Paul, W., and Temkin, R.J., "Amorphous Germanium: III" Optical Properties, Adv. Phys. 22 (1973), p. 643.
- 8) Janai, M., Allred, D.D., Booth, D.C., and Seraphin, B.O., "Optical Properties and Structure of Amorphous Silicon Prepared by CVD," Solar Energy Materials 1, 11, 1979.
- 9) Gurev, H.S., and Seraphin, B.O., "Progress in Chemical Vapor Deposition of Thin Silicon Films for Solar Energy Conversion," Fifth International Conf. on CVD, Electrochemical Society, Princeton, N.J., 1975, p. 667.

- 10) Masterson, K.D., "Spectrally Selective Surfaces for High-Temperature Photothermal Solar Energy Conversion," Proc. SPIE, 68, 1975, p. 147.
- 11) Seraphin, B.O., and Meinel, A.B., "Photothermal Solar Energy Conversion and the Optical Properties of Solids," in Seraphin, B.O., Ed., Optical Properties of Solids - New Developments, North-Holland, 1976, p. 927.
- 12) Carver, G.E., and Seraphin, B.O., "Chemical Vapor-Deposited Molybdenum Films of High Infrared Reflectance," Appl. Phys. Lett., 34 (4), 1979.
- 13) Carver, G.E., "CVD Molybdenum Films in Photothermal Converters," Solar Energy Materials, 1, 1979, p. 357.
- 14) Booth, D.C., Allred, D.D., and Seraphin, B.O., "Stabilized CVD Amorphous Silicon for High Temperature Solar Energy Conversion," Solar Energy Materials, 2, 1979, p. 107.
- 15) Zesch, J., Xerox Palo Alto Research Center, Private Communication, 1982.
- 16) Hey, P., Raouf, N., Booth, D.C., and Seraphin, B.O., in Tetrahedrally Bonded Amorphous Semiconductors, Carefree, Arizona, 1981, American Institute of Physics Conf. Proc. 73, p. 58.
- 17) Hey, P., and Seraphin, B.O., "The Role of Hydrogen in Amorphous Silicon Films Deposited by the Pyrolytic Decomposition of Silane," Solar Energy Materials, to be published.

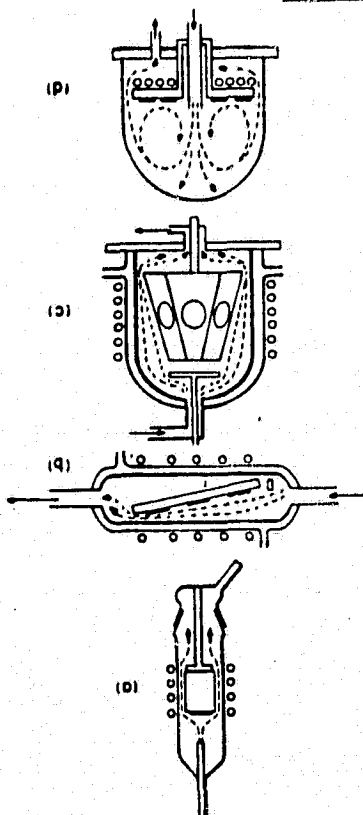
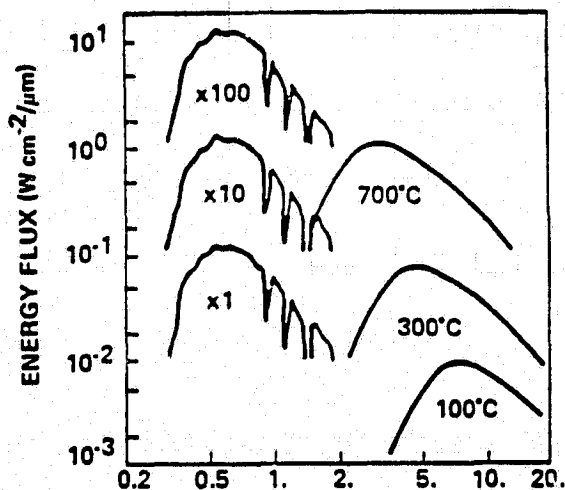


Figure 1. Schematic representation of reactors used for CVD of silicon: a) pedestal, b) horizontal, c) barrel, and d) pancake. From reference (4).

Figure 2. Spectral profile of the energy flux of solar input for three concentrations, and of reradiative loss at three converter temperatures.





ORIGINAL PAGE IS  
OF, POOR QUALITY

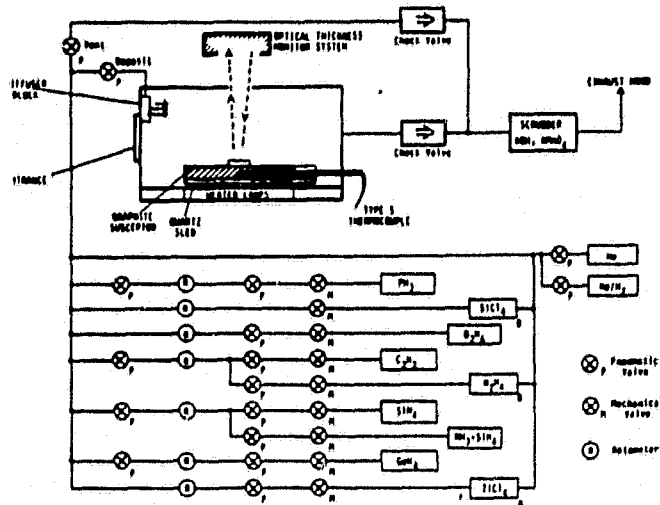


Figure 3. Schematic of CVD deposition system at University of Arizona including reactor and gas system.

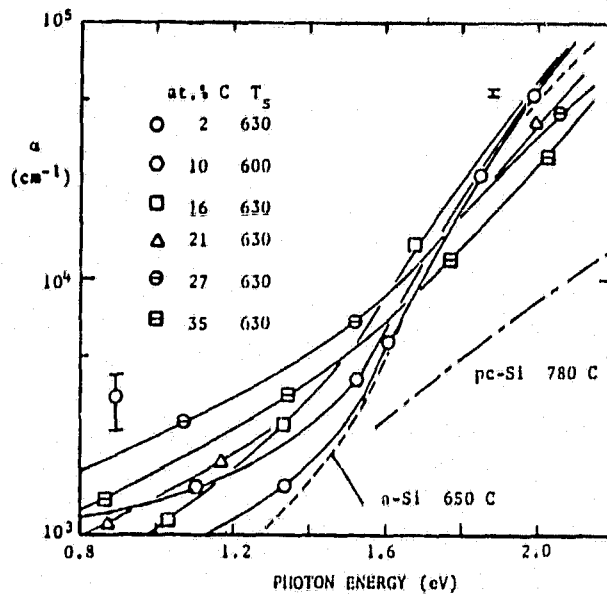
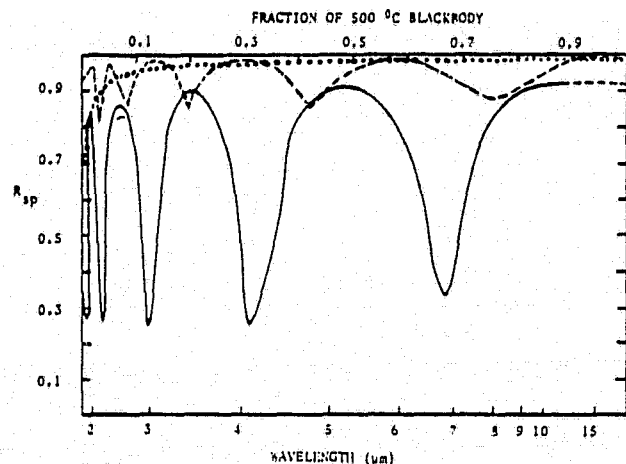
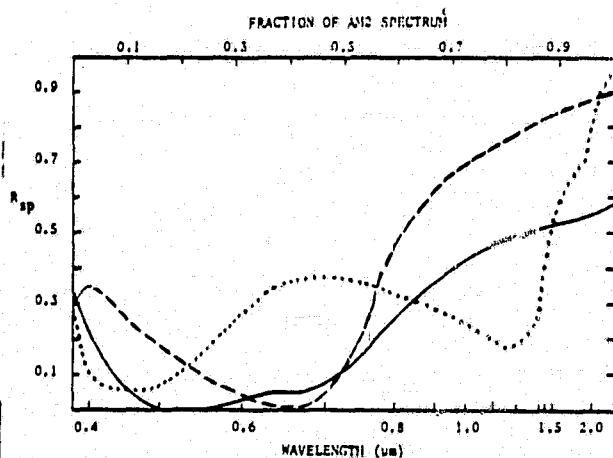


Figure 4. Absorption coefficient of a-Si:C alloys as a function of carbon concentration and photon energy, for fixed T<sub>s</sub>.

Figure 5. Measured specular reflectance R<sub>s</sub> of three tandem stacks:  
 - - - Si/Ag 1.6 μm - Si  
 — Si/Mo 1.4 μm - Si  
 ..... Si/Mo 60 nm



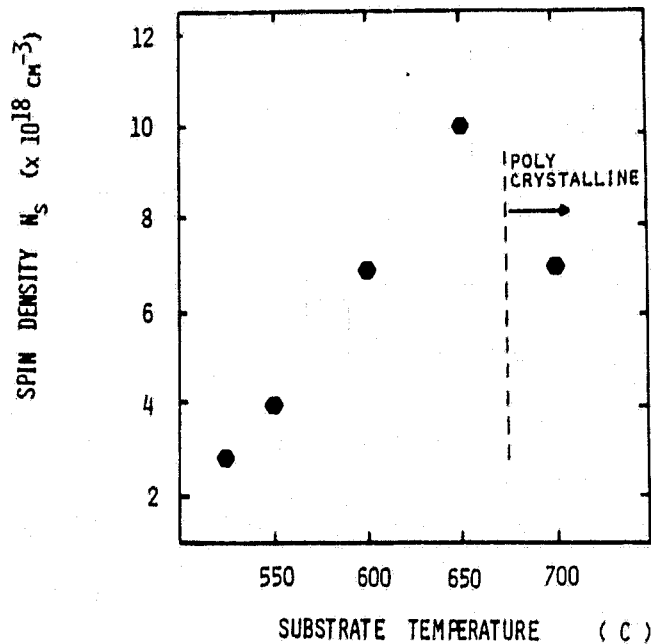


Figure 6. Spin density as measured by ESR as a function of  $T_S$  for CVD a-Si films (15).

Figure 7.  $\sigma(1/T)$  of hydrogenated a-Si for different post-deposition hydrogenation temperatures.  $T_S=600$  C,  $I_{RF}=27.5$ ,  $t_H=30$  minutes, full symbols= $\sigma_d$ , open symbols =  $\sigma_p$ .

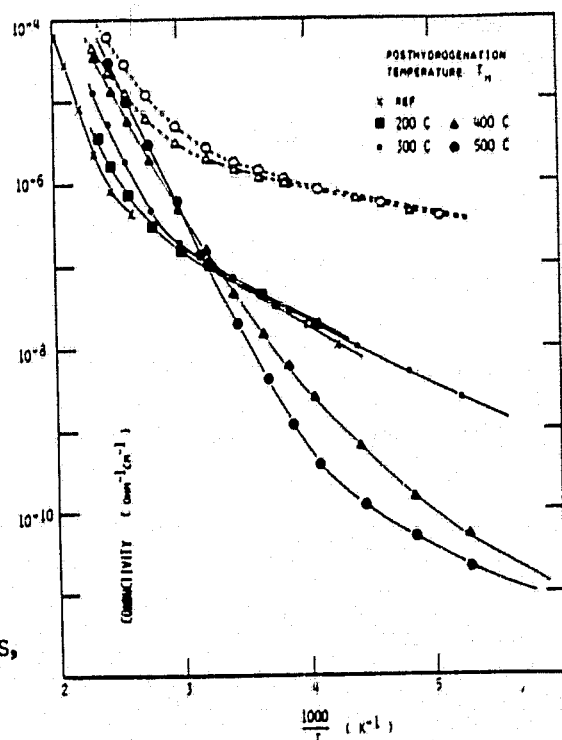
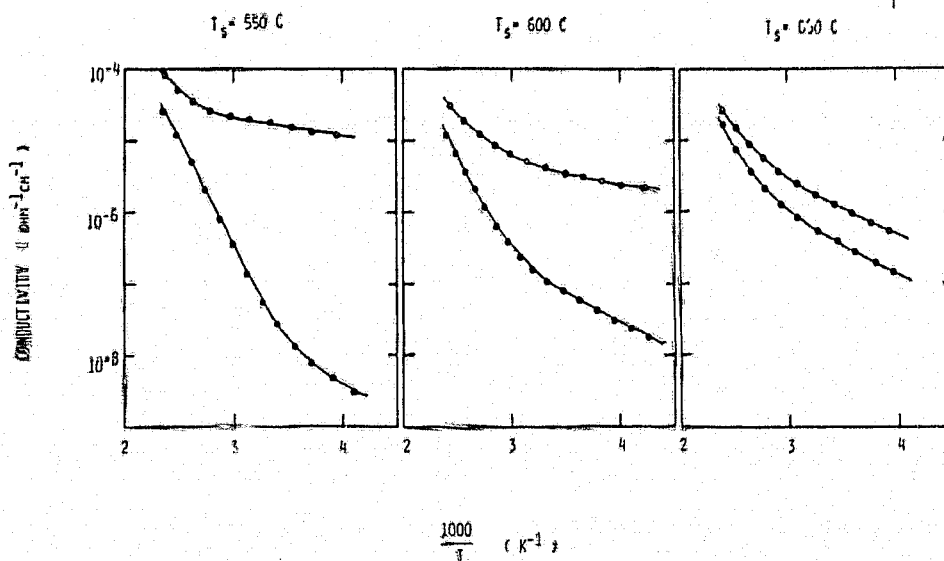


Figure 8.  $\sigma(1/T)$  of samples deposited at different temperatures  $T_S=500, 600$ , and  $650$  C and subsequently hydrogenated at  $T_H = 400$  C.  $I_{RF} = 27.5$ ,  $t_H = 30$  minutes, full symbols =  $\sigma_d$ , open symbols =  $\sigma_p$ .



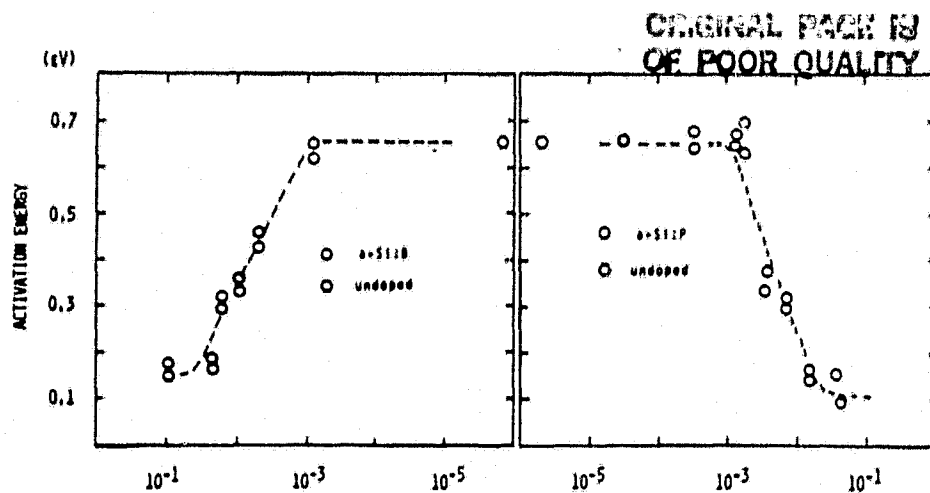


Fig. 9 (a)

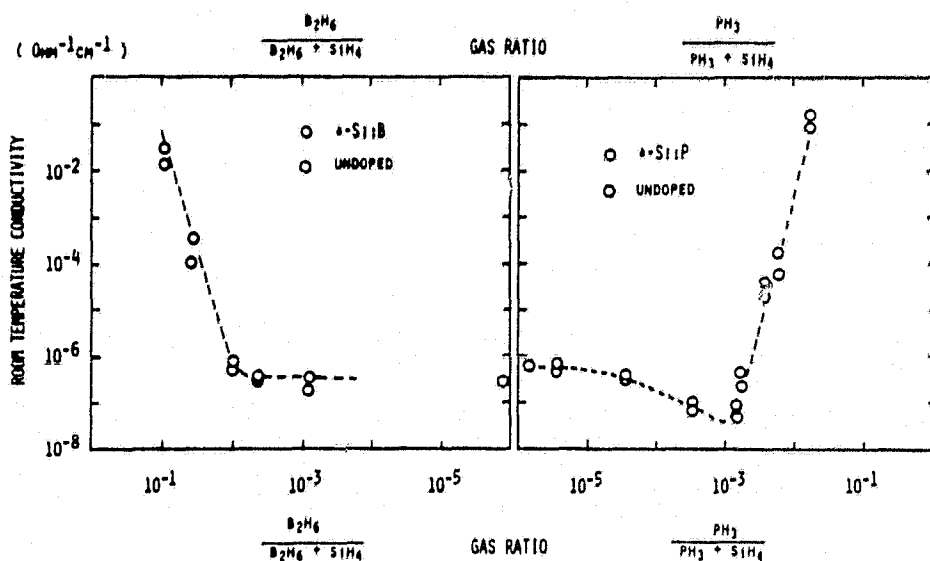


Fig. 9 (b)

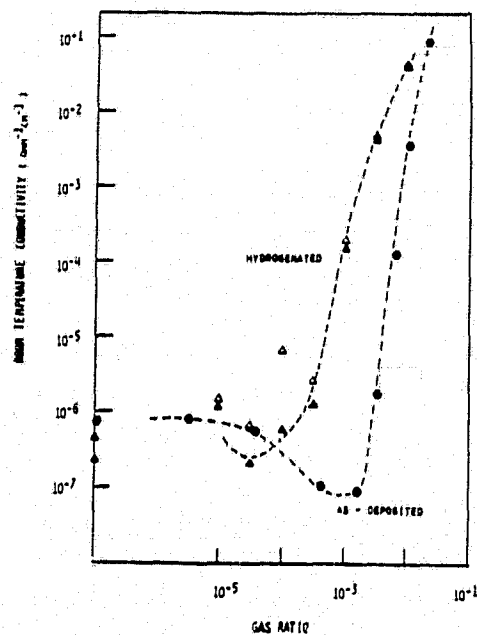


Fig. 9(a) Activation energy of CVD a-Si as a function of doping level.  $T_s = 600$  C.

Fig. 9(b) Room temperature conductivity of CVD a-Si as a function of doping level.  $T_s = 600$  C.

Fig. 10. Room temperature conductivity of CVD a-Si:H:P as a function of doping level.  $T_s = 600$  C,  $T_H = 400$  C,  $I_{RF} = 27.5$ ,  $t_H = 30$  minutes, full symbols =  $\sigma_d$ , open symbols =  $\sigma_p$ .

Fig. 10.

## DISCUSSION

SCOLARO: Did you do experiments below 550°C? It seems to me that you are getting better films at lower temperatures?

JACOBSON: The trouble is that the deposition rates begin to get so low below 550°C for this process that it becomes a difficult endeavor. We are approaching the lower limit of reasonable deposition rates.

SCOLARO: It is really noticeable how much your film improves as you go to the lower temperatures.

## Session VI: Alternative Polysilicon Processes

BRIGLIO (Chairman): In the last two days the talks have centered on the various phenomena in preparing silicon materials, such as reaction mechanisms, nucleation and growth of particles, and deposition processes. In this session we will address three processes that are being investigated as alternatives to the present production processes. On Monday, Jim Lorenz of Union Carbide, described progress by Union Carbide for the silane-to-silicon effort. Now we'll hear about work going on at SERI, Hemlock Semiconductor Corporation and SRI International.

# KINETICS OF SILICON ELECTRODEPOSITION

J. M. Olson, Karen Carleton  
Solar Energy Research Institute  
Golden, Colorado

## INTRODUCTION

The electrorefining of silicon using a silicon permeable  $\text{Si}:\text{Cu}_3\text{Si}$  anode is a promising technique for producing a solar-grade silicon (1). The electrorefining process has yielded, in a single step, a 99.9996% pure silicon in a dense, coherent, bulk form at a projected cost of \$7/kg. Of central importance to this refining technique are the kinetics of the silicon electrodeposition process. The kinetics of the heterogeneous electronucleation of silicon on carbon substrates, for example, will determine, to a large extent, the grain size and surface coverage. The morphological stability of the silicon-electrolyte interface, important from the standpoint of cost, will be affected by the kinetics of the homoelectrodeposition process. In the remainder of the paper we will first give a brief overview of the refining process and then cover some of the theoretical aspects of electrochemical nucleation and growth kinetics. Finally, results for the electrodeposition of silicon on carbon substrates will be presented.

## THE REFINING PROCESS

The basic components of an electrorefining process are: 1) an electrolyte, 2) an impure metal anode and 3) a suitable cathode or deposition electrode. If a small bias potential is applied to the anode, the metal (in our case, silicon) will be selectively transferred from the anode to the cathode. The selectivity is based upon the dispersion of electrochemical reduction potentials for the pertinent metal/metal ion couples. In molten salt systems, reduction potentials are not generally known, but the electronegativity usually scales with the reduction potential. Consequently, those metal impurities with an electronegativity greater than that of silicon (e.g., Cu, B, P, etc.) will tend to remain at the anode. Metals with an electronegativity less than that of silicon (e.g., Al, Ti, Zr, V, Cr, etc.) will, in a closed steady state system, not be segregated and will codeposit with the silicon on the cathode.

A schematic of our experimental electrorefining apparatus is shown in Fig. 1. The electrolyte is a mixture of LiF, KF, and  $\text{K}_2\text{SiF}_6$ . The  $\text{K}_2\text{SiF}_6$  can be formed in situ by reactively dissolving prepurified  $\text{SiF}_4(\text{g})$  in a KF-rich melt. The  $\text{SiF}_4$  is purified by passing it over a solid  $\text{CO}_2$  trap which removes primarily the  $\text{SO}_2$ , an impurity which we found tends to color the melt a pale yellow. A pre-electrolysis of the melt is required to remove dissolved oxides (particularly  $\text{SiO}_2$ ). This is accomplished by applying a potential of 2 V between two large area graphite electrodes. The impurity metals (including

278

Si) are deposited on the cathode and oxygen is discharged at the anode. This pre-electrolysis treatment is considered complete when the current (at 2 V) drops below 1.0 mA/cm<sup>2</sup>.

The impure anode is a composite of silicon and  $\eta$ -Cu<sub>3</sub>Si. It is solidified from a hypereutectic solution of copper and mgSi to form a two-phase system consisting of a primary silicon phase embedded in a Cu<sub>3</sub>Si matrix. Copper has an electronegativity greater than that of silicon and as mentioned will tend to remain at the anode. This composite anode has two important advantages over a simple, single-component (mgSi) anode. First, the eutectic temperature of the Si:Cu<sub>3</sub>Si system is 802° C. This facilitates the casting of "silicon" anode plates, a prerequisite for an efficient, low-cost, electrorefining process (2). Second, the use of this composite as an anode enhances the purity of the refined silicon by about two orders of magnitude as compared to previous work (1,3). This enhancement is due to the semipermeable nature of the  $\eta$ -Cu<sub>3</sub>Si phase. At the temperatures where the process is operated (750°-790° C), we discovered that the diffusion of silicon in the  $\eta$ -Cu<sub>3</sub>Si is greater than 10<sup>-5</sup> cm<sup>2</sup>/s which means that it is not difficult to extract silicon from a Si:Cu<sub>3</sub>Si anode. In contrast, the diffusion of other metal impurities is ostensibly much smaller. Essentially all impurities, independent of their electrochemical properties, tend to remain at the anode. The net result is summarized in Table I where we compare the purity of the mgSi feedstock with that of the refined silicon (1). As you can see all impurities, independent of their electrochemical properties are effectively segregated. Furthermore, recent results (4) suggest that the final purity of the refined silicon is determined more by the purity of the process environment than that of the impure anode. This implies that even purer silicon could be derived from such a refining operation.

#### ELECTROCHEMICAL NUCLEATION AND GROWTH KINETICS

Models of nucleation and growth processes in electrodeposition are characterized by three qualitative parameters (5,6): the growth mode, the limiting growth mechanism and the time dependence of the nucleation process. There are three fundamental growth modes: the growth can be one dimensional (a planar surface growing normal to itself), two dimensional (such as cylindrical nuclei growing radially) or three dimensional (hemispherical or spherical nuclei). Independent from the growth mode is the limiting growth mechanism. This rate determining step in the growth process can be either the interface kinetics (such as adatom surface diffusion or incorporation), the charge transfer kinetics, or the mass transfer of metal ions to the electrode surface. Finally, there are two broad categories for the time dependence of the nucleation process. If all the nuclei form at essentially the same time, nucleation is termed "instantaneous" and the nucleation density and related grain size are readily controlled. If nucleation continues to occur over a period of time, it is considered progressive, and the grain size is more difficult to control.

The growth mode and time dependence of the nucleation process are most easily determined from observations of the initial shape and size of the heterogeneous deposit. The limiting growth mechanism can be determined by a number of electrochemical transient measurement techniques. The first

technique which we will use is called cyclic voltammetry. As the name implies, it is a measurement of the dynamic current response of the system to a cyclical voltage excitation. Quantitative models of the voltammetric response for various electrodeposition mechanisms are available, but are not described here. Rather, qualitative observations of the voltammograms will be used as a basis or guide for experiments with a second, more quantitative technique. This second technique is called chronopotentiometry and is a measurement of the current-time response of a bare electrode to a potential step excitation. In processes other than deposition, the current decreases with time. However, for electrodeposition, once nucleation begins, the current increases due to an increasing surface area and a change from planar to two- or three-dimensional diffusion. This increasing current can be modeled as a function of time and the time dependence will be determined by the growth mode, the time dependence of the nucleation process, and the limiting growth mechanism. For example, for instantaneous nucleation and three dimensional kinetics limited growth (5)

$$I = 2\pi nFM^2 N_0 k \rho^{-1} t^2 \quad [1]$$

For instantaneous nucleation and three dimensional diffusion limited growth (6), the current-time response is given by

$$I = \pi nFM^{1/2} (2CD)^{3/2} \rho^{-1/2} t^{1/2} \quad [2]$$

Here  $N_0$  is the initial number of nuclei,  $k$  is the reaction rate constant,  $M$  and  $\rho$  are the molecular weight and density of the depositing metal,  $D$  and  $C$  are the diffusion coefficient and the concentration of the electrodepositing species,  $t$  is time, and the other terms have their usual meaning.

These models assume that only one process is controlling. Alternatively, more than one process may be considered rate controlling, such as both charge transfer kinetics and mass transfer control. In this case

$$I = (2\pi nFk C N_0 M^2 \rho^{-2}) (\alpha H^{-3} + 4t^{1/2} \alpha H^{-2} \pi^{-1/2} + 4t\alpha H^{-2} \pi^{-1}) \quad [3]$$

where  $H = k/D^{1/2}$  and  $\alpha = \exp(H^2 t) \operatorname{erfc}(Ht^{1/2})$ . This equation, along with those listed above, is used to analyze potential step transients for this system.

#### EXPERIMENTAL DETAILS

A vitreous carbon crucible containing the anode (silicon source) and the molten salt electrolyte is situated in a resistively heated furnace. The anode is solidified in situ from a hypereutectic solution of semiconductor grade silicon (16 w/o) and copper (99.999%). The electrolyte is a mixture of  $\text{KF}:\text{LiF}:\text{K}_2\text{SiF}_6$  (46 m/o:46 m/o:8 m/o).

The KF and LiF are dried in situ at pressures less than  $10^{-2}$  torr by slowly heating from  $100^\circ \text{C}$  up to  $300^\circ \text{C}$ . This drying procedure effectively prevents the formation of hydrolysis products that have a detrimental effect



on the morphology of the silicon electrodeposit. The molten salt is further purified by the pre-electrolysis step, as previously described.

The silicon reference electrode is formed in situ by depositing silicon on a 3 mm vitreous carbon rod. This electrode is stable for 2-3 days. Alternatively, an oxide free, single crystal silicon wafer may be used as a reference electrode. The working electrode is the rounded end of a 3 mm rod of either graphite or vitreous carbon with a geometric area of 0.3-0.4 cm<sup>2</sup>.

The chronoamperometric data are recorded with a Nicolet digital storage oscilloscope which is interfaced to an HP 9825 computer for curve fitting.

## RESULTS

### Cyclic Voltammetry

A typical cyclic voltammogram for the electrodeposition of silicon on graphite is shown in Fig. 2. The inflection at approximately 0 V is characteristic of a quasireversible deposition reaction, and the inflection point coincides with the reversible potential,  $E_0$ , for the silicon redox couple relative to silicon reference electrode. The nucleation threshold or onset of silicon deposition is slightly offset from this reversible potential by the nucleation overpotential. The surface increase loop implies that the area of the growth surface is increasing. This increasing surface area results in a larger current on the reverse scan than on the forward (cathodic) scan, and is due to either two- or three-dimensional growth. This multi-dimensional growth mode is confirmed by SEM micrographs of the initial stages of silicon electrodeposits on graphite; the silicon nuclei are hemispherical in shape. In addition, the nuclei are all the same size implying that the nucleation process is essentially instantaneous. Finally, anodic of  $E_0$  is a small cathodic current which we find is correlated with the prenucleation current of the chronoamperometric measurements (vide infra).

For a totally diffusion-controlled electrodeposition reaction, the current would be independent of the overpotential,  $\eta = E - E_0$ ; such currents are not usually observed in this system. For a quasireversible deposition reaction and currents less than the diffusion-limited value, the deposition rate is under mixed control with diffusion, interfacial kinetics, and charge transfer kinetics playing comparable roles. The contribution from interfacial kinetics is evident in the cyclic voltammogram for a polycrystalline silicon electrode shown in Fig. 3. Note that  $E_0$  is two-valued ( $E_0$  is also the potential where the total current is zero), and that the  $E_0$  for cathodically formed surfaces is 20 mV more negative than the  $E_0$  for anodically formed (i.e., etched) silicon surfaces. Etched surfaces are atomistically rough and require a smaller overpotential for growth than cathodically formed surfaces, that, in this case, are ostensibly smooth on an atomistic scale. This implies that there is an activation barrier associated with the adatom-lattice incorporation step and is probably responsible, along with diffusion and charge transfer kinetics, for limiting the deposition rate.

## Potential-Step Measurements

In Fig. 4, we show a series of potential-step, current-response curves for the electrodeposition of silicon on vitreous carbon. Initially the current is large as a result of double layer charging. This is followed by a current component which decays as  $t^{-1/2}$  and is associated with the prenucleation current observed in the cyclic voltammogram. At some time  $\tau$ , called the incubation time, the onset of nucleation occurs and the current begins to increase with time. To analyze the nucleation component of the resultant current it is first necessary to account for the effects of the prenucleation component. This prenucleation current is most likely a faradaic current associated with the reduction of residual impurities. Such currents are usually extrapolated into the region of interest and subtracted from the total current response to yield, in our case, the nucleation current component. In doing so we found that the current transient associated with the nucleation process was not adequately described by any of the existing theoretical models. This result is not surprising for the models of Equ. [1] and [2]. These models are for purely kinetics- or diffusion-limited growth and we showed in the previous section that for this system, neither case applied. However, the mixed control model (with instantaneous nucleation of three-dimensional nuclei) does not apply in this case either. Although Equ. [3] can be made to fit the nucleation current, the values of the resultant fit parameters are not self-consistent. In addition the fit parameters were also found to be a rather sensitive function of the prenucleation current extrapolation. Efforts in this area are continuing.

The current transients of Fig. 5 show some interesting qualitative features. First, the transients tend to saturate relatively quickly. The saturation is the result of the diffusion fields of individual nuclei overlapping to form essentially one diffusion field, the properties of which are independent of the shape and size of the individual nuclei. The time required to reach saturation is a function of the nucleation density,  $N_0$ , and the degree of stirring or convection in the electrolyte. The rapid saturation observed here is therefore the result of a large  $N_0$  and/or a large degree of convective mixing in the molten salt electrolyte. The latter has been observed directly and is qualitatively much greater than that usually observed in room temperature electrolytes. Second, the incubation time for the onset of nucleation decreases with increasing overpotential. This is expected from classical nucleation theory although the quantitative features are not fully understood. In Fig. 6, we compare potential-step experiments for graphite and vitreous carbon. Though both materials are made of carbon, their incubation times differ by an order of magnitude. One possible reason for this is that vitreous carbon has a greater number of active nucleation sites. This would yield a higher nucleation rate for a given overpotential. It would also imply that the grain size of electrodeposited silicon on graphite should be much larger than that on vitreous carbon. Differences in grain size between the two materials, however, are slight.

## CONCLUSIONS

We have shown that the electrodeposition of silicon from a  $\text{LiF:KF:K}_2\text{SiF}_6$  molten salt electrolyte is a process where the rate is limited by a combination of mass transfer diffusion in the electrolyte phase, interfacial reaction kinetics, and, possibly, charge transfer kinetics. This could possibly account for the stable growth morphology usually observed in this system. Efforts to model the nucleation and growth processes on carbon substrates were not successful, but supplementary qualitative observations indicated that the initial stages of heterogeneous deposition are characterized by the "instantaneous" nucleation of three-dimensional nuclei. This is one of the reasons why it is possible to decouple the silicon grain size from the final growth rate by the appropriate programming of the initial potential-time profile (7).

## REFERENCES

1. J.M. Olson and K.L. Carleton, J. Electrochem. Soc. 128, 2698 (1981).
2. D. Inman and S.H. White, J. Appl. Electrochem. 8, 375 (1978).
3. R. Monnier and J.C. Giacometti, Helv. Chem. Acta, 47, 345 (1964).
4. A. Kibbler, K.L. Carleton, and J.M. Olson (in print).
5. M. Fleischmann and H.R. Thirsk, Adv. in Electrochemistry and Electrochemical Engineering, Vol. 3 (P. Delahay and C.W. Tobias eds.) Interscience, New York (1963).
6. G.J. Hills, D.J. Schriffin, and J. Thompson, Electrochem. Acta, 19, 657 (1974).
7. K.L. Carleton and J.M. Olson (to be published).

ORIGINAL PAGE IS  
OF POOR QUALITY

TABLE I. Typical metal impurity concentration in the mgSi used to form the anode and in the refined, electrodeposited silicon.

Metal Impurity	mgSi (ppma)	Refined Si (ppma)
Al	3400.0	1.0
B	17.0	0.7
Ba	9.4	<0.02
Ca	290.0	<0.07
Cu	---	0.2
Cr	40.0	<0.2
Fe	>2500.0	0.1
Mg	85.0	0.9
Mn	550.0	0.03
Mo	1.4	<0.03
Ni	39.0	<0.1
P	14.5	3.0
S	7.0	0.4
Ti	290.0	<0.1
V	250.0	<0.05
Zr	13.0	<0.03

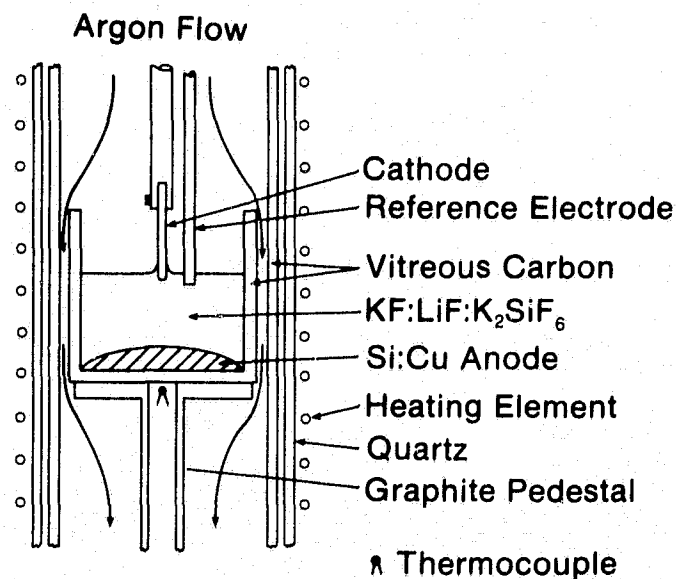


Fig. 1. Electrochemical cell for silicon deposition

ORIGINAL PAGE 13  
OF POOR QUALITY.

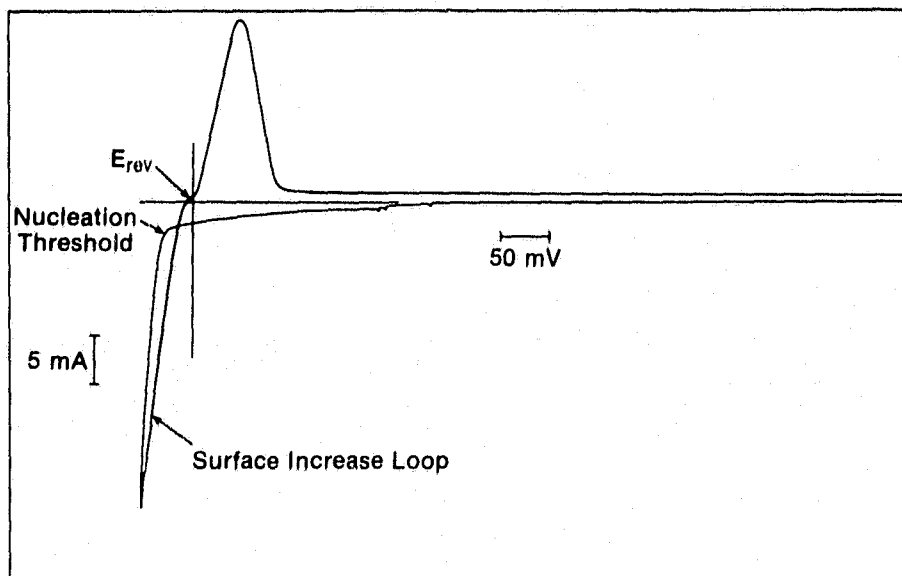


Fig. 2. Cyclic voltammogram for silicon deposition on graphite vs. Si reference in  $\text{LiF:KF:K}_2\text{SiF}_6$ ;  $T = 724^\circ \text{C}$ ; scan rate = 50 mV/s; area = 0.4  $\text{cm}^2$ .

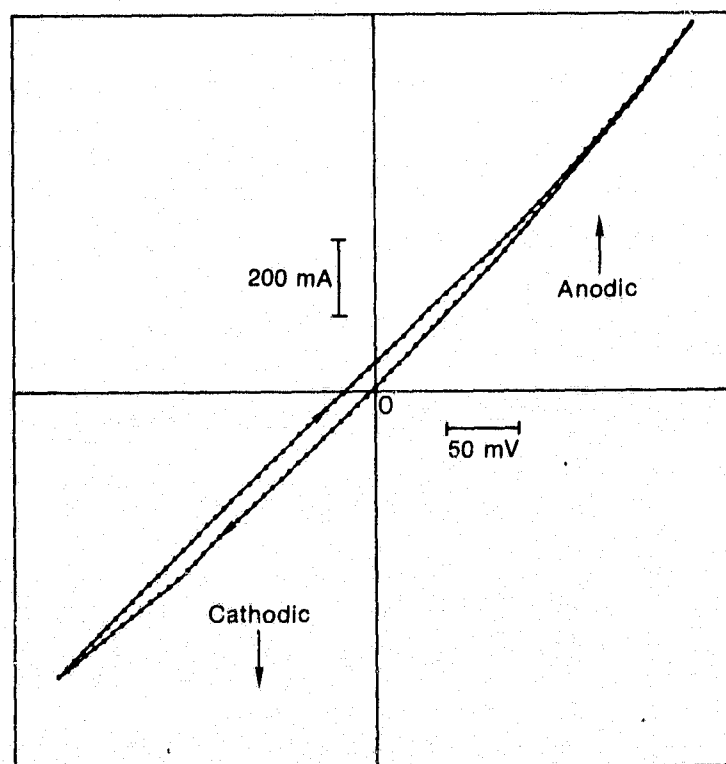


Fig. 3. Cyclic voltammogram polycrystalline silicon electrode in  $\text{KF:LiF:K}_2\text{SiF}_6$  electrolyte;  $T = 790^\circ$ ; scan rate = 1 mV/s; area = 10  $\text{cm}^2$ .

ORIGINAL PAGE IS  
OF POOR QUALITY

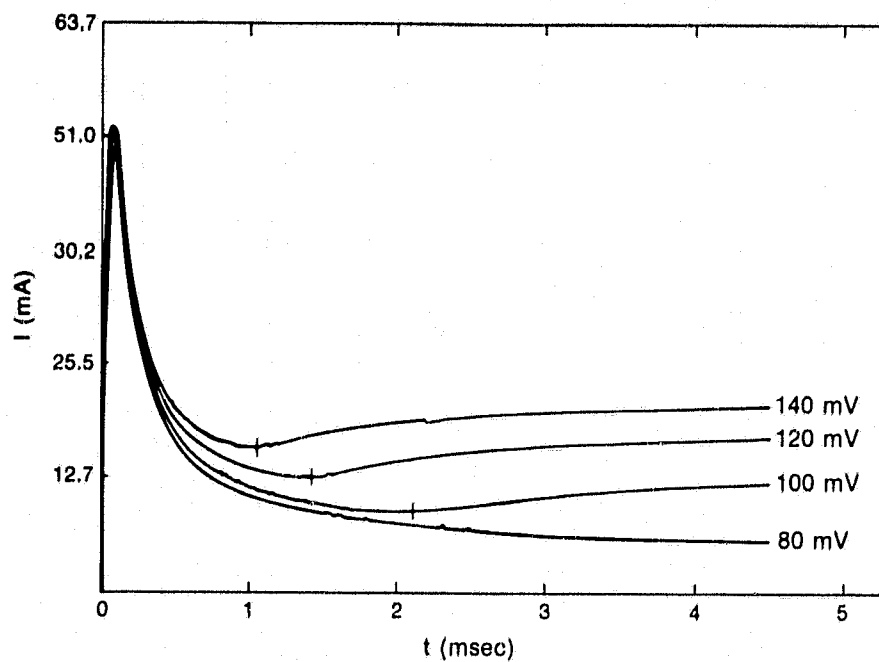


Fig. 4. Cathodic current transients for nucleation of silicon on vitreous carbon; initial potential = +1 V; area = 0.3 cm<sup>2</sup>.

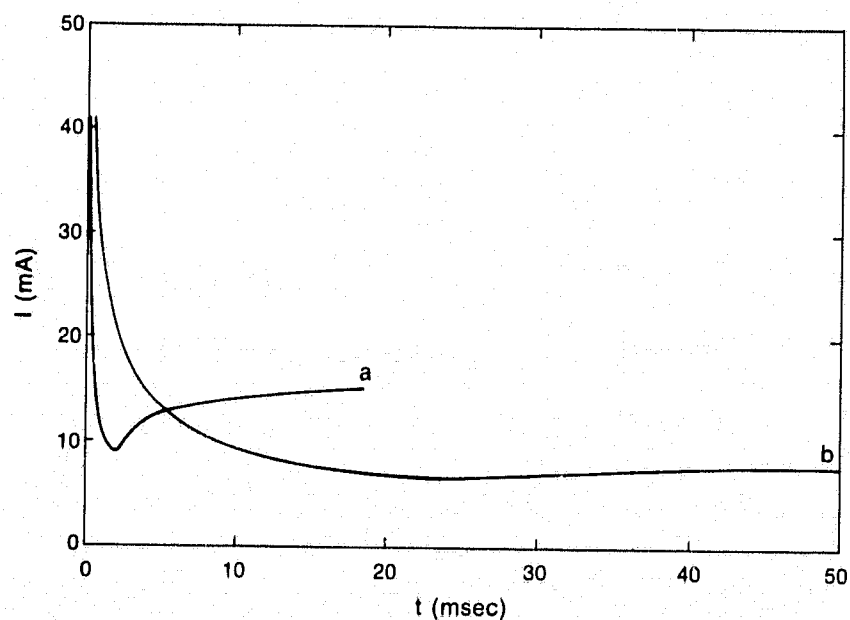


Fig. 5. Cathodic current transients for nucleation of silicon on a) vitreous carbon and b) graphite; potential step from +1 V to -100 mV; area = 0.3 cm<sup>2</sup>.

## DISCUSSION

ATWATER: You talked about nucleation on both vitreous carbon and graphite substrates. I wonder if you could be more specific about the type of graphite you used. We found when we did CVD on graphite that the formation of nuclei is not a function of the chemistry of the material but just the number of terraced ledges and kinks on the surface.

OLSON: This is an AXF Poco graphite. It is very fine grain.

ATWATER: Have you tried polishing the graphite? I would imagine you would have fewer nuclei then.

OLSON: Well, we have done that with almost no change in nucleation density as far as we could see. I don't know if you are familiar with that graphite, but it is fairly well polished as it comes from the manufacturer.

ATWATER: Also, you described something that went all the way toward a finished device. Have you built any devices with the material?

OLSON: Yes, we have made gold Schottky diodes on this material which are identical to controlled gold Schottky diodes produced on semiconductor-grade single-crystalline material. They have the same turn-on voltage, diode quality factors, and things like that. That is a low temperature process, simply evaporation of metal layer on the material. We got very excited and immediately threw the thing in the diffusion furnace to make a p-n junction and essentially got a resistor. No diode characteristics at all. So there is something happening in this material when you heat it up to the 1100°C that is required for the bond diffusion. And, of course, the efficiency was about 0.1%.

JEWETT: Your cyclic voltammogram showed almost nothing going on except your deposition process. Are you doing pre-electrolysis to clean up your electrolyte?

OLSON: Yes, that's one of the things you have to do to get those morphologically stable surfaces. The present dogma is that small concentrations of oxide species, like silicon dioxide, for example, have a very detrimental effect on the morphology of the material, causing it to be dendritic or needle-like in morphology.

JEWETT: Does the rate of deposition change the morphology? Are there problems with treeing and that sort of stuff?

OLSON: Of course. As you go to higher and higher current densities the growth morphology becomes unstable and this is reasonably well understood. Also, impurities can affect that. If you have a large amount of impurities, like an oxide, in there, then the maximum current density that you can run at is maybe 10 ma cm<sup>-2</sup> without dendritic breakdown.

BAILEY: Is there any reason why you couldn't have used a silicon casting which was coated with or plated with copper as your electrode?

OLSON: We have tried things like that, but the problem is that diffusion in this copper silicide is so rapid that it reconstructs fairly easily. If you do something like that, it reconstructs in areas of highest local current density and eventually what you do is essentially blow a hole in the outer copper lining and essentially end up with no diffusional barrier of filtering material between the metallurgical grade silicon and the electrolyte. We tried that, and it doesn't work. At least right now, we think you have to cast the material.

FITZGERALD: You mentioned that many of the impurities stayed behind because of this filtering effect. Could you comment on what fraction end up in the fused salt and how do you end up cleaning that up?

OLSON: Well, we can tell if there are impurity elements in the fused salt. They show up on the cyclicvoltammogram as excursions in the current with potential. So you can monitor the quality or the purity of the electrolyte by just looking at the cyclicvoltammogram. That doesn't change with time. Once we clean it up initially, it tends to remain that way unless we get some contamination from the furnace or something like that. It looks like all the impurities are staying in that metal. I can't give you exact numbers. All I can do is relate what the impurity concentration was initially in the anode and what we see in the cathode.

SCOLARO: It appears that you were not able to extract those elements you thought you could extract very well when compared to some others. The initial concentrations of boron and phosphorus, for instance, were 17 ppmw or something like that, and they went down to 3 or 1.5 ppmw, and something you thought you weren't supposed to separate, like aluminum, was 3200 ppmw and it went down to 1 ppmw. Do you know why you get that kind of effect?

OLSON: Yes. Well, I think we understand. The copper, boron and phosphorus are electrochemically segregated. At least based upon electronegativity. Something like aluminum, titanium, vanadium, and zirconium would not be electrochemically segregated in a normal electrorefining process, such as is found in the aluminum industry, for example. We see very strong segregation independent of the electrochemical properties of the elements. So you have to invoke some other segregation mechanism. The segregation mechanism that I am invoking is filtering of these elements by the lack of solid-state diffusion in the anode.

SETTY: Does the 5 kWh kg<sup>-1</sup> include the energy consumed in making the electrodes?

OLSON: No. That is about another 3 or 4 kWh kg<sup>-1</sup>. It only goes from 25 to 40 cents.

SETTY: What was the electrolyte temperature?



OLSON: The electrolyte temperature was in the range of 750 to 790°C.

SCOTT: Could you say something about the morphology in the orientation of the growth?

OLSON: If we have stable growth morphologies, we are tempted to say that the faces of the little pyramids are 111 facets, although we haven't proven this. This is something that is typically found in polycrystalline material or CVD material, but we haven't measured that sort of thing.

SCOTT: Could you get epitaxial growth on a doped silicon electrode or something like that?

OLSON: We have done that. We did silicon on silicon, and we got epitaxial growth. We got thick epitaxial layers on the order of 1 mm thick. That is a complicated problem; because if there is a thin layer of oxide on the material, the oxide is not conductive and the electrochemical process is dependent upon the transfer of the electrons across that interface. It is very difficult to get an overgrowth on an oxide layer and oxide layers become particularly important in electrochemistry, whereas in CVD they are important but not as important because you deposit to a certain extent on an oxide-covered surface.

MILSTEIN: I think two comments that you might make would have to do with terms of the space-time yield stating that perhaps in metric tons  $m^{-3}$ , and to answer Tom Fitzgerald's question, which dealt with impurities, it might be useful to state the length of the experiment for the reason that the numbers might change in a lengthy experiment.

OLSON: The first comment is well taken. Let's suppose that we were to scale this thing up to 100 metric tons per year. The size of the electrochemical reactor that would produce 100 metric tons per year at a linear growth rate of 100 microns per hour, which we have demonstrated in the laboratory, assuming that we operate the cell for 4000 hours per year (that's approximately 66% duty cycle) would be a medium sized desk. About 2  $m^3$ . In terms of the times that we have operated the process in the laboratory, we have had cells run for a month up to two months before something failed, either a heating element or a power failure. If there were going to be an accumulation of impurities in the electrolyte, we certainly would have seen them in that 1-to-2-month time span; and we didn't. The purity of the material at the end of the run was just as pure as it was at the beginning of the run.

SHANFIELD: When you cited 100 or 200 micron grains, how thick was the layer?

OLSON: You get grain selection. That is the grain size of the top surface. If you look at the grain size on the bottom side, it would be about 5 to 10 microns.

SHANFIELD: So it was about a 100-micron-thick layer.

OLSON: It was a 100- to 200-micron-thick layer.

SHANFIELD: What are the largest grains you have gotten?

OLSON: We have got them up to 1/2 millimeter.

SHANFIELD: With thick deposits?

OLSON: Thick deposits but not with complete surface coverage at this point.

SHANFIELD: Have you made any solar cells out of this material?

OLSON: As I mentioned before, we started with gold Schottky diodes. They looked very good. That's a low-temperature process. We then went to a high-temperature boron diffusion, and the material fell apart essentially in terms of its electrical characteristics. We are trying to understand that right now.

FELDER: What was the analytical technique you used to evaluate your impurities and have you been able to look at carbon?

OLSON: We used spark-source mass spectroscopy and with that we did look at carbon. Carbon is one of those elements which should segregate electrochemically and we found very low concentrations of carbon, even though these are carbon cells and carbon substrates.

FELDER: What was the order of magnitude of the carbon concentration?

OLSON: Sub-ppmw.

# The Hemlock Semiconductor Dichlorosilane-Based C.V.D. Process

James R. McCormick  
Manager Process Engineering and Research  
Hemlock Semiconductor Corp.  
Hemlock, Michigan 48626

## I. INTRODUCTION

Chemical vapor deposition (CVD) of high-purity polycrystalline silicon from trichlorosilane (TCS) feedstock forms the basis of the entire semiconductor-grade polycrystalline silicon industry. This process currently produces material of proven quality to meet the stringent requirements of the electronics industry at an acceptable price. Material produced by this process also meets all quality needs of the emerging photovoltaic industry. Process improvements, coupled with expanding capacity, have resulted in a steadily declining polycrystalline silicon price (measured in constant dollars); however, basic process changes are required to achieve the more dramatic cost reduction goals consistent with widespread commercialization of silicon photovoltaic power generation. The current polycrystalline silicon manufacturing process is briefly reviewed in this paper. Key features of an improved process, Hemlock Semiconductor Corporation's (HSC) Dichlorosilane (DCS) Based CVD Process, are presented along with a general process description. Process development efforts on the dichlorosilane based CVD process have been pursued with JPL/DOE support since 1979 and considerable data relating to all aspects of the technology have been developed. This paper will concentrate, in addition to the overall process description, on the following three key research areas:

- 1) The hazardous properties of dichlorosilane.
- 2) Catalyst evaluation for the redistribution of trichlorosilane.
- 3) Chemical vapor deposition of polycrystalline silicon from dichlorosilane feedstock.

The process currently employed in the manufacture of polycrystalline silicon is shown schematically in Figure 1. It consists of the hydrochlorination of metallurgical-grade silicon to produce trichlorosilane (TCS), purification of this material via distillation, reductive chemical vapor deposition of polycrystalline silicon from the trichlorosilane, and by-product recovery. Shortcomings in this process are:

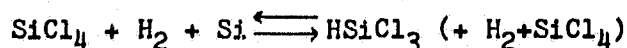
- 1) High capital cost due to low conversion rates at the CVD reactor.
- 2) High power consumption at the CVD reactor.
- 3) Low conversion efficiency (silicon in feedstock to silicon deposited).
- 4) Large silicon tetrachloride (STC) by-product stream.

PRECEDING PAGE BLANK NOT FILMED

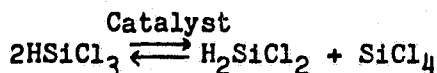
## II. HSC DICHLOROSILANE BASED CVD PROCESS

Shortcomings associated with the current process may be reduced by increasing CVD reactor efficiency and reprocessing the large silicon tetrachloride by-product stream. This is accomplished by the HSC process through the use of dichlorosilane as a reactor feedstock and the substitution of hydrogenation of silicon tetrachloride as the method of trichlorosilane production. The major chemical processes involved in this new production method are

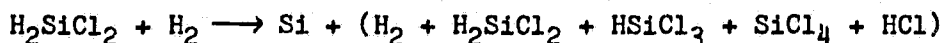
### Hydrogenation of Silicon Tetrachloride



### Dichlorosilane Synthesis



### Dichlorosilane Decomposition



The overall process shown schematically in Figure 2 consists of the hydrogenation of silicon tetrachloride to produce trichlorosilane, synthesis of dichlorosilane via the catalyzed redistribution of trichlorosilane, reductive chemical vapor deposition of polycrystalline silicon from dichlorosilane, and recovery/recycle of the decomposition by-products. The only remaining by-product stream shown in Figure 2 is hydrogen chloride which, of course, may be used in the hydrochlorination process for trichlorosilane production.

Key to the success of the process is the advantages associated with the use of dichlorosilane as a feedstock for the CVD reactor. Dichlorosilane is less stable than trichlorosilane both thermodynamically and kinetically.

In thermodynamic terms, dichlorosilane is a substantially better source of silicon than trichlorosilane. A perspective on equilibrium relationships between the two chlorosilanes is presented in Figure 3.<sup>2</sup> The figure shows the Cl/H ratio in the reactor feed stream (and vent, since no hydrogen or chlorine is deposited in the reactor) versus the equilibrium-determined Si/Cl ratio in the vent products (that is, not including the elemental silicon deposited). The figure can be used to ascertain the percent conversion into silicon for a range of feed compositions (Cl/H ratios), since

$$\text{Percent Conversion} = \frac{(\text{Si/Cl})_{\text{in}} - (\text{Si/Cl})_{\text{out}}}{(\text{Si/Cl})_{\text{in}}}$$

At a feed of 10 mole percent dichlorosilane in  $\text{H}_2$  and  $1050^\circ\text{C}$ , for example, the Cl/H ratio = .10, and:

$$\text{Percent Conversion} = (.50 - .20) / .50 = 60\%$$

Conversion efficiency of trichlorosilane under the same conditions is only 37%.

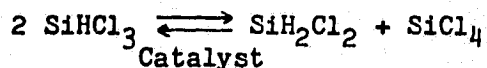
A further thermodynamic advantage of dichlorosilane relative to trichlorosilane is its lower sensitivity to increases in reactant concentration. For trichlorosilane, doubling the mole percent of reactant from 7% to 14% decreases the percent conversion into silicon from 40% to 31%. Dichlorosilane suffers proportionately less from concentration increases; an increase from 7% to 14% causes an equilibrium conversion decrease from 65% to only 58%.

Since equilibrium conditions do not, in fact, prevail in the anticipated CVD processes, the above equilibrium relationships will be modified by the kinetic realities. It has been demonstrated that, under conditions used for epitaxial deposition, formation of silicon from dichlorosilane is characterized by a lower activation energy than corresponding formation from trichlorosilane.<sup>3</sup> Typical values are 13 and 22 kcal/mole, respectively. Conditions utilized in epitaxial reactors typically involve substantially lower mole percent chlorosilane and flow rates than polysilicon production processes. However, recent work by Ban of RCA Laboratories has been conducted at mole fractions and temperatures compatible with the polycrystalline silicon production process.<sup>4</sup> Ban's results indicate that under conditions in which silicon tetrachloride and trichlorosilane are far from equilibrium, dichlorosilane has achieved equilibrium.

The high conversion efficiency associated with dichlorosilane decomposition results in increased deposition rate and reduced power consumption per unit of time. This high conversion efficiency, coupled with the lower molar chlorine content, also results in a substantially reduced recovery system size per kg of silicon produced.

### III. CATALYST EVALUATION

A preferred route to dichlorosilane production has been demonstrated to be the acid or base-catalyzed redistribution of trichlorosilane.



Dowex<sup>®</sup> MWA-1\* is a basic resin (methyl-amine organic polymer) that is capable of inducing a redistribution reaction at reasonable rates and at moderate temperatures. An experimental program was established to define reaction parameters using this solid, non-volatile catalyst.

The laboratory redistribution unit is shown schematically in Figure 4. This unit consists of a manifold which includes two stainless steel cylinders and a small diameter redistribution column. One cylinder contains trichlorosilane or mixed feeds of trichlorosilane and silicon tetrachloride. The second cylinder collects the effluent from the redistribution column. A coil of stainless steel tubing immersed in a recirculating oil bath that insures constant temperature operation serves as the redistribution column. Provisions exist for removal of samples for analysis by gas chromatography, waste removal, and automatic venting.

---

\* Manufactured by The Dow Chemical Co., Midland, Michigan

Data were collected to evaluate the kinetics of the trichlorosilane redistribution reaction at liquid flow rates greater than 5 ft/hr. Product composition data were fitted to the kinetic rate expression for reversible second order reactions of the form.<sup>5</sup>

$$2 \text{ TCS} = \text{DCS} + \text{STC}$$

$$\frac{k}{(1-X)(X/2)(X/2)}$$

where  $k = X_e/2t(1-X_e) \ln((X(1-2X_e)+X_e)/X_e-X)$   
 and  $k$  = kinetic rate constant ( $\text{min}^{-1}$ )  
 $t$  = residence time (min)  
 $X_e$  = equilibrium mole fraction  
 $X$  = mole fraction at time  $t$

As shown in Figure 5, a near equilibrium dichlorosilane concentration of 10 mole percent is observed in the effluent from the redistribution column. At velocities greater than 25 ft/hr, the kinetic rate constant reaches a constant value of approximately  $0.20 \text{ min}^{-1}$ . Data indicates that reasonably good mixing at the solid-liquid interface is present and that problems associated with liquid diffusion have been minimized at the higher velocities.

A process demonstration unit (PDU) capable of producing 70 lbs/hr of dichlorosilane was designed and constructed. This unit served to demonstrate the validity of laboratory data on a much larger scale and provided a source of high-purity dichlorosilane for chemical vapor deposition studies. This unit confirmed the laboratory data during a year of operation demonstrating a conversion efficiency of 12.5 %.

#### IV. DICHLOROSILANE SAFETY DATA

A thorough literature investigation<sup>6</sup> revealed discrepancies in combustion characteristics of dichlorosilane. Coincidental to the literature search, minor explosions had been experienced during catalyst evaluation experiments. An experimental program was implemented to measure autoignition temperature, explosion severity, and hydrolytic behavior of dichlorosilane, prior to the production of large quantities of dichlorosilane.

Hazards Research Corporation\* was engaged to perform the following tests:

- 1) Autoignition: determine temperature at which DCS/air mixtures spontaneously ignite.
- 2) Explosion Severity: determine rate of pressure rise upon ignition of DCS/air mixtures.
- 3) Hydrolytic: determine if ignition occurs when DCS is injected into water, or water into DCS.
- 4) Explosive Output: determine output of an unconfined vapor cloud explosion.

---

\* Hazards Research Corporation  
 200 East Main Street  
 Rockaway, New Jersey 07866

A summary of test results is presented in Figure 6.<sup>7</sup>

The low boiling point, broad flammability range, low autoignition temperature, and rapid rate of combustion combine to make dichlorosilane a much more hazardous material than trichlorosilane, silicon tetrachloride or hydrogen.

## V. CVD PROCESS EVALUATION

A small experimental CVD reactor was modified to characterize dichlorosilane as a reactor feedstock including quantitative determination of reaction products. A schematic of the experimental reactor showing the feed manifold and vent line configuration is shown in Figure 7. Rotameters were used to measure flow of various combinations of feed (TCS, DCS, or redistributed material) to the reactor. The reactor is composed of a heat shield, quartz bell jar, baseplate, and power supply. Feed and vent gas compositions were analyzed using a Bendix Model 170 gas chromatograph, a Perkin-Elmer Sigma 10 data system, and a North Star Horizon micro-computer.

To conserve time and dichlorosilane, experimental runs were segmented. Segmentation involves introducing trichlorosilane early in an experimental run to produce rods of adequate size, while dichlorosilane is used later in the run where reactor operating conditions are more severe and more representative of production reactor operation.

Optimization experiments utilizing a two-level experimental design were conducted to establish quantitative correlation between reactor operating parameters (total flow rate, mole percent dichlorosilane, and temperature) and measured responses (silicon deposition rate, conversion, and power consumption).

Nine DCS run segments, at conditions illustrated in Figure 8, were made along with replicate runs. Rod diameter ranges were classified as 26-32 mm, 33-39 mm, and 39-45 mm. The replicate experiments were made to confirm the assumption that rod diameter effects were minimal over the 26-45 mm range under these operating conditions. The eight experimental points (1-8) correspond to the corners of a cube in which the edges represent the variables: flow, mole percent DCS, and temperature.

Polynomial expressions describing the relationship between operating parameters and responses were developed using a least squares multiple regression analysis program.<sup>8</sup>

In general, the equations predict that an increase in any independent variable will result in an increase in silicon deposition rate and a decrease in power consumption with the stipulation that the reactor is not "feed starved." Dependence of conversion efficiency is more complex in that conversion is enhanced by increasing temperature, but diminished by increasing mole percent DCS and flow rate. A summary of data for the 9 cube locations is shown in Table 1.

The order of importance of each variable and interaction terms is listed below in descending order for each of the three responses.

Silicon Deposition Rate	Conversion Efficiency	Power Consumption
1. Flow	1. % DCS	1. Flow
2. Temp.	2. Temp.	2. % DCS
3. % DCS	3. Flow	3. Int. of Temp. X % DCS
4. Int. of Flow and Temp.	4. Int. of Temp. and % DCS	4. Temp.
5. Int. of Flow and % DCS	5. Int. of Flow and Temp.	5. Int. of Flow and Temp.
6. Int. of Temp. and % DCS	6. Int. of Flow and % DCS	6. Int. of Flow and % DCS

Further analysis of the data for varying rod diameter indicated that rod diameter was less important than any of the variables or interaction terms.

Results from the experimental design were verified by data collected using modified production reactors. The measured responses of deposition rate, conversion, and power consumption, for both reactor types are compared below with the original program goals.

	Deposition Rate $\text{gh}^{-1}\text{cm}^{-1}$	Conversion Mole Percent	Power Consumption kWh/kg
JPL Goal	2.00	40	60
Experimental Design	1.60	35.2	96
Modified Production Reactor	2.00	35.1	82

## VI. CONCLUSIONS

Considerable progress has been made toward demonstrating the full potential of dichlorosilane as a feedstock for a low-cost chemical vapor deposition route to high-purity polycrystalline silicon. Under proper flow and temperature conditions, the base catalyzed redistribution of trichlorosilane has been shown to be an attractive and cost effective method of dichlorosilane production. Hazards associated with the production and processing dichlorosilane were critically evaluated and, through the use of proper process design criteria, safe operation was demonstrated for a dichlorosilane production unit with a 500,000 pounds/yr capacity.

Deposition of high-purity polycrystalline silicon was conducted in both an experimental and modified production decomposition reactor. Preliminary data from modified production reactors confirm results obtained in the experimental reactor. The program goal for deposition rate was met, however, conversion efficiency remains lower than the targeted value of 40% and power consumption at the reactor remains approximately 20 kWh/kg over target. Further efforts in the areas of reactor design and process optimization are required to achieve all programs while assuring reliable reactor operation.



### Acknowledgements

The author would like to recognize and express his appreciation for the major contributions made in the dichlorosilane process development effort by Arvid Arvidson, Stewart Goldfarb, Frank Plahutnik, David Sawyer and Kenneth Sharp. Also contributing to the technical effort were Norman Deitering, Lloyd Ellis, Jeffery Fox, David Goffnet, Maurice Lovay and David Muller.

### References

1. Silicon Materials Outlook Study for 1980-85 Calendar Years, DOE/JPL - 1012-33, JPL Publication 79-110, 1 Nov. 1979.
2. L. Hunt and E. Sirtl, J. Electrochemical Soc., 119, 1741 (1972).
3. V. Ban, J. Electrochemical Society, 122, 1389 (1975).
4. Ibid.
5. Hemlock Semiconductor Corp., First Quarterly Report, Low-Cost Solar Array Project, DOE/JPL Contract No. 955533, January, 1980.
6. Kenneth G. Sharp, Arvid Arvidson, and Thomas C. Elvey, J. Electrochemical Soc., (to be Published).
7. William J. Cruice, Vapor Explosion Characteristics of Chlorosilanes In Air, HRC Report 4596, December 10, 1980.
8. Hemlock Semiconductor Corp., Third Quarterly Report, Low-Cost Solar Array Project, DOE/JPL Contract No. 955533, August, 1980.

Table 1. SUMMARY OF RESULTS OBTAINED FROM  
DCS DECOMPOSITION DESIGNED EXPERIMENT

CUBE LOCATION	DEPOSITION RATE GH-1CM-1	CONVERSION MOLE PERCENT	POWER CONSUMPTION KWH/KG
1	0.51	44.4	177
2	0.78	33.7	138.8
3	0.74	32.5	155.9
4	1.07	23.5	114.1
5	0.85	58.8	182.0
6	1.12	48.2	133.8
7	0.88	43.2	131.7
8	1.80	35.2	98.3
9	1.01	38.3	128.4

Figure 1. CURRENT POLYCRYSTALLINE SILICON PROCESS

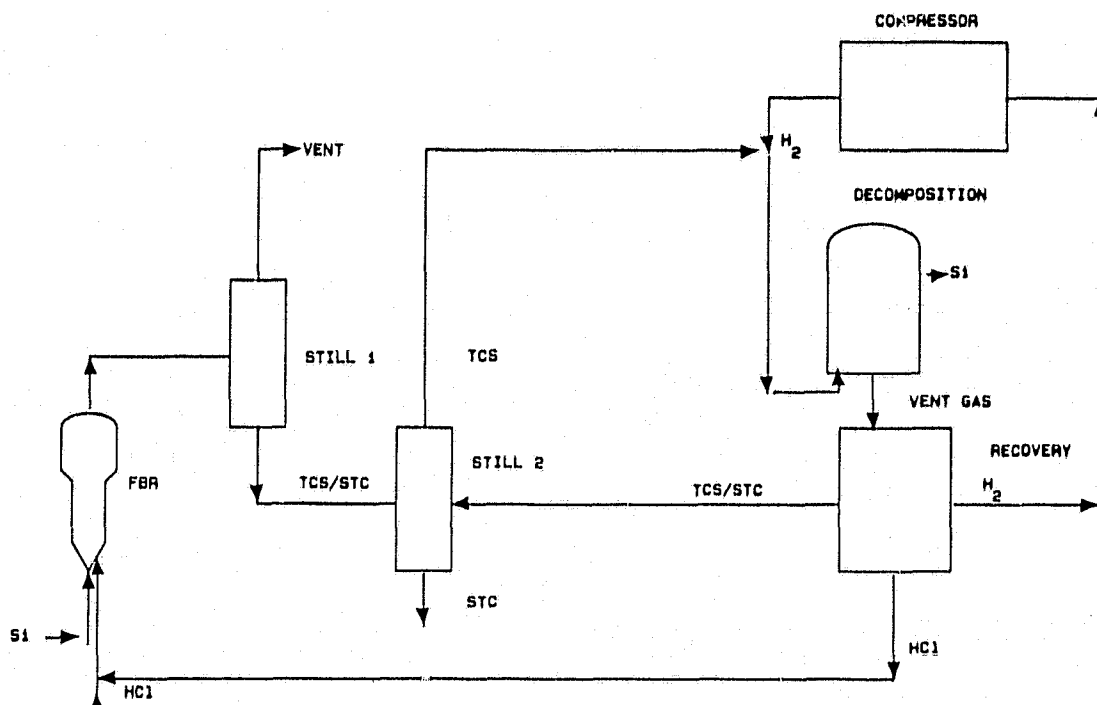


Figure 2. HSC LOW-COST SILICON PROCESS

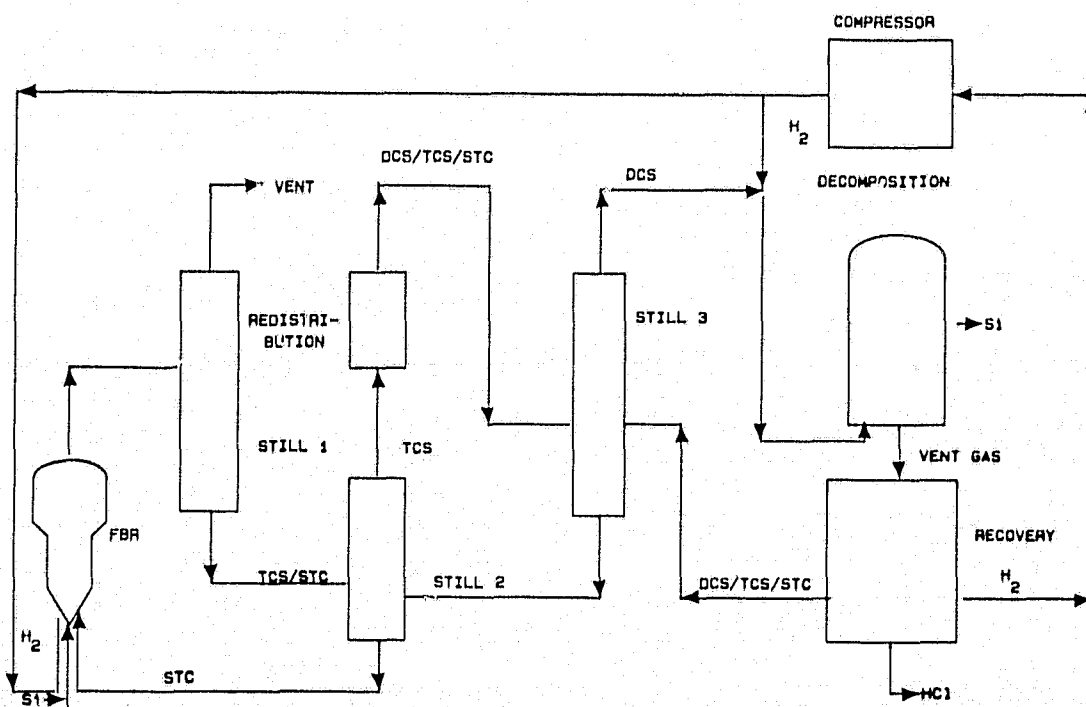


Figure 3. EQUILIBRIUM RELATIONSHIPS FOR SILICON GENERATION  
FROM CHLOROSILANES AT 1050 °C

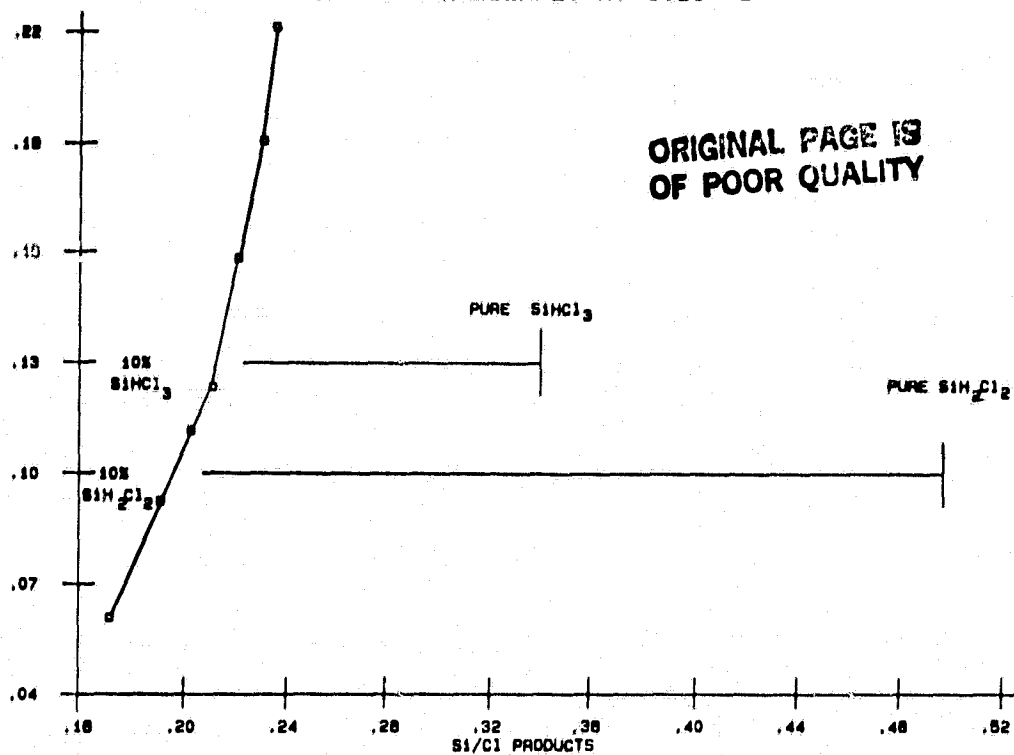
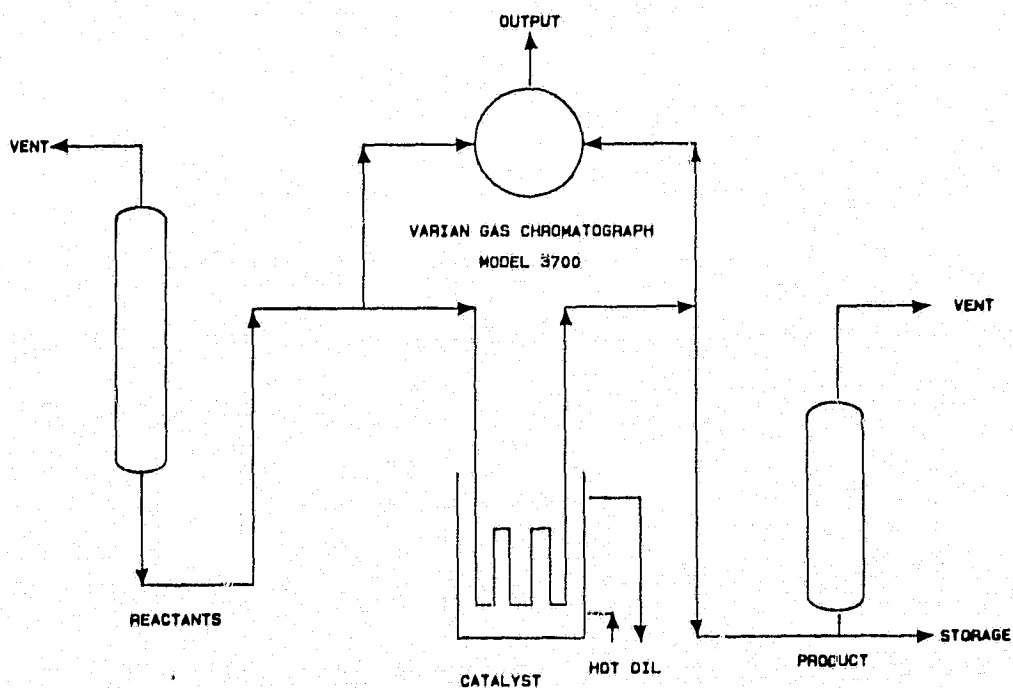


Figure 4. LABORATORY TRICHLOROSILANE REDISTRIBUTION UNIT



ORIGINAL PAGE IS  
OF POOR QUALITY

Figure 5. KINETIC DATA FROM REDISTRIBUTION OF  
TRICHLOROSILANE BY DOWEX® RESIN (77 °C, LIQUID)

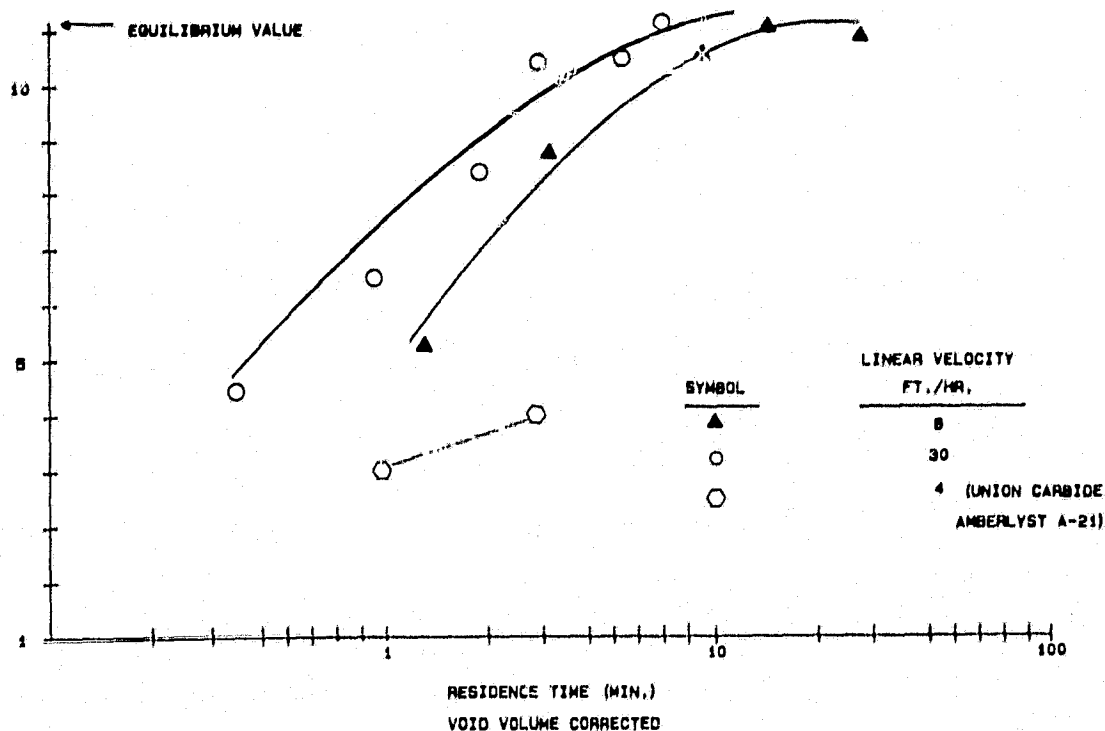


Figure 6. HAZARDS RESEARCH CORPORATION  
DATA FOR DICHLOROSILANE

PROPERTY	EXPERIMENTAL VALUE , FROM THIS WORK	PREVIOUS LITERATURE VALUE
AUTOIGNITION TEMP. (10 L. SPHERE)	55-60 °C	100 °C
EXPLOSION SEVERITY (10 L. SPHERE)	10 PSI/SEC MAX	NONE (H /AIR) 33,000 2
HYDROLYSIS	COPIUS EVOLUTION OF HCl; NO IGNITION	IGNITION MAY BE POSSIBLE
EXPLOSIVE OUTPUT (5 FT. CUBE, WITH PLASTIC SHEET FACES)	(1) UNEXPECTED IGNITION ON FLOW TERMINATION (2) SEVERITY > PROPYLENE/AIR; NO DETONATION OBSERVED	NONE
EXPL. SEVERITY (10% DCS/90% H )/AIR 2	55,000 (PSI/SEC) MAX	NONE

ORIGINAL PAGE IS  
OF POOR QUALITY

Figure 7. HSC DECOMPOSITION REACTOR

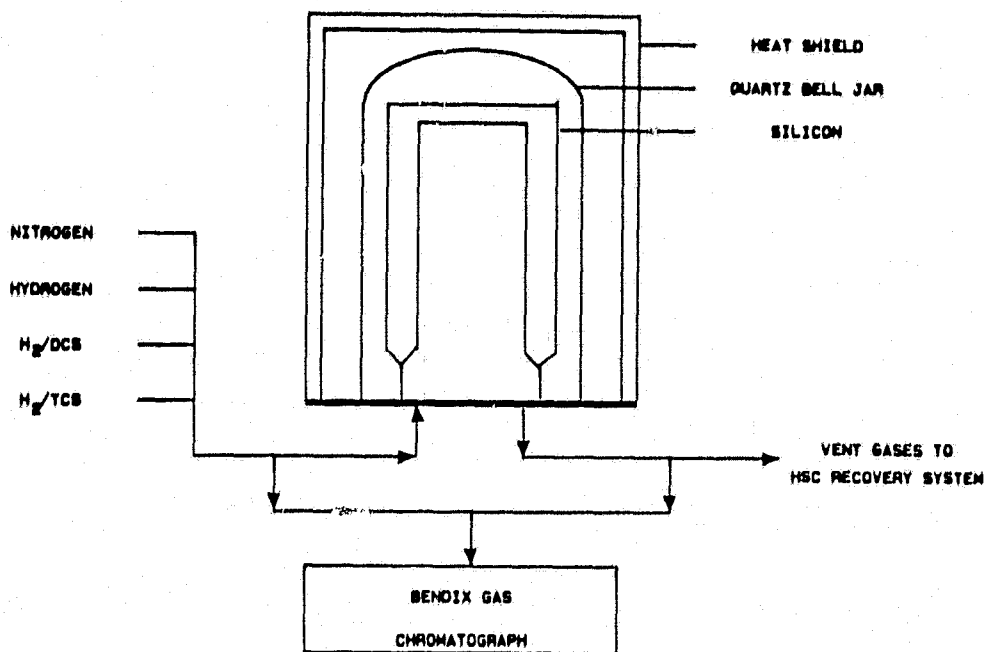
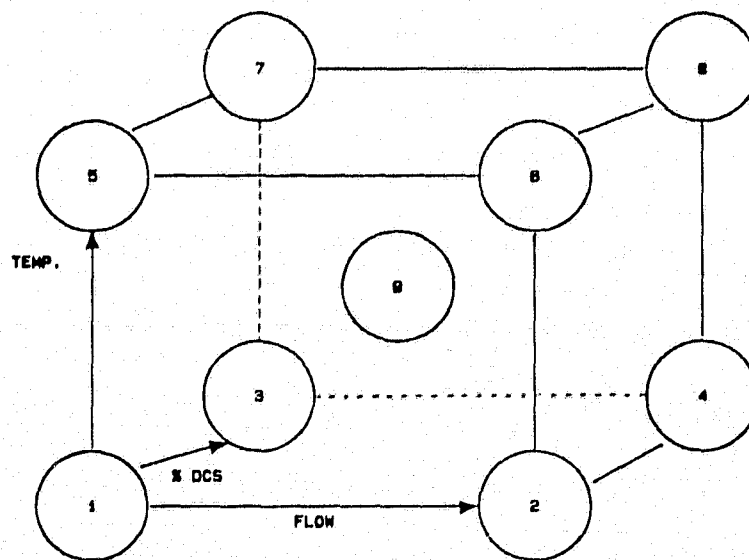


Figure 8. DICHLOROSILANE EXPERIMENTAL DESIGN



RANGE OF VARIABLES: FLOW 80 SCFH - 180 SCFH  
TEMP. 1020 DEGREES C - 1120 DEGREES C  
% DCS 6 - 12

## DISCUSSION

SETTY: You mentioned one other catalyst you are going to evaluate. Can you tell more about it?

MCCORMICK: No, I can't describe it here. It's a proprietary Dow-Corning catalyst.

# PRODUCTION OF SILICON BY THE REDUCTION OF SILICON TETRAFLUORIDE WITH SODIUM

A. Sanjurjo, K. Sancier  
SRI International, Menlo Park, CA 94025

## ABSTRACT

Solar grade silicon can be prepared by reducing  $\text{SiF}_4$  gas with Na metal to form Si and NaF. The  $\text{SiF}_4$  is obtained from inexpensive  $\text{H}_2\text{SiF}_6$  by precipitation and decomposition of  $\text{Na}_2\text{SiF}_6$ . The product Si can be separated from NaF by aqueous leaching or by melting above  $1450^\circ\text{C}$ .

## INTRODUCTION

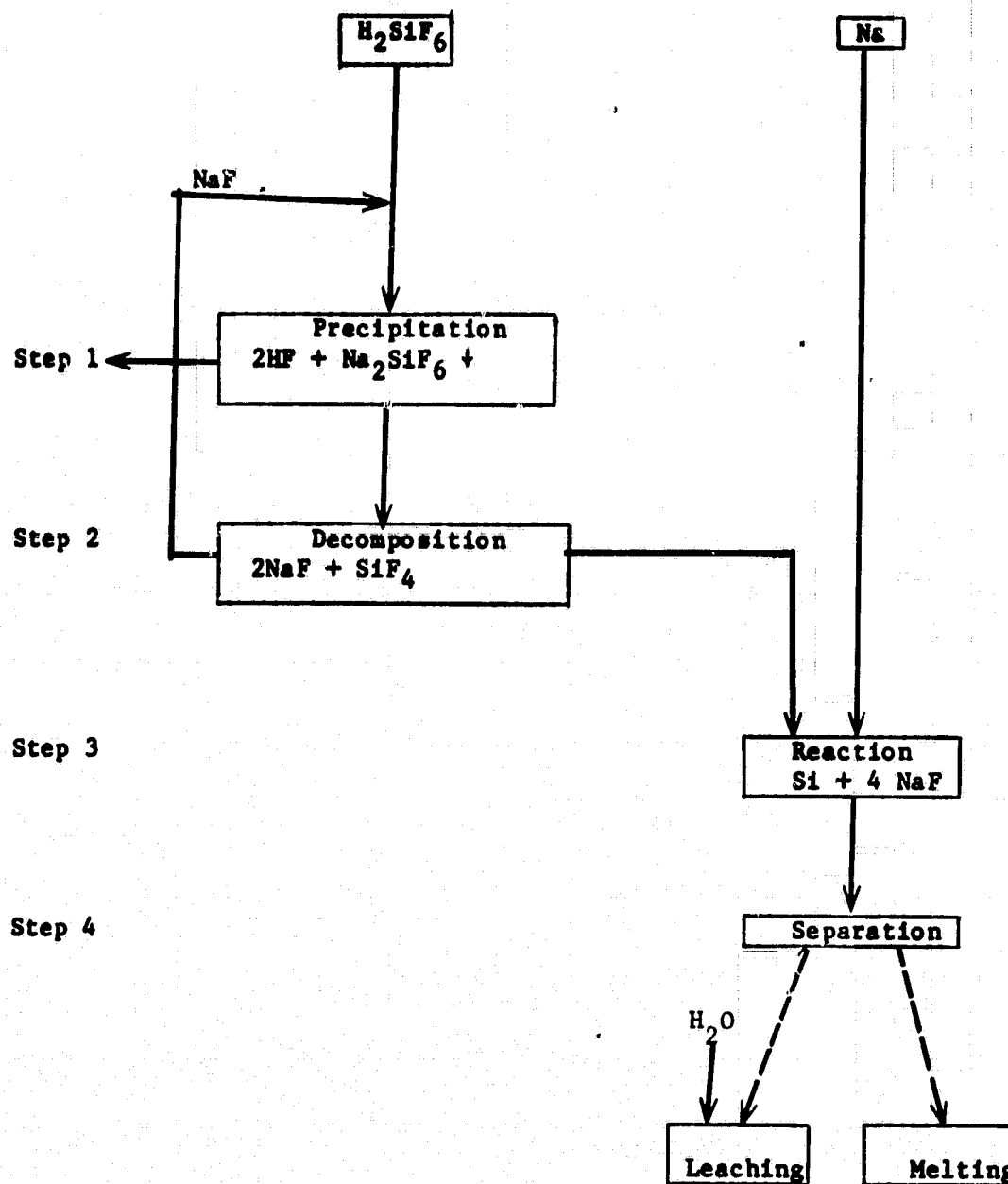
Silicon is an important material in modern semiconductor technology and is finding increased use in solar cells for the photovoltaic generation of electricity. Low cost silicon of high purity is needed to foster the continued development of solar photovoltaic systems. We have developed a process that offers a pathway to an industrial method that satisfies cost and purity requirements. The starting material is fluosilicic acid,  $\text{H}_2\text{SiF}_6$ , a low cost waste by-product of the phosphate fertilizer industry.  $\text{SiF}_4$  gas is prepared from  $\text{H}_2\text{SiF}_6$  and is reacted with sodium metal to produce a mixed reaction product consisting of Si and NaF. Aqueous leaching or melting can be used to separate NaF from Si. A general overview is presented here of the process which has been described in detail in previous publications (1).

The overall process consists of four major steps (Fig. 1): step 1, precipitation of  $\text{Na}_2\text{SiF}_6$ ; step 2,  $\text{SiF}_4$  generation; step 3, Na reduction of  $\text{SiF}_4$ ; and step 4, separation of Si from the Si-NaF mixture. A flow diagram of the process steps is shown in Fig. 1. The sequence of reactions is described below.

### Step 1: Precipitation of $\text{Na}_2\text{SiF}_6$

Sodium fluosilicate,  $\text{Na}_2\text{SiF}_6$ , was precipitated by adding sodium fluoride directly to an industrially available solution of fluosilic acid containing 23 wt%. The product  $\text{Na}_2\text{SiF}_6$  as determined by x-ray diffraction is a nonhygroscopic white powder that is very stable at room temperature and thus provides an excellent means for storing the silicon before it is decomposed to  $\text{SiF}_4$ . The Na salt was chosen because it best matched the desirable conditions of (a) low solubility of the fluosilicates coupled with high solubility of the fluoride, (b) ease of drying, and (c) low

ORIGINAL PAGE IS  
OF POOR QUALITY





temperature decomposition to generate  $\text{SiF}_4$ . Other fluosilicates such as those of Ba and K could also be used.

Impurities in the  $\text{H}_2\text{SiF}_6$  feed, the NaF, and the resulting  $\text{Na}_2\text{SiF}_6$  are shown in Table 1. During precipitation of the  $\text{Na}_2\text{SiF}_6$  most of the impurities remain in the  $\text{HF-H}_2\text{SiF}_6$  solution because of the high solubility of their fluosilicates, such as in the case of  $\text{MgSiF}_6$  or  $\text{CaSiF}_6$ , or their double salts such as  $\text{NaBF}_4$  or  $\text{NaPF}_6$ . By contrast, several transition metals that form soluble fluosilicates accumulated in the  $\text{Na}_2\text{SiF}_6$  precipitate. Studies to determine the form in which these impurities are incorporated in the precipitate indicate that they are not absorbed at the surface but are incorporated in the bulk of the sodium fluosilicate as insoluble fluorides.

Table 1

PLASMA EMISSION SPECTROSCOPY ANALYSIS,  
PARTS PER MILLION (wt)

Element	$\text{H}_2\text{SiF}_6^a$	$\text{NaF}^b$	$\text{Na}_2\text{SiF}_6$
Li	0.1		0.2
Na	450		
K	9.0		8.0
Mg	55		6.4
Ca	110	10	18
B	1.0		0.8
Al	8.0	<2.5	1.3
P	33		5
As	8.8		0.2
V	0.3	<5	0.3
Cr	0.8	<3.5	8.8
Mn	0.2	<4	0.4
Fe	13	<7	38
Co	0.54		0.7
Ni	1.17	<8	4.2
Cu	0.12	<4	0.6
Zn	1.4		1
Pb	14.5		5
Mo	11		1.0

<sup>a</sup>23 w/o waste by-product of phosphate fertilizer production.

<sup>b</sup>Emission spectroscopy.

Step 2:  $\text{Na}_2\text{SiF}_6$  Decomposition -  $\text{SiF}_4$  Generation

As  $\text{SiF}_4$  is needed, the  $\text{Na}_2\text{SiF}_6$  can be thermally decomposed at  $650^\circ\text{C}$  in a graphite-lined, gas-tight stainless steel retort.  $\text{SiF}_4$  gas prepared in this manner was determined by mass spectrometric analysis to be purer

than commercial grade  $\text{SiF}_4$ . Positively identified gaseous impurities are listed in Table 2; no metallic impurities were detected. Peaks corresponding to boron compounds, such as  $\text{BF}_3$ , were specially checked, but none were found.

Table 2  
MASS SPECTROMETRIC ANALYSIS OF  $\text{SiF}_4$

Ion	$\text{SiF}_4$ prepared at SRI from $\text{H}_2\text{SiF}_6$ (%)	commercial (%)
$\text{SiF}_3^+$	96.9	93.6
$\text{Si}_2\text{OF}_6^+$	3.04	4.24
$\text{SiOF}_2^+$	--	1.79
$\text{CCl}_3^+$	--	0.159
$\text{SO}_2\text{F}_2^+$	0.076	0.098
$\text{Si}_2\text{O}_2\text{F}_4^+$	--	0.081
$\text{SO}_2^+$	--	0.035

Although the  $\text{SiF}_4$  produced from  $\text{H}_2\text{SiF}_6$  was purer than the commercial grade, the commercial grade  $\text{SiF}_4$  was also used for experimental convenience. The possible presence of metallic impurities in commercial  $\text{SiF}_4$  was further determined by bubbling the gas through high purity  $\text{H}_2\text{O}$  and heating the resulting slurry with an excess of  $\text{HF}$  to drive off silicon as  $\text{SiF}_4$ . The final clear solution was then analyzed by plasma emission spectroscopy (PES). The results listed in Table 3 are representative of the impurity content to be found in the commercial grade  $\text{SiF}_4$  gas. The low content of B and P is of special significance for both semiconductor and solar cell applications.

The decomposition of  $\text{Na}_2\text{SiF}_6$  provides a purification step. By heating the solid in vacuum at  $450^\circ\text{C}$ , volatile impurity fluorides can be removed, and by keeping the temperature below  $700^\circ\text{C}$  during the decomposition less volatile fluorides (such as those of most transition metals) or more stable double salts will stay in the solid phase. Finally, certain volatile gases evolving within this temperature range can be condensed when the  $\text{SiF}_4$  gas is cooled to room temperature, such as the case of  $\text{TiF}_4$  which condenses at  $284^\circ\text{C}$ .

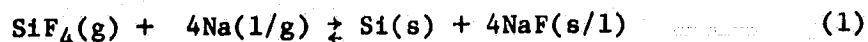
Table 3

IMPURITIES IN COMMERCIAL  $\text{SiF}_4$ 

Element	Impurity (ppm wt)
Li	<0.01
Na	1.1
K	0.2
Mg	1.3
Ca	1.0
B	<0.01
Al	0.7
P	0.06
As	0.2
V	<0.01
Cr	<0.01
Mn	0.2
Fe	0.04
Co	<0.01
Ni	<0.01
Cu	<0.01
Zn	<0.01
Pb	0.02
Mo	<0.01

Step 3:  $\text{SiF}_4$ -Na Reaction

The central operation of the process is the reduction of  $\text{SiF}_4$  by Na according to the reaction.



Although this reaction is thermodynamically favored at room temperature ( $\Delta G_{298\text{K}}^\circ = -146 \text{ kcal/mol Si}$ ), it has been found experimentally that Na has to be heated to about  $150^\circ \text{C}$  before any appreciable reaction can be observed. Once the reaction has been initiated, the released heat ( $\Delta H_{298\text{K}}^\circ = -164 \text{ kcal/mol Si}$ ) raises the temperature of the reacting Na, which in turn increases the reaction rate. Under adiabatic conditions, and stoichiometric quantities of  $\text{SiF}_4$  and Na, a temperature of  $2200^\circ \text{K}$  is predicted for reaction.

In practical non-adiabatic reactors it has been found that the temperature at the reaction zone depends on the pressure of  $\text{SiF}_4$  for a given geometry of the Na feed (2). Temperatures close to the melting point of silicon were obtained for  $\text{SiF}_4$  pressures around 1 atm. The main effect of higher temperatures is to increase the degree of segregation of the Si and NaF phases. In addition, it was observed that the particle size of the silicon grains in the Si-NaF product mixture increased with the pressure of the reaction (2).

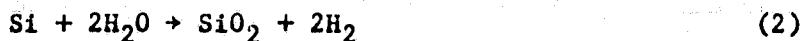
The complete segregation of phases Si and NaF can be achieved by heating the product mixture to 1450° C for 5 minutes (either externally or by using an adiabatic reactor). In this condition, Si collects at the bottom in a pool and NaF floats on top. At temperatures below the melting point of Si, NaF melts (998° C) and flows, producing partial segregation; however, no Si coalescence can be observed. In light of this evidence, the role of the SiF<sub>4</sub> in the segregation appears to be only indirect. It is the temperature reached by the r.p. during the reaction that is the main cause of the segregation and grain growth.

#### Step 4: Separation of Silicon from the Si-NaF Product Mixture

Silicon can be recovered from the product mixture by aqueous leaching or using the high temperature separation procedure.

#### Leach Separation

The reaction products obtained from the SiF<sub>4</sub>-Na reaction is a porous, brown mass of an intimate Si-NaF mixture from which Si can be readily recovered by aqueous leaching of the soluble NaF. The Si product obtained after leaching is a dark grey crystalline powder with particle size ranging from 0.1 to 1000 μm. Leaching is performed using aqueous acid solutions in a polypropylene container. The acid normality can be varied in the range 0.1 N to 1.0 N without affecting the recovery of silicon in the leaching process. When the F<sup>-</sup> concentration is about 10<sup>-5</sup> mole/liter, the leaching is stopped and the silicon is recovered by filtration or centrifugation and dried. The acidification of the leach solution is a precautionary measure to prevent increase in local pH due to reaction of H<sub>2</sub>O with unreacted sodium in the reaction product. High pH results in increased Si loss by oxidation according to the reaction.



It has been determined (3) that the rate of oxidation increases with increasing F<sup>-</sup> ion concentration in solutions for pH in the range of -0.8 to 10. This effect seems to be due to the effect of the F<sup>-</sup> in the otherwise stable surface SiO<sub>2</sub> layer on the Si. The contact time may be minimized by using forced filtration, which yields a 98% complete recovery of Si.

Several analytical methods have been used to characterize the very low levels of impurity elements in the silicon leached from the products of SiF<sub>4</sub>-Na reaction 1. These methods included spark source mass spectrometry (SSMS), neutron activation analysis (NA), plasma emission spectroscopy (PES), arc emission spectroscopy (AES), and a colorimetric chemical analysis for phosphorous. The use of several methods was both necessary and desirable since, at the low impurity levels encountered, each of the analytical techniques was used at the limit of resolution for several elements.

A typical analysis of the leached silicon powder is shown in column 2 of Table 4. In addition, to minimize errors due to sampling, a second silicon sample was prepared by melting and rapidly quenching powder silicon from a different batch. The analysis of this solid sample is given in column 3 of Table 4. To evaluate the accuracy of the analytical methods, a reference sample of ultra high purity semiconductor grade polycrystalline silicon with resistivity greater than  $1 \times 10^5$  ohm-cm was analyzed concurrently with the solid silicon samples of SRI silicon. The analysis of the reference material provided a base line that includes effects caused by sample preparation, accidental contamination, matrix and/or instrumental limitations and is shown in Table 4 column 5.

Table 4  
IMPURITY CONTENT OF SILICON RECOVERED  
BY LEACHING (ppm wt)

Element	Leached Silicon Powder	Melt	Semiconductor Si
		Consolidated Leached Silicon	
B	0.1	0.1	0.1
P	0.1	0.2(0.09) <sup>a</sup>	0.3
Al	1	0.8	0.4
Ga	0.06	0.1	
Ti	0.3	2.0	0.2
Zr	0.1	0.01	<0.3
Mo	0.3	b	
V	0.04	<0.3	
Cr	3	<3.5 <sup>c</sup>	0.8
Mn	0.1	0.1	b
Fe	20	<0.5	<0.5
Co	0.5	0.5	
Ni	4		
Cu	.7	0.2	
Zn	0.01	15	
F	0.1	<0.1	
Na	>160	1.0	9.0
K		0.01	<0.1
Ca		1.0	0.1
Mg	3	0.1	b

<sup>a</sup> Wet chemical analysis

<sup>b</sup> Not observed

<sup>c</sup> Arc emission spectroscopy; all others, spark source mass spectrometry.

The observed impurities can be introduced either with the reactants or by contamination during operation. The results listed in Table 3 show that SiF<sub>4</sub> can be considered free of metallic impurities. Therefore, the Na

feed, reactor materials, and possible contamination of the product during handling remain as the most probable sources of impurities in the Si.

Commercially available sodium which usually contains impurities in the ppm range for elements such as B, P, As, Ca, Al, and Fe, is a logical source of the impurities in the silicon. The impurities in Na can be divided roughly into three types according to their tendency to react with  $\text{SiF}_4$ , as classified by the free energy of reaction. The first type of impurity includes aluminum and elements from the groups IA, IIA. The free energy of reaction of  $\text{SiF}_4$  with these impurities ranges from -100 to -200 kcal/mole  $\text{SiF}_4$  at 1500 K. It is expected, therefore, that even when these impurities are present at the ppm level, they will react with the  $\text{SiF}_4$  to form the corresponding fluorides. Subsequently, the fluorides will be dissolved preferentially in the NaF phase. The second type of impurity includes transition metals such as Mo, W, Fe, Co, Ni, and Cu, and the elements P, As, and Sb. These elements exhibit positive free energies of reaction (up to 100 kcal/mole  $\text{SiF}_4$ ) and are not expected to react with  $\text{SiF}_4$ . Free metals impurities, such as Fe, Ni, or Cr, can react with the silicon resulting from the  $\text{SiF}_4$ -Na reaction to form silicides. Chemical analysis indicates similar proportion to the concentration of these elements in the Na feed and in silicon product. In any case, the concentration of Fe, Cr, Ni, and also Ti can be decreased by a factor of about  $10^4$ - $10^6$  by single-pass directional solidification or by the Czochralski crystal-pulling procedures used presently for solar cell manufacture. At the resulting level, these elements would not be detrimental to solar cell performance (4). Boron represents a third type of impurity. The free energy of reaction of this element with  $\text{SiF}_4$  is positive but small (5-20 kcal/mole  $\text{SiF}_4$  for temperatures up to 1500 K); therefore, some partial reaction can be expected and B will be distributed between the NaF and Si phases. The observed low content in silicon for this element, as well as for P and As could be due to the fact that these elements form complex fluorides, such as  $\text{NaBF}_4$ , and  $\text{NaPF}_6$ , that concentrate preferentially in the NaF phase and away from the Si phase. Since it is convenient to have dopant levels as low as possible to permit flexibility in subsequent doping procedures for solar cell applications, the low B and P content of Si produced by the  $\text{SiF}_4$ -Na process is of advantage.

The possibility of contamination from the reactor materials was minimized by the use of Ni and Grafoil liners that completely contained the reaction products and avoided contact or impurity transfer with the reactor walls. The Ni liner served merely as a mechanical retainer for the Grafoil sheet and did not contact the solid mixed reaction product. Both Ni and Inconel were selected for use in the reactor because of their stability in the presence of fluoride compounds.

Contamination during handling was, after the Na feed, probably the second most important source of impurity pick up. Airborne dust could have contacted the products either during their removal from the reactor or during sampling. Furthermore, although electronic grade acid and deionized water were used for leaching the NaF, the large volume of liquid used could have contributed to the accumulation of impurity in the silicon. Finally,

although the purity of the silicon produced by the  $\text{SiF}_4$  reaction is expected to be suitable for photovoltaic solar cells, by prepurification of the commercial grade Na and avoiding contamination during handling, semiconductor grade silicon could possibly be produced.

#### Melt Separation

An alternate separation method consists of heating the  $\text{SiF}_4$ -Na reaction product mixture without further treatment to temperatures above the melting point of Si ( $1412^\circ\text{C}$ ). At this temperatures, Si particles in the product mass coalesce into a pool at the bottom of a crucible, and the NaF is cleanly separated into an upper liquid layer.

Table 5  
IMPURITY CONTENT OF MELT-SEPARATED SILICON  
(ppm wt)

Element	Sample 1	Semiconductor Grade (Ref)
B	1.	0.1
P	1.	<0.6
As	0.5	<0.1
Al	1.	0.3
Ti	0.5	0.0
V	0.1	0.019
Zr		
Mo	0.1	<0.062
Cr		
Mn	<1.	0.04
Fe	20	2
Co	0.1	0.07
Ni	1.	0.0
Cu	1.	0.05
Zn	1.	0.4
Cd	<0.1	<0.01
Se	<1.0	<0.36
Pb	10	
Li	0.1	0.02
Na	328	3.7
K	<2.	<0.9
Mg	3.	0.9
Ca	5.	1
Sr	0.1	< 0.04

In independent sessile drop experiments, it was observed that NaF does not wet graphite while it readily wets silicon. When NaF is in contact with Si, especially surface oxidized silicon, fluosilicates species are produced at the interface and go into the NaF solution (5). This solution does wet graphite, but the NaF acts as a protective coating on the silicon preventing it from reacting with graphite and forming undesirable SiC. This wetting behavior allows for casting of silicon directly in reusable graphite crucibles (6). Typical values for the impurity content in the resulting silicon are shown in Table 5. As in the case of leach separation, solar grade silicon was obtained. When the silicon obtained by melt separation was separated from the NaF and heated in vacuum at 1200°C for 5 minutes, the Na content dropped below 10 ppm (6).

### CONCLUSIONS

Polycrystalline silicon of solar grade quality can be produced by reducing  $\text{SiF}_4$  gas with metallic Na.  $\text{SiF}_4$  is obtained from  $\text{H}_2\text{SiF}_6$  as an inexpensive by-product of the fertilizer industry. Silicon can be recovered from the Si-NaF mixture by either acidic aqueous leaching or by melt-separation at temperatures above 1410°C. In both cases, the resulting silicon has impurity levels at or below the maximum threshold [as determined by Westinghouse researchers (4)] at which impurity content results in degradation of cell efficiency.

### REFERENCES

1. A. Sanjurjo, L. Nanis, K. Sancier, R. Bartlett and V. Kapur, J. Electrochem. Soc., Vol. 128, No. 1 179, (1981).
2. A. Sanjurjo, L. Nanis, Bull. of Mat. Sci., Vol. 16, No. 4, 438, (1981).
3. K. Sancier, V. Kapur, J. Electrochem. Soc.
4. R. H. Hopkins et al., Final Rep. DOE/JPL-954331-81-14 (1982).
5. L. Nanis, A. Sanjurjo, and S. Westphal. Met. Trans. B. Vol. 12B, 535 (1981).
6. A. Sanjurjo, J. Electrochem. Soc., Vol. 128, No. 10, 2244 (1981).

### ACKNOWLEDGMENT

We are indebted to the technical contributions of many SRI members, especially to S. Leach, R. Emerson, D. Hildenbrand, K. Lau, R. Brittain, E. Farley, K. Kinoshita, S. Wing, R. Lespade. We also acknowledge the participation of former SRI members: L. Nanis, R. Bartlett, R. Weaver, V. Kapur, and S. Westphal. This work was funded in part by DOE/JPL under contract 954471.



## DISCUSSION

DeLUCA: If I understood you correctly, you used the reference material called semiconductor-grade silicon and you reported that the boron concentration was about .1 ppma and phosphorus was .6 ppma.

SANJURJO: Yes, but, I see your question. The sensitivity of the spark source mass spectroscopy system is established using semiconductor-grade silicon; that's what I tried to emphasize. It has no correlation whatsoever with the real purity. The purity of the semiconductor silicon we were using is probably very high, because the resistivity is more than  $10^4$  ohms, almost intrinsic. Measurements with this silicon were used to make sure that the system for analysis and handling could be trusted. The boron in our silicon, for example, was less than .1 ppma. Since we had to have the impurity measurements made outside of SRI, we did some internal checks on the values. I believe that the purity of our silicon is much higher than is indicated by these values. There were some other independent analyses for boron and phosphorus. These were done by a wet-type analytical method. These values were about 70 ppba, which is about the sensitivity level. This value is almost one level lower than the SSMS results.

THORNHILL: I've spent a great many years working with silicon and making devices from silicon and one of the things that I learned early on was to be very suspicious of the analysis of the starting material. The bottom line was always what kind of a device you could make. Has this material been made into crystals and photovoltaic devices?

SANJURJO: Unfortunately, JPL never gave us enough money to do it during the contract, but we are doing it at this time in our program. We will have the answers in a matter of months. I can tell you this much, we are producing a statistically significant number of solar cells so that the characterization should be valid.

# CLOSING COMMENT

LUTWACK: It is my pleasure now to first thank the speakers for presenting papers which were educational, stimulating and thought-provoking. I want to thank the people who attended for participating and making this a lively workshop. I hope all of you have enjoyed the workshop and have derived something of interest from the meeting. Perhaps you were educated in some areas. Perhaps some questions have been raised in your minds, and you will be stirred and provoked to increase their activities in some of the fields which have been discussed.

On behalf of the committee of the workshop, thank you very much for being here.

PRECEDING PAGE BLANK NOT FILMED